UNIVERSITY OF CALIFORNIA
RIVERSIDE

AdS Opacity, Soft Bombs, and Exotic Forces

A Dissertation submitted in partial satisfaction
of the requirements for the degree of

Doctor of Philosophy

in

Physics

by

Alexandria Nicole Costantino

December 2022

Dissertation Committee:

Dr. Philip Tanedo, Chairperson
Dr. José Wudka
Dr. Haibo Yu

The Dissertation of Alexandria Nicole Costantino is approved:

Committee Chairperson

University of California, Riverside

Acknowledgments

I would like to thank my friends and mentors for their support and guidance.

In particular, I am grateful to the members of my Ph.D. committee—Flip Tanedo, José Wudka, and Haibo Yu—for their mentorship and support. I would also like to thank Shan-Wen Tsai and Hillary Jenks for their mentorship, guidance, and support as well.

I am thankful to my longtime collaborator, Sylvain Fichet, with whom much of this work was completed. Work that appears in this thesis is based on previously published works [1–4] with whom Sylvain and Flip Tanedo were co-authors. I acknowledge the support of these co-authors and am thankful for their contributions.

I would like to thank my peers at UCR and at other institutions with whom I discussed physics, diversity and inclusion in STEM fields, or life in general. In particular, I would like to thank my friends in the particle theory group at UC Riverside, my friends within the Physics Organization for Women and the UnderRepresented, friends from my physics cohort at UCR, friends that I met through the TASI event of 2020, as well as others that I met through physics more broadly. This work would not have been possible without the collective support of my peers. I am extremely grateful for their support and friendship.

I am also grateful for the support that I received from the National Science Foundation through the Graduate Research Fellowship Program.

I dedicate this dissertation to my partner Rachel and to our two cats, George and Dustin.

ABSTRACT OF THE DISSERTATION

AdS Opacity, Soft Bombs, and Exotic Forces

by

Alexandria Nicole Costantino

Doctor of Philosophy, Graduate Program in Physics
University of California, Riverside, December 2022
Dr. Philip Tanedo, Chairperson

Effective field theory is arguably one of the most powerful theoretical tools that we have at our disposal as physicists. It enables us to describe the low-energy physics of a wide range of models with relatively few operators. In this thesis, we show how so-called "irrelevant" (higher-dimension) EFT operators lead to a number of novel, yet under-appreciated properties, both in flat and negatively-curved Anti de-Sitter spacetime.

In flat space, higher-dimension EFT operators give rise to spin-dependent quantum forces which arise at loop level. We determine these forces and show how they can be used to probe specific models of dark matter. We point out that the oft-discussed spin-dependent Yukawa forces have specific properties and are not representative of the behavior of generic potentials. Quantum forces from irrelevant EFT operators can and should serve as complimentary benchmark cases when discussing potential bounds from various *fifth-force experiments*. We discuss how the neutrino force, a famous example of a quantum force, can be used to determine the Dirac/Majorana origin of the neutrino mass.

In (4+1)-dimensional Anti de-Sitter spacetime, we show how the presence of higher-dimension EFT operators implies a number of novel properties for bulk particles. These include soft, high multiplicity cascade decays known as *soft bombs* and the merging of spectral resonances into a continuum at high energies. The negative curvature of AdS warps momentum scales, leading to a puzzle where particles created in one part of the space can appear to be outside the region of EFT invalidity in another part of the space. We provide the resolution to this puzzle and demonstrate the self-consistency of the EFT.

Contents

List of Figures

List of Tables

Chapter 1

Introduction

The Standard Model of particle physics and general relativity have been immensely successful, each providing accurate predictions of experimental observables over many length scales. However there remain a number of puzzles and anomalies which prompt us to consider the possibility that the Standard Model is not all that there is. The existence of dark matter, dark energy, and the hierarchy problem are just a few of the puzzles that motivate high energy physicists to theorize possible new physics.

In this thesis, two distinct extensions of the Standard Model paradigm will be discussed. In the first extension, we introduce an extra spatial dimension such that the Standard Model fields live on a 3-brane in a greater (4+1)-dimensional Anti-de Sitter (AdS) spacetime. Later, we present "exotic" (*i.e.* non-Yukawa) potentials that can arise from generic effective field theories (EFTs). We discuss applications such as Casimir-Polder forces from neutrinos as well as how exotic forces offer a possible probe of certain dark sector models.

1.1 AdS and CFT

Why might one study quantum field theory in anti-de Sitter space in the first place? AdS is a maximally symmetric background; it is a laboratory to understand Quantum Field Theory (QFT) in more general curved spacetime. In AdS the negative curvature regulates infrared divergences, which can teach us about flat space QFTs [8]. The AdS metric is conformally flat, such that boundary conformal theories in flat space can be studied by placing a conformal field theory (CFT) in the AdS bulk [9, 10]. But, perhaps more importantly, AdS turns out to be a unique window into strongly coupled gauge theories and into quantum gravity as a consequence of the AdS/CFT correspondence (for initial works see [11–18], for some reviews see [19–22]), which identifies a dual CFT living on the boundary of AdS.

QFT in AdS is also interesting for phenomenological reasons. Models in AdS can solve the electroweak hierarchy problem [23] and can also be used to model strongly coupled dark sectors [24–27] (via the AdS/CFT duality), both with reasonable modifications to 4d gravity [28, 29]. Quantum fields in AdS also offer some novel predictions not found in the Standard Model or particle extensions thereof. All quantum field theories exist on a renormalization group "flow" between ultraviolet and infrared conformal field theories. Thus, by better understanding CFTs (and by extension, QFT in AdS_5), we gain a deeper understanding of all QFTs.

The principal question we want to answer is: How do quantum dynamics affect the propagation of a field in AdS spacetime? Here we lay down preliminary observations to set the stage and sharpen the scope of our study.

1.1.1 Dressed Propagators and AdS Opacity

In Lorentzian flat space, propagators of perturbative quantum field theory are proportional to

$$\frac{i}{p^2 - m^2 + \Pi(p)} \,. \tag{1.1}$$

Π is the self-energy, *i.e.* the bilinear operator arising from quantum loops. This self-energy dresses the free propagator, yielding a Born series which sums to Eq. (1.1). Unitarity cuts relate the imaginary part of Π to processes ending in asymptotic states. ImΠ resolves singularities occurring in the timelike region $p^2 > 0$, making leading loop effects an unavoidable ingredient of QFT in the timelike region.

The presence of interactions results in a non-trivial self-energy operator Π dressing the propagating field, as shown in Eq. (1.1) above. One representation of a dressed propagator is as a Born series—a term of the series is pictured in Fig. 1.1. Another representation of dressing is via the equation of motion following from the quantum effective action, schematically

$$\sqrt{|\gamma|}\mathcal{D}\, G - G * \Pi = -i\delta \,. \tag{1.2}$$

Here $\mathcal{D}$ is the differential operator giving rise to the free equation of motion, γ the background metric on which the field propagates, δ a Dirac delta and G is the propagator. A perturbative treatment of the self-energy operator in Eq. (1.2) generates the Born series representation.

The qualitative differences in field propagation between the free and interacting theories are expected to occur most clearly in the *timelike* region of spacetime. This feature is not specific to flat space or AdS. It is expected simply because in the timelike regime, the

self-energy tends to develop singularities and become complex-valued. In particular, while the solutions of the free homogeneous EOM would tend to be oscillating, in the interacting theory Π can develop an imaginary component which introduces an exponential behaviour in the solutions. This then translates as an exponential damping in the Feynman propagator described in Eq. (1.2), where the effect comes from $\mathrm{Im}\Pi$. These rough considerations only rely on the analytical structure of Π, not on the existence of asymptotic states, hence they are valid for QFT in curved spacetime.[1]

The damping effect can be seen in Lorentzian flat space—though the position space propagator behaves as a power law in the free theory, it exponentially decays in the interacting theory. Assuming a constant imaginary part $\mathrm{Im}\Pi \equiv m\Gamma$ in Eq. (1.1) gives rise to a propagator decaying as

$$G(X, X') \sim \frac{m^{\frac{d}{2}-1}}{(\Delta X)^{\frac{d}{2}}} e^{-\frac{\Gamma \Delta X}{2}} \tag{1.3}$$

in $d+1-$dimensions, with $\Delta X = \sqrt{\eta_{MN} X^M X'^N} \in \mathbb{R}$ a timelike interval. The free theory behaviour amounts to having $\Gamma = 0$ in Eq. (1.3): there is no exponential decay in this case. This exponential suppression means that particles with $\mathrm{Im}\Pi \neq 0$ decay through time. This interpretation cannot be used in curved spacetimes, where intuitions using asymptotic states are not necessarily valid.

[1] We note in passing that the existence of asymptotic states are not necessarily guaranteed in curved spacetime. Consider the case of spacetime with a cosmological constant, of which AdS spacetime is a particular example. On this background, there is no vacuum state of minimal energy (because energy is not a conserved quantity). Without the existence of such a ground state, there are no asymptotic particle states, which are defined as excitations of the ground state. See *e.g.* [30] for more discussion on the topic. See also Sec. 2.2.1 of this thesis.

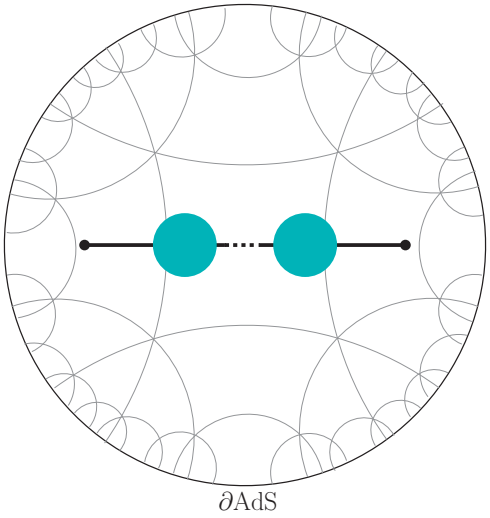

Figure 1.1: A propagator dressed by generic self-energy insertions, Π, in the bulk of AdS.

In Lorentzian AdS space—as in any other background—the propagator is also dressed by self-energy insertions, as pictured in Fig. 1.1. How does this dressed propagator behave in AdS? Some limited intuition from flat space might be used, but in any case an explicit, quantitative description of the effects of quantum dressing remains to be obtained.

In chapter 2 of this thesis, we solve the dressed equation of motion, Eq. (1.2) in AdS_5, for timelike momentum $p^2 > 0$ by working in the position-momentum space derived from Poincaré coordinates (p^μ, z). We find that the dressing may induce an exponential damping of the propagator in the $pz \gg 1$ region (the *conformally flat region*, see chapter 2). This damping behaviour occurs even if a single point is in the conformally flat region, *i.e.* $pz_< \ll 1$, $pz_> \gg 1$, which includes the boundary-to-bulk propagator with $pz \gg 1$ as a particular case. We refer to this exponential dampening as *the opacity of AdS*, or simply as *opacity*.

Opacity may have implications for extensions of the Standard Model of particles. This is for example relevant for extra-dimensional and holographic dark sector models. Consider the so-called "slice of AdS"—in which there are UV and IR branes that truncate the bulk. The exponential damping of the propagator indicates that particles in the UV region of the bulk cannot propagate to the IR brane (and vice versa) if they have sufficiently high absolute 4-momentum—either timelike or spacelike. Thus we say that we say that the IR brane *effectively emerges* for bulk propagators as their 4-momentum is decreased below a certain special value. This gives rise to the concept of an *emergent* sector which can only interact at sufficiently small values of absolute 4-momentum.

1.1.2 Soft Bombs and IR Emergence

In the "slice of AdS", as described in the previous paragraph, opacity suppresses propagation between UV and IR branes above some specific value of momentum $p > \widetilde{\Lambda}$. For sufficiently high four-momentum, the EFT will be invalid in the region near the IR brane. Thus one may conjecture that for $p \gg \widetilde{\Lambda}$, the theory is described by an effective Lagrangian without an IR brane. A workaround to this conjecture may be possible via bulk cascade diagrams. A cascade diagram can split the energy of an individual state into many offspring states which have $p_{\text{offspring}} < \widetilde{\Lambda}$ and can thus propagate to the IR region.

Across the $p \sim \widetilde{\Lambda}$ transition, do higher-point bulk correlators also effectively lose contact with the IR brane as the effective theory breaks down in that region of position–momentum space? If so, we say that the IR brane *effectively emerges* for bulk correlators as their energy is decreased through this KK–continuum transition.

Another way of phrasing the previous question is to ask whether the cascade decays induced by the bulk interactions may challenge the picture of effective emergence established by opacity. Previous studies of these cascade decays in AdS (obtained from the dual CFT) have indicated that they should be soft and highly spherical [31–37]. Hence in this thesis will we refer to these cascade decays as *soft bombs*.[2] Soft bombs can split the energy of individual excitations across many offspring states. Thus the soft bomb naïvely appears to be a way for a bulk field to propagate information to the IR brane even when the initial excitation is in a regime where it is not sensitive to the IR brane. The picture of effectively emergent IR brane physics thus depends on a careful understanding of soft bomb events from bulk decays.

In chapter 3 of this thesis, we study soft bombs events in the regime in which propagation to the IR brane is suppressed. There are multiple motivations for such a study:

- Earlier work on soft bombs in AdS_5 [40] did not take into account the opacity of AdS and the subsequent breakdown of the effective theory in the IR region of AdS. For $p > \widetilde{\lambda}$, propagation to the IR brane is exponentially suppressed and thus KK modes are no longer appropriate degrees of freedom. In this regime, we address kinematic considerations, such as the soft and spherical nature of the events. We also calculate occurrence probabilities for soft bomb events. To the best of our knowledge, such a calculation has not been presented in the literature.

[2] We note that soft bombs have also been referred to in the literature as "soft unclustered energy patterns" (SUEPs) [38, 39], "spherical events" [40], "fireworks" [37] or "jets at strong coupling."

- Understanding the soft bomb rate allows us to complete the picture of the emergence of the IR brane. Without soft bomb rates, it remains unclear whether the theory can actually be described by a high-energy effective theory with no IR brane in the continuum regime.

- Both IR brane emergence and the properties of soft bombs have phenomenological implications for models of physics beyond the Standard Model that involve a strongly–coupled hidden sector with an AdS dual. This holographic dark sector scenario has been recently put presented in [1, 27], see also [24–26, 41–43] for earlier and related attempts.

1.2 Exotic Forces

In the second portion of this thesis, our focus is not on (4+1)-dimensional AdS, but rather on "exotic" (non-Yukawa) forces. Why might one study new exotic forces in the first place?

1.2.1 Exotic Spin-Dependent Forces from A Hidden Sector

The existence of dark matter and dark energy suggests the possible existence of a light hidden sector. To avoid experimental observation, the particles in this hidden sector should have suppressed interactions with visible matter; these sectors are broadly referred to as *dark sectors*. The existence of a dark sector may imply that nature exhibits new macroscopic forces between visible sector particles. For example the exchange of a single bosonic particle induces a Yukawa-like potential. A multitude of experimental searches

probe the possible existence of spin-independent forces, see e.g. [44–46]. However, it is also possible that the dominant effects of a hidden sector force could be *spin-dependent*. These types of forces are more challenging to observe and relatively few experiments are designed to probe them.

Both theoretical and experimental efforts have focused primarily on Yukawa-like spin-dependent forces that arise from the exchange of a single massive boson. Spin-dependent forces from the axion were identified in [47]. More recently, Dobrescu and Mociou presented a dictionary between the field theoretical properties of new bosons and the types of spin-dependent macroscopic forces that they generate [48]. See [49] for a recent discussion that includes contact interactions, further phenomenology, and corrections of earlier literature. Conversely, experiments have been focused on the search for Yukawa-like forces, see e.g. [5, 50, 51].

In chapter 4 of this manuscript we present spin-dependent *exotic* forces. We define exotic to mean forces that are not Yukawa-like. The complementarity of the exotic and Yukawa-like potentials is manifested clearly in searches for spin-dependent forces. We point out that spin-dependent Yukawa forces have specific properties and are not representative of the behavior of generic spin-dependent potentials. Because of this, it is necessary to have a set of benchmark scenarios beyond the spin-dependent Yukawa case to interpret and design experiments. The main goal of chapter 4 is to fill a gap in the literature by presenting exotic potentials generated by explicit dark sector models. [3]

[3] See also [46, 52, 53] for related work on spin-independent potentials.

1.2.2 The Neutrino Casimir Force

There exists a great body of experimental evidence [54–57] to suggest that neutrinos undergo flavor oscillations and therefore have mass. A neutrino can be described as a 2-component fermion, and two distinct possibilities exist to generate its mass. One possibility is that neutrinos mass mix with an extra SM-singlet, in which case both can be described together in 4-component *Dirac* fermions. Alternatively, a neutrino mass can arise from lepton number-violating mass insertions, in which case neutrinos can be described as self-conjugate 4-component *Majorana* fermions.

The difficulty in distinguishing these possibilities lies in the "Majorana-Dirac confusion theorem" [58, 59]. In any amplitude, a neutrino propagator with 4-momentum $p \gg m_\nu$ has mass insertions suppressed as m_ν^2/p^2 and thus the mass generation mechanism cannot be observed. This is shown diagrammatically in Fig. 1.2. By unitary cuts the same property applies to external neutrino lines. [4]

Massive neutrinos have a mass of order $0.1\,\mathrm{eV}$ (see *e.g.* the upper bounds being placed by [61]). This is much smaller than the energy scale of most typical scattering experiments, and therefore the confusion theorem makes the mass generation mechanism difficult to observe. In the laboratory, one approach has been to search for processes that are forbidden for Dirac neutrinos but are allowed for Majorana neutrinos. Such processes include the lepton number-violating neutrinoless double beta decay [62–64] and the neutrinoless double

[4] The confusion theorem is a property of the SM. In contrast, gravity knows about all degrees of freedom and could identify whether an extra singlet neutrino exists, hence determining the nature of the neutrino mass. Existing approaches require one to consider the cosmological history of the Universe and depend on extra assumptions about physics beyond the SM (see *e.g.* [60]).

electron capture [65–67].

Another approach is to study the macroscopic forces that arise from the exchange of virtual neutrinos [7, 68]. In the low energy effective theory of the weak interaction, pairs of neutrinos can be exchanged, as shown in Fig. 1.3. This exchange results in long range *quantum* [5] forces between Standard Model fermions [2, 69–74]. On distances the order of $1/m_\nu$ or larger the confusion theorem no longer presents any issue as the neutrino mass is not negligibly small at that length scale. Hence by measuring the potential, one could in principle distinguish the Dirac versus Majorana nature of neutrinos.

Recently there has been renewed interest in this approach, for instance in [68]. These authors consider three generations of neutrinos (including mixing) in their calculation of the potential between point sources. They again find that a distinction between Majorana and Dirac neutrinos is possible when the separation of the point sources is on the order of $1/m_\nu$ or greater.

The sources considered in the previous works are pointlike. There also exists a force between extended macroscopic bodies: a neutrino Casimir force. In a realistic "fifth force" experimental setup aimed at establishing the nature of the neutrino masses, it is likely to be this Casimir force which is experimentally relevant, as the Compton wavelength of massive neutrinos is on the order of a micron, much larger than the atomic scale. In the case of sources with planar geometry, the potential is dominated by long wavelength contributions and therefore it is not obvious how the confusion theorem applies. It is with these motivations that in chapter 5 we present a study of the neutrino Casimir force in the

[5] Quantum forces have their leading contribution at loop level. See [1, 46, 53] for applications to dark sector searches.

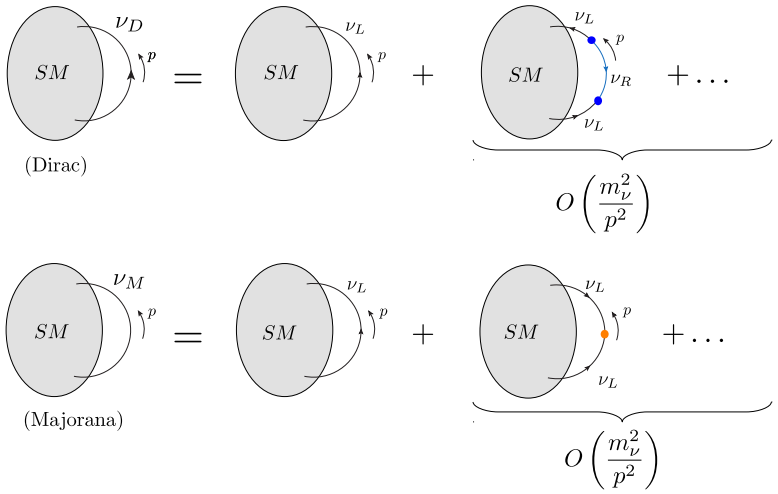

Figure 1.2: The Majorana-Dirac confusion theorem. The blob represents an arbitrary SM amplitude from which we single out an internal neutrino propagator. Dirac mass insertions (top) and Majorana mass insertions (bottom) become negligible for $p \gg m_\nu$ such that amplitudes become equivalent in this limit.

plate-plate and point-plate configurations. These can then serve as approximations of the force in more evolved geometries [75].

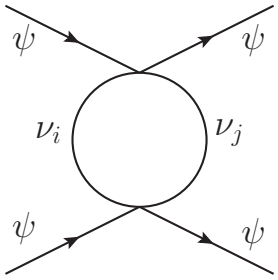

Figure 1.3: Quantum forces can be induced from the exchange of two neutrinos. The two virtual neutrinos can in principle have different masses $m_i \neq m_j$.

Chapter 2

Dressed Propagators and AdS Opacity

2.1 Chapter Abstract

We investigate how quantum dynamics affects the propagation of a scalar field in Lorentzian AdS. We work in momentum space, in which the propagator admits two spectral representations (denoted "conformal" and "momentum") in addition to a closed-form one, and all have a simple split structure. Focusing on scalar bubbles, we compute the imaginary part of the self-energy ImΠ in the three representations, which involves the evaluation of seemingly very different objects. We explicitly prove their equivalence in any dimension, and derive some elementary and asymptotic properties of ImΠ.

Using a WKB-like approach in the timelike region, we evaluate the propagator dressed with the imaginary part of the self-energy. We find that the dressing from loops

exponentially dampens the propagator when one of the endpoints is in the IR region, rendering this region opaque to propagation. This suppression may have implications for field-theoretical model-building in AdS. We argue that in the effective theory (EFT) paradigm, opacity of the IR region induced by higher dimensional operators censors the region of EFT breakdown. This confirms earlier expectations from the literature. Specializing to AdS_5, we determine a universal contribution to opacity from gravity.

2.2 Introduction

2.2.1 Preliminary Observations

in the introduction chapter, the principal question we want to answer is: How do quantum dynamics affect the propagation of a field in AdS spacetime? Here we provide supplementary background on recent related work in AdS to set the stage and sharpen the scope of our study.

A study of the dressed propagator involves evaluating loops in AdS and summing the Born series. But propagators in position space are complicated functions of the AdS geodesic distance, making every step a challenging calculation. Loops in AdS have been an intense topic of study, see [76–114]. AdS loops are often evaluated in position space and are given by fairly complex expressions. A summation of the Born series in the spectral formalism in the $O(N)$ model can be found in [101]. However the expressions involve spectral integrals and are fairly difficult to handle for further analysis. Hence to reduce the complexity of our calculations, we restrict our study to a scalar. We will study quantum effects induced both from matter interactions and from gravity on this propagating scalar.

We choose to investigate the dressed propagator by working in the position-momentum space derived from Poincaré coordinates (p^μ, z). Though some symmetry is lost when going in this Poincaré position-momentum space, various representations of the propagator become simultaneously available which take a simple form. Momentum space is also the natural language to study the loop summation and to connect with flat space QFT knowledge and tools. Among the above references, [112, 113] and [114] involve calculations in momentum space—the use of momentum space proves to be instrumental in these works. Momentum space has also been used in diverse studies of tree-level amplitudes [115–137] and in the calculation of cosmological observables [138–154].

When considering the effective field theory (EFT) of gravity, the theory necessarily becomes strongly coupled in the IR region of the Poincaré patch. This feature was pointed out at a qualitative level in [155], wherein it was suspected that rapid oscillations of the timelike propagator may render this region inaccessible, hence censoring superPlanckian effects. A more accurate analysis involving dressed propagators in the timelike region of AdS has been initiated in [110] and [3]. The present work also serves to reinforce and complete these EFT-oriented analyses.

As discussed in the introduction chapter, the imaginary part of the self-energy, $\mathrm{Im}\Pi$, will play an important role in the field propagation in AdS. Consequently $\mathrm{Im}\Pi$ will be a central object in our study.

In flat space, $\mathrm{Im}\Pi$ implements unitarity cuts. Unlike in flat space, AdS lacks asymptotic states to define a standard S-matrix, and thus a standard optical theorem [156,157]. However an AdS cut operation has been introduced in [158]—and a corresponding

operation has been identified in the dual conformal theory [159]. In the scope of the present work, we will note the interplay between the Im() and the AdS cut operations. We do not delve into the CFT side apart from using some elementary results.

At leading order in the loop expansion, ImΠ is expected to be finite in any space-time dimension. This is because the divergences renormalize local bilinear operators, which contribute to the real part of Π. The mass term in $\mathcal{D}$ may for instance be renormalized. We focus on a finite part of Π hence renormalization aspects do not require further discussion and can be ignored.

2.2.2 Summary of Results

Working in Poincaré position-momentum space (*i.e.* in Fourier-transformed Poincaré coordinates), three representations of the propagator become simultaneously available and take simple forms: a closed-form "canonical" representation, a conformal spectral representation, and a momentum spectral representation. Each of these representations is useful to illuminate different properties of the AdS loop.

We consider cubic couplings, such that the self-energies considered always have a bubble topology. We obtain the following results.

- We derive the imaginary part of the simplest scalar bubble in the three representations mentioned above. In the conformal spectral representation, AdS/CFT arises and we recover various results from the literature.[1] We prove the equivalence of all three

[1] In the conformal spectral representation, we show that ImΠ takes the form of a sum over double-trace propagators with coefficients that exactly match those from [79, 160]. When summing the Born series in the conformal spectral representation, we recover the anomalous dimension found in [93].

representations of ImΠ and show some of its elementary and asymptotic properties.

- We solve the dressed equation of motion for timelike momentum $p^2 > 0$ in the conformally flat region $pz \gg 1$ using a WKB-type approximation. We work in the momentum spectral representation of $\mathrm{Im}\,\Pi$ and the canonical representation of the propagator. To render the calculations analytically tractable and obtain a closed-form result, we employ kinematic and saddle-point approximations. This is a new method of studying the dressed propagator.

- The dressing induces an exponential damping of the propagator in the $pz \gg 1$ region. This damping behaviour occurs even if a single point is in the conformally flat region, *i.e.* $pz_< \ll 1$, $pz_> \gg 1$, which includes the boundary-to-bulk propagator with $pz \gg 1$ as a particular case. This regime has no flat-space equivalent—the $pz \ll 1$ region vanishes if one Weyl-transforms to flat space. Renormalizable interactions may not give rise to an exponential damping, but operators of sufficiently high dimension—as present in an EFT—will induce it. This is pictured in Fig. 2.1.

- In the EFT paradigm, the EFT breaks down when higher dimensional operators give contributions of the same order. In AdS this occurs at sufficiently large pz, *i.e.* in the IR region of the Poincaré patch. Working in the EFT paradigm, we find that the exponential damping censors the region of EFT breakdown.

- In case of a scalar field theory in AdS_5, the leading damping occurs from the $\Phi^3 - \Phi\partial_M\Phi\partial^M\Phi$ bubble. The timelike propagator behaves schematically as

$$G(p; z, z') \propto e^{-c\frac{k}{\Lambda}(pz_>)^2} \tag{2.1}$$

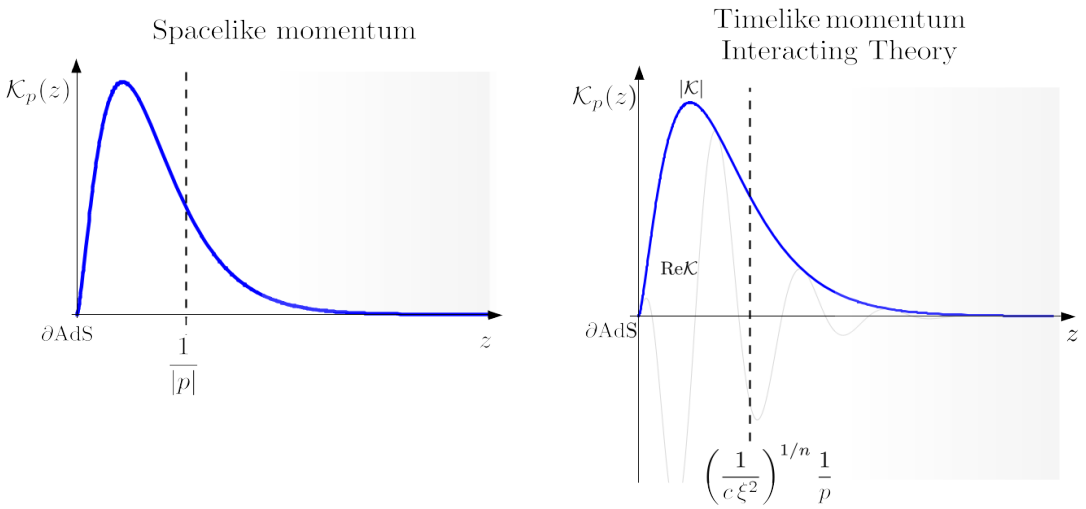

Figure 2.1: AdS boundary-to-bulk propagators in Poincaré position-momentum space (p^μ, z). For spacelike momentum the propagator decays exponentially for $|p|z \gg 1$ (left). For timelike momentum, exponential decay is induced by interactions at the quantum level for $c\,\xi^2(pz)^n \gg 1$. The dimensionless coupling ξ parameterizes some cubic interaction and $c \ll 1$ encodes a loop factor suppression. In both cases, AdS becomes "opaque" to propagation at large enough z.

where the coefficient $c = O(10^{-2})$ (see Sec. 2.6.4) includes suppression by a loop factor and estimates from 5D dimensional analysis. Here k is the AdS curvature and Λ characterizes the strength of couplings in the EFT.

- A partial contribution from bulk gravity in AdS_5 leads to the suppression

$$G(p; z, z') \propto e^{-c'\kappa^2(pz_>)^4} \tag{2.2}$$

with $c' = O(10^{-6})$ and $\kappa = \frac{k}{M_{\rm Pl}}$. This effect depends only on the strength of gravity κ.

2.2.3 Outline

Our investigation takes the following steps. We lay down the basic formalism and derive the scalar propagator in various representations in Sec. 2.3. Asymptotic properties of Poincaré position-momentum space are also discussed. Using the conformal spectral representation, we evaluate a bubble diagram and sum the Born series in Sec. 2.4. This involves AdS/CFT—the CFT elements required for the calculations are also given. In Sec. 2.5 we derive the expressions of ImΠ in the various representations, as well as their equivalence proofs. We proceed to prove some general properties of ImΠ.

In Sec. 2.6 we adopt the EFT viewpoint and study the dressed propagator in the conformally flat region. We present a WKB-like approach and justify some related assumptions needed to tackle the calculations analytically. We use this approach to derive the behavior of the dressed propagator in a given regime. Aspects of EFT validity, arbitrary dimensions, higher order diagrams and deformed AdS backgrounds are also discussed. A universal contribution from gravity to opacity is then calculated in Sec. 2.7. Closing remarks and possible future directions (including implications for field-theoretical AdS model-building) are given in Sec. 2.8.

2.3 A Scalar Field in AdS$_{d+1}$

We focus on a scalar quantum field theory in $(d+1)$-dimensional Anti-de Sitter (AdS) spacetime with $d > 2$. The action has the form

$$S = S_{\rm EH} + \int d^{d+1}X\sqrt{g}\left(\frac{1}{2}\partial_M\Phi\partial^M\Phi - \frac{1}{2}m_\Phi^2\Phi^2 + \dots\right) \tag{2.3}$$

where $S_{\rm EH}$ is the Einstein-Hilbert action. The metric of the AdS background is denoted as γ_{MN} such that $g_{MN} = \gamma_{MN} + \dots$ where the ellipses represent fluctuations of the metric. The background metric in Poincaré coordinates is

$$ds^2 = \gamma_{MN}\, dX^M dX^N = \frac{1}{(kz)^2}\left(\eta_{\mu\nu} dx^\mu dx^\nu - dz^2\right) \tag{2.4}$$

with k the AdS curvature and $z \in [0, \infty]$.[2] The AdS boundary is at $z = 0$, the Poincaré horizon at $z \to \infty$. We use a mostly-minus metric such that $\eta = \text{diag}(1, -1, -1, \dots)$.

The ellipses in Eq. (2.3) represent operators with more fields and/or more derivatives, including interactions such as $\frac{1}{3!}\Phi^3$, $\frac{1}{3!}\Phi\partial_M\Phi\partial^M\Phi$. Interactions play a central role in this work and will be specified further on. The Einstein-Hilbert action is expanded in Sec. 2.7, which considers gravity-scalar interactions. In the other sections, we focus on scalar interactions.

Regarding the free part of the scalar action, it is often useful to parameterize the scalar mass as

$$m_\Phi^2 \equiv \left(\alpha^2 - \frac{d^2}{4}\right) k^2 \,. \tag{2.5}$$

The Breitenlohner-Freedman bound is satisfied for $\alpha^2 \geq 0$ in any dimension. In general we have $\alpha \in \mathbb{R}$. Throughout this work we restrict to $\alpha \in \mathbb{R}_+$ without loss of generality. In any dimension the $\alpha = 1/2$ value corresponds to a conformally massless scalar, see Sec. 2.3.3 for details.

In this work we focus on exact AdS, with no departure or truncation of the metric in the UV (towards the boundary) or in the IR (towards the Poincaré horizon). However our

[2] Poincaré coordinates render manifest the $SO(1,1) \times SO(1, d-1)$ subgroup of the $SO(2, d)$ isometry group of AdS_{d+1}, which encodes dilatation and d-dimensional Poincaré isometries.

results will also be relevant in the context of deformed AdS backgrounds. This is discussed in Sec. 2.6.7.

2.3.1 Free and Dressed Propagator

The equation of motion for the free field—when all interactions are neglected—can be obtained by extremizing the fundamental action. This gives

$$\mathcal{D}\Phi_{\rm cl} \equiv \frac{1}{\sqrt{\gamma}}\partial_M(\gamma^{MN}\sqrt{\gamma}\partial_N\Phi_{\rm cl}) + m_\Phi^2\Phi_{\rm cl} = 0 \tag{2.6}$$

where with have introduced the differential operator $\mathcal{D}$. The Green's function of $\mathcal{D}$ is the propagator of the free field, $G^{(0)}(X,X') = \langle\Phi(X)\Phi(X')\rangle_{\rm free}$, satisfying

$$\mathcal{D}_X G^{(0)}(X,X') = \frac{-i}{\sqrt{\gamma}}\delta^{(d+1)}(X-X')\ . \tag{2.7}$$

In the presence of interactions, the propagator is dressed by self-energy insertions, *i.e.* by bilinear operators resulting from the quantum dynamics. This is described using the partition function and derived quantities such as the quantum effective action.

The dressed equation of motion can be obtained from the partition function

$$Z = \int \mathcal{D}[\text{fields}]\, e^{iS} \tag{2.8}$$

by using invariance under an infinitesimal change of the field variable $\Phi(X) \to \Phi(X)+\epsilon(X)$. An explicit derivation is given in App. A. The result for the propagator dressed by a generic self-energy $i\Pi(X,X')$ is given by

$$\mathcal{D}_X G(X,X') - \frac{1}{\sqrt{\gamma}}\Pi * G(X,X') = \frac{-i}{\sqrt{\gamma}}\delta^{(d+1)}(X-X') \tag{2.9}$$

where $*$ is the convolution product, $A*B(X,X') = \int d^{d+1}Y A(X,Y)B(Y,X')$.

Treating the self-energy operator perturbatively, one can verify that Eq. (2.9) implies the well-known Born series representation of the dressed propagator $G = \sum_{n=0}^{\infty} G^{(n)}$ with

$$G(X, X') = G^{(0)}(X, X') + G^{(1)}(X, X') + \ldots = G^{(0)}(X, X') + G^{(0)} * i\Pi * G^{(0)}(X, X') + \ldots \tag{2.10}$$

For example, from the perturbative solving of Eq. (2.9), the first nontrivial term satisfies

$$\mathcal{D}_X G^{(1)}(X, X') = \frac{1}{\sqrt{\gamma}} \Pi * G^{(0)}(X, X') \,, \tag{2.11}$$

which gives the contribution Eq. (2.10) using that the solution to $\mathcal{D}\Phi = J$ is given by $\Phi(X) = i \int d^{d+1}Y \sqrt{|\gamma|} G^{(0)}(X, Y) J(Y)$. The higher order terms are obtained recursively, generating the Born series representation of G.

2.3.2 Three Representations in Poincaré Coordinates

The free Feynman propagator in the Poincaré coordinates (x^μ, z) defined in Eq. (2.7) is derived in Ref. [161]. Here we rather work in momentum space along the Minkowski slices, using Fourier transform

$$\Phi(p^\mu, z) = \int d^d x \Phi(x^\mu, z) e^{i\eta_{\mu\nu} p^\mu x^\nu} \,. \tag{2.12}$$

When working in Fourier-transformed Poincaré coordinates, the d-dimensional Poincaré isometries $SO(1, d-1)$ remains manifest, and the dilatation isometry becomes $(p^\mu, z) \to (p^\mu/\lambda, \lambda z)$.[3] One discrete symmetry is lost: the inversion $X^M \to \frac{X^M}{(X_N X^N)}$. As a counterpart to position space, position-momentum space offers supplemental insights. These are discussed throughout this section.

[3]This follows from requiring invariance of the Fourier transform Eq. (2.12) under these symmetries.

We define $p^2 = \sqrt{\eta_{\mu\nu} p^\mu p^\nu}$. Notice that the quantity pz is invariant under dilatations in addition to $SO(1, d-1)$ transformations. It is thus a good quantity to characterize points in the position-momentum space. The pz invariant appears throughout this work.

In position-momentum space the EOM operator becomes

$$\mathcal{D} = \Box + m_\Phi^2 = k^2 \left(-z^2 p^2 - z^{d+1} \partial_z \left(z^{1-d} \partial_z \right) + \left(\alpha^2 - \frac{d^2}{4} \right) \right) . \tag{2.13}$$

The EOM of the propagator is then given by

$$\mathcal{D}_z G^{(0)}(p; z, z') = -i(kz)^{d+1} \delta(z - z') . \tag{2.14}$$

$G^{(0)}(p; z, z')$ corresponds to the reduced 2-point function defined by factoring out a Dirac delta function associated with overall momentum conservation,

$$\langle \Phi(p^\mu, z) \Phi(p'^\mu, z') \rangle_{\text{free}} = G^{(0)}(p; z, z') (2\pi)^d \delta^{(d)}(p^\mu - p'^\mu) . \tag{2.15}$$

In the following we often use the shortcut $G(p; z, z') = G_p(z, z')$.

In Lorentzian space, the physical p^2 takes both signs. Since we have chosen the mostly minus metric, we have $p^2 < 0$ for spacelike momentum, $p^2 > 0$ for timelike momentum. In the free theory, p^2 is made slightly complex to resolve the non-analyticities arising for timelike momentum. This corresponds to the inclusion of an infinitesimal imaginary shift $p^2 + i\epsilon$, $\epsilon \to 0$. $\epsilon > 0$, the "Feynman prescription", is consistent with causality and defines the Feynman propagator. The $i\epsilon$ shift will often be left implicit in our notations.

In Fourier space, the homogeneous solutions to the EOM are linear combinations of

$$z^{d/2} J_\alpha (pz) , \quad z^{d/2} Y_\alpha (pz) , \tag{2.16}$$

using the bulk mass parameter α introduced in Eq. (2.5). It is also useful to use the basis

$$z^{d/2} I_\alpha \left(\sqrt{-p^2} z \right) , \quad z^{d/2} K_\alpha \left(\sqrt{-p^2} z \right) , \tag{2.17}$$

which shows explicitly the occurence of a branch cut for timelike momentum $p^2 > 0$. In this case one has the identities

$$I_\alpha \left(\sqrt{-p^2} z \right) K_\alpha \left(\sqrt{-p^2} z \right) = \begin{cases} \dfrac{i\pi}{2} J_\alpha (pz) H_\alpha^{(1)} (pz) & \text{if} \quad \epsilon > 0 \\ -\dfrac{i\pi}{2} J_\alpha (pz) H_\alpha^{(2)} (pz) & \text{if} \quad \epsilon < 0 \end{cases} \tag{2.18}$$

We now derive three different representations of the propagator.

Canonical Representation

A direct solving of Eq. (2.14) is possible using standard ODE techniques (see App. A of [162]). In this reference a solving has been done for $d = 4$, but the generalization to arbitrary dimension is straightforward.

The propagator takes the general form

$$G_p(z, z') = \frac{i}{C} F_<(z_<) F_>(z_>) \tag{2.19}$$

with $z_< = \min(z, z')$, $z_> = \max(z, z')$. The $F_{<,>}$ functions are linear combinations of the solutions Eq. (2.16) and are determined such that the propagator decays at $z \to 0, \infty$. In the timelike regime, this decay is ensured by the $i\epsilon$ prescription. [4] An equivalent method is to assume boundary conditions on branes placed at $z \neq 0, \infty$, and then send those branes to $z \to 0$ and $z \to \infty$. The overall coefficient C is related to the Wronskian $W = F_< F_>' - F_<' F_>$ such that $C = W(z)/(kz)^{d-1}$ [162].

[4] The $i\epsilon$ is presumably replaced by a physical effect in the interacting theory. We explicitly show how this occurs in Sec. 2.6.

Since we have chosen $\alpha > 0$, the condition that Eq. (2.19) does not diverge as $z \to \{0, \infty\}$ dictates that $F_<(z) = z^2 I_\alpha\left(\sqrt{-p^2}z\right)$ and $F_>(z) = z^2 K_\alpha\left(\sqrt{-p^2}z\right)$. We thus find

$$G_p^{(0)}(z,z') = -\frac{i}{k}(kz)^{d/2}(kz')^{d/2} I_\alpha\left(\sqrt{-p^2}z_<\right) K_\alpha\left(\sqrt{-p^2}z_>\right) \tag{2.20}$$

with $C = -k$. In the timelike regime we obtain

$$G_p^{(0)}(z,z') = \begin{cases} \dfrac{\pi}{2k}(kz)^{d/2}(kz')^{d/2} J_\alpha(pz_<) H_\alpha^{(1)}(pz_>) & \text{if} \quad \epsilon > 0 \\ -\dfrac{\pi}{2k}(kz)^{d/2}(kz')^{d/2} J_\alpha(pz_<) H_\alpha^{(2)}(pz_>) & \text{if} \quad \epsilon < 0. \end{cases} \tag{2.21}$$

Spectral Representations

The homogeneous solutions Eq. (2.16) depends on two external continuous parameters, α and p. The physical value of α is real and the physical value of p can be either purely real or imaginary, but both of these parameters can be analytically continued everywhere into the complex plane.

Each of these parameters can be used to develop a spectral representation of the propagator. What is required is a spectral function $\Omega_X(z,z')$ solution of the homogeneous EOM $\mathcal{D}\Omega_X(z,z') = 0$ and satisfying a completeness relation of the form

$$\int dX \Omega_X(z,z') \propto \delta(z - z') \tag{2.22}$$

where the integration is over some specified domain and where X is either α or p in our case. As we will see below, an integral representation of $G^{(0)}$ can be easily obtained whenever Ω_X is known. The completeness relation can be difficult to guess directly. However it can be built starting from the propagator, possibly with an appropriate analytic continuation of the relevant parameter.

Conformal Spectral Representation

Here we consider the spectral representation based on the bulk mass parameter α. In this subsection we indicate explicitly the α dependence of $G^{(0)}$ and of $\mathcal{D}$ via subscripts. The α parameter plays a central role in the AdS/CFT and CFT literature. α is directly related to the conformal dimension of the operators in the conformal field theory, see Sec. 2.4 for further details.

A spectral function in α is found to be

$$\Omega_\alpha(z,z') = \frac{i\alpha\sin(\pi\alpha)(kz)^{\frac{d}{2}}(kz')^{\frac{d}{2}}}{\pi^2} K_\alpha\left(\sqrt{-p^2}z\right) K_\alpha\left(\sqrt{-p^2}z'\right) . \tag{2.23}$$

We find it satisfies the completeness relation

$$\int_{-i\infty}^{i\infty} d\hat{\alpha}\, \Omega_{\hat{\alpha}}(z,z') = (kz)^{d+1}\frac{\delta(z-z')}{k} . \tag{2.24}$$

The direct proof of Eq. (2.24) is not trivial, we give it in App. B. The spectral function also satisfies the homogeneous EOM $\mathcal{D}_{z;\alpha}\Omega_\alpha(z,z') = 0$.

The propagator with bulk mass parameter α (*i.e.* with bulk mass $(\alpha^2 - d^2/4)k^2$) expressed in the conformal spectral representation takes the form

$$G^{(0)}_{p,\alpha}(z,z') = \frac{i}{k}\int_{-i\infty}^{i\infty} d\hat{\alpha}\, P(\hat{\alpha},\alpha)\,\Omega_{\hat{\alpha}}(z,z') , \qquad P(\hat{\alpha},\alpha) = \frac{1}{\hat{\alpha}^2-\alpha^2} . \tag{2.25}$$

One can notice that $\mathcal{D}_{z;\alpha}\Omega_\alpha(z,z') = 0$ implies

$$\mathcal{D}_{z;\alpha}\Omega_{\hat{\alpha}}(z,z') = (\alpha^2-\hat{\alpha}^2)k^2\Omega_{\hat{\alpha}}(z,z') . \tag{2.26}$$

By using Eq. (2.26) and the completeness relation Eq. (2.24), one can show that Eq. (2.25) obeys the EOM.

One can also verify that the spectral function satisfies

$$\Omega_\alpha(z,z') = \frac{\alpha}{2\pi}\left(G^{(0)}_{p,\alpha}(z,z') - G^{(0)}_{p,-\alpha}(z,z')\right) . \tag{2.27}$$

This can be used to prove Eq. (2.25). Substituting Eq. (2.27) into Eq. (2.25), and using that $G^{(0)}_{p,\alpha}(z,z') \propto \left(\frac{z_<}{z_>}\right)^\alpha$ for large $\mathrm{Re}(\alpha) > 0$ as discussed in and below Eq. (2.39), we can close the contour of the $\int d\hat{\alpha}$ integral of $G^{(0)}_{p,\hat{\alpha}}(z,z')$ clockwise towards the positive reals and the contour integral of $G^{(0)}_{p,-\hat{\alpha}}(z,z')$ counterclockwise towards the negative reals. This picks respectively the $\hat{\alpha} = \alpha$ and $\hat{\alpha} = -\alpha$ poles of the $P(\hat{\alpha},\alpha)$ measure. The residues combine to prove Eq. (2.25).

The conformal spectral representation obtained here amounts to the Fourier transform of the so-called split representation of the AdS propagator, usually taken in position space in the AdS/CFT literature. The split representation in position space involves a convolution of two boundary-to-bulk propagators [163]. In our position-momentum space formalism, such boundary convolution integral changes into a product. The "split" feature simply corresponds to the fact that $\Omega_\alpha(z,z')$ factors into the product of the $z^2 K_\alpha\left(\sqrt{-p^2}z\right)$, $z'^2 K_\alpha\left(\sqrt{-p^2}z'\right)$ solutions. This is not surprising since $\Omega_\alpha(z,z')$ has to satisfy the homogeneous EOM for both z and z'. This dictates that $\Omega_\alpha(z,z')$ must factor into a product of solutions of the free EOM.

Momentum Spectral Representation

Here we consider the spectral representation based on the absolute 4-momentum p. In this subsection we need to indicate explicitly the p dependence of $\mathcal{D}$ in subscript.

A spectral function in p is found to be

$$\Omega_p(z,z') = \frac{p}{k}(kz)^{d/2}(kz')^{d/2}J_\alpha(pz)J_\alpha(pz')\,. \tag{2.28}$$

It satisfies the homogeneous EOM. Moreover $\Omega_p(z,z')$ satisfies the completeness relation

$$\int_0^\infty dp\,\Omega_p(z,z') = (kz)^{d-1}\delta(z-z')\,. \tag{2.29}$$

This follows directly from the identity

$$\int_0^\infty d\hat{p}\hat{p}J_\alpha(\hat{p}z)J_\alpha(\hat{p}z') = z^{-1}\delta(z-z')\,. \tag{2.30}$$

The propagator with momentum p expressed in the momentum spectral representation takes the form

$$G_p^{(0)}(z,z') = i\int_0^\infty d\hat{p}\,P(\hat{p},p)\,\Omega_{\hat{p}}(z,z')\,, \qquad P(\hat{p},p) = \frac{1}{p^2-\hat{p}^2}\,. \tag{2.31}$$

One can notice that $\mathcal{D}_{z;p}\Omega_p(z,z') = 0$ implies

$$\mathcal{D}_{z;p}\Omega_{\hat{p}}(z,z') = (\hat{p}^2-p^2)(kz)^2\Omega_{\hat{p}}(z,z')\,. \tag{2.32}$$

By using Eq. (2.32) and the completeness relation Eq. (2.29), one can show that Eq. (2.31) obeys the EOM. We note that for timelike $\hat{p}$ the spectral function is given by

$$\Omega_{\hat{p}}(z,z') = \frac{\hat{p}}{\pi}\left(G^{(0)}_{\hat{p}+i\epsilon}(z,z') - G^{(0)}_{-\hat{p}+i\epsilon}(z,z')\right) \tag{2.33}$$

using that

$$J(x)H^{(1)}(y) = -(J(-x^*)H^{(1)}(-y^*))^* \tag{2.34}$$

for $\mathrm{Im}(x,y) > 0$.

We see that the structure of these expressions is similar to those of the conformal spectral representation. For instance Ω_p has a split structure just like Ω_α, since it satisfies the homogeneous EOM for both z and z'. The analogy is completed by extending the integration over $\hat{p} \in [-\infty, +\infty]$ —and including an overall factor of $1/2$. This then reproduces a structure similar to the integral Eq. (2.25) when taking spacelike momentum $p^2 < 0$ such that the poles are imaginary. It follows that Eq. (2.31) can be derived from Eq. (2.33) by closing the contour of the $\hat{p}$ integral. [5] Alternatively one could use the known result, Eq. (10.22.69) of [164].

The form of the spectral function Eq. (2.33) is reminiscent of the Källén-Lehmann spectral representation from flat space QFT (see e.g. [165, 166]). This is because using Eq. (2.33) with Eq. (2.34) amounts to picking the discontinuity of $G^{(0)}$ across the branch cut in p,

$$\mathrm{Disc}[G_p^{(0)}(z,z')]_{p\in R^+} = \frac{\pi}{k}(kz)^{d/2}(kz')^{d/2}J_\alpha(pz)J_\alpha(pz')\,. \tag{2.35}$$

Eq. (2.31) is then equivalent to

$$G_p^{(0)}(z,z') = \frac{i}{2\pi}\int_0^\infty d\hat{p}^2 \frac{\mathrm{Disc}[G_{\hat{p}}^{(0)}(z,z')]_{\hat{p}\in R^+}}{p^2-\hat{p}^2}\,, \tag{2.36}$$

which follows from Cauchy's integral formula.

2.3.3 Asymptotics in Poincaré Coordinates

In Poincaré momentum space, the factorized structure of the propagator implies that the asymptotic behaviour of the propagator can be independently understood for the

[5] One has $G_{\hat{p}}^{(0)} \propto e^{-\mathrm{Im}\,\hat{p}|z-z'|}$ at large $|\hat{p}|$. One closes the contour upward for both terms. The residues from each term have opposite signs and add up.

z and z' endpoints. The behaviour is dictated by Bessel functions asymptotics, where the relevant quantities to expand about are either the pz, pz' invariants or the α parameter.

In contrast, notice that in full position space, the propagator admits asymptotic behaviours as a function of the chordal distance $\xi = \frac{(z-z')^2 - x^\mu x_\mu}{zz'}$. Hence the asymptotic behaviour in position space involves information from both endpoints, the endpoints are not disentangled like in position-momentum space.

A given propagator has three distinct regimes: ($pz_< \ll 1$, $pz_> \ll 1$), ($pz_< \gg 1$, $pz_> \gg 1$), and ($pz_< \ll 1$, $pz_> \gg 1$). Expanding the Bessel functions at fixed complex α, the three asymptotic regimes are [6]

$$G_p^{(0)}(z,z') \approx -i \left(k^2 zz'\right)^{\frac{d-1}{2}} \frac{\sin\left(pz_< - \varphi\right) e^{i(pz_> - \varphi)}}{p} \quad \text{if} \quad pz, pz' \gg 1 \tag{2.37}$$

$$G_p^{(0)}(z,z') \approx -i \frac{\sqrt{\pi}}{\Gamma(\alpha+1)} \left(k^2 zz'\right)^{\frac{d-1}{2}} \left(\frac{pz_<}{2}\right)^{\alpha+1/2} \frac{e^{i(pz_> - \varphi)}}{p} \quad \text{if} \quad pz_< \ll 1\,,\ pz_> \gg 1\,. \tag{2.38}$$

$$G_p^{(0)}(z,z') \approx -\frac{i}{2k\Gamma(\alpha+1)} \left(k^2 zz'\right)^{d/2} \left(\Gamma(\alpha) \left(\frac{z_<}{z_>}\right)^{\alpha} + \Gamma(-\alpha) e^{-i\pi\alpha} \left(\frac{p^2 z_< z_>}{4}\right)^{\alpha}\right) \quad \text{if} \quad pz, pz' \ll 1 \tag{2.39}$$

for $\alpha \notin \mathbb{Z}$ with $\varphi = \frac{\pi(2\alpha-1)}{4}$. Note that for spacelike momentum $p^2 < 0$, the expressions Eq. (2.37) and Eq. (2.38) are exponentially suppressed for $|p| z_> \gg 1$. Some other features of these expressions are discussed further below.

[6] The exact criterion for Bessel asymptotics depends on α, throughout the paper we write simply $pz \ll 1$, $pz \gg 1$ for convenience.

The limit of large bulk mass/conformal dimension at fixed pz, pz' is equivalent to the limit taken in Eq. (2.39) when $\alpha \notin \mathbb{Z}$. When $\mathrm{Re}(\alpha)$ is large and positive, the first term in Eq. (2.39) dominates. When $\mathrm{Re}(\alpha)$ is large and negative, it is the second term that dominates. This limit is useful for Mellin-Barnes-type integrals appearing in the conformal spectral representation.

Conformally Massless Scalar

Here we further discuss the behaviour of the solutions at $pz \gg 1$.

Consider a scalar in $d+1$-dimensional flat space with mass m_0^2. A conformal Weyl transform from flat space ($\mathcal{R} = 0$) to curved space ($\mathcal{R} \neq 0$) gives an additional mass contribution uniquely fixed by the geometry,

$$m_\Phi^2 = \frac{d-1}{4d}\mathcal{R} + m_0^2 \,. \tag{2.40}$$

We have $\mathcal{R} = -d(d+1)k^2$ in AdS. Setting $m_0 = 0$ in Eq. (2.40) then gives

$$m_\Phi^2 = \frac{1-d^2}{4}k^2 \,. \tag{2.41}$$

We refer to a scalar with such mass as a *conformally massless* scalar—since it becomes massless when Weyl-transforming from AdS to flat space.

In position-momentum space, a scalar field in the $pz \gg 1$ regime *behaves asymptotically as a conformally massless scalar*, *i.e.* its mass is set to Eq. (2.41), or equivalently has $\alpha = 1/2$ in any dimension. This property can be noted by inspecting the solutions to the EOM for arbitrary α at $pz \gg 1$. The α dependence remains only in phases which are irrelevant for solutions to the homogeneous EOM. An α-dependence also remains in higher order terms $O\left(\frac{1}{pz}\right)$ of the asymptotic expansion of the Bessel functions.

This implies that $G_p^{(0)}(z,z')$ in the $pz, pz' \gg 1$ regime (Eq. (2.39)) is equivalent to a *massless* propagator in $d+1$-dimensional flat space under a Weyl transformation. This is shown in next section where we study the flat space limit in more details. In contrast, for $G_p^{(0)}(z,z')$ in the $pz_< \ll 1$ and $pz_> \gg 1$ (Eq. (2.38)), only "one half" of the propagator has such conformally massless behaviour. In next section we make clear the propagators in the $pz_< \ll 1$, $pz_> \ll 1$ and $pz_< \ll 1$, $pz_> \gg 1$ regimes have no equivalent in flat space.

The Flat Space Limit

Here we study the flat space limit in order to bring perspective to the asymptotic behaviours Eqs. (2.37)-(2.39). This limit is defined by the Weyl transform

$$\gamma_{MN} \to (kz)^2 \gamma_{MN} \tag{2.42}$$

which takes AdS space to flat space with a boundary at $z = 0$ [167].

Since the Weyl transform amounts to undoing the overall $1/(kz)^2$ factor of the metric Eq. (2.4), such transform also amounts to take the AdS curvature to zero, $k \to 0$ —keeping track of the k-dependence of the bulk mass. Such zero-curvature limit is best taken by first switching from Poincaré coordinates to the y-coordinates

$$z = \frac{e^{ky}}{k}\,, \quad \gamma_{MN} dX^M dX^N = e^{-2ky}\eta_{\mu\nu} dx^\mu dx^\nu - dy^2 \tag{2.43}$$

in which it is manifest that $k \to 0$ gives the $(d+1)$ Minkowski metric. The AdS boundary is at $y = -\infty$.

For any point which is not on the boundary, taking $k \to 0$ gives $z - z' \to y - y'$, $kz \to 1$, while sending z, z' to infinity. This last feature implies that, for any fixed p, there

is no $pz \ll 1$ regime in the flat space limit. Instead, any (p^μ, z) point of the position-momentum space ends up satisfying $pz \gg 1$. We refer to $pz \gg 1$ as the *conformally flat region*.

This feature illuminates how the propagator behaves under the flat space limit. For $k \to 0$ both endpoints have $pz \gg 1$, $pz' \gg 1$, such that the propagator is in the conformally flat regime of Eq. (2.37). Taking $kz \to 1$ and $\alpha \to 1/2$ in this expression reproduces the massless scalar propagator in $d+1$-dimensional flat space with a boundary.

Conversely, the flat space limit makes clear that the $pz \ll 1$, $pz' \ll 1$ and $pz_< \ll 1$, $pz_> \gg 1$ asymptotic regimes shown in Eqs. (2.39), (2.38) have *no* flat space equivalent. Instead these regimes vanish in the flat space limit. These non-conformally flat regimes include the cases of one or two endpoints on the AdS boundary and are thus key for AdS/CFT features. Our study of dressing will focus on the $pz_< \ll 1$, $pz_> \gg 1$ regime in Sec. 2.6.

2.4 Bubble and Dressing in the Conformal Spectral Representation

This section focuses on the self-energy and the dressed propagator in the conformal spectral representation. In this representation, the AdS/CFT correspondence [7] naturally arises [183].

The evaluation of the dressed propagator is the primary goal of this work as

[7] For AdS/CFT see [11–13], subsequent early works [14–18], and some yet unmentioned recent developments [168–182]. Some lecture notes and reviews are [19–22].

a whole. The advantage of the conformal spectral representation is that CFT objects naturally appear, which greatly simplifies the evaluation and allows us to use known CFT results. This approach allow us to obtain the dressed propagator written as a spectral integral. Though exact, this representation of the dressed propagator is not convenient for the purpose of obtaining a simple and intuitive idea of its behaviour in position-momentum space. This aspect will instead be tackled in Sec. 2.5 and Sec. 2.6 with the help of the momentum spectral and canonical representations.

From the dressed propagator in the conformal spectral representation, we can use a simple trick to obtain a form of the self-energy, Π, itself. We will use this form in the calculations of Sec. 2.5. The self-energy is a necessary component of our analysis in Sec. 2.6.

Some results of this section connect to earlier results from AdS/CFT works [93, 101]. The calculations we present here in momentum space offers various cross-checks with these works, and perhaps a different perspective.

2.4.1 Bubble Diagram

We consider a cubic interaction of the form [8]

$$S \supset \int dX^M \sqrt{|\gamma|} \lambda \Phi \Phi_1 \Phi_2 \,. \tag{2.44}$$

The coupling has dimension $[\lambda] = \frac{5-d}{2}$, we introduce the dimensionless coupling

$$\hat{\lambda}^2 = \lambda^2 k^{d-5} \,. \tag{2.45}$$

The external propagating field is chosen to be Φ. The Φ_1, Φ_2 fields form the self-

[8] The results can be trivially extended to the cubic self-interaction of a scalar field via the interaction $\frac{\lambda}{3!}\Phi^3$. A symmetry factor of 1/2 has then to be taken in the bubble amplitude.

energy bubble. In the conformal representation calculations it is convenient to use $\bar{\alpha}$ for the external field and no bar for the dummy variable α to be integrated over. The bulk masses for Φ, $\Phi_{1,2}$ are parametrized as

$$m_{\Phi}^2 = \left(\bar{\alpha}^2 - \frac{d^2}{4}\right) k^2 \,, \quad m_{\Phi_{1,2}}^2 = \left(\bar{\alpha}_{1,2}^2 - \frac{d^2}{4}\right) k^2 \,. \tag{2.46}$$

The respective free propagators are noted $G^{(0)}$ and $G_{1,2}^{(0)}$.

This cubic interaction gives rise to dressing by bubble self-energy diagrams as shown in Fig. 2.2 (left). The bubble amplitude is given by

$$i\Pi(p;u,v) = -\frac{\lambda^2}{(ku)^{d+1}(kv)^{d+1}} \int \frac{d^d q}{(2\pi)^d} G_1^{(0)}(q+p;u,v) G_2^{(0)}(q;v,u) \tag{2.47}$$

where we have included the metric factors coming from the vertices. This Π is the self-energy entering in the dressed equation of motion Eq. (2.9).

2.4.2 A Bit of AdS/CFT in Momentum Space

The elements of AdS and CFT needed for calculating the dressed propagator in the conformal spectral representation are collected in App. C. Here we give a brief description of these AdS/CFT ingredients together with an outline of the upcoming calculation.

In momentum space, the spectral function Ω_α can be decomposed as the product

$$\Omega_\alpha(z,z') \sim \mathcal{K}_\alpha^+(p,z)\mathcal{K}_\alpha^-(p,z') \tag{2.48}$$

where $\mathcal{K}_\alpha^\pm(p,z)$ are boundary-to-bulk propagators defined in App. C.5. Writing all the propagators in this form for a given term of the Born series gives the diagram in Fig. 2.2 (center), where each line represents a $\mathcal{K}$ propagator.

The z-coordinate of each internal vertex (blue points in Fig. 2.2) are integrated over in each term of the Born series. Each cubic vertex gives rise to convolutions of three $\mathcal{K}^{\pm}_{\alpha_i}(p_i, z)$ with distinct α_i and d-momentum p_i. Each of these triple-K integrals give rise to a CFT three-point correlator in d-dimensional Minkowski space, as given by

$$\int dz \sqrt{|\gamma|} \mathcal{K}^{\pm}_{\alpha}(p_1, z) \mathcal{K}^{\pm}_{\alpha}(p_2, z) \mathcal{K}^{\pm}_{\alpha}(p_3, z) \sim \langle\!\langle \mathcal{O}_1(p_1) \mathcal{O}_2(p_2) \mathcal{O}_3(p_3) \rangle\!\rangle \,. \tag{2.49}$$

This is AdS/CFT in action. The coefficient is given in Eq. (C.25). Only α and d-momentum integrals remain. This is pictured in Fig. 2.2 (right).

Each bulk bubble gives rise to two CFT three-point correlators connected together via the pairing described in App. C.3, forming a (non-amputated) CFT bubble. The evaluation of the CFT bubble in momentum space is given in App. C.4

$$\int \frac{d^d q}{(2\pi)^d} \langle\!\langle \mathcal{O}_a(p) \mathcal{O}_1(q) \mathcal{O}_2(-p-q) \rangle\!\rangle \langle\!\langle \widetilde{\mathcal{O}_1}(-q) \widetilde{\mathcal{O}}_2(p+q) \widetilde{\mathcal{O}}_b(-p) \rangle\!\rangle \sim \delta_{ab} \delta(\alpha - \alpha') + s.t. \tag{2.50}$$

where $\widetilde{\mathcal{O}}$ denotes the shadow transform of $\mathcal{O}$ (see App. C.3) and $s.t$ is short for shadow transform.

Finally, the $\delta(\alpha \pm \alpha')$ arising from each CFT bubble eliminates a $\int d\alpha$ integral from one of the $G^{(0)}$ connected to it. This implies that for any term of the Born series, a single $\int d\alpha$ integral ultimately remains. This allows the Born series to be summed.

In the next sections we proceed with the calculation of the dressed propagator per se.

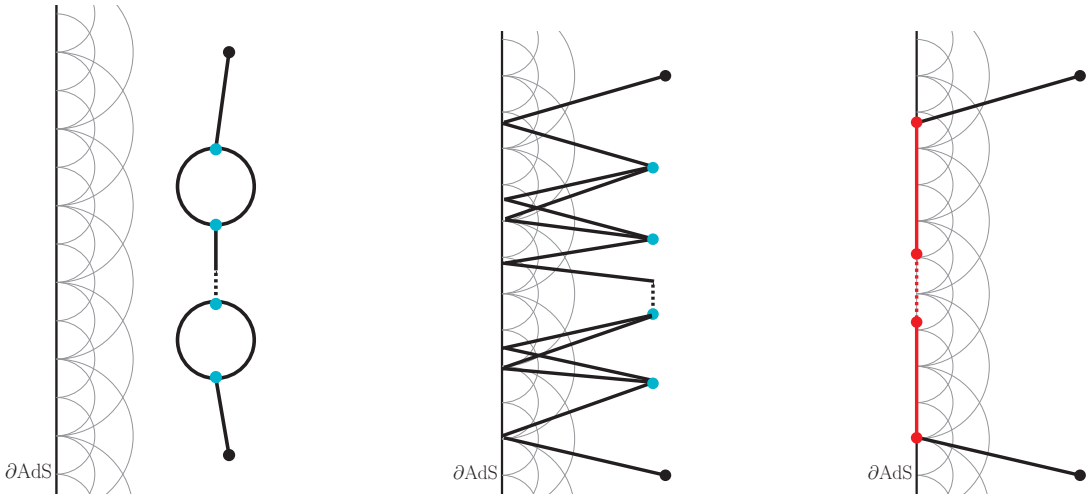

Figure 2.2: Left: A bulk line dressed by bubble self-energy diagrams. Center: Rewriting using the conformal spectral (*i.e.* split) representation. Right: Structure after integrating intermediate bulk points. Each solid red line represents a conformal bubble integral.

2.4.3 One Bubble Insertion

In this subsection, we work out the details of the $G^{(1)}$ term of the Born series $G = \sum_{n=0}^{\infty} G^{(n)}$ which is the term with one insertion, see Eq. (2.10). Computation of higher terms is similar, and the full series will be summed in next subsection.

The $G^{(1)}$ term of the series reads

$$\begin{aligned} G^{(1)}(z,z') &= G^{(0)} * i\Pi * G^{(0)}(z,z') \\ &= \int_{-i\infty}^{i\infty} d\alpha \int_{-i\infty}^{i\infty} d\alpha' \left(\frac{i}{k}\right)^2 P(\alpha,\bar{\alpha}) P(\alpha',\bar{\alpha})\, \Omega_{\alpha}^{(0)} * i\Pi * \Omega_{\alpha'}^{(0)}(z,z') \end{aligned} \tag{2.51}$$

with the measures

$$P(\alpha,\bar{\alpha}) = \frac{1}{\alpha^2 - \bar{\alpha}^2}\,, \quad P(\alpha',\bar{\alpha}) = \frac{1}{\alpha'^2 - \bar{\alpha}^2}\,. \tag{2.52}$$

We single out the convolution appearing in Eq. (2.51),

$$\Omega_{\alpha}^{(0)} * i\Pi * \Omega_{\alpha'}^{(0)}(z,z') = \int du \int dv\; \Omega_{\alpha}^{(0)}(z,u)\, i\Pi(u,v)\, \Omega_{\alpha'}^{(0)}(v,z') \tag{2.53}$$

and introduce the conformal spectral representation for the bubble and the external legs. We write all spectral functions in terms of the boundary-to-bulk propagators as shown in Eq. (C.24), giving

$$\int du \int dv\ \Omega^{(0)}_{\alpha}(z,u)\, i\Pi(u,v)\, \Omega^{(0)}_{\alpha'}(v,z') \tag{2.54}$$
$$= \left(\frac{1}{4\pi}\right)^4 \left(\frac{\lambda}{k}\right)^2 \int \frac{du}{(ku)^{d+1}} \int \frac{dv}{(kv)^{d+1}} \int_{-i\infty}^{i\infty} d\alpha_1 \int_{-i\infty}^{i\infty} d\alpha_2\, P(\alpha_1,\bar{\alpha}_1) P(\alpha_2,\bar{\alpha}_2) \times$$
$$\int \frac{d^d q}{(2\pi)^d} \mathcal{K}^+_{\alpha}(p;z) \mathcal{K}^-_{\alpha}(p;u) \mathcal{K}^+_{\alpha_1}(q+p;u) \mathcal{K}^-_{\alpha_1}(q+p;v) \mathcal{K}^+_{\alpha_2}(q;v) \mathcal{K}^-_{\alpha_2}(q;u) \mathcal{K}^+_{\alpha'}(p;v) \mathcal{K}^-_{\alpha'}(p;z').$$

The diagram involves products of boundary-to-bulk propagators—it corresponds to Fig. 2.2 (center) with a single bubble.

In $G^{(1)}$ there are two triple-K integrals, one corresponding to each vertex. Using results from App. C.5, we have

$$\int \frac{du}{(ku)^{d+1}} \mathcal{K}^-_{\alpha}(p;u) \mathcal{K}^+_{\alpha_1}(q+p;u) \mathcal{K}^-_{\alpha_2}(q;u) = c_{\alpha,-\alpha_1,\alpha_2} k^{d/2-1} \langle\!\langle \widetilde{\mathcal{O}}(p) \mathcal{O}_1(-p-q) \widetilde{\mathcal{O}}_2(q) \rangle\!\rangle \tag{2.55}$$

$$\int \frac{dv}{(kv)^{d+1}} \mathcal{K}^+_{\alpha'}(p;v) \mathcal{K}^-_{\alpha_1}(q+p;v) \mathcal{K}^+_{\alpha_2}(q;v) = c_{-\alpha',\alpha_1,-\alpha_2} k^{d/2-1} \langle\!\langle \mathcal{O}(-p) \widetilde{\mathcal{O}}_1(p+q) \mathcal{O}_2(-q) \rangle\!\rangle\ . \tag{2.56}$$

We see that a CFT bubble integral arises in the last line of Eq. (2.54) when performing the intermediate bulk point integrations. This is shown in Fig. 2.2 (right). The evaluation of the CFT bubble in momentum space is given in Eq. (C.20). Both terms of the right-hand side of Eq. (C.20) give identical contribution by shadow symmetry ($\alpha \leftrightarrow -\alpha$).

Putting the pieces together, we have

$$\Omega_{\alpha}^{(0)} * i\Pi * \Omega_{\alpha'}^{(0)}(z,z') = 2\delta(\alpha-\alpha')\frac{\lambda^2 k^{d-4}}{(4\pi)^4}\, 2\pi\mathcal{B}_{\mathcal{O}}\, \mathcal{K}_{\alpha}^{+}(pz)\mathcal{K}_{\alpha'}^{-}(pz) \tag{2.57}$$
$$\times \int d\alpha_1 d\alpha_2 P(\alpha_1,\bar{\alpha}_1)P(\alpha_2,\bar{\alpha}_2)c_{\alpha,-\alpha_1,\alpha_2}c_{-\alpha',\alpha_1,-\alpha_2},$$

where $\mathcal{B}_{\mathcal{O}}$ is given in Eq. (C.19). In Eq. (2.57) we are left with two boundary-to-bulk propagators associated with the two endpoints of $G^{(1)}$. Since $\alpha = \alpha'$ from the Dirac delta, these two boundary-to-bulk propagators can be combined into a spectral function using Eq. (C.24). We thus obtain

$$\begin{aligned}\Omega_{\alpha}^{(0)} * i\Pi * \Omega_{\alpha'}^{(0)}(z,z') &= \delta(\alpha-\alpha')\lambda^2 k^{d-4}\,\frac{1}{4\pi}\mathcal{K}_{\alpha}^{+}(pz)\mathcal{K}_{\alpha'}^{-}(pz)\,\mathcal{B}(\alpha) \\ &= \delta(\alpha-\alpha')\lambda^2 k^{d-4}\, i\mathcal{B}(\alpha)\,\Omega_{\alpha}^{(0)}(z,z'),\end{aligned} \tag{2.58}$$

where we introduced the dimensionless bubble function

$$\begin{aligned}\mathcal{B}(\alpha) &= -2\frac{1}{(4\pi)^3}\,2\pi\mathcal{B}_{\mathcal{O}} \times \int d\alpha_1 d\alpha_2\, P(\alpha_1,\bar{\alpha}_1)P(\alpha_2,\bar{\alpha}_2)\, c_{\alpha,-\alpha_1,\alpha_2}c_{-\alpha,\alpha_1,-\alpha_2} \\ &= -\frac{1}{2^5\pi^{4+d/2}}\frac{1}{\Gamma(d/2)\Gamma(d/2-\alpha)\Gamma(d/2+\alpha)}\int d\alpha_1 d\alpha_2 \frac{\alpha_1\alpha_2\sin(\pi\alpha_1)\sin(\pi\alpha_2)}{(\alpha_1^2-\bar{\alpha}_1^2)(\alpha_2^2-\bar{\alpha}_2^2)} \\ &\times \Gamma\left(\tfrac{\alpha+\alpha_1+\alpha_2+d/2}{2}\right)\Gamma\left(\tfrac{\alpha-\alpha_1+\alpha_2+d/2}{2}\right)\Gamma\left(\tfrac{\alpha+\alpha_1-\alpha_2+d/2}{2}\right)\Gamma\left(\tfrac{-\alpha+\alpha_1+\alpha_2+d/2}{2}\right) \\ &\times \Gamma\left(\tfrac{-\alpha-\alpha_1-\alpha_2+d/2}{2}\right)\Gamma\left(\tfrac{-\alpha+\alpha_1-\alpha_2+d/2}{2}\right)\Gamma\left(\tfrac{-\alpha-\alpha_1+\alpha_2+d/2}{2}\right)\Gamma\left(\tfrac{\alpha-\alpha_1-\alpha_2+d/2}{2}\right)\end{aligned} \tag{2.59}$$

This bubble function is proportional to the one obtained in [93]. An additional cross-check is obtained further below.

In Eq. (2.58) we have reduced the convolutions in $G^{(1)}$ into a nontrivial algebraic

factor. We complete the evaluation by putting Eq. (2.58) back into Eq. (2.51), which gives

$$
\begin{aligned}
G^{(1)}(z,z') &= G^{(0)} * i\Pi * G^{(0)}(z,z') \qquad (2.60)\\
&= \int_{-i\infty}^{i\infty} d\alpha \int_{-i\infty}^{i\infty} d\alpha' \left(\frac{i}{k}\right)^2 P(\alpha,\bar{\alpha})P(\alpha',\bar{\alpha})\ \delta(\alpha-\alpha')\lambda^2 k^{d-4} i\mathcal{B}(\alpha)\Omega_{\alpha}^{(0)}(z,z')\\
&= \frac{i}{k}\int_{-i\infty}^{i\infty} d\alpha\, P^2(\alpha,\bar{\alpha})\ \left[-\hat{\lambda}^2\mathcal{B}(\alpha)\right]\Omega_{\alpha}^{(0)}(z,z').
\end{aligned}
$$

2.4.4 The Spectral Born Series

The above steps can be reproduced for an arbitrary number of bubble insertions. One finds the n-bubble contribution to be

$$
G^{(n)}(z,z') = \frac{i}{k}\int_{-i\infty}^{i\infty} d\alpha\, P(\alpha,\bar{\alpha})\ \left[-\hat{\lambda}^2 P(\alpha,\bar{\alpha})\mathcal{B}(\alpha)\right]^n \Omega_{\alpha}^{(0)}(z,z'). \qquad (2.61)
$$

We see that a geometric series appears and hence the full Born sum can be performed. This is because spectral transforms turn convolutions into products, as discussed in [101]. Here we have recovered this feature via direct calculation. There is no analog to this property in the momentum spectral representation, because unlike in the conformal representation the bubble integral does not conserve the spectral variable $\hat{p}$.

Summing the Born series, we find that the complete dressed propagator in the conformal spectral representation is

$$
\sum_{n=0}^{\infty} G^{(n)}(z,z') = G(z,z') = \left(\frac{i}{k}\right)\int_{-i\infty}^{i\infty} d\alpha\, \frac{1}{P(\alpha,\bar{\alpha})^{-1}+\hat{\lambda}^2\mathcal{B}(\alpha)}\Omega_{\alpha}^{(0)}(z,z'). \qquad (2.62)
$$

Thus it turns out that in the conformal spectral representation the dressing amounts to a deformation of the $P(\alpha,\bar{\alpha})$ measure and $\hat{\lambda}^2\mathcal{B}(\alpha)$ effectively has the role of a "spectral self-energy". In particular we can see that the $\alpha = \pm\bar{\alpha}$ poles of the free spectral function $P(\alpha,\bar{\alpha})$ get shifted by the $\hat{\lambda}^2\mathcal{B}(\alpha)$ term.

2.4.5 Aside: Anomalous Dimension from the Dressed Propagator

For sufficiently small coupling $\hat{\lambda} \ll 1$ we can approximate $\mathcal{B}(\alpha) \approx \mathcal{B}(\bar{\alpha})$ near the $\alpha = \pm\bar{\alpha}$ poles. Other poles exist whenever $\hat{\lambda} \neq 0$, but the corresponding residues are expected to be small for $\hat{\lambda} \ll 1$ and are not our focus.[9] The $\mathcal{B}(\bar{\alpha})$ constant can be seen as a correction to the bulk mass,

$$m_\Phi^2|_{\text{dressed}} = \left(\bar{\alpha}^2 - \frac{d^2}{4} - \mathcal{B}(\bar{\alpha})\right) k^2 \,. \tag{2.63}$$

In the dual CFT, the correction amounts to an anomalous dimension γ shifting the conformal dimensions $\Delta_\pm$. We define γ such that

$$\Delta_\pm|_{\text{dressed}} = \Delta_\pm \pm \gamma = \frac{d}{2} \pm \bar{\alpha} \pm \gamma \,, \tag{2.64}$$

with

$$\gamma = -\frac{\mathcal{B}(\bar{\alpha})}{2\bar{\alpha}} \,. \tag{2.65}$$

The fact that the sign of the correction flips between Δ_+ and Δ_- is enforced from the AdS side since it is a correction on $\bar{\alpha}$ and since $\Delta_\pm = \frac{d}{2} \pm \bar{\alpha}$. The sign flip is also clear from the CFT side in order for shadow symmetry to be respected.

We find that the imaginary part of $\mathcal{B}(\bar{\alpha})$ vanishes. To note this, close the contours in Eq. (2.59) and use the residue theorem. The residues are real and hence by counting

[9] From direct evaluation [93, 101], $\mathcal{B}(\alpha)$ features an infinite set of simple poles. $\mathcal{B}(\alpha)$ goes to $\pm\infty$ when approaching each pole from either side. Hence for any $\hat{\lambda} \neq 0$, $1/(P(\alpha,\bar{\alpha})^{-1} + \hat{\lambda}^2\mathcal{B}(\alpha))$ has an infinite set of poles contributing to Eq. (2.62). For $\hat{\lambda} \ll 1$ these extra residues are expected to vanish with $\hat{\lambda}$. Otherwise, there would be a discontinuity in $G(z,z')$ (and thus in the spectrum of operators obtained from related Witten diagrams) when turning on $\hat{\lambda}$. See [101] for a related study of $\mathcal{B}(\bar{\alpha})$ in the $O(N)$ model.

factors of i, we determine that $\mathcal{B}(\bar{\alpha})$ is purely real. This is consistent with the conclusions in [93]. Thus the leading correction to $\bar{\alpha}$ is purely real.

We find that our result Eq. (2.65) precisely matches the anomalous dimension found in [93] (Eq. (2.37) in that reference). In that reference the anomalous dimension was evaluated by looking at the $\log(\Delta X)$ term in a on-shell bubble amplitude in position space. Here we have confirmed their result with a different approach. From Eq. (2.62) other higher order effects such as wave-function renormalization could be studied.

2.4.6 The Self-Energy as a Spectral Transform

To obtain a useful form of Π in the conformal spectral representation, we apply the EOM operator $\mathcal{D}$ on both sides of $G^{(1)}(z,z') = G^{(0)} * i\Pi * G^{(0)}(z,z')$. Using the free EOM Eq. (2.14), we obtain

$$\mathcal{D}_z\mathcal{D}_{z'}G^{(1)}(z,z') = -i\frac{1}{\sqrt{|\gamma|}_z\sqrt{|\gamma|}_{z'}}\Pi(z,z') = -i(kz)^{d+1}(kz')^{d+1}\Pi(z,z'). \tag{2.66}$$

$G^{(1)}$ in the conformal spectral representation has been computed in Eq. (2.60). Using it in Eq. (2.66) gives

$$\begin{aligned}\mathcal{D}_z\mathcal{D}_{z'}G^{(1)}(z,z') &= \frac{i}{k}\int_{-i\infty}^{i\infty} d\alpha\, P^2(\alpha,\bar{\alpha})\, \left[-\hat{\lambda}^2\mathcal{B}(\alpha)\right] \mathcal{D}_z\mathcal{D}_{z'}\Omega_\alpha^{(0)}(z,z') \\ &= -ik^3\int_{-i\infty}^{i\infty} d\alpha\, \hat{\lambda}^2\mathcal{B}(\alpha)\Omega_\alpha^{(0)}(z,z')\,.\end{aligned} \tag{2.67}$$

In doing so we have thus obtained

$$i(kz)^{d+1}(kz')^{d+1}\Pi(z,z') = i\hat{\lambda}^2k^3\int_{-i\infty}^{i\infty} d\alpha\,\mathcal{B}(\alpha)\Omega_\alpha^{(0)}(z,z')\,. \tag{2.68}$$

This establishes that $\hat{\lambda}^2k^3\mathcal{B}(\alpha)$ is the spectral transform of $(k^2zz')^{d+1}\Pi$. This is the form of the self-energy that we will use in the conformal spectral calculation of Sec. 2.5.2.

2.5 Representations and Properties of ImΠ

In this section we evaluate a self-energy bubble diagram $i\Pi$ in the three different representation shown in Sec. 2.3. Our focus is on the imaginary part ImΠ. The equivalence of the expressions in various representations is nontrivial, hence we demonstrate it explicitly in Sec. 2.5.4. The various representations render manifest different properties of the self-energy. These properties are discussed in Sec. 2.5.5.

Throughout this section the interaction considered is a cubic coupling between three inequivalent real scalar fields

$$S \supset \int dX^M \sqrt{|\gamma|} \lambda \Phi \Phi_1 \Phi_2 \,. \tag{2.69}$$

We introduce $\alpha_{1,2}$ to parameterize the bulk masses of the $\Phi_{1,2}$ fields. When working in the conformal spectral representation, we change our convention $\alpha_{1,2} \to \bar{\alpha}_{1,2}$ as done in Sec. 2.4. Our results are trivially extended to a cubic self-interaction via the operator $\frac{\lambda}{3!}\Phi^3$ and taking into account a $\frac{1}{2}$ symmetry factor in the loop.

In our calculations, we focus on p^2 close to the real line. For $p^2 \in \mathbb{R}_-$, we are permitted to stay exactly on the real line. The propagator has a branch cut for timelike momentum however, so taking $p^2 \in \mathbb{R}_+$ is not well defined (see Sec. 2.3.2). Instead, one must give p^2 a small imaginary part $p^2 \to p^2 + i\epsilon$ to resolve the branch ambiguity. We allow for either $\epsilon > 0$ or $\epsilon < 0$ in our calculations. We show in Sec. 2.5.5 that the sign of ϵ controls the sign of ImΠ.

The self-energy of Φ is given by

$$\Pi_p(z, z') = \frac{i\lambda^2}{(k^2 z z')^{d+1}} \int \frac{d^d q}{(2\pi)^d} G_1^{(0)}(p+q, z, z') G_2^{(0)}(q, z', z). \tag{2.70}$$

Eq. (2.70) serves as the starting point for the following calculations.

2.5.1 ImΠ in the Canonical Representation

We substitute the canonical propagator Eq. (2.20) into Eq. (2.70) and use the infinite series-representations of the Bessel functions,

$$I_\alpha(\sqrt{-p^2}z) = \sum_{m=0}^{\infty} \frac{1}{m!\Gamma(m+\alpha+1)} \left(\frac{\sqrt{-p^2}z}{2}\right)^{2m+\alpha} \tag{2.71}$$

$$K_\alpha(\sqrt{-p^2}z) = \frac{\pi}{2\sin(\pi\alpha)} \sum_{m=0} \frac{1}{m!} \left(\frac{\sqrt{-p^2}z}{2}\right)^{2m} \times \left[\frac{1}{\Gamma(m-\alpha+1)} \left(\frac{\sqrt{-p^2}z}{2}\right)^{-\alpha} - \frac{1}{\Gamma(m+\alpha+1)} \left(\frac{\sqrt{-p^2}z}{2}\right)^{\alpha}\right]. \tag{2.72}$$

In this representation, the self-energy is

$$\Pi_p(z,z') = \frac{-i\pi^2\lambda^2}{4k^4 z z' \sin(\pi\alpha_1)\sin(\pi\alpha_2)} \int \frac{d^dq}{(2\pi)^d} \sum_{s,t=0}^{\infty} \sum_{n,m=0}^{\infty} \frac{(-1)^{n+m+s+t}}{n!m!s!t!} \times \frac{1}{\Gamma(n+\alpha_2+1)} \frac{1}{\Gamma(s+\alpha_1+1)} \left(\frac{qz_<}{2}\right)^{2s+\alpha_1} \left(\frac{(p+q)z_<}{2}\right)^{2n+\alpha_2} \left(\frac{qz_>}{2}\right)^{2t} \left(\frac{(p+q)z_>}{2}\right)^{2m} \times \left[\frac{\left(\frac{qz_>}{2}\right)^{-\alpha_1}}{\Gamma(t-\alpha_1+1)} - \frac{\left(\frac{qz_>}{2}\right)^{\alpha_1} e^{-i\alpha_1\pi\mathrm{Sign}(\epsilon)}}{\Gamma(t+\alpha_1+1)}\right] \left[\frac{\left(\frac{(p+q)z_>}{2}\right)^{-\alpha_2}}{\Gamma(m-\alpha_2+1)} - \frac{\left(\frac{(p+q)z_>}{2}\right)^{\alpha_2} e^{-i\alpha_2\pi\mathrm{Sign}(\epsilon)}}{\Gamma(m+\alpha_2+1)}\right]. \tag{2.73}$$

$\Pi_p(z,z')$ contains many terms, each of which go like

$$\Pi_p(z,z') \sim \int \frac{d^dq}{(2\pi)^d} \left((p+q)^2\right)^a \left(q^2\right)^b \tag{2.74}$$

for some a, b. To each term, we apply the identity

$$\left((p+q)^2\right)^a \left(q^2\right)^b = \int_0^1 dx \frac{\left(x\,(p+q)^2 + (1-x)q^2\right)^{a+b}}{x^{a+1}(1-x)^{b+1}} \frac{\Gamma(-a-b)}{\Gamma(-a)\Gamma(-b)}. \tag{2.75}$$

The integral on the right-hand side converges for $\mathrm{Re}(a), \mathrm{Re}(b) < 0$. However, provided the final result of the calculation is analytic in a, b, the result can be extended by analytical

continuation such that restrictions on a, b are ultimately lifted. [10]

Shifting the loop momentum $l \equiv q + px$, we obtain

$$\Pi_p(z, z') \sim \int_0^1 dx \int \frac{d^d l}{(2\pi)^d} \frac{(l^2 + x(1-x)p^2)^{a+b}}{x^{a+1}(1-x)^{b+1}} \frac{\Gamma(-a-b)}{\Gamma(-a)\Gamma(-b)}. \tag{2.76}$$

We evaluate the loop integral with

$$\int \frac{d^d l}{(2\pi)^d} \left(l^2 + \Delta\right)^c = \frac{i(-i\text{Sign}(\epsilon))^d}{(4\pi)^{\frac{d}{2}}} \frac{\Gamma\left(-c - \frac{d}{2}\right)}{\Gamma(-c)} \Delta^{c+\frac{d}{2}}. \tag{2.77}$$

Again, the loop integrals are performed in the domain of (c, d) where the integral on the left-hand-side converges. The functions on the right-hand-side are analytic in c anywhere away from c integer, hence the final result will be ultimately analytically continued in c. The particular points where a divergence appear require renormalization. However such divergences are in the real part of Π and are irrelevant for the study of ImΠ.

Putting Eqs. (2.75) and (2.77) together yields

$$\Pi_p(z, z') \sim \frac{i(-i\text{Sign}(\epsilon))^d}{(4\pi)^{\frac{d}{2}}} \left(p^2\right)^{a+b+\frac{d}{2}} \frac{\Gamma\left(-a-b-\frac{d}{2}\right)}{\Gamma(-a)\Gamma(-b)} \int_0^1 dx x^{b+\frac{d}{2}-1}(1-x)^{a+\frac{d}{2}-1}. \tag{2.78}$$

We identify the remaining integral as being the integral representation of the Beta function.

[10] Although the details of analytic continuation are usually left implicit, it is interesting to know how it concretely happens in the intermediate steps. The Feynman parametrization Eq. (2.75) follows from the integral representation of Gamma functions valid for $\text{Re}(a), \text{Re}(b) < 0$, which involves integrals along the real line. The analytical continuation of the Feynman parametrization relies on analytically continued Gamma functions, whose integral representation involves Hankel contours in the complex plane. It turns out that the x parameter must follow a *Pochhammer* contour appropriately wrapping the 0 and 1 points in the complex plane. The Pochhammer contour in x gives rise to the analytically continued integral representation of the hypergeometric function, lifting the $\text{Re}(a), \text{Re}(b) < 0$ restriction in Eq. (2.75) and ultimately giving rise to the analytically continued Beta function in *e.g.* Eq. (2.78).

Evaluating the integral, we obtain [11]

$$\Pi_p(z,z') \sim \frac{i(-i\mathrm{Sign}(\epsilon))^d}{(4\pi)^{d/2}} \left(p^2\right)^{a+b+d/2} \frac{\Gamma(-a-b-d/2)}{\Gamma(-a)\Gamma(-b)} \frac{\Gamma(a+d/2)\Gamma(b+d/2)}{\Gamma(a+b+d)}. \tag{2.79}$$

There are four terms in Eq. (2.73) corresponding to the four sign pairings of α_1, α_2 in the exponents. All but the $z_>^{\alpha_1+\alpha_2}$ term have either $a \in \mathbb{N}$ or $b \in \mathbb{N}$ or both. These terms vanish trivially on account of the $\Gamma(-a)\Gamma(-b)$ function in the denominator of Eq. (2.79). The disappearance of the $z_>^{-\alpha_1-\alpha_2}$ term can also be shown by taking the imaginary part of Π. In particular for even d when $\Gamma(-a-b-d/2)$ diverges, we find that the $z_>^{-\alpha_1-\alpha_2}$ term is purely real.

Making everything explicit again and taking the imaginary part, we have

$$\begin{aligned}
&\mathrm{Im}\Pi_p(z,z') = \qquad\qquad (2.80)\\
&\mathrm{Im}\Bigg[\frac{\pi^2\lambda^2 p^d e^{-i\pi(\alpha_1+\alpha_2+d/2)\mathrm{Sign}(\epsilon)}}{4k^4 zz' \sin(\pi\alpha_1)\sin(\pi\alpha_2)(4\pi)^{d/2}} \sum_{s,t=0}^{\infty}\sum_{n,m=0}^{\infty} \left(\frac{pz}{2}\right)^{2n+2s+\alpha_1+\alpha_2} \left(\frac{pz'}{2}\right)^{2m+2t+\alpha_1+\alpha_2} \times \\
&\frac{(-1)^s}{s!\Gamma(s+\alpha_1+1)} \frac{(-1)^t}{t!\Gamma(t+\alpha_1+1)} \frac{(-1)^n}{n!\Gamma(n+\alpha_2+1)} \frac{(-1)^m}{m!\Gamma(m+\alpha_2+1)} \times \\
&\frac{\Gamma(-n-m-s-t-\alpha_1-\alpha_2-d/2)}{\Gamma(-n-m-\alpha_2)\Gamma(-s-t-\alpha_1)} \frac{\Gamma(s+t+\alpha_1+d/2)\Gamma(n+m+\alpha_2+d/2)}{\Gamma(s+t+n+m+d+\alpha_1+\alpha_2)}\Bigg],
\end{aligned}$$

where we removed the $<,>$ subscripts because the expression is symmetric upon relabeling. We regroup the complex exponential with the factors of p in Eq. (2.80) to make the $\sqrt{-p^2}$ factor appear explicitly. This involves reabsorbing the $i\epsilon$ into p^2, where it remains implicitly,

[11] S.F. thanks M. Quiros for providing insight on this loop integral calculation in an early unpublished work [184].

yielding

$$\mathrm{Im}\Pi_p(z,z') = \sum_{n,m,s,t=0}^{\infty} \frac{\lambda^2\pi^2}{4\pi^{d/2}k^4\,(zz')^{1+d/2}\sin(\pi\alpha_1)\sin(\pi\alpha_2)}\times \tag{2.81}$$
$$\frac{(-1)^s}{s!\Gamma(s+\alpha_1+1)}\frac{(-1)^t}{t!\Gamma(t+\alpha_1+1)}\frac{(-1)^n}{n!\Gamma(n+\alpha_2+1)}\frac{(-1)^m}{m!\Gamma(m+\alpha_2+1)}\times$$
$$\frac{\Gamma(-n-m-s-t-\alpha_1-\alpha_2-d/2)}{\Gamma(-n-m-\alpha_2)\Gamma(-s-t-\alpha_1)}\frac{\Gamma(s+t+\alpha_1+d/2)\Gamma(n+m+\alpha_2+d/2)}{\Gamma(s+t+n+m+d+\alpha_1+\alpha_2)}\times$$
$$\mathrm{Im}\left[\left(\frac{\sqrt{-p^2}z}{2}\right)^{2n+2s+\alpha_1+\alpha_2+d/2}\left(\frac{\sqrt{-p^2}z'}{2}\right)^{2m+2t+\alpha_1+\alpha_2+d/2}\right].$$

In this form, $\mathrm{Im}\Pi_p(z,z')$ explicitly vanishes for spacelike momentum. Using Euler's reflection formula

$$\Gamma(x)\Gamma(1-x) = \frac{\pi}{\sin(\pi x)} \quad \text{for} \quad x \notin \mathbb{Z}, \tag{2.82}$$

and taking the imaginary part, Eq. (2.81) can be written as

$$\mathrm{Im}\Pi_p(z,z') = \tag{2.83}$$
$$\frac{\mathrm{Sign}(\epsilon)\pi\lambda^2p^d}{4k^4zz'(4\pi)^{d/2}}\sum_{n,m,s,t=0}^{\infty}\left(\frac{pz}{2}\right)^{2n+2s+\alpha_1+\alpha_2}\left(\frac{pz'}{2}\right)^{2m+2t+\alpha_1+\alpha_2}\times$$
$$\frac{(-1)^s}{s!\Gamma(s+\alpha_1+1)}\frac{(-1)^t}{t!\Gamma(t+\alpha_1+1)}\frac{(-1)^n}{n!\Gamma(n+\alpha_2+1)}\frac{(-1)^m}{m!\Gamma(m+\alpha_2+1)}\times$$
$$\frac{\Gamma(n+m+\alpha_2+1)\Gamma(s+t+\alpha_1+1)}{\Gamma(n+m+s+t+\alpha_1+\alpha_2+d/2+1)}\frac{\Gamma(s+t+\alpha_1+d/2)\Gamma(n+m+\alpha_2+d/2)}{\Gamma(s+t+n+m+d+\alpha_1+\alpha_2)}.$$

Eq. (2.83) represents our final result for $\mathrm{Im}\Pi_p(z,z')$ in the canonical representation.

2.5.2 $\mathrm{Im}\Pi$ in the Conformal Spectral Representation

Some preliminary work was done in Sec. 2.4 to calculate $\mathrm{Im}\Pi$ in the conformal spectral representation. Here we start from the identity Eq. (2.68), repeated here:

$$\mathrm{Im}(k^2zz')^{d+1}\Pi(z,z') = \mathrm{Im}\left[\hat{\lambda}^2k^3\int_{-i\infty}^{i\infty}d\alpha\,\mathcal{B}(\alpha)\Omega_\alpha^{(0)}(z,z')\right]. \tag{2.84}$$

In this subsection only, we follow the convention of Sec. 2.4 and use $\alpha, \alpha_1, \alpha_2$ to denote integration variables. We use $\bar{\alpha}_1, \bar{\alpha}_2$ for the bulk mass parameters, Eq. (2.5). We expand the Bessel functions in a series using Eq. (2.72) and use the $\alpha \leftrightarrow -\alpha$ shadow symmetry of the integrand to write the four terms in $\Omega_\alpha^{(0)}(z, z')$ as two. We have

$$\mathrm{Im}\Pi(z, z') = \tag{2.85}$$
$$\mathrm{Im}\left[\frac{i\hat{\lambda}^2 k^3}{(k^2 z z')^{d/2+1}} \int_{-i\infty}^{i\infty} d\alpha\, \mathcal{B}(\alpha) \frac{\alpha}{2\sin(\pi\alpha)} \sum_{m,n=0}^{\infty} \frac{1}{m!n!} \left(\frac{\sqrt{-p^2}z'}{2}\right)^{2n} \left(\frac{\sqrt{-p^2}z}{2}\right)^{2m} \times \right.$$
$$\left. \frac{1}{\Gamma(n-\alpha+1)} \left(\frac{\sqrt{-p^2}z'}{2}\right)^{-\alpha} \left(\frac{1}{\Gamma(m-\alpha+1)} \left(\frac{\sqrt{-p^2}z}{2}\right)^{-\alpha} - \frac{1}{\Gamma(m+\alpha+1)} \left(\frac{\sqrt{-p^2}z}{2}\right)^{\alpha}\right)\right].$$

The imaginary part of the above expression will ultimately come from $\mathrm{Im}\left(-p^2\right)^a$ for some a. That is, all other factors of i from applications of the residue theorem conspire to produce a real prefactor. In the second term of Eq. (2.85) above, the two powers of α cancel, and hence a is necessarily an integer. Thus we find that this second term vanishes upon taking the imaginary part, as it is purely real. The poles from the $1/\sin(\pi\alpha)$ factor sit at integer α, which again yields integer a upon applying the residue theorem. Hence these residues do not contribute to $\mathrm{Im}\Pi(z, z')$.

Following this preliminary result, only the first term in the bracket in Eq. (2.85) contributes to the imaginary part, and only the poles within the bubble function $\mathcal{B}(\alpha)$ are relevant. We close the α-contour towards the negative reals, where the integrand vanishes exponentially on account of the Gamma functions. This selects an infinite number of residues from the four relevant Gamma functions within the bubble function, Eq. (2.59). The sets of poles that we enclose are located at

$$\alpha = \pm\alpha_1 \pm \alpha_2 - \frac{d}{2} - 2l \qquad \text{for} \qquad l \in \mathbb{N}\,. \tag{2.86}$$

The corresponding four sets of residues all take the same form, but with relative sign flips ($\alpha_1 \leftrightarrow -\alpha_1$ and/or $\alpha_2 \leftrightarrow -\alpha_2$). We have

$$\mathrm{Im}\Pi(z,z') = \mathrm{Im} \sum_{m,n,l=0}^{\infty} \int d\alpha_1 d\alpha_2 \left(\mathcal{I}_{\alpha_1,\alpha_2} + \mathcal{I}_{-\alpha_1,\alpha_2} + \mathcal{I}_{\alpha_1,-\alpha_2} + \mathcal{I}_{-\alpha_1,-\alpha_2}\right) \tag{2.87}$$

for

$$\begin{aligned}
&\mathcal{I}_{\alpha_1,\alpha_2} \equiv \qquad\qquad (2.88)\\
&\frac{\hat{\lambda}^2 k^3}{(k^2 z z')^{d/2+1}} \left(\frac{\sqrt{-p^2}z}{2}\right)^{2m+2l+\alpha_1+\alpha_2+d/2} \left(\frac{\sqrt{-p^2}z'}{2}\right)^{2n+2l+\alpha_1+\alpha_2+d/2} \times\\
&\frac{1}{2^4\pi^{1+d/2}} \frac{1}{l!m!n!} \frac{(2l+\alpha_1+\alpha_2+d/2)\csc(\pi(\alpha_1+\alpha_2+d/2))}{\Gamma(d/2)\Gamma(2l+\alpha_1+\alpha_2+d)\Gamma(l+\alpha_1+\alpha_2+1)} \frac{\alpha_1\alpha_2}{(\alpha_1^2-\bar{\alpha}_1^2)(\alpha_2^2-\bar{\alpha}_2^2)} \times\\
&\frac{\Gamma\left(l+d/2\right)\Gamma\left(l+\alpha_1+d/2\right)\Gamma\left(l+\alpha_2+d/2\right)\Gamma\left(2l+\alpha_1+\alpha_2+1\right)\Gamma\left(l+\alpha_1+\alpha_2+d/2\right)}{\Gamma(n+2l+\alpha_1+\alpha_2+d/2+1)\Gamma(m+2l+\alpha_1+\alpha_2+d/2+1)\Gamma\left(l+\alpha_1+1\right)\Gamma\left(l+\alpha_2+1\right)},
\end{aligned}$$

where we have simplified the expression by using the reflection formula Eq. (2.82). All four terms are equivalent—as can be seen by $\alpha_j \to -\alpha_j$ relabelings—and hence the integrand amounts to $4\mathcal{I}_{\alpha_1,\alpha_2}$.

We then perform the α_1 and α_2 integrals. We close the integrals towards the positive reals, where the integrand vanishes exponentially on account of the Gamma functions. Within the contour, there are poles at $\alpha_i = \bar{\alpha}_i$ from the $P\left(\bar{\alpha}_i, \alpha_i\right)$ measures (see Eq. (2.52)) and poles at $\alpha_1+\alpha_2+d/2 \in \mathbb{Z}_+$ from $\csc(\pi(\alpha_1+\alpha_2+d/2))$. The residues from the cosecant only give a contribution to $\mathrm{Re}\Pi(z,z')$ because they give rise to even powers of $\sqrt{-p^2}$. The residues from the $P\left(\bar{\alpha}_i, \alpha_i\right)$ measures yield a contribution to $\mathrm{Im}\Pi(z,z')$.

We obtain

$$\begin{aligned}\mathrm{Im}\Pi(z,z') = -\sum_{m,n,l=0}^{\infty} \frac{\hat{\lambda}^2 k^3}{\left(k^2 z z'\right)^{d/2+1}} \frac{1}{2^2 \pi^{d/2-1}} \frac{1}{l!m!n!} \times \\ \frac{\Gamma\left(l+\bar{\alpha}_1+\bar{\alpha}_2+d/2\right)\left(2l+\bar{\alpha}_1+\bar{\alpha}_2+d/2\right)\csc(\pi(\bar{\alpha}_1+\bar{\alpha}_2+d/2))}{\Gamma(d/2)\Gamma(n+2l+\bar{\alpha}_1+\alpha_{2,0}+d/2+1)\Gamma(m+2l+\bar{\alpha}_1+\bar{\alpha}_2+d/2+1)} \times \\ \frac{\Gamma\left(l+d/2\right)\Gamma\left(l+\bar{\alpha}_1+d/2\right)\Gamma\left(l+\bar{\alpha}_2+d/2\right)\Gamma\left(2l+\bar{\alpha}_1+\bar{\alpha}_2+1\right)}{\Gamma(2l+\bar{\alpha}_1+\bar{\alpha}_2+d)\Gamma(l+\bar{\alpha}_1+\bar{\alpha}_2+1)\Gamma\left(l+\bar{\alpha}_1+1\right)\Gamma\left(l+\bar{\alpha}_2+1\right)} \times \\ \mathrm{Im}\left[\left(\frac{\sqrt{-p^2}z}{2}\right)^{2m+2l+\bar{\alpha}_1+\bar{\alpha}_2+d/2}\left(\frac{\sqrt{-p^2}z'}{2}\right)^{2n+2l+\bar{\alpha}_1+\bar{\alpha}_2+d/2}\right].\end{aligned} \tag{2.89}$$

The self-energy becomes real for spacelike momenta, which is straightforward to note in this form. For timelike momenta, the imaginary part is given by

$$\begin{aligned}\mathrm{Im}\Pi(z,z') = \\ \mathrm{Sign}\left(\epsilon\right)\sum_{m,n,l=0}^{\infty} \frac{(-1)^{n+m}}{m!n!l!}\left(\frac{pz}{2}\right)^{2m+2l+\bar{\alpha}_1+\bar{\alpha}_2+d/2}\left(\frac{pz'}{2}\right)^{2n+2l+\bar{\alpha}_1+\bar{\alpha}_2+d/2} \times \\ \frac{\hat{\lambda}^2 k^3}{2^2\pi^{d/2-1}\left(k^2 z z'\right)^{d/2+1}} \frac{\Gamma\left(l+d/2\right)\Gamma\left(l+\bar{\alpha}_1+d/2\right)\Gamma\left(l+\bar{\alpha}_2+d/2\right)\Gamma\left(2l+\bar{\alpha}_1+\bar{\alpha}_2+1\right)}{\Gamma(d/2)\Gamma(2l+\bar{\alpha}_1+\bar{\alpha}_2+d)\Gamma(l+\bar{\alpha}_1+\bar{\alpha}_2+1)} \times \\ \frac{(2l+\bar{\alpha}_1+\bar{\alpha}_2+d/2)\Gamma\left(l+\bar{\alpha}_1+\bar{\alpha}_2+d/2\right)}{\Gamma\left(l+\bar{\alpha}_1+1\right)\Gamma\left(l+\bar{\alpha}_2+1\right)\Gamma(n+2l+\bar{\alpha}_1+\bar{\alpha}_2+d/2+1)\Gamma(m+2l+\bar{\alpha}_1+\bar{\alpha}_2+d/2+1)}.\end{aligned} \tag{2.90}$$

We recognize the sums over n, m as the series representation of the Bessel function J,

$$J_{2l+\bar{\alpha}_1+\bar{\alpha}_2+d/2}\left(x\right) = \sum_{j=0}^{\infty} \frac{(-1)^j\left(\frac{x}{2}\right)^{2j+2l+\bar{\alpha}_1+\bar{\alpha}_2+d/2}}{j!\Gamma(j+2l+\bar{\alpha}_1+\bar{\alpha}_2+d/2+1)}. \tag{2.91}$$

This gives

$$\begin{aligned}\mathrm{Im}\Pi(z,z') = \\ \frac{\mathrm{Sign}\left(\epsilon\right)\hat{\lambda}^2 k^3}{2^2\pi^{d/2-1}\left(k^2 z z'\right)^{d/2+1}} \sum_{l=0}^{\infty}(2l+\bar{\alpha}_1+\bar{\alpha}_2+d/2) J_{2l+\bar{\alpha}_1+\bar{\alpha}_2+d/2}\left(pz\right) J_{2l+\bar{\alpha}_1+\bar{\alpha}_2+d/2}\left(pz'\right) \times \\ \frac{\Gamma\left(l+d/2\right)\Gamma\left(l+\bar{\alpha}_1+d/2\right)\Gamma\left(l+\bar{\alpha}_2+d/2\right)\Gamma\left(2l+\bar{\alpha}_1+\bar{\alpha}_2+1\right)\Gamma\left(l+\bar{\alpha}_1+\bar{\alpha}_2+d/2\right)}{\Gamma(d/2)\Gamma(l+1)\Gamma(2l+\bar{\alpha}_1+\bar{\alpha}_2+d)\Gamma(l+\bar{\alpha}_1+\bar{\alpha}_2+1)\Gamma\left(l+\bar{\alpha}_1+1\right)\Gamma\left(l+\bar{\alpha}_2+1\right)}.\end{aligned} \tag{2.92}$$

Eq. (2.92) represents our final result for $\mathrm{Im}\Pi_p(z,z')$ in the conformal spectral representation. In Sec. 2.5.5, we identify this result as being a sum over the imaginary part of propagators.

2.5.3 ImΠ in the Momentum Spectral Representation

We again start from Eq. (2.70) and express the propagator in the p-spectral representation, Eq. (2.31). We introduce a Feynman parameter and shift the loop momentum, $l \equiv q + px$. This yields

$$\Pi_p(z,z') = \frac{-i\lambda^2}{(k^2 z z')^{d+1}} \int_0^1 dx \int_0^\infty dm_1 \Omega_{m_1}(z,z') \int_0^\infty dm_2 \Omega_{m_2}(z,z') \int \frac{d^d l}{(2\pi)^d} \frac{1}{(l^2-\Delta)^2} \tag{2.93}$$

for

$$\Delta \equiv x m_2^2 + (1-x) m_1^2 - x(1-x)p^2. \tag{2.94}$$

We evaluate the loop integral in arbitrary dimension with

$$\int \frac{d^d l}{(2\pi)^d} \frac{1}{(l^2-\Delta)^2} = \frac{i\Gamma\left(2-\frac{d}{2}\right)}{(4\pi)^{d/2}} \Delta^{d/2-2}\,. \tag{2.95}$$

The left-hand side integral converges for $d < 4$. However it can be analytically continued in d. For odd d, we write the square root as

$$\sqrt{\Delta}\Big|_{\mathrm{Re}\Delta \gg \mathrm{Im}\Delta} \approx i\sqrt{|\Delta|}\Theta\left(-\mathrm{Re}\Delta\right) \mathrm{Sign}\left(\mathrm{Im}\Delta\right) + \sqrt{|\Delta|}\Theta\left(\mathrm{Re}\Delta\right)\,, \tag{2.96}$$

valid for Δ near the real line. For even d, we take $d = d_0 \pm \varepsilon$ for $\varepsilon \ll 1$ and use the reflection formula Eq. (2.82). We obtain

$$\int \frac{d^d l}{(2\pi)^d} \frac{1}{(l^2-\Delta)^2}\Big|_{d_0 \text{ even}} = \frac{i\pi(-1)^{d_0/2-1}}{(4\pi)^{d_0/2} \sin\left(\pm\frac{\pi\varepsilon}{2}\right) \Gamma\left(\frac{d_0}{2}-1\right)} \Delta^{d_0/2-2} \Delta^{\pm\varepsilon/2}\,. \tag{2.97}$$

We expand Eq. (2.97) for $\varepsilon \ll 1$ using

$$\Delta^{\pm\varepsilon/2} \approx 1 \pm \frac{\varepsilon}{2}\log\Delta\,, \qquad \sin\left(\pm\frac{\pi\varepsilon}{2}\right) \approx \pm\frac{\pi\varepsilon}{2}. \tag{2.98}$$

We note that the log can be described in terms of arctan and a step function,

$$\log(\Delta) = \log|\Delta| + i\arctan\left(\frac{\mathrm{Im}\Delta}{\mathrm{Re}\Delta}\right) + i\pi\Theta(-\mathrm{Re}\Delta)\,\mathrm{Sign}(\mathrm{Im}\Delta)\ . \tag{2.99}$$

For Δ near the real line, the arctan term is small and can be dropped. The 1 and $\log|\Delta|$ terms yield contributions to the self-energy that are purely real and hence vanishes when taking the imaginary part.

With these simplifications, we can combine results for both even and odd d to obtain

$$\mathrm{Im}\left[i\int\frac{d^dl}{(2\pi)^d}\frac{1}{(l^2-\Delta)^2}\right]_{\mathrm{Re}\Delta\gg\mathrm{Im}\Delta} \approx \frac{\pi(-\Delta)^{d/2-2}}{(4\pi)^{d/2}\Gamma\left(\frac{d}{2}-1\right)}\Theta(-\mathrm{Re}\Delta)\,\mathrm{Sign}(\mathrm{Im}\Delta)\ , \tag{2.100}$$

valid for $d > 2$. Taking the imaginary part of the self-energy, we now have

$$\begin{aligned}\mathrm{Im}\Pi_p(z,z') =& \frac{-\pi}{(4\pi)^{d/2}\Gamma\left(\frac{d}{2}-1\right)}\frac{\lambda^2}{(k^2zz')^{d+1}}\int_0^1 dx\ \times \\ & \int_0^\infty dm_1\Omega_{m_1}\int_0^\infty dm_2\Omega_{m_2}(-\Delta)^{d/2-2}\Theta(-\mathrm{Re}\Delta)\,\mathrm{Sign}(\mathrm{Im}\Delta)\ .\end{aligned} \tag{2.101}$$

We find that for spacelike momenta $p^2 < 0$, $\mathrm{Re}\Delta > 0$ and hence $\mathrm{Im}\Pi = 0$. Specializing to timelike momenta $p^2 > 0$, we have

$$\mathrm{Sign}(\mathrm{Im}\Delta) = -\mathrm{Sign}(\epsilon)\,, \tag{2.102}$$

where $\epsilon > 0$ is the Feynman prescription for the propagator. The step function truncates the integrals over m_1, m_2 and x. We now have

$$\mathrm{Im}\Pi_p(z,z') = \frac{\mathrm{Sign}(\epsilon)\,\pi}{(4\pi)^{d/2}\Gamma\left(\frac{d}{2}-1\right)}\frac{\lambda^2}{(k^2zz')^{d+1}}\int_0^p dm_1\Omega_{m_1}\int_0^{p-m_1} dm_2\Omega_{m_2}\int_{x_-}^{x_+} dx(-\Delta)^{d/2-2} \tag{2.103}$$

for

$$x_\pm \equiv \frac{p^2 + \left(m_1^2 - m_2^2\right) \pm \sqrt{\left(p^2 - (m_1 - m_2)^2\right)\left(p^2 - (m_1 + m_2)^2\right)}}{2p^2} \,. \tag{2.104}$$

Notice that $-\Delta = (x_+ - x)(x - x_-)p^2$. To evaluate the integral, we change variables to $y = (x - x_-) / (x_+ - x_-)$ and recognize the integral representation of the Beta function,

$$\int_0^1 dy y^{n_1}(1-y)^{n_2} = \frac{\Gamma(n_1+1)\Gamma(n_2+1)}{\Gamma(n_1+n_2+2)} \equiv \mathrm{B}(n_1+1, n_2+1) \,. \tag{2.105}$$

$n_1 = n_2 = \frac{d}{2} - 2$ in the current case, and thus we obtain

$$\Xi(d, p, m_1, m_2) \equiv \frac{1}{\Gamma\left(\frac{d}{2}-1\right)} \int_{x_-}^{x_+} dx (-\Delta)^{d/2-2} = 2p^{2-d} K^{d-3} \frac{\Gamma\left(\frac{d}{2}\right)}{\Gamma\left(d-1\right)} \tag{2.106}$$

Here $K = K(p, m_1, m_2)$ is the standard four-dimensional two-body kinematic factor,

$$K(p, m_1, m_2) \equiv \sqrt{\left(p^2 - (m_1+m_2)^2\right)\left(p^2 - (m_1-m_2)^2\right)} \,. \tag{2.107}$$

The $\Xi(d, p, m_1, m_2)$ function is the two-body kinematic factor in arbitrary dimension d. Thus we obtain

$$\begin{aligned} \mathrm{Im}\Pi_p(z, z') = \mathrm{Sign}\,(\epsilon) \frac{2\pi}{(4\pi)^{d/2}} \frac{\Gamma\left(\frac{d}{2}\right)}{\Gamma\left(d-1\right)} \frac{\lambda^2}{\left(k^2 z z'\right)^{d+1}} \times \\ \int_0^p dm_1 \Omega_{m_1} \int_0^{p-m_1} dm_2 \Omega_{m_2} p^{2-d} K(p, m_1, m_2)^{d-3} \,. \end{aligned} \tag{2.108}$$

Eq. (2.108) represents our final result for $\mathrm{Im}\Pi_p(z, z')$ in the momentum spectral representation.

2.5.4 Proofs of Equality

The equivalence of the representations of ImΠ obtained in Secs. 2.5.1, 2.5.2, 2.5.3 is not manifest. In the canonical representation, a key piece of the calculation was a loop integral with non-integer powers. In the conformal spectral representation, AdS/CFT naturally

arises: CFT correlators appear and combine to form a CFT bubble diagram. Finally in the momentum spectral representation, a generalized two-body kinematic threshold emerges—with no intrinsic dependence on α. These three evaluations thus involve rather different objects and methods.

In this section, we prove the equality of these various representations of ImΠ.

Canonical—Momentum Spectral Equivalence

Here we relate the self-energy from the calculation in the momentum spectral representation to the calculation in the canonical representation. We start from Eq. (2.101) in the momentum spectral representation and substitute in the spectral functions Ω_m in terms of the Bessel functions explicitly

$$\begin{aligned}\mathrm{Im}\Pi_p(z,z') =& \mathrm{Sign}(\epsilon)\frac{\pi^2}{(4\pi)^{d/2+1}\Gamma\left(\frac{d}{2}-1\right)}\frac{\lambda^2}{k^4 z z'}\int_0^1 dx\int_0^\infty dm_1^2\int_0^\infty dm_2^2\times \\ & J_{\alpha_1}(m_1 z)J_{\alpha_1}(m_1 z')J_{\alpha_2}(m_2 z)J_{\alpha_2}(m_2 z')(-\Delta)^{d/2-2}\Theta\left(-\mathrm{Re}\Delta\right)\,.\end{aligned} \tag{2.109}$$

We use the step function to cut the m_1, m_2 integrals instead of the x integral. We also expand out the Bessel functions in terms of the series

$$J_\alpha(z) = \sum_{m=0}^{\infty}\frac{(-1)^m}{m!\Gamma(m+\alpha+1)}\left(\frac{z}{2}\right)^{2m+\alpha}. \tag{2.110}$$

We obtain

$$\begin{aligned}
&\mathrm{Im}\Pi_p(z,z') = \qquad (2.111)\\
&\frac{\mathrm{Sign}(\epsilon)\pi^2}{(4\pi)^{d/2+1}\Gamma\left(\frac{d}{2}-1\right)}\frac{\lambda^2}{k^4 zz'}\int_0^1 dx\int_0^{xp^2} dm_1^2\int_0^{(1-x)(xp^2-m_1^2)/x} dm_2^2\times\\
&\sum_{s,t,m,n=0}^{\infty}\frac{(-1)^{s+t+n+m}}{s!t!n!m!\Gamma(s+\alpha_1+1)\Gamma(t+\alpha_1+1)\Gamma(m+\alpha_2+1)\Gamma(n+\alpha_2+1)}\times\\
&\left(\frac{m_1 z}{2}\right)^{2s+\alpha_1}\left(\frac{m_1 z'}{2}\right)^{2t+\alpha_1}\left(\frac{m_2 z}{2}\right)^{2n+\alpha_2}\left(\frac{m_2 z'}{2}\right)^{2m+\alpha_2}(-\Delta)^{d/2-2}.
\end{aligned}$$

We perform the integral over m_2, then the integral over m_1, and lastly the integral over x. Each of these integrals can be expressed as the integral representation of the Beta function, Eq. (2.105). Thus we obtain

$$\begin{aligned}
&\mathrm{Im}\Pi_p(z,z') = \qquad (2.112)\\
&\frac{\mathrm{Sign}(\epsilon)p^d\pi^2}{(4\pi)^{d/2+1}}\frac{\lambda^2}{k^4 zz'}\sum_{s,t,m,n=0}^{\infty}\left(\frac{pz}{2}\right)^{2s+2n+\alpha_1+\alpha_2}\left(\frac{pz'}{2}\right)^{2t+2m+\alpha_1+\alpha_2}\times\\
&\frac{(-1)^{s+t+n+m}}{s!t!n!m!\Gamma(s+\alpha_1+1)\Gamma(t+\alpha_1+1)\Gamma(m+\alpha_2+1)\Gamma(n+\alpha_2+1)}\times\\
&\frac{\Gamma(1+s+t+\alpha_1)\Gamma(1+m+n+\alpha_2)}{\Gamma\left(1+s+t+n+m+\alpha_1+\alpha_2+\frac{d}{2}\right)}\frac{\Gamma\left(\frac{d}{2}+s+t+\alpha_1\right)\Gamma\left(\frac{d}{2}+m+n+\alpha_2\right)}{\Gamma(d+s+t+n+m+\alpha_1+\alpha_2)},
\end{aligned}$$

which is exactly Eq. (2.83).

Equivalence with the Conformal Spectral Representation

It is difficult to show the exact equivalence between the conformal spectral representation and either the canonical or momentum spectral representation. The proof involves sums over generalized hypergeometric functions ${}_4F_3$ which are nontrivial to perform. It is not as difficult to show the equivalence order by order in $pz_<$. Here we present a proof of equivalence for $pz_< \ll 1$ with arbitrary $pz_>$.

We take the self-energy in the canonical representation Eq. (2.83) to leading order in $pz_<$,

$$\mathrm{Im}\Pi_p(z,z') = \frac{\mathrm{Sign}(\epsilon)\pi\lambda^2 p^d}{4k^4 zz'(4\pi)^{d/2}} \frac{1}{\Gamma(\alpha_1+1)} \frac{1}{\Gamma(\alpha_2+1)} \left(\frac{pz_<}{2}\right)^{\alpha_1+\alpha_2} \times \tag{2.113}$$
$$\sum_{n,s=0}^{\infty} \left(\frac{pz_>}{2}\right)^{2n+2s+\alpha_1+\alpha_2} \frac{(-1)^{s+n}}{s!n!} \frac{\Gamma(s+\alpha_1+d/2)\Gamma(n+\alpha_2+d/2)}{\Gamma(s+n+d+\alpha_1+\alpha_2)\Gamma(n+s+\alpha_1+\alpha_2+d/2+1)}.$$

We introduce $j \equiv s+n$ and reorganize the sums

$$\mathrm{Im}\Pi_p(z,z') = \frac{\mathrm{Sign}(\epsilon)\pi\lambda^2 p^d}{4k^4 zz'(4\pi)^{d/2}} \frac{1}{\Gamma(\alpha_1+1)} \frac{1}{\Gamma(\alpha_2+1)} \left(\frac{pz_<}{2}\right)^{\alpha_1+\alpha_2} \times \tag{2.114}$$
$$\sum_{j=0}^{\infty} \frac{(-1)^j \left(\frac{pz_>}{2}\right)^{2j+\alpha_1+\alpha_2}}{\Gamma(j+d+\alpha_1+\alpha_2)\Gamma(j+\alpha_1+\alpha_2+d/2+1)} \sum_{s=0}^{j} \frac{\Gamma(s+\alpha_1+d/2)\Gamma(j-s+\alpha_2+d/2)}{s!(j-s)!}.$$

We directly evaluate the sum over s with Mathematica [185]. We obtain

$$\mathrm{Im}\Pi_p(z,z') = \frac{\mathrm{Sign}(\epsilon)\pi\lambda^2 p^d}{4k^4 zz'(4\pi)^{d/2}} \frac{1}{\Gamma(\alpha_1+1)} \frac{1}{\Gamma(\alpha_2+1)} \left(\frac{pz_<}{2}\right)^{\alpha_1+\alpha_2} \times \tag{2.115}$$
$$\sum_{j=0}^{\infty} \frac{(-1)^j \left(\frac{pz_>}{2}\right)^{2j+\alpha_1+\alpha_2} \Gamma\left(\alpha_1+\frac{d}{2}\right) \Gamma\left(\alpha_2+\frac{d}{2}+j\right) {}_2F_1\left(\alpha_1+\frac{d}{2}, -j; -\alpha_2-j-\frac{d}{2}+1; 1\right)}{j!\Gamma(j+d+\alpha_1+\alpha_2)\Gamma(j+\alpha_1+\alpha_2+d/2+1)}.$$

We now use a known result for this special case of the hypergeometric function—Eq. (15.4.20) of [164]—reprinted here:

$${}_2F_1(a,b;c;1) = \frac{\Gamma(c)\Gamma(c-a-b)}{\Gamma(c-a)\Gamma(c-b)}. \tag{2.116}$$

We obtain

$$\mathrm{Im}\Pi_p(z,z') = \frac{\mathrm{Sign}(\epsilon)\pi\lambda^2 p^d}{4k^4 zz'(4\pi)^{d/2}} \frac{1}{\Gamma(\alpha_1+1)} \frac{1}{\Gamma(\alpha_2+1)} \left(\frac{pz_<}{2}\right)^{\alpha_1+\alpha_2} \times \tag{2.117}$$
$$\sum_{j=0}^{\infty} \frac{(-1)^j \left(\frac{pz_>}{2}\right)^{2j+\alpha_1+\alpha_2} \Gamma\left(\alpha_1+\frac{d}{2}\right) \Gamma\left(\alpha_2+\frac{d}{2}+j\right) \Gamma(-\alpha_1-\alpha_2-d+1)\Gamma(-\alpha_2-j-\frac{d}{2}+1)}{j!\Gamma(j+d+\alpha_1+\alpha_2)\Gamma(j+\alpha_1+\alpha_2+d/2+1)\Gamma(-\alpha_1-\alpha_2-j-d+1)\Gamma(-\alpha_2-\frac{d}{2}+1)}.$$

We simplify further by using Euler's reflection formula, Eq. (2.82), and trigonometric identities. We obtain

$$\begin{aligned}\mathrm{Im}\Pi_p(z,z') =& \frac{\mathrm{Sign}(\epsilon)\pi\lambda^2}{4k^4(zz')^{d/2+1}\pi^{d/2}} \frac{\Gamma\left(\alpha_1+\frac{d}{2}\right)\Gamma\left(\alpha_2+\frac{d}{2}\right)}{\Gamma(\alpha_1+1)\Gamma(\alpha_2+1)} \frac{1}{\Gamma(d+\alpha_1+\alpha_2)} \times \\ & \left(\frac{pz_<}{2}\right)^{\alpha_1+\alpha_2+d/2} \sum_{j=0}^{\infty} \frac{(-1)^j \left(\frac{pz_>}{2}\right)^{2j+\alpha_1+\alpha_2+d/2}}{j!\Gamma(j+\alpha_1+\alpha_2+d/2+1)}.\end{aligned} \tag{2.118}$$

We recognize the remaining sum as the series representation of the Bessel function J as given in Eq. (2.91). Thus we obtain

$$\mathrm{Im}\Pi_p(z,z') = \frac{\mathrm{Sign}(\epsilon)\pi\lambda^2}{4k^4(zz')^{d/2+1}\pi^{d/2}} \frac{\Gamma\left(\alpha_1+\frac{d}{2}\right)\Gamma\left(\alpha_2+\frac{d}{2}\right)}{\Gamma(\alpha_1+1)\Gamma(\alpha_2+1)} \frac{J_{\alpha_1+\alpha_2+d/2}(pz_>)}{\Gamma(d+\alpha_1+\alpha_2)} \left(\frac{pz_<}{2}\right)^{\alpha_1+\alpha_2+d/2}. \tag{2.119}$$

The conformal spectral result is given by Eq. (2.92). To leading order in $pz_<$, $l=0$ and we take the small argument limit of the $pz_< \ll 1$ Bessel function. Upon application of the recurrence formula for the Gamma functions, we immediately obtain Eq. (2.119).

We have checked the equality of the next-to-leading order terms in $pz_<$. This calculation goes just as above, but with more terms that nontrivially sum. When attempting to show equality generally (for any $pz_<$), sums over generalized hypergeometric functions ${}_4F_3$ emerge which are difficult to evaluate. We expect equality to hold to all orders in $pz_<$.

2.5.5 Properties of the Self-Energy

Based on our results, here we discuss some properties of the imaginary part of the bubble diagram $\mathrm{Im}\Pi$.

Elementary Features

- **The self-energy becomes real for spacelike momentum $p^2 < 0$, *i.e.***

$$\mathrm{Im}\Pi|_{p^2<0} = 0\,. \tag{2.120}$$

This is easily shown from the conformal spectral or canonical representations, where we note that $\mathrm{Im}\Pi \propto \mathrm{Im}\left(-p^2\right)^\gamma$ for some power γ. When the momenta becomes spacelike $-p^2 > 0$, $\mathrm{Im}\Pi$ subsequently vanishes. In the momentum spectral representation, we note that the Heaviside Θ-function in Eq. (2.100) cannot be satisfied for spacelike momenta, and hence $\mathrm{Im}\Pi = 0$.

- $\mathrm{Im}\Pi$ **is finite for nonzero z, z' and finite timelike momentum p.**

This can be shown from any of the representations. Consider for instance the canonical representation Eq. (2.83). At fixed p and z, z', when going to high enough order in a given sum, the Gamma functions in the denominator imply that the absolute value of the ratios of two subsequent terms is strictly smaller than 1. This implies that the series (absolutely) converges, therefore $\mathrm{Im}\Pi$ is finite.

- **If $z = z'$,** $\mathrm{Im}\Pi$ **carries the same sign as ϵ,** *i.e.*

$$\mathrm{Sign}\left(\mathrm{Im}\Pi(z,z)\right) = \mathrm{Sign}(\epsilon)\,. \tag{2.121}$$

This property can be shown from the momentum spectral representation Eq. (2.108). For $z = z'$, both spectral functions are positive since $\propto (J_\alpha(m_i z))^2$. Hence the integrals are positive and $\mathrm{Sign}\left(\mathrm{Im}\Pi\right) = \mathrm{Sign}\left(\epsilon\right)$. This property can also be shown in the conformal spectral representation by noting that the self-energy can be written as a

sum over squares when $z = z'$. Along the same lines, we show that $\text{Sign}\left(\text{Im}\Pi(z,z')\right) = \text{Sign}(\epsilon)$ if $p|z-z'| \ll 1$, *i.e.* when z and z' are close enough (see below).

Asymptotic Features

- **At large $pz \to \infty$ with timelike momentum p, $\text{Im}\Pi$ becomes asymptotically local, with**

$$\text{Im}\Pi_p(z,z')\Big|_{p\to\infty} \propto \frac{p^{d-3}}{z^4}\frac{\sin(p(z-z'))}{z-z'}\Big|_{p\to\infty} \sim \frac{p^{d-3}}{z^4}\delta(z-z')\,. \tag{2.122}$$

We show this in the momentum spectral representation. Details are given in App. D. In short, at large pz the spectral functions rapidly oscillate such that their average can be pull out from the mass integrals. The averages asymptotically give rise to a nascent Dirac delta in z. The remaining mass integral depends only on p and must scale as p^{d-3}. This limit makes clear that $\text{Im}\Pi_p(z,z')$ is peaked on $z \sim z'$, and that it becomes increasingly peaky with $pz \gg 1$ since in this limit it approaches a Dirac delta. This asymptotic feature should not be seen as a literal divergence. These properties are more difficult to show in the conformal spectral and canonical representations.

- **At small pz, pz' with timelike momentum p, the behaviour of $\text{Im}\Pi$ is**

$$\text{Im}\Pi_p(z,z')\Big|_{pz\ll 1, pz'\ll 1} \propto (zz')^{\alpha_1+\alpha_2-1}p^{d+2\alpha_1+2\alpha_2} = (zz')^{\Delta_1+\Delta_2-d-1}p^{2\Delta_1+2\Delta_2-d}\,. \tag{2.123}$$

This behaviour can be shown from any of the representations, and can be directly read from *e.g.* Eq. (2.83) by taking the first term of the series. The scaling in p is consistent with the one found in [114]. For the last equality we used $\Delta_i = \frac{d}{2} + \alpha_i$. If

z approaches zero, $\mathrm{Im}\Pi_p(z,z')$ goes as $z^{\alpha_1+\alpha_2-1}$, which diverges if $\alpha_1+\alpha_2<1$. In physical expressions, however, $\mathrm{Im}\Pi_p(z,z')$ is always multiplied by extra metric factors which remove this possibly divergent behavior near the boundary. Such z,z' factors appear for instance in Eq. (2.139), thus justifying the saddle-point expansion.

Double-Trace Formula from Conformal Spectral Representation

Starting from the conformal spectral representation of $\mathrm{Im}\Pi$ Eq. (2.92), we notice that each term of the sum can be rewritten as the discontinuity of a free propagator with bulk mass parameter $\alpha_1+\alpha_2+d/2$ along the timelike branch cut (see Eq. (2.35)). This is equivalently given by the imaginary part of $iG^{(0)}$,

$$\mathrm{Im}\left[iG^{(0)}_{\alpha_1+\alpha_2+d/2+2l}(z,z')\right]=\mathrm{Sign}\,(\epsilon)\,\frac{\pi}{2k}(kz)^{d/2}(kz')^{d/2}J_{\alpha_1+\alpha_2+d/2+2l}(pz)J_{\alpha_1+\alpha_2+d/2+2l}(pz') \tag{2.124}$$

In terms of conformal dimension, using $\Delta_i=\alpha_i+d/2$, this propagator amounts to the exchange of operators with dimension $\Delta_1+\Delta_2+2l$. We recognize the structure of the well-known "double-trace" formula [79, 160] which gives the product of position-space propagators $G^{(0)}_{\alpha_1}(X,Y)G^{(0)}_{\alpha_2}(X,Y)$ as an infinite sum over $G^{(0)}_{\alpha_1+\alpha_2+d/2+2l}(X,Y)$.

Making the imaginary part of $iG^{(0)}$ explicit in Eq. (2.92), we obtain

$$\mathrm{Im}\Pi_p(z,z')=\frac{\hat{\lambda}^2k^3}{(k^2zz')^{d+1}}\sum_{l=0}^{\infty}a_{\Delta_1,\Delta_2,l}\,\mathrm{Im}\left[iG^{(0)}_{\alpha_1+\alpha_2+d/2+2l}(z,z')\right] \tag{2.125}$$

with

$$a_{\Delta_1,\Delta_2,l}=\frac{2l+\alpha_1+\alpha_2+d/2}{2\pi^{d/2}}\times \tag{2.126}$$
$$\frac{\Gamma\left(l+d/2\right)\Gamma\left(l+\alpha_1+d/2\right)\Gamma\left(l+\alpha_2+d/2\right)\Gamma\left(2l+\alpha_1+\alpha_2+1\right)\Gamma\left(l+\alpha_1+\alpha_2+d/2\right)}{\Gamma(d/2)\Gamma(l+1)\Gamma(2l+\alpha_1+\alpha_2+d)\Gamma(l+\alpha_1+\alpha_2+1)\Gamma\left(l+\alpha_1+1\right)\Gamma\left(l+\alpha_2+1\right)}\,.$$

Using Legendre's duplication formula

$$\frac{\Gamma(2z)}{\Gamma(z)} = \frac{2^{2z-1}}{\sqrt{\pi}}\Gamma\left(z+\frac{1}{2}\right) \tag{2.127}$$

it turns out that one can re-write $a_{\Delta_1,\Delta_2,l}$ in terms of Pochammer functions $(x)_n = \Gamma(x+n)/\Gamma(x)$, obtaining

$$a_{\Delta_1,\Delta_2,l} = \frac{\left(\frac{d}{2}\right)_l}{2\pi^{d/2}l!}\frac{(\Delta_1+\Delta_2+2l)_{1-d/2}\,(\Delta_1+\Delta_2+l-d+1)_l}{(\Delta_1+l)_{1-d/2}\,(\Delta_2+l)_{1-d/2}\,(\Delta_1+\Delta_2+l-d/2)_l}\,. \tag{2.128}$$

This matches precisely the coefficients of the double-trace formula [79]. With Eq. (2.125), we have thus recovered the imaginary part of the double-trace formula by direct calculation starting from the conformal spectral representation. [12]

Relation to AdS Unitarity Methods

Unitarity methods in AdS have recently been investigated in [114, 158]. These methods typically aim to compute the double discontinuity of the dual CFT correlators from the AdS side [159], and therefore focus on full Witten diagrams. However amputated diagram such as our bubble $i\Pi$ encapsulate essential information about the Witten diagram they are a part of. Let us consider the interplay between our results for ImΠ and existing AdS unitarity methods.

In [158], a **Cut** operation was introduced in the space of conformal dimensions. [13] This **Cut** applies in the conformal spectral representation: It picks the poles of the $P(\alpha,\bar{\alpha})$ measure enclosed by the corresponding α-contour integral. One can apply this operation

[12] Upon Fourier-transform and appropriate translation into our Lorentzian conventions.

[13] A $\widehat{\textbf{Cut}}$ operation is also introduced, which involves an extra projection and applies only to full Witten diagrams. Here our focus is on the **Cut** operation only.

to the bubble diagram in the conformal spectral representation (Sec. 2.5.2). Consider the $\mathbf{Cut}_{12}$ operation, which cuts both lines of the bubble in the sense defined above. This cut amounts to selecting the poles of $P(\alpha_1, \bar{\alpha}_1)$ and $P(\alpha_2, \bar{\alpha}_2)$ in the α_1, α_2 integrals. This is intuitively what the Im operation would do in flat space. What is the effect of Im on the AdS bubble as compared to $\mathbf{Cut}_{12}$? We have seen by direct calculation in Sec. 2.5.2 that the Im does the same work as $\mathbf{Cut}_{12}$ because other residues are real and are thus projected out. We conclude that

$$\mathrm{Im}(\mathbf{Cut}_{12}\Pi) = \mathbf{Cut}_{12}(\mathrm{Im}\Pi) = \mathrm{Im}\Pi\,. \tag{2.129}$$

These identities imply that the Im projection is at least as strong as $\mathbf{Cut}_{12}$, *i.e.* $\mathrm{Im}\Pi \subset \mathbf{Cut}_{12}\Pi$. The equality of the operations is not guaranteed. The evaluation of $\mathbf{Cut}_{12}\Pi$ in our formalism would require further investigation.

In [114], unitarity cuts in the momentum spectral representation have been explored. Following this reference, we can evaluate a cut of the Π bubble instead of evaluating its imaginary part. To do so, we implement Cutkosky rules in the propagator Eq. (2.31), cutting the $P(\hat{p}, p)$ using the substitution

$$P(\hat{p}, p) \propto \delta\left(p^2 - \hat{p}^2\right)\,. \tag{2.130}$$

With such substitution in Eq. (2.31), one can evaluate the integral in $\hat{p}$, which gives rise to the AdS Wightman propagator [114] given schematically by [14]

$$G_p^W(z, z') \propto (zz')^{d/2} J_\alpha(pz) J_\alpha(pz')\,. \tag{2.131}$$

Pursuing the evaluation of the cut of Π along these lines, we obtain a product of four Bessel

[14] We thank the authors of [114] for pointing this out in private correspondence.

J functions. Expanding the Bessel functions as a series and performing the loop integrals as in Sec. 2.5.1, we ultimately find that the cut diagram reproduces the result of $\mathrm{Im}\Pi$ in the canonical representation Eq. (2.92).

2.6 Opacity of AdS

In this section we solve the dressed equation of motion in the timelike regime. This is done using an improved version of the WKB method [15] and other approximations. Our focus is on the effect of the imaginary contribution $\mathrm{Im}\Pi_p(z, z')$.

As discussed in Sec. 2.3.3, three distinct regimes can be distinguished in position-momentum space, depending on whether the invariants pz, pz' are smaller or larger than 1. In the $pz, pz' \ll 1$ regime, the effects of dressing are expected to be small because the self-energy gets suppressed by higher powers of pz with respect to the terms in the free EOM operator $\mathcal{D}_z$ (see *e.g.* Eq. (2.83) or (2.123)). The behaviour of the dressed propagator for $pz, pz' \gg 1$ could be understood from a flat space viewpoint by using a Weyl transform (see Sec. 2.3.3). Hence we do not focus on these cases. Our focus in this section is rather on the non-trivial $pz_< \ll 1$, $pz_> \gg 1$ regime, which has no flat space analog since the $pz \ll 1$ vanishes in the flat space limit. Note this regime includes the boundary-to-bulk propagators (Sec. C.5) as a particular case.

Recall that for spacelike momentum, the propagator in the $|p|z_< \ll 1$, $|p|z_> \gg 1$

[15] Also known as the Carlini–Liouville–Green–Rayleigh–Gans–Jeffreys–Wentzel–Kramers–Brillouin approximation.

regime decays as

$$G_p(z, z') \propto \exp\left(-|p| z_>\right) \tag{2.132}$$

irrespective of $z_<$. This can be seen from Eq. (2.38) using that p is imaginary in the spacelike region. The purpose of this section is to show that a similar exponential decay happens for *timelike* momentum in the *interacting* theory. This exponential fall-off directly results from the imaginary part of Π, which introduces a damping in the EOM solutions, which would otherwise be oscillating.

We have provided various representations of $\mathrm{Im}\Pi$ in Sec. 2.5. The momentum spectral representation—made available by working in position-momentum space—turns out to be the most convenient to pursue the calculation and make intuitive approximations.

In this section we will work within the effective field theory (EFT) paradigm. Before delving into the dressing calculations, some details about EFT are given in Sec. 2.6.1.

2.6.1 Interactions and Effective Field Theory

Matter interactions have been left implicit in the action Eq. (2.3). In Secs. 2.4, 2.5, we have restricted the calculation to a non-derivative scalar cubic coupling for simplicity.

Here we are interested more broadly in the low-energy effective field theory (EFT) viewpoint, in which the action S encodes local interactions with arbitrary high number of fields and derivatives. In addition to scalar cubic interactions with no derivatives—which are renormalizable for $d \leq 6$ —cubic interactions with an arbitrary number of extra derivatives

are also present in principle. We consider the cubic couplings [16]

$$S \supset \int dX^M \sqrt{|\gamma|} \left(\lambda \Phi \Phi_1 \Phi_2 - \zeta \Phi \partial_M \Phi_1 \partial^M \Phi_2 + \ldots \right) \tag{2.133}$$

where the ellipses denote scalar cubic couplings with higher number of derivatives. In Sec. 2.7, cubic matter-gravity interactions will be considered.

Following the EFT paradigm, these interactions of higher dimension are suppressed by a typical energy scale Λ, the EFT cutoff. The natural relation for the couplings in Eq. (2.133) is expected to be $\zeta/\lambda \sim 1/\Lambda^2$, *i.e.* each derivative brings an extra $1/\Lambda$ factor. Conversely, the EFT action is valid only up to a proper distance scale of order $\Delta X \sim 1/\Lambda$.

How does the cutoff appear in our Poincaré position-momentum space? To see it, one can compare the effects of operators of different order, *e.g.* the two operators in Eq. (2.133), or the scalar kinetic term and a bilinear four-derivative operator $\Lambda^{-2}\Box(\partial_M \Phi \partial^M \Phi)$, in some physical amplitude. [17] This shows that the cutoff of the EFT is reached for

$$pz \sim \frac{\Lambda}{k} \,. \tag{2.134}$$

This happens because higher derivatives operators necessarily come together with extra powers of kz. More generally, at the value set by Eq. (2.134), operators with arbitrary number of derivatives become equally important in the amplitudes, signalling that the low-energy EFT has reached its limit and that a deeper UV-completion should be used instead. We in fact recover the scaling of Eq. (2.134) in our results Eq. (2.168). This feature is well-known, see [3, 110, 155, 186–188] for further details.

[16] In the EFT, other two-derivative cubic interactions such as $\Phi_1 \partial_M \Phi \partial^M \Phi_2$ can be reduced to the ones in Eq. (2.133) using integration by parts and the equation of motion.

[17] One can *e.g.* examine the correction to the free propagator from $\Lambda^{-2}\Box(\partial_M \Phi \partial^M \Phi)$.

2.6.2 Solving the Dressed EOM

The dressed EOM can be treated with standard solving techniques just like the free case (see Sec. 2.3.2 and Eq. (2.19)), such that the dressed canonical propagator admits the structure

$$G(p;z,z') = \frac{i}{\widetilde{C}}\widetilde{F}_<(z_<)\widetilde{F}_>(z_>)\,. \tag{2.135}$$

The $\widetilde{F}_i$ satisfies the homogeneous dressed EOM

$$\mathcal{D}\widetilde{F}_i(z) - \frac{1}{\sqrt{|\gamma|}}\Pi * \widetilde{F}_i(z) = 0\,. \tag{2.136}$$

The quantum dressing affects both solutions $\widetilde{F}_<$ and $\widetilde{F}_>$. Our focus is on the $pz_< \ll 1$, $pz_> \gg 1$ regime, and we are interested in the effect of dressing on the $\widetilde{F}_>$ part of the propagator. As discussed above, the effects of dressing on $\widetilde{F}_<$ and $\widetilde{C}$ are small—this follows from *e.g.* Eq. (2.123)—and are neglected for our purposes.

A WKB-like Approximation

In the $pz_> \gg 1$ regime we know from Sec. 2.3.3 that $\widetilde{F}_>$ is conformally equivalent to a massless flat space solution, which is a e^{ipz} exponential—the asymptotic AdS solution is $z^{\frac{d-1}{2}}e^{ipz}$. This feature implies that we can use developed WKB-type methods to find the solution $\widetilde{F}_>$ as a suitable perturbation of the free solution $F_>$. The WKB ansatz of $\widetilde{F}_>$ for timelike momentum, assuming $\epsilon > 0$ and taking the $pz \gg 1$ limit, is the asymptotic form [18]

$$\widetilde{F}_>(z)\Big|_{pz\gg 1} \approx \widetilde{F}_>^{\text{c.m.}}(z) = z^{\frac{d-1}{2}}e^{ipz+S(z)}\,. \tag{2.137}$$

[18] We dropped an irrelevant multiplicative constant as compared to the convention of the free case of Sec. 2.3.2. By construction such factors cancel in the full expression, see Sec. 2.3.2.

The $S(z)$ function is determined perturbatively. Setting $S \to 0$ gives the asymptotic conformally massless solution of the free EOM, noted $F_>^{\text{c.m.}}(z)$. In our analysis, we show that $S(z) < 0$. Thus we find that loop corrections are consistent with the $\epsilon > 0$ prescription of the free theory.

Plugging $\widetilde{F}_>^{\text{c.f.}}(z)$ into the dressed equation of motion gives

$$S'(z) = -\frac{e^{-ipz}}{2p} \int_0^\infty du \, \text{Im}\Pi(z,u)(k^2 z)^{\frac{d-1}{2}} F_>(u) \tag{2.138}$$

at first order, assuming $|S'| \ll p$, $|S''| \ll p|S'|$ and $|S|$ not arbitrarily large.[19] These conditions are satisfied for $pz \gg 1$.

Upon extracting the $u^{\frac{d-1}{2}}$ prefactor from $F_>(u)$, we note that the resulting integrand is highly peaked at $z \sim u$ —as expected from locality. Upon inspecting $\left(k^2 z\, u\right)^{\frac{d-1}{2}} \text{Im}\Pi(z,u)$, one can also confirm that the dominant contributions to $S(z)$ do indeed come from the $pz \gg 1$ region. Further, the steepness of the peak increases with pz. This can be checked in the amplitudes of Sec. (2.6.4), see *e.g.* Eq. (2.151). Additional supporting details are discussed in Sec. 2.5.5.

Having a peak at $z \sim u$, and having $pz \gg 1$ by assumption, we can safely use the $pu \gg 1$ approximation for the convoluted propagator such that $F_>(u) \approx F_>^{\text{c.m.}}(u)$ in Eq. (2.138). This gives

$$S(z) = -\frac{1}{2p} \int_z d\widetilde{z} \int_0^\infty du \, \text{Im}\Pi(\widetilde{z},u) \left(k^2 \widetilde{z}\, u\right)^{\frac{d-1}{2}} e^{+ip(u-\widetilde{z})} \tag{2.139}$$

[19] More precisely, taking $e^{-S(z)+S(u)} \sim 1$ (with $S < 0$) on the right-hand side of Eq. (2.138) is valid as long as the rest of the integrand is sufficiently peaked. In Sec. 2.6.2, we use a saddle-point approximation for the rest of the integrand which gives $e^{-\frac{1}{2C}p^2(z-u)^2}$. So long as $e^{-S(z)+S(u)}$ does not compete with $e^{-\frac{1}{2C}p^2(z-u)^2}$, our approximation is valid. The breakdown occurs at values of $|S|$ sensibly larger than 1.

where we have integrated S' to obtain S.

The integration constant for the last $d\widetilde{z}$ integral would be determined by a matching condition at $z = z'$ in the propagator. Such condition is not accessible analytically in the asymptotic regime considered, since $z_> \gg z_<$. However we will see that the integration constant is essentially irrelevant for our analysis.

Aside on an Elementary Approximation

For large pz, the integrand in Eq. (2.139) is highly peaked. The most basic approximation that we can perform is to take $\left(k^2\, z\, u\right)^{\frac{d-1}{2}}\, \mathrm{Im}\Pi(z,u)$ to be proportional to a Dirac distribution, *i.e.* assuming exact locality along the z direction. Under this approximation we have

$$(z\,u)^{\frac{d-1}{2}}\ \mathrm{Im}\Pi(z,u) \approx I(z)\delta(z-u), \quad I(z) = \int_0^\infty du\ (z\,u)^{\frac{d-1}{2}}\ \mathrm{Im}\Pi(z,u)\,. \tag{2.140}$$

In this limit, the convolution $\Pi * F_>(z)$ becomes a product $I(z)F_>(z)$. The convolution being gone, the problem reduces to a standard WKB one in which the EOM is perturbed by a potential $I(z)$. This approximation reproduces the large p limit of the self-energy established in Sec. 2.5.5. Even though the integrand in Eq. (2.139) is very peaked at large pz, it multiplies an exponential which oscillates in pz and thus cannot be treated as a function varying slowly with respect to $\mathrm{Im}\Pi$. Thus this approximation scheme is potentially inaccurate and a more refined approach is necessary.

Saddle-Point Approximation

As an improved approximation, we take $\left(k^2\, z\, u\right)^{\frac{d-1}{2}}\, \mathrm{Im}\Pi(z,u)$ as a Gaussian centered on $\widetilde{z} = u$, whose width is controlled by the second derivative at this point. [20] This is the saddle-point approximation. It allows us to treat $\left(k^2\, z\, u\right)^{\frac{d-1}{2}}\, \mathrm{Im}\Pi(z,u)$ as peaked while also accounting for the complex exponential. The saddle-point approximation will allow us to perform the integrals analytically.

We write Eq. (2.139) as

$$S(z) = -\frac{1}{2p}\int_z d\widetilde{z}\int_0^\infty du\, e^{-f(\widetilde{z},u)+ip(u-\widetilde{z})} \tag{2.141}$$

for

$$f(z,u) = -\log\left(\left(k^2\, z\, u\right)^{\frac{d-1}{2}}\, \mathrm{Im}\Pi(z,u)\right). \tag{2.142}$$

The maximum of $\left(k^2\, z\, u\right)^{\frac{d-1}{2}}\, \mathrm{Im}\Pi(z,u)$ being at $z = u$, $f(z,u)$ has a minimum at $z \sim u$ up to a small $O(1/pz)$ suppressed shift. Expanding $f(z,u)$ about this minimum, we have

$$S(z) = -\frac{1}{2p}\int_z d\widetilde{z}\int_0^\infty du\, e^{-f(\widetilde{z},\widetilde{z})+ip(u-\widetilde{z})-\frac{1}{2}\left(\partial_u^2 f(\widetilde{z},u)\big|_{u=\widetilde{z}}\right)(u-\widetilde{z})^2} \tag{2.143}$$

where $\partial_u^2 f(z,u)\big|_{u=z}$ is given by

$$\partial_u^2 f(z,u)\big|_{u=z} \approx -\left.\frac{\partial_u^2\left(\left(k^2\, z\, u\right)^{\frac{d-1}{2}}\, \mathrm{Im}\Pi(z,u)\right)}{\left(\left(k^2\, z\, u\right)^{\frac{d-1}{2}}\, \mathrm{Im}\Pi(z,u)\right)}\right|_{u=z} + \left(\partial_u f(z,u)\big|_{u=z}\right)^2 \equiv C_p\,(z)\, p^2. \tag{2.144}$$

[20] While performing this approximation, $\mathrm{Im}\Pi(z,u) > 0$ is required. While this is not strictly the case for $\mathrm{Im}\Pi(z,u)$ globally, it is true on the $z \sim u$ peak. A side effect of the kinematic approximation discussed in Sec. 2.6.3 is to smooth the oscillations of $\mathrm{Im}\Pi(z,u)$. This smoothed version satisfies $\mathrm{Im}\Pi(z,u) > 0$ everywhere.

Note that $\partial_u f(z,u)|_{u=z} = 0$ by construction. The p^2 factor we have extracted in our convention will naturally appear in the upcoming explicit calculations. We now have

$$S(z) = -\frac{1}{2p}\int_z d\widetilde{z}\,(k\widetilde{z})^{d-1}\,\mathrm{Im}\Pi(\widetilde{z},\widetilde{z})\int_0^\infty du\, e^{ip(u-\widetilde{z})-\frac{1}{2}C_p(\widetilde{z})p^2(u-\widetilde{z})^2}, \tag{2.145}$$

which is a Gaussian integral. Evaluating this integral gives

$$S(z) \approx -\frac{1}{2p^2}\int_z d\widetilde{z}\,\mathrm{Im}\Pi_p(\widetilde{z},\widetilde{z})\,(k\widetilde{z})^{d-1}\sqrt{\frac{2\pi}{C_p(\widetilde{z})}}e^{-\frac{1}{2C_p(\widetilde{z})}}\,. \tag{2.146}$$

Compared to the delta-function approximation shown in Eq. (2.140), it turns out that an extra factor $e^{-\frac{1}{2C_p(z)}}$ appears above in Eq. (2.146) —inducing an extra suppression of the S function. This extra effect reflects the departure from the standard WKB problem taken into account by the saddle-point approximation. It encodes the fact that the perturbation to the EOM is a convolution $\Pi * G$, and not a mere potential multiplying G as would be approximated by Eq. (2.140). We will use this improved WKB-like approximation in our analysis.

2.6.3 Kinematic Approximation for ImΠ in Any Dimension

We turn to the imaginary part of the self-energy itself. In Sec. 2.5, we gave the exact form of ImΠ from a Φ^3 interaction in various forms. In this section, we allow for a more general form that could arise from the derivative cubic interactions in Eq. (2.133).

Using the momentum spectral representation established in Sec. 2.5.3, the imaginary part of the bubble diagram takes the structure

$$\mathrm{Im}\Pi_p(z,z') = \tag{2.147}$$
$$\frac{c_a c_b \pi}{(4\pi)^{d/2}k^4 zz'}\int_0^p dq_1\int_0^{p-q_1} dq_2 q_1 q_2 \mathcal{V}_a\, J_{\alpha_1}(q_1 z)J_{\alpha_2}(q_2 z)\mathcal{V}_b\, J_{\alpha_1}(q_1 z')J_{\alpha_2}(q_2 z')\Xi(d,p,q_1,q_2)\,.$$

The $\mathcal{V}_i \equiv \mathcal{V}_i(q_1, q_2, \partial_z, \partial_{z'})$ are operators encoding the Lorentz structure of the vertices. The c_i are the overall dimensionful coefficient of the vertices. Dimensions are such that $[c_i \mathcal{V}_i] = \frac{5-d}{2}$. The $\Xi(d, p, q_1, q_2)$ function is the d-dimensional 2-body kinematic function appearing in the momentum spectral representation (see Sec. 2.5.3). Its dimension is $[\Xi] = d - 4$.

Eq. (2.147) is exact, but is in general difficult to evaluate. In any dimension the $\Xi(d, p, q_1, q_2)$ function drops to zero at the $p = q_1 + q_2$ threshold. Away from the threshold $p \gg q_1 + q_2$, K tends to p^2 and the kinematic function simplifies to

$$\Xi(d, p, q_1, q_2) \approx \Xi(d, p, 0, 0) = \frac{2p^{d-4}\Gamma\left(\frac{d}{2}\right)}{\Gamma\left(d-1\right)} \tag{2.148}$$

giving for instance

d	3	4	5	6
$\Xi(d, p, 0, 0)$	$\frac{\sqrt{\pi}}{p}$	1	$\frac{\sqrt{\pi}}{4}p$	$\frac{p^2}{6}$

Following these observations, we introduce a kinematic threshold approximation for which $\Xi(d, p, q_1, q_2)$ is replaced by $\Theta\left(q_1 < \frac{p}{2}\right)\Theta\left(q_2 < \frac{p}{2}\right)\Xi(d, p, 0, 0)$. We have checked this approximation gives a typical error of $O(10\%)$ upon z integration. Numerical examples are shown in App. E. The approximate expression for $\mathrm{Im}\Pi_p$ becomes

$$\mathrm{Im}\Pi_p(z, z') \approx \tag{2.149}$$
$$\frac{c_a c_b \pi}{(4\pi)^{d/2} k^4 z z'} \int_0^{p/2} dq_1 \int_0^{p/2} dq_2 q_1 q_2 \mathcal{V}_a \, J_{\alpha_1}(q_1 z) J_{\alpha_2}(q_2 z) \mathcal{V}_b \, J_{\alpha_1}(q_1 z') J_{\alpha_2}(q_2 z') \Xi(d, p, 0, 0) \, .$$

Additionally, when working in the $pz, pz' \gg 1$ regimes, it turns out that the propagators can be accurately approximated as the conformally massless ones, such that one can also take $\alpha_{1,2} = 1/2$ in Eq. (2.149). This last approximation is not strictly necessary to render the evaluation of the WKB function S analytically tractable, but it will simplify the following expressions and integrals.

2.6.4 Bubbles in AdS_5

In the following subsections, we calculate the various contributions to the self-energy coming from the cubic vertices in Eq. (2.133). A detailed calculation of the $\Phi^3 - \Phi^3$ bubble was performed in Sec. 2.5. Abridged versions of all bubble calculations are given in App. F.

Here we specialize to the $d = 4$ case, *i.e* five-dimensional AdS. Results in other dimension are qualitatively similar, this is discussed in Sec. 2.6.5. As described in the previous subsection, to leading order we can set $\alpha_{1,2} = 1/2$ to simplify our expressions in the $pz \gg 1$ region.

$\Phi^3 - \Phi^3$ Bubble

The contribution to ImΠ from the bubble induced by two $\lambda\Phi\Phi_1\Phi_2$ vertices is given by

$$\mathrm{Im}\Pi_{\lambda\lambda}(z_1, z_2) = \frac{\lambda^2}{16\pi k^4 z_1 z_2} \int dq_1 dq_2 q_1 q_2 J_{\alpha_1}(q_1 z_1) J_{\alpha_1}(q_1 z_2) J_{\alpha_2}(q_2 z_1) J_{\alpha_2}(q_2 z_2) \frac{K(p; q_1, q_2)}{p^2} \,. \tag{2.150}$$

Details of the calculation are given in Sec. 2.5.3. An abridged version is provided in App. F.1.

We now set $\alpha_{1,2} = 1/2$. Performing the mass integrals using the kinematic threshold approximation gives

$$\mathrm{Im}\Pi_{\lambda\lambda}(z_1, z_2) \approx \lambda^2 \frac{\left(z_2 \cos\left(\frac{pz_2}{2}\right) \sin\left(\frac{pz_1}{2}\right) - z_1 \cos\left(\frac{pz_1}{2}\right) \sin\left(\frac{pz_2}{2}\right)\right)^2}{4\pi^3 \, k^4 \, z_1^2 z_2^2 (z_1^2 - z_2^2)^2} \,. \tag{2.151}$$

Finally, to complete the evaluation of the WKB function S in Eq. (2.146), we consider ImΠ

at same point $z_1 = z_2 = z$. Keeping the leading term in $pz \gg 1$ gives

$$\mathrm{Im}\Pi_{\lambda\lambda}(z,z) = \lambda^2 \frac{p^2}{64\pi^3 (kz)^4} \left(1 + O\left(\frac{1}{pz}\right)\right) \tag{2.152}$$

and

$$C_{\lambda\lambda}(z) = \frac{1}{6} + O\left(\frac{1}{pz}\right) . \tag{2.153}$$

We note $\mathrm{Im}\Pi_{\lambda\lambda}(z,z)$ has oscillating terms but they are subleading in $1/pz$ and thus do not appear in Eq. (2.152). The same feature is true in the other diagrams we evaluate.

$\Phi^3 - \Phi(\partial\Phi)^2$ Bubble

We evaluate the contribution to $\mathrm{Im}\Pi$ from the bubble induced by one $\lambda\Phi\Phi_1\Phi_2$ and one $\xi\Phi\partial_M\Phi_1\partial^M\Phi_2$ vertex. We get

$$\begin{aligned} \mathrm{Im}\Pi_{\lambda\zeta}(z_1,z_2) \supset & -\lambda\zeta \frac{z_2^2}{k^2\, z_1 z_2} \int dq_1 dq_2 q_1 q_2 \\ & \frac{1}{16\pi}\left(q_1^2 + q_2^2 - \frac{p^2}{2} - \partial_{z_2}\partial_{z_2}\right) J_{\alpha_1}(q_1 z_1) J_{\alpha}(q_1 z_2) J_{\alpha_2}(q_2 z_1) J_{\beta}(q_2 z_2) \\ & + \Big(1 \leftrightarrow 2\Big) . \end{aligned} \tag{2.154}$$

Details of the calculation are given in App. F.2. Taking $z_1 = z_2 = z$, $\alpha_{1,2} = 1/2$, and expanding for large pz, we obtain

$$\mathrm{Im}\Pi_{\lambda\zeta}(z,z) = \lambda\zeta \frac{p^4}{96\pi^3 (kz)^2} \left(1 + O\left(\frac{1}{pz}\right)\right) \tag{2.155}$$

and

$$C_{\lambda\zeta}(z) = \frac{2}{15} + O\left(\frac{1}{pz}\right) . \tag{2.156}$$

$\Phi(\partial\Phi)^2 - \Phi(\partial\Phi)^2$ **Bubble**

We evaluate the contribution from two $\xi\Phi\partial_M\Phi_1\partial^M\Phi_2$ vertices. Intermediate details of the derivation are similar to the other contributions but more cumbersome. Details are given in App. F.3. Proceeding similarly we get

$$\mathrm{Im}\Pi_{\xi\xi}(z,z) = \zeta^2\frac{113\,p^6}{46080\pi^3}\left(1+O\left(\frac{1}{pz}\right)\right) \tag{2.157}$$

and

$$C_{\xi\xi}(z) = \frac{213}{1582} + O\left(\frac{1}{pz}\right) . \tag{2.158}$$

2.6.5 Opacity from the Dressing

We have all the ingredients to describe the behaviour of the dressed propagator in the timelike, $pz_< \ll 1$, $pz_< \gg 1$ regime of Poincaré position-momentum space induced by the above bubble diagrams.

We plug the various contributions into the WKB formula Eq. (2.146) —which gives the argument of the exponential WKB ansatz. We integrate from a point z_0 to z with $z_0 \ll z$ and satisfying $pz_0 \gg 1$ such that the asymptotic behaviour is valid. Using the full functions, the contribution to $S(z)$ from $z_0 < 1/p$ should be negligible. The dependence on z_0 will be essentially irrelevant for our purposes, for concreteness we let $z_0 \sim 1/p$.

We obtain

$$S_{\lambda\lambda}(z) = -\sqrt{\frac{3}{2}}\frac{e^{-3}}{128\pi^{5/2}}\frac{\lambda^2}{k}\log(pz) \tag{2.159}$$
$$\approx -3\cdot 10^{-5}\,\frac{\lambda^2}{k}\log(pz)$$

$$S_{\lambda\zeta}(z) = -\sqrt{\frac{5}{6}}\frac{e^{-15/4}}{128\pi^{5/2}}\,\lambda\zeta k\,(pz)^2 \tag{2.160}$$
$$\approx -1\cdot 10^{-5}\,\lambda\zeta k\,(pz)^2$$

$$S_{\zeta\zeta}(z) = -\sqrt{\frac{791}{446}}\frac{11e^{-791/223}}{46080\pi^{5/2}}\,\zeta^2 k^3\,(pz)^4 \tag{2.161}$$
$$\approx -5\cdot 10^{-7}\,\zeta^2 k^3\,(pz)^4.$$

The z_0 dependence is negligible in $S_{\lambda\zeta}$, $S_{\zeta\zeta}$ because of $z_0 \ll z$.

Following the WKB analysis of Sec. 2.6.2, we conclude that the dressed propagator in the timelike region behaves as

$$G_p(z,z') \sim e^{S(z_>)}\,, \tag{2.162}$$

with S functions given by Eqs. (2.159)-(2.161). Neglecting the effect of $S_{\lambda\lambda}$ which varies very slowly, the dressed propagator is damped for

$$S_{\lambda\zeta}\left(pz|_{\text{opacity}}\right) \sim -1\,. \tag{2.163}$$

The condition Eq. (2.163) translates as a condition on pz for given couplings and AdS curvature—or vice-versa.

Hence we have found that the bubble diagrams found above dictate the exponential damping of the propagator in the IR region of timelike Poincaré position-momentum space.

In the propagator, when $pz_>$ gets larger than the value set by Eq. (2.163), the propagator gets exponentially suppressed, making the corresponding IR region effectively opaque to propagation.

Dimensional Analysis and EFT Censorship

We go further by using knowledge from the EFT paradigm, which provides estimate for the couplings. Dimensional analysis at strong coupling (*i.e.* "naive dimensional analysis", here denoted NDA) for an EFT in five dimensions dictates that [188–190]

$$\lambda \sim \sqrt{\ell_5 \Lambda}\,, \qquad \zeta \sim \sqrt{\frac{\ell_5}{\Lambda^3}} \tag{2.164}$$

where $\ell_5 = 24\pi^3$ is the 5D loop factor. Using Eq. (2.164) in $S_{\lambda\zeta}$, $S_{\zeta\zeta}$ we have

$$S_{\lambda\zeta} \approx -1 \cdot 10^{-5}\, \ell_5 \frac{k}{\Lambda}\,(pz)^2\,, \quad S_{\zeta\zeta} \approx -5 \cdot 10^{-7}\, \ell_5 \frac{k^3}{\Lambda^3}(pz)^4\,. \tag{2.165}$$

Λ and k can also be related by NDA. It was found in Ref. [3] that

$$\Lambda \gtrsim \pi k\,. \tag{2.166}$$

This condition follows from avoiding the strong coupling of momentum modes in the momentum spectral representation. This relation is also tied to the large N expansion in the dual CFT, see Eq. (2.170).

Taking $\Lambda \sim \pi k$, we find that the damping condition $S_{\lambda\zeta} \sim 1$ is attained for

$$pz|_{\text{opacity}} \sim 20\,. \tag{2.167}$$

For larger Λ, the value of pz for which the damping occurs gets larger.

But what of the contribution from the higher dimension operators? According to the standard EFT paradigm, all contributions should become the same order at the limit

of validity of the EFT. Thus by comparing $S_{\lambda\zeta}$ and $S_{\zeta\zeta}$, we robustly determine the validity region of the EFT. Using $\frac{\zeta}{\lambda} \sim \frac{1}{\Lambda^2}$, it turns out that $S_{\lambda\zeta} \sim S_{\zeta\zeta}$ for

$$(pz)^2 \sim 10\frac{\Lambda^2}{k^2}\,, \tag{2.168}$$

which makes the familiar z-dependent cutoff of Poincaré position-momentum space appear once again. For $\Lambda \sim \pi k$, the region of EFT breaking starts at $pz = O(10)$ and thus qualitatively matches the region of opacity. For $\Lambda > \pi k$, the damping occurs before the breaking of the EFT. This is because

$$pz|_{\text{opacity}} \propto \sqrt{\frac{\Lambda}{k}}\,, \qquad pz|_{\text{EFT breaking}} \propto \frac{\Lambda}{k}\,. \tag{2.169}$$

We conclude the damping induced by interactions prevents the propagator to enter the region of EFT breaking. In short, we can say that opacity *censors* the region of EFT breaking.[21] This is valid in particular for the boundary-to-bulk propagator.

A first sketch of these features was done in [110] and further insights were given in [3]. Censorship of the IR region for timelike momenta was also qualitatively predicted in [155]. Our analysis validates all of these conclusions.

Aside on the Dual CFT

Here we mention how the above quantities match to the dual CFT. Using dimensional analysis in the holographic action and comparing to correlators of a gauge theory

[21] Throughout we have used NDA on the renormalizable λ coupling. As an alternative scenario, one could assume that λ is smaller than its strong coupling estimate. In such case the region of EFT breaking cannot be obtained using the $S_{\lambda\zeta} \sim S_{\zeta\zeta}$ criterion. Instead the effect of a next-to-leading higher dimensional operator has to be evaluated and compared to *e.g.* $S_{\lambda\zeta}$ or $S_{\zeta\zeta}$. We expect similar conclusions regarding the exponential damping and EFT breakdown.

with adjoint fields, Ref. [3] finds

$$\frac{\pi k}{\Lambda} \sim \frac{1}{N^2} \tag{2.170}$$

where N is the number of colors. Hence the ubiquitous Λ/k ratio is directly related to N. $N \gg 1$ corresponds to $\Lambda \gg k$, in agreement with Eq. (2.166).

Qualitative Behavior for $\mathbf{AdS}_{d+1}$

Finally we comment about the behavior of the damping for other dimensions of spacetime. To estimate the behavior, we use the kinematic approximation Eq. (2.149), in which the scaling of the kinematic function is

$$\Xi(d, p, 0, 0) \propto p^{d-4}. \tag{2.171}$$

In addition, contributions from higher dimensional operators grow with higher powers of pz, coming from the extra derivatives in the vertices of the bubble. This knowledge is enough to estimate the behavior of $\mathrm{Im}\Pi$ in any dimension.

In $d = 4$, we have obtained that $S_{\lambda\lambda}$, $S_{\lambda\zeta}$, $S_{\zeta\zeta}$ grow respectively as $\log(pz)$, $(pz)^2$, $(pz)^4$, hence the leading contribution to the exponential damping comes from $S_{\lambda\zeta}$.[22] Notice that $S_{\lambda\zeta}$ is the leading contribution from the higher dimensional operators of the EFT, since the λ coupling is renormalizable in $d = 4$.

In $d > 4$ the contribution from the $\lambda\lambda$ bubble to the S function goes as $S \propto \lambda^2 (pz)^{d-4}$. Hence the exponential suppression already happens from the cubic coupling λ in these dimensions. For $d = 3$ the first polynomial contribution to S is from the $\lambda\zeta$ bubble, which grows as $\propto pz$. For $d = 2$, it is from the $\zeta\zeta$ bubble which grows as $\propto (pz)^2$.

[22] Notice the $S_{\zeta\zeta}$ contribution is of same order as a mixed contribution from the $\lambda\Phi\Phi_1\Phi_2$ and a higher dimensional operator such as $\Phi\partial_M\partial_N\Phi_1\partial^M\partial^N\Phi_2$.

We conclude that, for any dimension of spacetime, when considering an effective field theory in AdS—implying a tower of higher derivative operators, the interactions render the IR region of Poincaré position-momentum space opaque to propagation. Conversely, the IR region of EFT breakdown, which exists because of the presence of these higher derivative operators, gets censored. These features are summarized in Fig. 2.1.

2.6.6 Structure of Higher Order Diagrams

One may wonder what happens to the exponential damping when one takes into account higher order diagrams into account in the self-energy dressing the propagator. For instance the internal lines of the bubble considered so far are themselves dressed by bubble subdiagrams, and so on.

A convenient way to get the answer is to use the momentum spectral representation and introduce a UV and IR brane such that the momentum modes get discretized—they become the familiar Kaluza-Klein modes. The optical theorem can then be used in the regime of momentum where these modes are narrow.

Using this approach, it becomes clear that the contribution of higher order diagrams to $\mathrm{Im}\Pi$ appear when the mass integrals in Eq. (2.108) go beyond the leading order kinematic threshold, *e.g.* beyond the two-body threshold in case of a bubble. Instead of being cut at the two-body threshold, the integrand is now non zero for higher masses. These higher order regions of the integrand come with additional loop factor suppression—*i.e.* the additional phase space suppression in the halved diagram. The region of the mass integrals where the two-body channel is opened is essentially unaffected by these subleading corrections.

In summary, higher order corrections give small higher order additions to ImΠ, the main contribution to opacity comes from the leading order 1PI diagram. Using results from [3] on cascade topologies in the continuum regime where the branes become irrelevant, these conclusions generalize to the un-truncated Poincaré patch.

2.6.7 Application to Asymptotically AdS Backgrounds

Our study has been focused on the entire Poincaré patch $z \in [0, \infty]$ of AdS. In some models, the metric in the IR region can naturally get deformed and become singular. This is instrumental for AdS/QCD, see *e.g.* [191–200]. In many instances, models are built which truncate the UV and/or IR regions—leading to UV/IR branes. This well-known setup has applications across physics beyond the Standard Model, for *e.g.* recent holographic dark sector applications see [1, 24–27, 41].

How do our findings about AdS opacity apply to such deformed AdS backgrounds?

In the case of an IR brane, propagation to the brane will be exponentially damped at sufficiently high momentum, such that the propagators become agnostic of the IR region and do not know about the IR brane—neither in the spacelike regime, nor in the timelike regime (see earlier discussion in [3, 110]). This conclusion readily extends to asymptotically AdS backgrounds with an IR deformation which can be described as an effective IR brane as in [199].

In the presence of a UV brane, one can check using limits of the propagator from [3] that the effects of the UV brane on the propagator become negligible when the endpoints are away from it. Whenever one of the endpoints of the propagator is away from the UV brane, the locality property of ImΠ dictates that both endpoints of the relevant dressing

diagrams will be away from the brane. The exponential damping is usually relevant deep in the IR, and hence the existence of the UV brane is irrelevant and our conclusions hold.

A wide class of backgrounds is described by a conformally flat metric of the form

$$ds^2 = e^{-2A(z)} \left(\eta_{\mu\nu} dx^\mu dx^\nu - dz^2 \right) . \tag{2.172}$$

In particular, deformed AdS backgrounds typically admit such a description. [23] Like in Poincaré position coordinates, this metric has d-dimensional Poincaré isometries in the x^μ coordinates. Hence for an arbitrary warping $A(z)$ we can Fourier-transform to position-momentum space (p^μ, z) as we did in the exact AdS case. This implies that the canonical and spectral representations of the propagator may be used in more general backgrounds. The last remaining ingredient is to obtain the solution of the Fourier-transformed free EOM. In any case, the split structure of the spectral functions should automatically hold throughout, as explained in Sec. 2.3.

In summary, we conclude that our results on opacity of the Poincaré momentum-space apply to a broad range of deformed/truncated AdS backgrounds, and that our formalism itself may also be generalized to other metrics of the form Eq. (2.172).

2.7 Opacity from Gravity in AdS_5

Even if cubic matter interactions are absent—which could happen for symmetry reasons or if they are vanishing/negligible altogether, there is always a cubic interaction between AdS gravity and matter. This is true for any matter field since the graviton couples linearly to the matter stress tensor as $h_{MN} T^{MN}$. Hence bulk gravity always produces a

[23] This metric appears in certain 5D supergravities, see *e.g.* [201].

bubble contribution to the self-energy of a matter field, thereby inducing a universal, 1-loop contribution to the "opacity" of the IR region (see discussions in Sec. 2.6).

For this work we consider propagation of a scalar field and we focus only on the $d = 4$ case. In $d = 4$, the bulk graviton splits into five degrees of freedom, two of helicity-two, two of helicity-one, one of helicity-zero, each with their own coupling to the stress-energy tensor. The trace of the metric is a non-physical, ghosty degree of freedom which also contributes to the loop. We closely follow the formalism of [202]. [24]

The pure gravity part of the action is

$$S_{\rm EH} = M_*^3 \int d^5X \sqrt{g} \left(\mathcal{R} - \Lambda_5\right) \tag{2.173}$$

with $\Lambda_5 = -12k^2$. The canonically normalized metric fluctuation around the AdS background γ_{MN} is defined by

$$g_{MN} = \gamma_{MN} + \sqrt{\frac{2}{M_*^3}} h_{MN} \,. \tag{2.174}$$

The expansion of the gravity action Eq. (2.173) up to quadratic order is well-known (see *e.g.* [203, 204]), giving the action for the 5d graviton h_{MN},

$$\begin{aligned} S^h = \int d^5X \sqrt{\gamma} \Bigg(& \frac{1}{2} \nabla_R h_{MN} \nabla^R h^{MN} - \frac{1}{2} \nabla_R h \nabla^R h + \nabla_M h^{MN} \nabla_N h \\ & - \nabla_M h^{MN} \nabla^R h_{RN} + k^2 (h_{MN}^2 + h^2) + \sqrt{\frac{1}{2M_*^3}} h^{MN} T_{MN} \Bigg) \end{aligned} \tag{2.175}$$

where

$$T_{MN} = -2 \frac{\delta \mathcal{L}_\Phi}{\delta \gamma^{MN}} + \gamma_{MN} \mathcal{L}_\Phi \,. \tag{2.176}$$

Following [202], all degrees of freedom of the graviton can be disentangled using field redefinitions and Faddeev-Popov gauge fixing. Defining $\hat{h}_{MN} = (kz)^2 h_{MN}$ then splitting the

[24] Except that we use the opposite metric signature.

graviton components as

$$\widetilde{h}_{\mu\nu} = \hat{h}_{\mu\nu} - \frac{1}{4}\eta_{\mu\nu}h^{\rho}_{\rho}\,, \quad B_\mu = \frac{\sqrt{2}}{kz}\hat{h}_{\mu 5}\,, \quad \chi = \frac{1}{2}\left(\hat{h}^{\mu}_{\mu} - 2\hat{h}_{55}\right)\,, \quad \phi = \frac{\sqrt{3}}{\sqrt{2}(kz)^2}\hat{h}_{55}\,, \tag{2.177}$$

and defining the sources

$$\widetilde{T}_{\mu\nu} = T_{\mu\nu} - \frac{1}{4}\eta_{\mu\nu}T^{\rho}_{\rho}\,, \quad \widetilde{T}_{55} = T_{55} + \frac{1}{2}T^{\rho}_{\rho}\,, \tag{2.178}$$

the graviton action $S^h = \int dx^M \mathcal{L}^h$ takes the simple form

$$\begin{aligned}\mathcal{L}^h =& \frac{1}{2}\left(\frac{1}{(kz)^3}(\partial_R\widetilde{h}_{\mu\nu})^2 + \frac{1}{kz}(\partial_R B_\mu)^2 + kz(\partial_R\phi)^2 - \frac{1}{(kz)^3}(\partial_R\chi)^2\right) \\ &+ \frac{1}{\sqrt{M_*^3}}\left(\frac{1}{\sqrt{2}(kz)^3}\widetilde{h}^{\mu\nu}\widetilde{T}_{\mu\nu} + \frac{1}{(kz)^2}B^\mu T_{\mu 5} + \frac{1}{2\sqrt{2}(kz)^3}\chi T^{\mu}_{\mu} + \frac{1}{\sqrt{3}kz}\phi\widetilde{T}_{55}\right)\,.\end{aligned} \tag{2.179}$$

In Eqs. (2.177)-(2.179) all contractions are done with the Minkowski metric. As expected the χ field has "wrong-sign" kinetic term and is an unphysical degree of freedom. Its contribution naturally combines with the one of the $\widetilde{h}_{\mu\nu}$ field.

The graviton degrees of freedom in Eq. (2.179) are diagonal, hence their contributions to the self-energy are disentangled such that

$$\mathrm{Im}\,\Pi_p(z,z') = \mathrm{Im}\,\Pi^h_p(z,z') + \mathrm{Im}\,\Pi^B_p(z,z') + \mathrm{Im}\,\Pi^\phi_p(z,z') + \mathrm{Im}\,\Pi^\chi_p(z,z')\,. \tag{2.180}$$

In this work we focus on the contribution of the scalar component ϕ of the graviton multiplet. The Feynman propagator of ϕ is given by

$$G^\phi(z,z') = \frac{\pi}{2k}J_0(pz_<)H^{(1)}_0(pz_>) \tag{2.181}$$

with $\langle\phi(p,z)\phi(p',z')\rangle = G^\phi(z,z')(2\pi)^4\delta^{(4)}(p^\mu - p'^\mu)$.

The stress-energy tensor of the bulk scalar Φ is

$$T_{MN} = -\partial_M\Phi\partial_N\Phi + \frac{1}{2}\gamma_{MN}\left(\partial_R\Phi\partial^R\Phi - m^2_\phi\Phi^2\right)\,, \tag{2.182}$$

giving the source

$$\widetilde{T}_{55} = -\frac{3}{2}(\partial_5\Phi)^2 - \frac{1}{2\,(kz)^2}m_\Phi^2\Phi^2\,, \tag{2.183}$$

which couples to the ϕ component of the graviton multiplet. Using integration by parts, we rewrite the relevant term of the Lagrangian as

$$\mathcal{L}^h \supset \Phi\partial_5\left(\frac{\sqrt{3}}{2kz\sqrt{M_*^3}}\phi\partial_5\Phi\right) - \frac{m_\Phi^2}{2(kz)^3\sqrt{3M_*^3}}\phi\Phi^2. \tag{2.184}$$

We perform the graviton loop calculation in App. F.4. We find

$$\begin{aligned}\mathrm{Im}\Pi^\phi(z_1,z_2) = \frac{1}{48\pi\,M_*^3}\left(\frac{m_\Phi^2}{2(kz_1)^2} - \frac{3}{2}\partial_{z_1}\partial_{z_1}^{G_\Phi}\right)\left(\frac{m_\Phi^2}{2(kz_2)^2} - \frac{3}{2}\partial_{z_2}\partial_{z_2}^{G_\Phi}\right) \\ \frac{1}{z_1z_2}\int dq_1dq_2q_1q_2\left[z_1^2z_2^2J_\alpha(q_1z_1)J_\alpha(q_1z_2)\right]J_0(q_2z_1)J_0(q_2z_2)\,.\end{aligned} \tag{2.185}$$

Here the $\partial_z^{G_\Phi}$ derivatives act on the internal Φ propagator only (*i.e.* only the term in square brackets), whereas the ∂_z derivatives act on everything to the right.

Using the WKB approximation scheme introduced and justified in Sec. 2.6, we then obtain

$$\mathrm{Im}\Pi^\phi(z,z) = \kappa^2\frac{7\,p^6}{30720\pi^3\,k^3}\left(1+O\left(\frac{1}{pz}\right)\right) \tag{2.186}$$

$$C^\phi(z) = \frac{24}{49} + O\left(\frac{1}{pz}\right), \tag{2.187}$$

where we have introduced the 5D gravity coupling strength

$$\kappa \equiv \sqrt{\frac{k^3}{M_*^3}} = \frac{k}{M_{Pl}}\,. \tag{2.188}$$

This contribution is similar to the effect from the $\Phi(\partial\Phi)^2 - \Phi(\partial\Phi)^2$ scalar bubble—which is not surprising since the number of derivatives in the vertices is the same. The argument of the exponential of the WKB ansatz given by Eq. (2.146) is found to be

$$S^{\phi}(z) = -\frac{49e^{-49/48}}{491520\sqrt{3}\pi^{5/2}}\,\kappa^2\,(pz)^4 \tag{2.189}$$
$$\approx -1\cdot 10^{-6}\,\kappa^2\,(pz)^4$$

This shows explicitly that bulk gravity itself induces opacity of the IR region in Poincaré position-momentum space, *i.e.* $G_p(z,z') \sim e^{S^{\phi}(z_>)}$. The contribution is universal in the sense that it depends only on the strength of the AdS gravity coupling κ.[25]

In five dimensions, the gravity Lagrangian is understood as an EFT from which the leading term is the Einstein-Hilbert one. Studying higher order effects from the graviton EFT would require one to include the effect of higher dimension interactions such as $\mathcal{R}\mathcal{L}_{\text{matter}}$. This is beyond the scope of this work, in which the main focus has been on scalar fields. Since we do not attempt to evaluate higher order contributions from the EFT, we do not comment on the interplay between EFT breakdown and IR opacity in this section. It would be interesting to check if the superPlanckian region is censored as a result of opacity from graviton loops, along the lines of Sec. 2.6.5.

2.8 Discussion

In this work, we have investigated how quantum dynamics affects the propagation of a scalar field in Lorentzian AdS_{d+1}. Our main results are presented in Sec. 2.2.2. This section contains a summary, comments on the implications of this work and possible future directions.

[25] 5D dimensional analysis shows that the maximal value of κ is $O(1)$ to avoid higher curvature terms. For completeness we also remind that $\kappa^2 \sim \frac{1}{N^2}$ when matching the theory to a 4D CFT [19].

In the first part of this work, we studied the simplest scalar bubble in momentum-position space. Different objects appear depending on the representation used. In the canonical representation, loop integrals with non-integer powers are the key ingredient. In the momentum spectral representation, a generalized two-body kinematic threshold emerges. In the conformal spectral representation, AdS/CFT arises: CFT correlators naturally appear and combine to form a CFT bubble diagram.[26] By direct computation, we find that the conformal spectral result for ImΠ takes the form of a sum over double-trace propagators, with coefficients that match exactly those from [79, 160]. We have provided explicit equivalence proofs between these representations.

We prove a number of global and asymptotic properties of the imaginary part of the bubble via the various representations. Asymptotics and convenient approximations are best obtained in the momentum spectral representation. In particular this representation shows that ImΠ tends to be peaked at large pz.

To study concretely how loops affect propagation in AdS, we directly solve the dressed equation of motion. To do so, we introduce a WKB-type method adapted to a convolution term $\Pi * G^{(0)}$ and use a saddle-point approximation of ImΠ. The most interesting regime is when the propagator endpoints satisfy $pz_< \ll 1$, $pz_> \gg 1$, which includes the boundary-to-bulk propagators with $pz \gg 1$ as a particular case. This regime has no flat-space equivalent—the $pz \ll 1$ region vanishes if one Weyl-transforms to flat space.

We adopt the EFT viewpoint in which Lagrangians contain an infinite series of

[26] We obtained the anomalous dimension via resummation and verified that it matches exactly the one found in [93] by another method.

higher dimensional operators and evaluate the effect of bubbles from leading and next-to-leading operators in AdS_5. We find that interactions of high-enough order in the bulk of AdS induce an exponential damping of the propagator for timelike momentum at large pz. The damping renders the IR region of the Poincaré patch opaque to propagation. This exponential damping is similar to the one induced by the Feynman $i\epsilon$ prescription in the free case. We thus conclude that loop corrections are consistent with the $i\epsilon$ prescription.

By definition, an EFT breaks down when higher dimensional operators give contributions of the same order. In AdS this occurs at sufficiently large pz, *i.e.* in the IR region of the Poincaré patch. Estimating the operator coefficients using standard dimensional analysis, we find that the region of EFT breakdown falls behind the region of exponential suppression, meaning that this region is effectively *censored*. A qualitative generalization to AdS_{d+1} is presented.

A first sketch of these features was proposed in [110]. Censorship of the IR for timelike momenta was also qualitatively predicted in [155], though the mechanism by which their predicted behavior occurs is fundamentally different. Our analysis validates all of these conclusions.

The damping behavior observed is not unique to AdS, it may occur in any space-time background whenever the self-energy of the propagating field develops an imaginary part. In flat space such damping is associated to decaying particles via the S-matrix optical theorem, but such interpretation is not required in general—as exemplified by our AdS findings. The key aspect is rather that Π develop an imaginary part in some region.

Going beyond scalar loops, we have evaluated a contribution from the leading

graviton loop in AdS_5. Opacity of the IR region again occurs, and depends only on the strength of AdS gravity controlled by $k/M_{\rm Pl}$. We do not comment on EFT breaking in this context since it would require to evaluate the effect of graviton-matter vertices from higher dimensional operators.

2.8.1 Possible Implications and Future Directions

There are some immediate extensions to our study. It would be interesting to derive the approximate behavior of the dressed propagator as obtained in Sec. 2.6 from the conformal spectral representation as given in Sec. 2.4. Other directions include the study of propagating fields with non-zero spin or to investigate the effect of a larger variety of self-energies including those from fermion or graviton loops.

The formalism developed here for AdS may be useful for more general backgrounds—namely those admitting a warped, conformally-flat metric of the form described in Eq. (2.172). A direct consequence of working in the Poincaré momentum space (p^μ, z) is that the propagators have a split structure in pz, pz', both in the spectral representations and in the canonical one. Moreover, whenever the solutions to the free EOM in momentum-position space are analytical, we can expect the various representations (canonical, conformal and momentum spectral) of the propagator to have analytical expressions.

This study has been focused on AdS_{d+1}. We have essentially not discussed aspects of the dual CFT, apart from using some basic elements which naturally arise in the calculations. The bubble topology is the simplest loop diagram, and as such may be seen as a laboratory to study unitarity in AdS. AdS/CFT unitarity methods have recently been developed [114, 158]. Our detailed analysis of $\mathrm{Im}\Pi$ in its various forms could be useful in

these types of studies. [27]

On a more phenomenological note, our results on the exponential damping of the propagator may have implications for extensions of the Standard Model of particles. This is for example relevant for extra-dimensional and holographic dark sector models. Consider the so-called "slice of AdS"—in which there are UV and IR branes that truncate the bulk. Our results indicate that particles in the UV cannot propagate to the IR brane if they have sufficiently high absolute 4-momentum—either timelike or spacelike. This gives rise to the concept of an *emergent* sector which can only interact at sufficiently small values of absolute 4-momentum, as discussed in [3]. This is discussed in more detail in chapter 3.

Our work may have implications for AdS/QCD, since timelike bulk processes are related to timelike fragmentation functions in the gauge theory. One may note that opacity of AdS in the spacelike regime played a role in the AdS/CFT deep-inelastic study of [205]. Hence timelike opacity should also be important in the study of the cross-symmetric process, *e.g.* e^+e^- annihilation into states of the strongly-coupled gauge theory.

[27] We have found that $\mathrm{Im}(\mathbf{Cut}\Pi) = \mathbf{Cut}(\mathrm{Im}\Pi) = \mathrm{Im}\Pi$, where the AdS **Cut** operation acts on poles in the conformal spectral representation. We have also found that upon cutting the bubble in the momentum spectral representation, we obtain the imaginary part in the canonical representation.

Chapter 3

Soft Bombs and the Continuum Regime of AdS

3.1 Chapter Abstract

We consider a scalar field in a slice of Lorentzian five-dimensional AdS at arbitrary energies. We show that the presence of bulk interactions separate the behavior of the theory into two different regimes: Kaluza–Klein and continuum. We determine the transition scale between these regimes and show that UV brane correlation functions are independent of IR brane-localized operators for four-momenta beyond this transition scale. The same bulk interactions that induce the transition also give rise to cascade decays. We study these cascade decays for the case of a cubic self-interaction in the continuum regime. We find that the cascade decay progresses slowly towards the IR region and gives rise to soft spherical final states, in accordance with former results from both gravity and CFT. We

identify a recursion relation between integrated squared amplitudes of different leg numbers and thus evaluate the total rate. We find that cascade decays in the continuum regime are exponentially suppressed. This feature completes the picture of the IR brane as an emergent sector as seen from the UV brane. We briefly discuss consistency with the holographic dual description of glueballs and some implications for dark sector models.

3.2 Introduction

The overarching idea throughout this chapter is that the bulk correlators effectively lose contact with the IR brane above some specific value of momentum $p > \widetilde{\Lambda}$. At the qualitative level, this can be argued from the breakdown of the effective theory in the IR region (using e.g. Refs. [155, 186]). Quantitatively, this requires one to account for bulk loops that dress the propagator [110]. Throughout this chapter we say that the IR brane *effectively emerges* for bulk correlators as their energy is decreased through the $p \sim \widetilde{\Lambda}$. transition.

We begin our study by outlining the regimes of field theory in a slice of 5D AdS, as obtained in this chapter. The fundamental scales fixed by geometry are the AdS curvature, k, and the IR brane position, $1/\mu$. The Kaluza–Klein scale is $\mu \ll k$ and represents the mass gap in the dual gauge theory. In the presence of interactions, the theory has a 5D cutoff Λ and a transition scale $\widetilde{\Lambda}$ that is explained below. These have a hierarchy $\Lambda > k > \widetilde{\Lambda} > \mu$ that define four different energy regimes:

- 4D regime, $E < \mu$. In this limit, Kaluza–Klein modes are integrated out and only sufficiently light 4D modes such as gauge or Goldstone bosons remain in the spectrum.

- Kaluza–Klein regime, $\mu < E < \widetilde{\Lambda}$. The theory in this regime has a tower of regularly spaced narrow resonances. The resonances in this energy window are narrow glueballs in the dual gauge theory.

- Continuum regime, $\widetilde{\Lambda} < E < k$. In this regime, the effective theory breaks down in the IR region of AdS. Quantum corrections mix the KK modes and merge them into a continuum. An observer on the UV brane effectively sees pure AdS. The theory can equivalently be described by a holographic CFT with no mass gap.

- Flat space regime, $k < E < \Lambda$. Here the curvature of AdS becomes negligible, and KK modes from any other compact dimensions appear. No simple CFT dual is expected in this regime.

One may conjecture that for $p \gg \widetilde{\Lambda}$, the theory is described by an effective Lagrangian without an IR brane. As described in the introductory chapter, a workaround to this conjecture may be possible via bulk cascade diagrams (i.e. soft bombs). A cascade diagram can split the energy of an individual state in the continuum regime into many offspring states reaching into the KK regime. The evaluation of the rate for such event would imply that the high energy theory already knows about the IR brane, which would invalidate the proposal that there is effectively no IR brane in the continuum regime. A careful investigation of the soft bomb rates is thus required.

In summary, this chapter *i)* establishes the existence of a continuum regime in the presence of interactions and *ii)* studies soft bomb events in this regime. The chapter is organized as follows. Section 3.3 establishes the basic five-dimensional formalism in a slice of AdS. In particular, we present the classical propagator for a scalar field in mixed

position–momentum space. Interactions in the bulk of AdS play a central role in our study. Section 3.4 provides the necessary tools for dimensional analysis at strong coupling. In Section 3.5, we dress the propagator with quantum corrections. The imaginary part of the self-energy induces distinct KK and continuum regimes. The transition scale is understood both qualitatively from the viewpoint of effective theory validity and from the viewpoint of the opacity of the IR region resulting from the dressing of the propagator by bulk fields. In Section 3.6 we identify a recursion relation that relates the continuum-regime cascade decay rates with arbitrary number of legs. Section 3.7 presents the general picture of soft bomb events in the continuum regime. Building on this, we spell out the notion of IR brane emergence. Asymptotically AdS backgrounds and implications for holographic dark sectors are also discussed. In Section 3.8 we connect our analysis to strongly coupled gauge theories using AdS/CFT. We discuss CFT soft bombs, establish the relation between bulk matter interactions and large-N expansion, and analyse the transition scale in the EFT of glueballs. Conclusions are given in Sec. 3.9.

3.3 A Bulk Scalar in a Slice of AdS

In studies of the gravity–scalar system, a general ansatz for the metric preserving the 4D Poincaré invariance is

$$ds^2 = g_{MN}\, dX^M dX^N = e^{-2A(y)}\eta_{\mu\nu}dx^\mu dx^\nu - dy^2 \ , \tag{3.1}$$

where $\eta_{\mu\nu}$ is the 3+1-dimensional Minkowski metric with $(+,-,-,-)$ signature. This metric appears in certain 5D supergravities, see *e.g.* [201]. It can depart from AdS and develop a singularity at large y, beyond which spacetime ends, see *e.g.* [191–193, 196, 198, 199]. In

other classes of models, an IR brane truncating the y coordinate is explicitly included. In this paper we focus on the simplest example of a slice of AdS for which the metric is exactly anti-de Sitter. Using the conformally flat coordinates $z = e^{ky}/k$, the metric is

$$ds^2 = g_{MN}\, dX^M dX^N = (kz)^{-2} \left(\eta_{\mu\nu} dx^\mu dx^\nu - dz^2\right) \ . \tag{3.2}$$

Space is truncated at endpoints

$$z_{\rm UV} = k^{-1} \qquad \text{and} \qquad z_{\rm IR} = \mu^{-1} > z_{\rm UV} \ , \tag{3.3}$$

which correspond to the positions of a UV and IR brane, respectively.

3.3.1 Action

A generic effective theory on this background involves gravitons and matter fields of different spins. In this manuscript we focus on the case of a scalar field Φ with non-derivative, cubic interactions. We expect that the results of this study generalize readily to any other type of field. The action for this field is

$$S = \int d^5X \sqrt{g} \left(\frac{1}{2} \nabla_M \Phi \nabla^M \Phi - \frac{1}{2} m_\Phi^2 \Phi^2 + \frac{1}{3!} \lambda \Phi^3 \right) + S_{\rm UV} + S_{\rm IR} + \cdots \tag{3.4}$$

where we explicitly write the kinetic, mass and interaction terms. The ellipses denote additional contributions from gravity and higher-dimensional operators that are suppressed by powers of the effective theory's cutoff. A convenient parameterization of the scalar mass is

$$m_\Phi^2 \equiv (\alpha^2 - 4) k^2 \ . \tag{3.5}$$

The Breitenlohner-Freedman bound requires $\alpha^2 \geq 0$ [206, 207]. In this chapter we routinely take α to be non-integer. The actions $S_{\rm UV}$ and $S_{\rm IR}$ encode brane-localized operators. These

can include mass terms for the scalar which are conveniently parameterized with respect to dimensionless parameters $b_{\rm UV}$ and $b_{\rm IR}$ as (see, e.g. [188]),

$$S_{\rm UV} + S_{\rm IR} \supset \frac{1}{2}\int d^5X\sqrt{\bar{g}}\left[(\alpha - 2 - b_{\rm UV})k\delta(z - z_{\rm UV}) - (\alpha - 2 + b_{\rm IR})k\delta(z - z_{\rm IR})\right]\Phi^2 \,. \tag{3.6}$$

We leave these parameters unspecified and simply assume that $b_{\rm UV} \neq 0$. There is a special mode in the spectrum with mass $\sim b_{\rm UV}k$. For $b_{\rm UV}$ sufficiently small, this mode may affect the physical processes studied here. We assume this special mode is heavy such that it is irrelevant in our analysis. $\bar{g}_{\mu\nu}$ is the induced metric on the brane so that $\sqrt{\bar{g}} = (kz)^{-4}$. Other degrees of freedom may be localized on the brane and interact with Φ. [1] In the context of our analysis, such brane modes provide asymptotic states for the bulk scattering amplitudes.

3.3.2 The Scalar Propagator

The classical equation of motion obtained by varying the bulk action for the scalar field, Φ, is

$$D\Phi \equiv \frac{1}{\sqrt{g}}\partial_M(g^{MN}\sqrt{g}\partial_N\Phi) + m_\Phi^2\Phi = 0 \,. \tag{3.7}$$

The Feynman propagator is the Green's function of the D operator,

$$D_X\Delta(X, X') = \frac{-i}{\sqrt{g}}\delta^{(5)}(X - X') \,. \tag{3.8}$$

[1] There are hints that a brane-localized degree of freedom always arises from a bulk field and is thus necessarily accompanied by a tower of Kaluza-Klein modes [162]. This tower can be decoupled from the brane so that it is consistent to consider only the brane-localized mode.

Rather than work in position-space coordinates, $X^M = (x^\mu, z)$, we Fourier transform along the 4D Minkowski slices: $\Phi_p(z) \equiv \int e^{i\eta_{\mu\nu}x^\mu p^\nu}\Phi(x^\mu, z)$. We call this Poincaré position-momentum space. The AdS dilatation isometry becomes $(p^\mu, z) \to (p^\mu/\lambda, \lambda z)$ so that pz is an invariant. Here p is the Minkowski norm $p = \sqrt{\eta_{\mu\nu}p^\mu p^\nu}$, which is real (imaginary) for timelike (spacelike) four-momentum, p^μ. In these coordinates, the propagator is, see *e.g.* [162],

$$\Delta_p(z,z') = i\frac{\pi k^3 (zz')^2}{2}\frac{\left[\widetilde{Y}_\alpha^{UV} J_\alpha(pz_<) - \widetilde{J}_\alpha^{UV} Y_\alpha(pz_<)\right]\left[\widetilde{Y}_\alpha^{IR} J_\alpha(pz_>) - \widetilde{J}_\alpha^{IR} Y_\alpha(pz_>)\right]}{\widetilde{J}_\alpha^{UV}\widetilde{Y}_\alpha^{IR} - \widetilde{Y}_\alpha^{UV}\widetilde{J}_\alpha^{IR}}\,, \quad (3.9)$$

where $z_{<,>}$ is the lesser/greater of the endpoints z and z'. The p-dependent quantities $\widetilde{J}^{UV,IR}$ are

$$\widetilde{J}_\alpha^{UV} = \frac{p}{k}J_{\alpha-1}\left(\frac{p}{k}\right) - b_{UV}J_\alpha\left(\frac{p}{k}\right) \qquad \widetilde{J}_\alpha^{IR} = \frac{p}{\mu}J_{\alpha-1}\left(\frac{p}{\mu}\right) + b_{IR}J_\alpha\left(\frac{p}{\mu}\right), \quad (3.10)$$

with similar definitions for $\widetilde{Y}^{UV,IR}$.

For timelike momentum, the propagator (3.9) has poles set by the zeros of the denominator. This propagator can always be written formally as an infinite sum over 4D poles. Let us introduce the matrix notation

$$\mathbf{f}(z) = [\, f_n(z)\,] \qquad \mathbf{D} = \left[\, \frac{\delta_{nr}}{p^2 - m_n^2}\,\right], \quad (3.11)$$

where $\mathbf{f}$ is a one-dimensional infinite vector and $\mathbf{D}$ is an infinite diagonal matrix indexed by the Kaluza–Klein (KK) numbers n and r. The propagator in the Kaluza-Klein representation is

$$\Delta_p(z,z') = i\,\mathbf{f}(z)\cdot\mathbf{D}\cdot\mathbf{f}(z')\,. \quad (3.12)$$

Amplitude calculations often feature sums over KK modes. We can represent these sums as contour integrals [110],

$$\sum_{n=0}^{\widetilde{n}} U(m_n) f_n(z) f_n(z') = -\frac{1}{2\pi} \oint_{\mathcal{C}[\widetilde{n}]} dq^2 U(q^2) \Delta_q(z, z') \ , \tag{3.13}$$

where the contour $\mathcal{C}\left[\widetilde{n}\right]$ in momentum space encloses the first $\widetilde{n}$ poles. U can be any function that does not obstruct the contour with singularities. The identity (3.13) is a useful link between the KK and closed form representations of the propagator.

3.4 Interactions: Dimensional Analysis

A key ingredient of our study is the magnitude of the couplings of the bulk scalar from an effective field theory (EFT) perspective. In the presence of interactions, a five-dimensional theory is understood to be an EFT with some ultraviolet cutoff Λ beyond which the EFT becomes strongly coupled. This cutoff is tied to the strength of interactions through dimensional analysis in the strong coupling limit through so-called naïve dimensional analysis (NDA) [189, 208–211]; see e.g. [188] for a pedagogical introduction of NDA to 5D theories. The crux of this analysis is to compare amplitudes of different loop order or involving higher dimensional operators. Let us define the loop factors

$$\ell_5 = 24\pi^3 \qquad \text{and} \qquad \ell_4 = 16\pi^2 \ . \tag{3.14}$$

3.4.1 Gravitational Interactions

The interactions of the graviton in AdS is controlled by the dimensionless coupling

$$\kappa = \frac{k}{M_{\rm Pl}} \, . \tag{3.15}$$

The reduced 4D and 5D Planck masses are related by $M_5^3 = M_{\rm Pl}^2 k$. By NDA, the cutoff in the gravity sector

$$\Lambda_{\rm grav}^3 = \ell_5 M_5^3 = \ell_5 \kappa M_{\rm Pl}^3 \ . \tag{3.16}$$

In order to keep higher order gravity terms under control, κ should be at most $\mathcal{O}(1)$ [189, 190].

The gravity cutoff $\Lambda_{\rm grav}$ is sometimes taken as a universal scale setting the strength of all interactions in the effective Lagrangian. However, in the EFT the typical strength of interactions in various sectors can in principle be different with different strong coupling scales. Strongly-interacting matter cannot influence the strength of gravity, which is protected by diffeomorphism invariance and set by the background geometry. In particular, matter interactions are at least as strong as gravity. The strong coupling scale of pure matter interactions can thus be lower than $\Lambda_{\rm grav}$. Notice that gravity can even be removed, $M_{\rm Pl} \to \infty$, while the matter cutoff remains unchanged. [2]

3.4.2 Matter Interactions

We assume that a universal cutoff Λ sets the strength of interactions in the matter sector of our theory. To make this connection manifest in D-dimensions, one writes the fundamental action in terms of dimensionless fields $\hat{\Phi}$ with ℓ_D factored out [188, 189]:

$$S_D = \frac{N_s \Lambda^D}{\ell_D} \int d^D X \hat{\mathcal{L}} \left[\hat{\Phi}, \partial/\Lambda \right] \ . \tag{3.17}$$

[2] In a UV completion, the Λ, $\Lambda_{\rm grav}$ scales would likely be correlated and a fine-tuning might be needed to separate these scales.

N_s counts the number of species in the Lagrangian; for the present study we set $N_s = 1$. NDA states that an $\mathcal{O}(1)$ coupling in $\hat{\mathcal{L}}$ corresponds to a strong interaction strength. The dimensionful Lagrangian is recovered by canonically normalizing the fields. For the case of a cubic interaction, the NDA coupling dictated by (3.17) is $\lambda \sim (\ell_5 \Lambda)^{1/2}$.

The gravitational cutoff Λ_{grav} is related to the AdS curvature k through (3.15) and (3.16). One may determine a similar relation between the matter cutoff Λ and k by considering the effective 4D interactions between specific KK modes. When expanding the 5D field in terms of canonically normalized 4D modes, $\Phi = kz \sum_n \widetilde{f}_n(z)\phi_n(x)$, one finds that $\widetilde{f}_n(1/\mu)$ is of order $\sqrt{k}$.[3] Because KK modes are localized towards the IR brane, this implies that the order of magnitude of an effective 4D coupling between KK modes is obtained from the 5D coupling by multiplying by powers of $\sqrt{k}$ and the warp factor $w = \mu/k$. For a given KK mode, the 4D NDA action is

$$S_{\text{KK}} = \frac{w^4 \Lambda^4}{\ell_4} \int d^4x \hat{\mathcal{L}} \left[\hat{\phi}, \partial/(w\Lambda) \right] \tag{3.18}$$

following the same conventions of (3.17). Notice that the cutoff only appears through the warped down cutoff scale $w\Lambda = \widetilde{\Lambda}$; we discuss this feature in Section 3.5.1.

Consider a general monomial interaction $\lambda_{5\text{D}} \Phi^n / n!$ in the 5D action with $n > 2$. 5D NDA, (3.17), reveals that the strong coupling coefficient is

$$\lambda_{5\text{D}} = {\ell_5}^{n/2-1} \Lambda^{5-3n/2} \,. \tag{3.19}$$

An interaction between n KK modes with $\mathcal{O}(1)$ dimensionless couplings is then

$$\lambda_{4\text{D}} \sim {\ell_5}^{n/2-1} \Lambda^{5-3n/2} k^{n/2-1} w^{4-n} \,. \tag{3.20}$$

[3]The KK mode normalization is $\int dz (kz)^{-1} \widetilde{f}_n(z) \widetilde{f}_m(z) = \delta_{mn}$. One has $\widetilde{f}_m(z) = (kz)^{-1} f_m(z)$, where the f_m are introduced in Sec. 3.3.

On the other hand, the 4D NDA value for λ_4 is

$$\lambda_4 = {\ell_4}^{n/2-1} \Lambda^{4-n} w^{4-n} \,. \tag{3.21}$$

For the effective theory of KK modes to be valid, one must require the effective λ_4 in (3.20) to be smaller than or equal to its strong coupling estimate, (3.21). This implies

$$\Lambda > \frac{\ell_5}{\ell_4} k \,. \tag{3.22}$$

This universal relation arises because the $\sqrt{k}$ and the loop factors have the same powers in the NDA estimates, which are in turn fixed by field counting. When (3.22) is not saturated, the effective 4D couplings of KK monomials are suppressed by powers of $(\ell_5 k/\ell_4 \Lambda)^{1/2}$ with respect to their strong coupling value. This systematic suppression factor is reminiscent of the large N suppression in the dual CFT, see Section 3.8.2.

3.4.3 Value of the Cubic Coupling

In this chapter we consider a scalar field, whose natural mass scale would be $\mathcal{O}(\Lambda)$, as reflected by NDA. While the NDA value of the cubic coupling is $\lambda \sim (\ell_5 \Lambda)^{1/2}$, for this manuscript we set it to a smaller value

$$\lambda \sim m_\Phi \frac{\ell_5^{1/2}}{\Lambda^{1/2}} \,. \tag{3.23}$$

This value is consistent with a bulk mass parametrically lower than Λ: the self-energy bubble diagram from λ gives a $\mathcal{O}(m_\Phi^2)$ contribution, in accordance with NDA. The λ coupling tends to zero in the free limit $\Lambda \to \infty$ (i.e. $N \to \infty$) as it should.

3.5 The Kaluza–Klein and Continuum Regimes of AdS

We study the behavior of the effective theory using the results of the free theory in Section 3.3 and the interaction strengths in Section 3.4. Quantum corrections from the bulk interactions 'dress' the bulk propagator and cause it to have qualitatively different behavior depending on the four-momentum, p. We show how these corrections separate the Kaluza–Klein and continuum regimes of a bulk scalar.

3.5.1 The Transition Scale

The homogeneity of AdS implies a homogenous 5D cutoff on proper distances smaller than $\Delta X \sim 1/\Lambda$. In the conformal coordinate system the cutoff is z-dependent with respect to the Minkowski distance, since $\sqrt{\eta_{\mu\nu}\Delta x^\mu \Delta x^\nu} \sim kz/\Lambda$. In position–momentum space the condition amounts to $p \sim \Lambda/(kz)$. This implies that the 5D cutoff for an observer at position z in the bulk is warped down to $\Lambda/(kz)$.

One can see this from an EFT perspective: the effects of higher-dimensional operators in the action are enhanced by powers of z. For example, consider dressing the propagator with a higher derivative bilinear, $\Box(\partial_\mu \Phi)^2/\Lambda^2$ with an $\mathcal{O}(1)$ coefficient as dictated by NDA (see Eq. (3.17)). This term dominates for

$$pz \gtrsim \Lambda/k\,. \tag{3.24}$$

For a fixed p, this implies that the EFT breaks down in the IR region of AdS, $z \gtrsim (\Lambda/k)/p$; see e.g. [110, 155, 186]. The cutoff is warped below the scale p for values of z beyond this region. Therefore propagation into this region of position–momentum space falls outside the EFT's domain of validity.

It follows that the theory also contains a scale

$$\widetilde{\Lambda} = \Lambda \frac{\mu}{k}\,, \tag{3.25}$$

the warped down cutoff at the IR brane. At energies $p > \widetilde{\Lambda}$, the correlation functions cannot know about the IR brane since it is in the region of position–momentum space hidden by the EFT validity condition (3.24). In short, for $p > \widetilde{\Lambda}$ the IR brane is "outside of the EFT," see Section 3.7.

This is a hint that the behavior of the theory undergoes a qualitative change at $\widetilde{\Lambda}$. The IR brane imposes a boundary condition that leads to discrete KK modes. Thus for $p < \widetilde{\Lambda}$, one can expect that the theory features KK modes. On the other hand, for $p > \widetilde{\Lambda}$ the IR brane is outside the EFT, hence no KK modes should exist. Instead, an observer should see a continuum of states.

3.5.2 Dressed Propagator

The free propagator in (3.9) encodes narrow KK modes. It amounts to $\Lambda \to \infty$ or $N \to \infty$. The continuum behavior becomes apparent when one dresses the free propagator with quantum corrections. [4] These quantum corrections resolve the poles in the free propagator with timelike momenta as they do in 4D Minkowski space. Including these effects corresponds to evaluating the leading $1/N^2$ effect on the propagator of the strongly coupled dual theory; in our case this is $1/N^2 \sim \lambda^2/k$.

[4] The exact calculation of diagrams in AdS has recently been an intense topic of research, see e.g. [93, 95, 96, 101, 108, 158] for loop-level diagrams and [112, 119, 124, 137] for developments in position–momentum space. Throughout this paper we instead use approximate propagators.

We focus on bulk self-energy corrections from a cubic self-interaction. Brane-localized self-energies only modify the boundary conditions and are thus unimportant for our purposes. In contrast to the free propagator, the Green's function equation for the dressed propagator satisfies

$$D_X \Delta(X, X') - \frac{1}{\sqrt{g}} \int dY \, \Pi(X, Y) \Delta(Y, X') = -\frac{i}{\sqrt{g}} \delta^{(5)}(X - X') \,, \tag{3.26}$$

where $i\Pi(X, Y)$ are 1PI insertions that dress the propagator. In our case, the leading $i\Pi$ insertion is induced by the scalar bubble induced by the $\lambda\Phi^3$ interaction. We are interested only in the imaginary part of the self-energy, which is finite.

A calculation of $i\Pi(X, Y)$ is performed analytically in [110] with self-consistent approximations in the limit of strong coupling and moderate bulk masses $\alpha = \mathcal{O}(1)$. One of the tricks for the analytical estimate is to expand the non-local self-energy as a series of local insertions, which amounts to a ∂_z expansion. Using this method, we estimate of the contribution from the $|p| > 1/z_<$ regime. The imaginary part of the 1-loop bubble induces a shift of p,

$$\Delta_p^{\text{dressed}}(z, z') \sim \Delta_{p(1+ic)}^{\text{free}}(z, z') \qquad\qquad c \sim a \frac{\lambda^2}{\ell_5 k} \,, \tag{3.27}$$

where c is loop-induced and estimated to have $a \sim \mathcal{O}(1/10)$ with a large uncertainty. [5] Using the NDA value of λ in (3.23) and taking $m_\Phi = \mathcal{O}(k)$, one finds $c \sim ak/\Lambda \sim a/(\pi N^2)$. The $|p| > 1/z_<$ regime provides a larger contribution to a than the result previously presented from the $|p| < 1/z_>$ regime [110]. This extends the validity of our calculations to weaker coupling, hence allowing large N. A self-consistent numerical solution to the integro-differential

[5] This estimate is confirmed in the upcoming detailed analysis of [4].

equation of motion, (3.26), may be required to obtain the general dressed propagator. We leave this for future work.

3.5.3 The Two Regimes

The self-energy dressing of the propagator presents distinct Kaluza–Klein and continuum regimes. The poles of the free propagator are set by zeros of its denominator. For momenta much larger than the IR brane scale, $p \gg \mu$, the asymptotic form of the Bessel functions lead to a propagator that is approximately proportional to

$$\Delta_p(z, z') \propto \frac{1}{\sin\left(\frac{p}{\mu} - \frac{\pi}{4}(1+2\alpha)\right)} \,. \tag{3.28}$$

The effect of the dressing, (3.27), softens the poles and causes them to merge at a scale

$$p \sim \frac{\mu}{c} \sim \frac{\widetilde{\Lambda}}{a} \,. \tag{3.29}$$

Above this scale the propagator describes a continuum rather than distinct Kaluza–Klein modes. Thus we observe that the dressing of the propagator reaffirms the existence of distinct KK and continuum regimes separated by a transition scale controlled by $\widetilde{\Lambda} = (\mu/\Lambda)k$. Let us comment further on both sides of the transition.

3.5.4 Kaluza–Klein Regime: $p < \widetilde{\Lambda}$

For momenta less than the transition scale $\widetilde{\Lambda}$, UV correlation functions are sensitive to the physics of the IR brane. The IR brane provides a boundary condition for the bulk equation of motion and hence imposes a discrete spectrum of KK modes. These modes may be narrow. However, as the KK mass approaches the transition scale, the KK modes

must merge to form a continuum. To see this, one may use the full form of the dressed KK propagator from (3.26). This propagator is given by

$$\Delta_q(z,z') = i\,\mathbf{f}(z)\cdot\left[\mathbf{D}^{-1} + i\,\mathrm{Im}\,\mathbf{\Pi}\right]^{-1}\cdot\mathbf{f}(z') \tag{3.30}$$

where

$$i\mathbf{\Pi} \equiv \int du \int dv\, i\Pi(u,v)\mathbf{f}(u)\otimes\mathbf{f}(v)\,. \tag{3.31}$$

The imaginary part of $\mathbf{\Pi}$ gives rise to a "width matrix" for the KK resonances. Critically, $\mathrm{Im}\,\mathbf{\Pi}$ is *not* diagonal: the KK modes mix due to this non-diagonal, imaginary contribution to the mass matrix. The KK modes may merge into a continuum either because they become broad, or because of the mixing induced by $\mathrm{Im}\,\mathbf{\Pi}$. This property of the AdS propagator is suggestive of how heavy glueballs in the strongly-coupled dual tend to merge near the $\widetilde{\Lambda}$ cutoff, see Section 3.8.3.

At low enough four-momentum p, the narrow-width approximation applies to the KK modes. The KK modes can then be treated as asymptotic 4D states. The optical theorem applies to these light KK modes. In contrast, when approaching the transition scale, the KK modes cannot be seen as asymptotic states due to large widths and KK-mode mixing. This is consistent with the properties of non-truncated AdS.

3.5.5 Continuum Regime: $p > \widetilde{\Lambda}$

When p is above the transition scale, $\widetilde{\Lambda}$, the oscillating pieces of the propagator are smoothed. Within this regime, the endpoints of the propagator define additional scales for which the propagator realizes different behavior.

Continuum regime, low momentum. In the continuum regime with low momentum, $|p| > \widetilde{\Lambda}$ and $|p| < z_>^{-1}$, and away from the poles, the propagator is

$$\Delta_p(z, z') \approx \Delta_{\rm UV} + \Delta_{\rm heavy} + \Delta_{\rm light} \ , \tag{3.32}$$

where the pieces are

$$\Delta_{\rm UV} = \quad i\frac{(b_{UV}+2\alpha)(kz)^{2-\alpha}(kz')^{2-\alpha}}{\alpha\left(p^2/(\alpha-1)k + 2b_{UV}k\right)} \qquad \Delta_{\rm heavy} = -i\frac{(kz)^2(kz')^2}{2\alpha k}\left(\frac{z_<}{z_>}\right)^\alpha \tag{3.33}$$

$$\Delta_{\rm light} = -i\frac{\Gamma(-\alpha)(kz)^2(kz')^2}{\Gamma(\alpha+1)2b_{UV}^2 k} g(z_<)g(z_>)\left(\frac{-p^2}{4k^2}\right)^\alpha \qquad g(z) = \frac{b_{\rm UV}+2\alpha}{(zk)^\alpha} - b_{\rm UV}(zk)^\alpha \, . \tag{3.34}$$

Notice that the dependence on the μ parameter has dropped this expression. This is a manifestation of the propagator's agnosticism of the IR brane in this regime. Conversely, this implies that when varying p from UV scales to IR scales, the IR brane is effectively emergent when p drops below $\widetilde{\Lambda}$.

The content of each term in (3.32) is also instructive. The first term, $\Delta_{\rm UV}$ represents a 4D mode localized near the UV brane. [6] This 4D mode is assumed to be very heavy, $b_{\rm UV} = \mathcal{O}(1)$, such that it does not play a role in the processes of in this manuscript. The second term, $\Delta_{\rm heavy}$ is analytic and encodes the collective effect of heavy KK modes. The third term, $\Delta_{\rm light}$ is nonanalytic and encodes the collective effect of light modes.

[6] In our convention, the 4D mode squared mass is positive for negative $b_{\rm UV}$.

Continuum regime, high momentum. In the continuum regime with high momentum, $|p| > \widetilde{\lambda}$ and $z_>^{-1} < |p| < z_<^{-1}$, the numerator of the propagator oscillates:

$$\Delta_p(z,z') \propto \frac{\cos\left(p\mu^{-1} - pz_>\right)}{\cos\left(p\mu^{-1} + \varphi_-\right)} \times \begin{cases} 1 & \text{for } z_>^{-1} < p < z_<^{-1} \\ \\ \cos\left(pz_< - \varphi_+\right) & \text{for } p > z_<^{-1}\,, \end{cases} \tag{3.35}$$

where we have written phase shifts as $\varphi_\pm = \pi\left(1 \pm 2\alpha\right)/4$. Upon dressing, the non-oscillatory part of the propagator in this region scales as

$$\Delta_p(z,z') \sim \begin{cases} e^{-|p|z_>} & \text{for } p_\mu \text{ spacelike} \\ \\ e^{-cpz_>} & \text{for } p_\mu \text{ timelike} \end{cases}. \tag{3.36}$$

This is an important feature: the IR region of AdS is opaque to propagation for both spacelike and timelike momenta. The regions of opacity are somewhat different—the suppression for spacelike momentum occurs at $z \sim 1/|p|$, while the suppression for timelike momentum occurs at $z \sim 1/cp$. Substituting in c, we see that the suppression in the timelike regime occurs for

$$pz_> \gtrsim \frac{\Lambda}{ak}\,. \tag{3.37}$$

This behavior is similar to the region of EFT breaking in (3.24). Therefore the opacity of the space effectively censors the region where the EFT breaks down. This behavior was qualitatively predicted in Ref. [155]. For the specific case with an endpoint on the IR brane, $z_> = 1/\mu$, the opacity threshold (3.37) is the same as the scale at which the Kaluza–Klein poles disappear, (3.29). The two effects are, of course, closely related: the poles vanish precisely when the IR brane becomes opaque to the propagator.

In the continuum regime, KK modes are not appropriate variables to describe the theory because the f_n profiles fall into a spacetime region where the EFT breaks down, (3.24). Instead, the meaningful variables are those localized on the UV brane. These remain in the theory up to the ultimate cutoff $p \sim \Lambda$. This was already observed in [186] from EFT considerations, and is completely consistent with the holographic formalism needed for AdS/CFT.

3.6 Cascade Decays in the Continuum Regime

The same bulk interactions that induce opacity in the IR region necessarily induce cascade decays in the bulk. These cascade decays, in turn, may appear to be a possible loophole to the arguments in the previous section. In particular, it is possible that a continuum with $p \gg \widetilde{\Lambda}$ undergoes cascade decays down the KK regime, ending in light narrow KK states and/or in IR-localized states. In such a process, it may seem that for *any* initial momentum the cascade decay 'knows' that an IR brane exists. This appears to circumvent the picture obtained in Section 3.5, where the theory at $p \gg \widetilde{\Lambda}$ does not know at all about the IR brane. We evaluate explicitly this process in this section and discuss implications in Section 3.7.

The properties of cascade decays initiated in the KK regime are fairly well-understood and are summarized in Section 3.7.1. We instead focus on the cascade decays starting in the continuum regime. This regime is always present unless interactions are removed ($\Lambda \to \infty$). Furthermore, in the strong coupling limit $\Lambda \sim k$, there is essentially no KK regime and all propagation is in the continuum regime. We seek to determine the overall shape and the

total probability for a cascade decay event to occur in the continuum regime.

The bulk of AdS does not permit asymptotic states or a conventional S-matrix (see e.g. [156, 157]). However the 4D modes localized on the branes, which have a 4D Minkowski metric, can provide usual asymptotic states. We thus consider decays that are initiated on the UV brane. The decay may end back on the UV brane or reach asymptotic states on the IR brane. It can also end in narrow KK modes which are effectively asymptotic states in the limit of the 4D narrow width approximation.

3.6.1 The Decay Process

The explicit evaluation of a generic decay diagram with an arbitrary number of legs is, in principle, challenging because there are many phase space and position integrals to perform over a non-trivial integrand. However, it turns out that a recursive approach can be adopted based on simplifying approximations. We build on this approach to estimate the total rate for a generic decay.

For intermediate steps in this calculation, it is convenient to formally write the final states as KK modes, even if the corresponding momenta are in the continuum regime. Sums over KK modes may then be re-expressed in terms of the closed form propagator at the end of the calculation.

Measurable event rates, such as cross sections and decay widths, depend on the integral of the squared amplitude over phase space. To emphasize that our approach does not depend on how the continuum is created, we work at the level of this integrated square amplitude, denoted as P_M. For the diagram in Fig. 3.1 with $M+1$ final states,

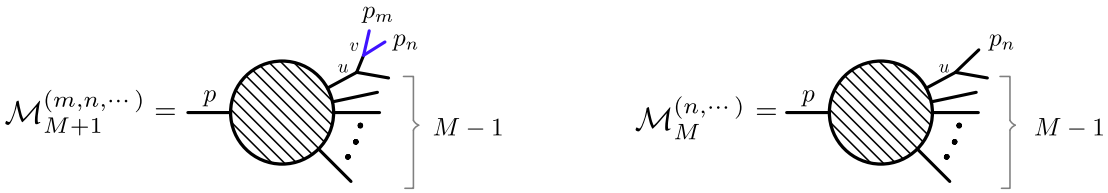

Figure 3.1: The cascade decay amplitudes. u and v are coordinates in the z direction. In our recursive approach, we relate the integrated square amplitude of the left diagram to that of the right diagram.

$$P_{M+1} \equiv \int \sum_{\mathrm{FS}(M+1)} |\mathcal{M}_{M+1}|^2 (2\pi)^4 d\Phi_{M+1}. \tag{3.38}$$

The sum over FS$(M+1)$ is shorthand for a sum over all possible combinations of $(M+1)$ KK modes that are kinematically allowed final states. $d\Phi_{M+1}$ is the volume element of the $(M+1)-$body Lorentz-invariant phase space [212]. We label specific specific final state KK numbers and four-momenta as m, p_m and n, p_n. The amplitude for a given set of final state KK modes is expressed as

$$\mathcal{M}_{M+1}^{(m,n,\cdots)} = \int du\ \mathcal{I}_M^{(\cdots)}(u) \int_{1/k}^{1/\mu} dv \frac{\lambda \Delta_q(u,v)}{(kv)^5} f_m(v) f_n(v)\ . \tag{3.39}$$

$\mathcal{I}_M^{(\ldots)}(u)$ is the amplitude that has been amputated just before the propagator that produces the m and n modes, see Fig. 3.1.

The $\mathcal{M}_M$ amplitude, shown on the right-hand side of Fig. 3.1, is

$$\mathcal{M}_M^{(n,\cdots)} = \int du\ \mathcal{I}_M^{(\cdots)}(u) f_n(u). \tag{3.40}$$

The corresponding integrated square amplitude is

$$P_M \equiv \int \sum_{FS(M)} |\mathcal{M}_M|^2 (2\pi)^4 d\Phi_M\ . \tag{3.41}$$

We now relate P_{M+1} to P_M.

3.6.2 Recursion Relation

Propagators with timelike momentum are suppressed beyond $z_> \sim 1/(cp)$, as seen in (3.36). We assume for simplicity that $c \sim 1$. This implies that our evaluation assumes nearly strong coupling, i.e. Λ is not far from k. Following this, the position integrals effectively have no support beyond $z \sim 1/p$. Note that this is equivalent to only considering contributions from the $\mu < |p| < z_>^{-1}$ region of position–momentum space, see (3.32).

We have numerically evaluated contributions from the $|p| > z_>^{-1}$ regions and found that they tend to be smaller or of the same order as the results from this section for c near unity. These contributions can be somewhat larger for smaller c, though a detailed analysis is beyond the scope of this manuscript.

We square the amplitude and write sums on KK modes as integrals over the propagator using (3.13). In the continuum regime, only the third term of the continuum propagator in (3.32) contributes to the contour integral because it carries a branch cut. By deforming the contour to fit snugly around the branch cut, we determine that

$$\sum_{n=0}^{\widetilde{n}} U(m_n^2) f_n(z) f_n(z') = -\frac{1}{2\pi} \oint_{\mathcal{C}[\widetilde{n}]} dq^2\, U(q^2) \Delta_q(z,z') = \frac{-1}{2\pi} \int_0^{m_{\widetilde{n}}^2} dq^2\, U(q^2) \mathrm{Disc}[\Delta_q(z,z')]\,. \tag{3.42}$$

In terms of the propagator, P_{M+1} then reads

$$P_{M+1} = 4\pi^2 \sum_{\mathrm{FS}(M-1)} \int d\Phi_{M+1} \int du \int du'\, \mathcal{I}_M(u)\, \mathcal{I}_M^*(u') \int_{1/k}^{1/q} dv \int_{1/k}^{1/q} dv'\, \frac{\lambda^2 \Delta_q(u,v) \Delta_q^*(u',v')}{(kv)^5 (kv')^5} \times \tag{3.43}$$

$$\int dp_1^2\, \mathrm{Disc}[\Delta_{p_1}(v,v')] \int dp_2^2\, \mathrm{Disc}[\Delta_{p_2}(v,v')]\,.$$

The integrals over the p_1^2, p_2^2 variables implement the sum over KK modes in (3.42). The

integrands in (3.43) carry positive powers of v and v' so that the $dv\,dv'$ integrand is largest at the upper limit, $v,\, v' \sim 1/q$. Because q is the momentum flowing through the parent this implies that the cascade decay progresses slowly towards the IR region.

We break up the phase space using the standard recursion relation, see e.g. [212],

$$d\Phi_{M+1} = d\Phi_2(q; p_1, p_2)\, d\Phi_M\, (2\pi)^3 dq^2\,. \tag{3.44}$$

We get

$$P_{M+1} = (2\pi)^4 \sum_{\mathrm{FS}(M-1)} \int d\Phi_M \int du \int du'\, \mathcal{I}_M(u)\, \mathcal{I}_M^*(u') \int_{1/k}^{1/q} dv \int_{1/k}^{1/q} dv'\ \frac{\lambda^2}{(kv)^5 (kv')^5} \times \tag{3.45}$$

$$\int dp_1^2\, \mathrm{Disc}[\Delta_{p_1}(v, v')] \int dp_2^2\, \mathrm{Disc}[\Delta_{p_2}(v, v')] \int \frac{dq^2}{64\pi^4 q^2} K(q, p_1, p_2) \Delta_q(u, v) \Delta_q^*(u', v') \,.$$

Here $K(q, p_1, p_2)$ is the 2-body kinematic factor,

$$K(q, p_1, p_2)^2 \equiv \left[q^2 - (p_1 + p_2)^2\right] \left[q^2 - (p_1 - p_2)^2\right]\,. \tag{3.46}$$

We approximate the integrals over p_1^2 and p_2^2 as

$$\int_0^q dp_1 \int_0^{q-p_1} dp_2\ p_1^{2\alpha+1} p_2^{2\alpha+1} K(q, p_1, p_2) \approx \int_0^{q/2} dp_1 \int_0^{q/2} dp_2\ p_1^{2\alpha+1} p_2^{2\alpha+1} q^2\,. \tag{3.47}$$

This approximation introduces a $\mathcal{O}(1)$ error that depends on α.[7] Note that the dominant contribution to the integral in (3.47) comes from the region near the upper limit. This indicates that the continua tend to decay near kinematic threshold. Thus the cascades gives rise to soft spherical final states, in accordance with former results from both gravity and CFT sides.

[7]The error monotonically increases from $\sim 25\%$ for α near 0 to $\sim 30\%$ for α near 1.

Integrating over p_1^2, p_2^2, v, and v', we have

$$P_{M+1} = C_\alpha \sum_{FS(M-1)} (2\pi)^4 \int d\Phi_M \int \frac{dq^2}{k} \left(\frac{q}{k}\right)^{2\alpha} \int du \int du' \, \mathcal{I}_M(u) \, \mathcal{I}_M^*(u') (ku)^{2+\alpha} (ku')^{2+\alpha} \,, \tag{3.48}$$

where the constant prefactor is

$$C_\alpha = \frac{8^{4(1-\alpha)} \lambda^2}{\alpha^4 \pi^4 k} \left(\frac{\Gamma(1-\alpha)\sin(\pi\alpha)}{\Gamma(1+\alpha)} \right)^2 \frac{|(2+3\alpha)4^\alpha - (\alpha+2)\frac{\Gamma(1-\alpha)}{\Gamma(1+\alpha)} e^{i\alpha\pi}|^2}{(2+3\alpha)^2(2+\alpha)^2(1+\alpha)^2} \,. \tag{3.49}$$

One may replace the dq^2 in favor of a sum over the continuum of KK final states by applying (3.42). This yields a recursion relation

$$P_{M+1} = r \int \sum_{\mathrm{FS}(M)} \left| \int du \; \mathcal{I}_M(u) f_n(u) \right|^2 (2\pi)^4 d\Phi_n = r \, P_M \,. \tag{3.50}$$

The fact that one obtains a simple relation is a consequence of the integrand having a specific momentum dependence and is nontrivial. This relation is clearly useful since it can be used to give an estimate of a total rate with arbitrary number of legs.

The recursion coefficient r is given by

$$r \equiv \frac{\lambda^2}{k} \frac{1}{1024^{1+\alpha}} \frac{1}{2\pi^3 \alpha^3} \left(\frac{|(2+3\alpha)4^\alpha - (2+\alpha)\frac{\Gamma(1-\alpha)}{\Gamma(1+\alpha)} e^{i\alpha\pi}|^2}{(2+3\alpha)^2(2+\alpha)^2(1+\alpha)^2} \right) \frac{\Gamma(1-\alpha)\sin(\pi\alpha)}{\Gamma(1+\alpha)} \,. \tag{3.51}$$

Even for the strongly coupled case, $\lambda^2 \sim \ell_5 k$, this coefficient is much smaller than one.

3.7 Soft Bombs and the Emergence of the IR Brane

The recursion relation (3.51) allows us to study the qualitative features of a complete cascade decay event. An event initiated on the UV brane with timelike momentum $P > \widetilde{\Lambda}$ starts in the continuum regime and decays as a cascade of continua. This decay eventually reaches the KK regime.

3.7.1 Shape

The differential event rate—the integrand in the expression for P_M—determines the most likely configurations in phase space. The phase space approximation (3.47) shows that decays tend to occur near threshold with final momenta evenly split between the offspring. The event thus tends to be soft and spherical. This confirms the *soft bomb* picture obtained in the KK regime [40], in string calculations (see e.g. [31]) and in the gauge theory dual [33, 36].

The integrand in (3.45) shows that vertices tend to occur at $z \sim 1/p$ where p is the momentum of the parent continuum. There is a sense of progression in the fifth dimension: the cascade decay proceeds from the UV to the IR with each offspring moving further into the IR than its parent.

Let p_f be the average momentum of states after some number of branchings. The soft bomb then leaves the continuum regime and enters the KK regime at $p_f \sim \widetilde{\Lambda}$. This is roughly the scale at which the KK modes become narrow. These features are summarized in Fig. 3.2.

3.7.2 Total Rate

The soft bomb enters the regime of narrow KK modes when the offspring have average momenta $p_f \sim \widetilde{\Lambda}$. At this scale, the narrow width approximation is valid and the recursion (3.50) halts because subsequent decays factorize. This highlights a key feature of the continuum regime in contrast to the KK regime: the phase space suppression factors are not compensated by narrow poles due to the breakdown of the narrow width approximation.

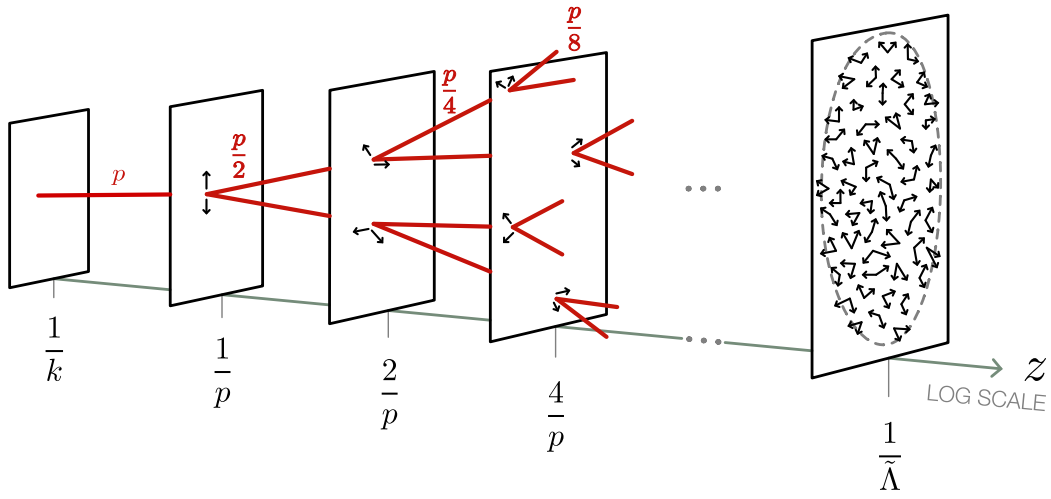

Figure 3.2: A typical field-theoretical soft bomb event in AdS_5 in the continuum regime $p > \widetilde{\Lambda}$. The rate for such an event to occur is exponentially suppressed.

This is why cascade events starting in the continuum regime are suppressed.

One can estimate the total rate of cascade decays using the recursion (3.50). A continuum cascade initiated with momentum P stops at momentum $p_f \sim \widetilde{\Lambda}$. Assuming an equal split of momenta among a total of M offspring gives

$$M \sim P/\widetilde{\Lambda} \, . \tag{3.52}$$

The recursion relation (3.50) shows that the rate is suppressed by r^{M-1}.

$$P_M \sim r^{P/\widetilde{\Lambda}} \, . \tag{3.53}$$

Since $r \ll 1$, the soft bomb is exponentially suppressed as a function of P for initial timelike momenta in the continuum regime $P > \widetilde{\Lambda}$.

3.7.3 Emergence of the IR Brane

The suppression of the soft bomb rate in the continuum regime completes our picture of quantum field theory in AdS for timelike momenta. We can now make a statement

about the 'disappearance' of the IR brane in QFT first hinted in Section 3.5.1.

Consider, for example, a UV-localized field φ that couples to the bulk scalar, Φ. The collision of two φ states can induce a cascade decay $\varphi\varphi \to \Phi \to \Phi\Phi \to \cdots$ When the center-of-mass four-momentum is in the KK regime, $P < \widetilde{\Lambda}$, the event rate is determined by the $\varphi\varphi \to \Phi^{(n)}$ amplitude to create an on-shell KK mode $\Phi^{(n)}$ with mass $m_n \sim P$. In contrast, in the continuum regime, $P > \widetilde{\Lambda}$, the cascade is initiated with 5D continua that have no poles and thus no notion of being on-shell. Narrow KK modes only appear after the cascade has produced enough offspring for the typical momentum to drop below $\widetilde{\Lambda}$. The amplitude to calculate includes the entire cascade up to, and including, the first narrow KK modes. The rate for a cascade in the continuum regime is suppressed with respect to that in the KK regime by the tiny factor $r^{P/\widetilde{\Lambda}}$ in (3.53).

This suppression implies that continua produced tend not to cascade down to many narrow KK states which can interact with an IR brane, but instead tend to go promptly into UV-brane states with no cascade. Thus in the continuum regime, the theory truly does not know about the IR brane. The observables—including decays—in this regime of the theory can be equivalently obtained in AdS background with *no* IR brane.

Formally this statement can be spelled out using the partition function of the theory

$$e^{iE[J]} = \left\langle e^{i\int_{z_{\rm UV}}^{z_{\rm IR}} dz d^4p\, \Phi J} \right\rangle = \int \mathcal{D}[\text{fields}] \exp i \left(\int_{z_{\rm UV}}^{z_{\rm IR}} dz d^4p \left(\mathcal{L}_{\rm bulk} + \Phi J \right) + S_{\rm UV} + S_{\rm IR} \right), \tag{3.54}$$

where $E[J]$ is the generating functional of the connected correlators. Our claim is that in

the $p \gg \widetilde{\Lambda}$ regime, the correlators are equivalently described by

$$e^{iE[J]\big|_{p\gg\tilde{\Lambda}}} \approx \int \mathcal{D}[\text{fields}] \exp i \left(\int_{z_{\text{UV}}}^{\infty} dz d^4p \left(\mathcal{L}_{\text{bulk}} + \Phi J \right) + S_{\text{UV}} \right) \equiv e^{iE[J]\big|_{z_{\text{IR}}\to\infty}} . \quad (3.55)$$

On the right-hand side, $E[J]\big|_{z_{\text{IR}}\to\infty}$ amounts to the theory with the IR brane removed. In other words, the IR brane—and the fields and operators localized on it—effectively vanishes for $p \gg \widetilde{\Lambda}$. Conversely, the IR brane affects correlators for lower p and is thus effectively emergent. [8]

Finally we notice that the continuum regime is exactly described by an appropriate CFT model as dictated by the AdS/CFT correspondence. Apart from the UV brane which amounts to a UV cutoff in the CFT, the theory is exactly AdS in the continuum regime.

3.7.4 Optical Theorem

In Section 3.5.4 we observed that in the Kaluza–Klein regime, KK modes are valid asymptotic states that obey the optical theorem. In the continuum regime, even though the rate of cascade decays is exponentially suppressed, the imaginary part of the bulk self-energy $\operatorname{Im}\Pi$ is not. This does not contradict the optical theorem, though it may appear to do so when using the intuition from KK modes. This is because unlike the KK regime, the continuum regime has no narrow state on which one may perform a unitarity cut. Thus the loop-level contribution to the self-energy is *not* related to a decay—the optical theorem does not apply.

[8] For the purpose of taking functional derivatives, the source J can formally be any distribution. If instead J is given a physical meaning, it is typically localized towards the UV brane to avoid any backreaction of the metric towards the IR. In the context of holography, J is exactly localized on $z = z_{\text{UV}}$, giving rise to UV-localized variables as done in Section 3.8.2.

One may insist on identifying propagators of light KK modes with narrow widths upon which one may perform a unitarity cut. Because of the "near-threshold" property of KK vertices in Section 3.7.1, these light KK modes only appear at high loop order. A unitarity cut on this high-loop order diagram ultimately reproduces the typical soft bomb diagram in Figure 3.2 that ends in states with $m_{\rm KK} \sim \widetilde{\Lambda}$. Such diagrams only amount to a tiny portion of $\operatorname{Im}\Pi$.

3.7.5 Asymptotically AdS Backgrounds

Our study focuses on a slice of pure AdS with no departure from AdS in the IR region. The qualitative features of our results can apply to models whose backgrounds are deformed in the IR. One kind of model is the slice of AdS stabilized by the Goldberger–Wise mechanism. This produces a non-negligible backreaction of the metric near the IR brane. Another class of model are those where the metric develops a naked curvature singularity in the IR—the soft-wall models, see *e.g.* [191–193, 196, 198, 199] for some points of entry in the literature. Such models are typically asymptotically AdS towards the UV brane, with the IR deformation becoming relevant near the IR brane/singularity.

One can apply the reasoning of Section 3.5 to these models. By dimensional analysis, there is some typical scale $\hat{\mu}$ associated with the IR region. A transition scale $\Lambda\hat{\mu}/k$ thus also exists, above which the IR region should drop from the correlation functions if the EFT is to remain under control.

More quantitatively, one can integrate out the IR region and encapsulate it into an effective IR brane with non-trivial form factors localized on it [199]. This holographic projection of the IR region demonstrates that the two regimes can indeed be meaningfully

separated. The effective IR brane contains the details of the model-dependent KK regime. Since the bulk is pure AdS, our results from Sections 3.3-3.7 apply. This immediately shows that at high enough p, the effective IR brane leaves the theory, leaving thus a (quasi-)AdS continuum regime like the one described in this paper. Conversely, when decreasing p, the deviation from AdS gradually emerges from the viewpoint of a UV-brane observer.

3.7.6 Holographic Dark Sector

The soft bomb suppression rate has phenomenological implications for theories where a dark (or hidden) sector is confined to the IR brane and the Standard Model is confined to the UV brane, as recently proposed in [27]. Suppose, for concreteness, that the decay chain ends in stable IR brane particles that could naturally be identified with dark matter.

A standard way to search for dark matter at colliders is to look for missing energy signatures. In our holographic dark sector scenario, the suppression of the cascade decay rate in the continuum regime implies that the missing energy spectrum should vanish around the $\widetilde{\Lambda}$ scale. This characteristic of the holographic dark sector framework is completely distinct from standard 4D dark sectors.

Another standard constraint on dark sectors with light states that couple to the Standard Model is stellar cooling from the emission of dark states. In the holographic dark sector scenario, stars emit KK modes with narrow widths when the temperature of the star is roughly between μ and $\widetilde{\Lambda}$. In contrast, if the star is hotter than $\widetilde{\Lambda}$, the center-of-mass energy for dark state production is typically in the continuum regime. One may then expect that the anomalous cooling rates are then exponentially suppressed within the AdS

model. One must be cautious with this intuition, however, as the finite-temperature system may be better described by an AdS–Schwarzschild geometry [213]. The phenomenology of this situation may lead to new possibilities to get around the stellar cooling bounds that constrain standard dark sectors.

These effects are very interesting from a phenomenological viewpoint: they may alleviate experimental constraints and change the experimental complementarity of dark matter searches. The direct detection signatures of this type of framework are studied in [42], which also discusses some qualitative differences of timelike correlation functions in models of near-conformal sectors. We explore these effects in upcoming phenomenological studies.

3.8 AdS/CFT

This paper focused primarily on the physics of 5D Anti-de Sitter spacetime. In this section we connect our analysis to the properties of the dual gauge theory by the AdS/CFT correspondence. First we briefly discuss consistency of our soft bomb picture with the one obtained in the CFT literature. We will then show how dimensional analysis (see Section 3.4) applied to the holographic action naturally relates to the dual large-N expansion. Finally we study the transition scale in the dual low-energy EFT of glueballs.

3.8.1 CFT Soft Bombs

There is strong evidence that gauge theories with large 't Hooft coupling exhibit vastly different behaviour than weakly-coupled gauge theories, see e.g. [205]. [9]

In [36], the fragmentation of a jet at large 't Hooft coupling was qualitatively studied using properties of spacelike and timelike anomalous dimensions. The jet is assumed to be created from well-defined asymptotic states such as in e^+e^- annihilation. In our AdS dual this is realized using asymptotic states localized on the UV brane. The jet evolves and ends at some infrared scale $\Lambda_{\rm IR}$ at which the parton momenta are measured. In our AdS dual this $\Lambda_{\rm IR}$ corresponds to the infrared scale $\widetilde{\Lambda}$ that we have determined in Section 3.5.

Ref. [36] finds that parton splitting tends to be democratic because there is no reason for soft or collinear phase space configurations to be preferred—all partons tend to have minimum momentum $p_f \sim \Lambda_{\rm IR}$. Hence, cascades give rise to spherical events with a large number of low-momentum final states. This matches our explicit AdS calculation in Section 3.7.1. The total number of offspring is found to be $n \sim P/\Lambda_{\rm IR}$, which corresponds to (3.52), with $\Lambda_{\rm IR} \sim \widetilde{\Lambda}$.

We conclude that the shape of an AdS soft bomb event is consistent with findings on the CFT side.

3.8.2 Dimensional Analysis and Large N

In Section 3.4.2 we have shown that 4D KK mode interactions are naturally suppressed by powers of $(\ell_5 k/\ell_4\Lambda)$. Here we show that this suppression corresponds to the

[9] In the gauge theory context, the strongly-coupled analog of jets have sometimes been referred to as "spherical events" or "jets at strong coupling" instead of "soft bombs" as done here.

large N suppression in the dual CFT. To see this correspondence, instead of KK modes, we must consider the 5D theory in AdS using an appropriate variable—the value of the bulk field on the UV brane

$$\hat{\Phi}_0(x) \equiv \hat{\Phi}(X)\Big|_{\text{UV brane}}. \tag{3.56}$$

Φ is the dimensionless bulk field in (3.17). The bulk field in the action is rewritten as $\hat{\Phi} = \hat{\Phi}_0 K$, where K is the classical field profile sourced by $\hat{\Phi}_0$. In terms of this holographic variable, the partition function (3.54) takes the form $\int \mathcal{D}\hat{\Phi}_0 \exp\left(iS_5[\hat{\Phi}_0 K]\right)$, where S_5 is the 5D action for which the 5D NDA in (3.17) applies.

The leading term of the effective action in the semiclassical expansion is the classical holographic action

$$\Gamma_{\text{hol}} = \frac{\Lambda^5}{\ell_5}\int d^4x \mathcal{L}_{\text{hol}}\left[\hat{\Phi}_0, \partial/\Lambda\right] + \cdots, \tag{3.57}$$

where the ellipses represent quantum terms that are irrelevant for our discussion. The Lagrangian $\mathcal{L}_{\text{hol}}$ has dimension -1. To recover a 4D NDA formulation as in (3.17), we need to introduce a dimensionless Lagrangian. From explicit calculation (see e.g. [13, 188]), the quadratic part of $\mathcal{L}_{\text{hol}}$, $\frac{1}{2}\hat{\Phi}_0\Pi[\partial^2]\hat{\Phi}_0$, is proportional to the inverse of $\Delta_q(z_0, z_0)$ and contains an analytic part representing a 4D mode. Schematically, it is

$$\Pi[\partial^2] \sim -\frac{1}{k}\frac{\partial^2 + m_0^2}{\Lambda^2} + \ldots \tag{3.58}$$

up to an $\mathcal{O}(1)$ coefficient. In the language of AdS/CFT, this is the kinetic term of the 4D source probing the CFT. The exact expression can be read directly from the propagator (3.32) and is not needed here.

We introduce the dimensionless Lagrangian $\frac{1}{k}\hat{\mathcal{L}}_{\rm hol} = \mathcal{L}_{\rm hol}$, such that the dimensionless source described in (3.58) is canonically normalized. The action now can be rearranged as

$$\Gamma_{\rm hol} = \left(\frac{\ell_4\Lambda}{\ell_5 k}\right)\frac{\Lambda^4}{\ell_4}\int d^4x\hat{\mathcal{L}}_{\rm hol}\left[\hat{\Phi}_0, \partial/\Lambda\right] + \cdots\,, \tag{3.59}$$

where we explicitly write the Λ^4/ℓ_4 factor appear in accordance with 4D NDA. The factor in parenthesis is the same suppression as obtained in Section 3.4.2. From (3.57) it is clear that this factor systematically appears alongside $\hbar$ in the semiclassical expansion of the holographic action.

We may now perform dimensional analysis on the canonically normalized holographic variable,

$$\Phi_0 = \left(\frac{\ell_4\Lambda}{\ell_5 k}\right)^{1/2}\frac{\Lambda}{\ell_4^{1/2}}\hat{\Phi}_0\,. \tag{3.60}$$

Functional derivatives with respect to Φ_0 are suppressed as

$$\frac{\delta^n\Gamma_{\rm hol}}{\delta\Phi_0(x_1)\delta\Phi_0(x_2)\cdots} \propto \left(\frac{\ell_5 k}{\ell_4\Lambda}\right)^{n/2-1} \tag{3.61}$$

at leading order. Hence by applying dimensional analysis at 5D and 4D levels in the holographic action, we have shown that a small parameter ($\sqrt{\ell_5 k/\ell_4\Lambda}$) systematically suppressing the interactions and controlled by the AdS curvature appears.

The AdS/CFT correspondence dictates that the above quantity reproduces the connected n-point functions of a conformal gauge theory with adjoint fields and large N. The main contribution to the correlator at large N is suppressed as [21, 214]

$$\langle\mathcal{O}\mathcal{O}\ldots\rangle_{\rm con} \propto \frac{1}{N^{n-2}} \tag{3.62}$$

with canonical normalization such that the 2pt function does not scale with N. Comparing the AdS expression (3.61) and the CFT expression (3.62), we see that the suppression factor in AdS corresponds to the $1/N^2$ suppression of the CFT,

$$\frac{\ell_5 k}{\ell_4 \Lambda} \sim \frac{1}{N^2}\,. \tag{3.63}$$

We thus obtain a precise, field-theoretical version of the correspondence between the $1/N$ expansion in the CFT and the parameters of the AdS effective field theory. At fixed AdS curvature k, and i.e. fixed 't Hooft coupling, the $N \to \infty$ limit corresponds to the $\Lambda \to \infty$ limit. This sets all interactions to zero and therefore produces a free 5D theory. The relation (3.63), when put in the holographic action (3.59), gives $\Gamma_{\rm hol} = N^2 \frac{\Lambda^4}{\ell_4} \int d^4x \hat{\mathcal{L}}_{\rm hol}$. The N^2 factor accompanying $\hbar$ in this action is a hallmark feature of AdS/CFT [19].

3.8.3 Dual Interpretation of Transition Scale

In this section we consider the dual gauge theory interpretation of the transition scale using $\Lambda/k \sim N^2 \ell_5/\ell_4$ as established in (3.63). In the following discussion, we estimate $\ell_5/\ell_4 \sim \pi$. Interactions vanish in the $\Lambda \to \infty$ limit. In this limit, the AdS theory thus contains an infinite tower of free, stable KK modes.[10] This is the AdS manifestation of the infinite tower of stable glueballs when $N \to \infty$.

For finite N, the transition scale is

$$\widetilde{\Lambda} \sim N^2 \pi \mu\,. \tag{3.64}$$

[10] A confined gauge theory produces a spectrum with particles of arbitrary spin. In the QFT approach to AdS/QCD, glueballs of a given spin corresponds to a given field on the AdS side, see *e.g.* [191]. Focusing on a bulk scalar amounts to focusing on the sector of scalar glueballs.

The scale controlling the mass of the KK modes, $\pi\mu$ appears. The KK masses grow linearly, hence the transition is reached around the mass of the N^2-th KK mode.

The $\widetilde{\Lambda}$ scale would be the cutoff of the glueball EFT. Does the value (3.64) make sense from the gauge theory side? Recall that the large-N theory contains, in principle, many glueballs at low energy. It is thus described by an EFT containing many species. The interactions between glueballs are set by the $\widetilde{\Lambda}$ scale and suppressed by powers of $1/N$. In the loop diagrams, such suppression is compensated by the multiplicity of glueballs. For N^2 glueballs, the cutoff of the EFT becomes $\widetilde{\Lambda}$. This feature can be seen by using 4D NDA applied to the glueball theory with arbitrary number of species N_s and $D = 4$. The prefactor of (3.17) is

$$\frac{N_s \widetilde{\Lambda}^4}{N^2 \ell_4}\,, \tag{3.65}$$

which indicates strong coupling when the number of glueballs N_s is of order N^2. This paints a consistent picture: the N^2 modes of the KK regime in AdS match the N^2 glueballs of the gauge theory.

These considerations are only about the number of species and do not tell us about glueball masses. However we also know that an infinite tower of glueballs is needed to reproduce the logarithmic momentum dependence of the correlator between gauge currents [214]. At finite N, the width over mass ratio of the n^{th} glueball is expected to grow as $\Gamma_n/m_n \sim n/N^2$. The $(1/N)^2$ factor comes from the $1/N$ suppressed cubic vertices, and the n factor comes from the number of accessible decay channels into lighter glueballs. Hence the glueballs tend to become broad at $n \sim N^2$, which signals the transition to a continuum. Since there is a tower of glueballs, the cutoff of the glueball EFT has to be around the mass

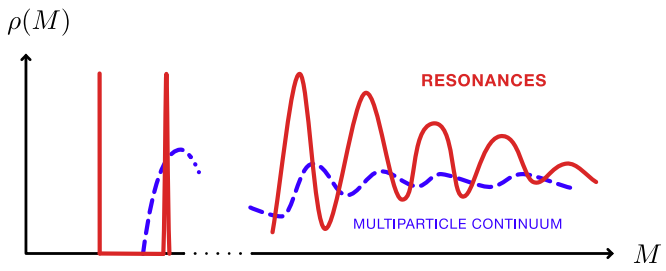

Figure 3.3: Schematic spectral density of the two-point correlator of the large-N glueball EFT. The solid line shows the glueball resonances merging into a continuum when approaching the cutoff of the EFT. The merging of resonances that we describe is distinct from the multiparticle continuum, which we show schematically for completeness.

of the N^2-th glueball, *i.e.* $\widetilde{\Lambda} \sim m_{N^2}$. This matches the picture obtained on the AdS side in (3.64), where the N^2-th KK mode is indeed of order of $\widetilde{\Lambda}$. Notice this reasoning relies on state-counting and only requires enough of a hierarchy between masses for the decays to occur. This is a very mild condition. In this work the mass distribution obtained from the AdS side is $m_n \sim n$, but the same line of reasoning would apply to *e.g.* a Regge-like spectrum $m_n \sim \sqrt{n}$.[11]

The spectral density of glueballs obained from the above considerations is summarized in Fig. 3.3.

[11] For completeness we notice that at energies approaching the cutoff, $\widetilde{\Lambda}$, contributions from the multiparticle continuum should become sizeable. This is expected since, by definition, at the EFT cutoff the contributions from all loop orders become same order of magnitude—the EFT becomes strongly coupled. The multiparticle contributions are suppressed by additional $1/N$ factors and by loop factors $1/\ell_4$ which define the perturbative expansion in the EFT. Near the cutoff, the $1/N$ suppression is compensated by the multiplicity of states in the loop(s). Hence near the cutoff, one both expects that the resonances merge into a tree-level continuum and that loop-level continua become of same order as the tree-level one. This is included in Figure 3.3.

3.9 Conclusion

We revisit the behaviour of an effective theory of interacting matter fields in a slice of AdS_5. We work in Poincaré position-momentum space—the AdS Poincaré patch Fourier-transformed along Minkowski slices.

We study new features induced by bulk interactions for timelike four-momenta. These correspond to including the leading $1/N^2$ effects in the strongly coupled dual theory. We show using dimensional analysis that there is a transition scale, $\widetilde{\Lambda}$, above which bulk propagators lose contact with the IR brane because the latter falls beyond the domain of validity of the effective theory. The scale separates the Kaluza–Klein and continuum regimes of the bulk propagator. The continuum regime would be absent if interactions were not taken into account. Conversely the continuum regime is the only one present in the limit of strong interactions.

For timelike momenta the transition between the KK and continuum regimes occurs because the propagator is dressed by bulk interactions, a leading $1/N^2$ effect. This induces an exponential suppression of the propagator in the region where the EFT would become invalid. This censorship property was qualitatively predicted in [155]. Our treatment invokes approximations to loop integrals; more details of opacity in AdS may be better elucidated with future formal developments.

In the CFT dual, the existence of the transition scale corresponds to the fact that the effective theory of glueballs cannot contain infinitely many species. It becomes strongly coupled if more than approximately N^2 glueballs are included in the spectrum. Beyond the transition scale, a gauge theory with no mass gap should appear. This is indeed what we

demonstrate in the AdS theory.

For timelike bulk propagators, the IR brane is effectively absent when $p > \widetilde{\Lambda}$. However, cascade decays could allow correlators with energy beyond $\widetilde{\Lambda}$ to be sensitive to the IR brane because the momentum is split between many offspring states. We therefore study cascade decays to better understand the notion of IR brane emergence. We focus on a scalar with a bulk cubic interaction and investigate the squared matrix element integrated over final states that are the main ingredients of observable event rates. In the continuum regime, there exists a recursion relation between cascades of different branching depth, which we use to estimate the rate for arbitrarily deep cascade.

We have checked that contributions from other effects are subleading. These include direct decays into an IR brane localized state or into light KK modes via a tower of off-shell KK modes. We found that the contribution from the region in which the propagator is exponentially suppressed may be of the same order, but that this does not change our conclusions.

In chapter 6, we provide additional concluding remarks and paint a broader picture of soft bombs in the continuum regime of AdS.

Chapter 4

Exotic Spin-Dependent Forces from a Hidden Sector

4.1 Chapter Abstract

New dynamics from hidden sectors may manifest as long-range forces between visible matter particles. The well-known case of Yukawa-like potentials occurs via the exchange of a single virtual particle. However, more exotic behavior is also possible. We present three classes of exotic potentials that are generated by relativistic theories: (i) quantum forces from the loop-level exchange of two virtual particles, (ii) conformal forces from a conformal sector, and (iii) emergent forces from degrees of freedom that only exist in the infrared regime of the theory. We discuss the complementarity of spin-dependent force searches in an effective field theory framework. We identify well-motivated directions to search for exotic spin-dependent forces.

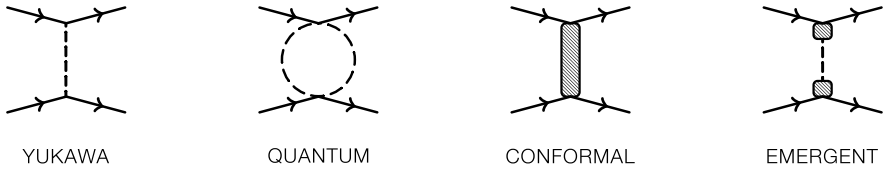

Figure 4.1: t-channel diagrams generating long-range forces in the scenarios we consider. Shaded regions represent strong dynamics.

4.2 Introduction

As stated in the introductory chapter, the main goal of this chapter is to fill a gap in the literature by presenting exotic potentials generated by explicit dark sector models. [1] As a preliminary study, we systematically consider the experimental complementarity of exotic and Yukawa-like potentials from an effective field theory perspective. The general aspects of effective theory and experimental complementarity are discussed in Sections 4.3 and 4.4. In Sections 4.5– 4.7 we identify and examine three kinds of exotic potentials based on how they are generated in a microscopic theory:

- *Quantum*: The potential is generated by particles that couple bilinearly to nucleons. The leading contribution is generated at loop-level.
- *Conformal*: The potential is generated by approximately conformal dynamics.
- *Emergent*: The potential is generated by low-mass states that exist in the infrared limit of the theory, analogous to pions in QCD.

These potentials are sketched in Fig. 4.1 and can serve as benchmarks for experimental studies.

[1] See also [46, 52, 53] for related work on spin-independent potentials.

4.3 Effective Field Theory

We assume that the dark sector interacts with nucleons via local effective operators. Because the relevant distance scales are longer than the inverse QCD confinement scale, $\Lambda_{\rm QCD}$, it is sufficient to use a relativistic effective theory of nucleons without specifying the microphysics of dark sector–partonic interactions.

4.3.1 Effective Operators and Potentials

The low-energy effective Lagrangian between nucleons and the dark sector is of the form

$$\mathcal{L} \supset \mathcal{O}_N \mathcal{O}_{\rm DS} \ . \tag{4.1}$$

We focus on bilinear nucleon operators $\mathcal{O}_{\rm N} = \bar{N}\Gamma N$ with some Lorentz structure Γ. We consider the following nucleon bilinears:

$$\begin{aligned} &\mathcal{O}_N^{\rm S} = \bar{N}N && \mathcal{O}_N^{\rm V} = \bar{N}\gamma^\mu N && \mathcal{O}_N^{\rm T} = \bar{N}\sigma^{\mu\nu}N \\ &\mathcal{O}_N^{\rm P} = \bar{N}i\gamma^5 N && \mathcal{O}_N^{\rm A} = \bar{N}\gamma^\mu\gamma^5 N \ . \end{aligned} \tag{4.2}$$

We focus on the case where only one of these operators is active in the effective Lagrangian. A pseudo-tensor operator $\bar{N}\sigma^{\mu\nu}\gamma^5 N$ also exists, but is redundant with the tensor operator in the scope of our study. [2] Nucleon bilinears with more complex Lorentz structures also exist but have higher dimension, such that the ones considered here are the most important. [3]

[2] This is a consequence of the relation $i\gamma^5\sigma^{\mu\nu} = \frac{i}{2}\varepsilon^{\mu\nu\alpha\beta}\sigma_{\alpha\beta}$.

[3] The complexity of the Lorentz structures grows together with the dimensionality of $\mathcal{O}_{\rm SM}\mathcal{O}_{DS}$ because either more derivatives or a more intricate UV origin—such as higher loop diagrams—are needed to form complex Lorentz structures.

While the $\mathcal{O}^{S,P,V,A}$ operators can have renormalizable couplings to spin-0 and spin-1 mediators, the tensor operator has to couple to other fields through a higher-dimensional operator such as a gauge field strength. We remark on ultraviolet completions of this coupling in Appendix G.

The leading relativistic $2 \to 2$ scattering amplitude contributing to long-range potential between nucleons N_1 and N_2 through operators $\mathcal{O}_N^I$ and $\mathcal{O}_N^J$ is

$$i\mathcal{M}_{IJ} \propto \langle N_{1,\text{out}}| \mathcal{O}_N^I |N_{1,\text{in}}\rangle \, \Sigma_{\text{DS}} \, \langle N_{2,\text{out}}| \mathcal{O}_N^J |N_{2,\text{in}}\rangle \tag{4.3}$$

where $I \in \{S, V, T, P, A\}$. The quantity Σ_{DS} encodes the intermediate states generated by the dark sector operators $\mathcal{O}_{\text{DS}}$. The class of 'exotic' long range potential is encoded in Σ_{DS}. We provide non-relativistic limits of $\langle N_{\text{out}}| \mathcal{O}_N^I |N_{\text{in}}\rangle$ in Appendix J.

The potential between nucleons is proportional to the spatial Fourier transform of the amplitude with respect to the exchanged three-momentum $\boldsymbol{q}$,

$$V_{IJ}(\boldsymbol{r}) = -\frac{1}{4m_N^2} \int \frac{d^3q}{(2\pi)^3} e^{i\boldsymbol{q}\cdot\boldsymbol{r}} \mathcal{M}_{IJ} \ . \tag{4.4}$$

The non-relativistic limit is taken by keeping the leading order terms in $|\boldsymbol{p}|/m_N$, where m_N is the nucleon mass and $\boldsymbol{p}$ is the characteristic nucleon three-momentum. The cutoff of the effective theory should in principle be taken into account when performing the Fourier integral[4]. We show in Appendix H that effects from the cutoff are negligible when implementing a smooth cutoff avoiding spurious non-analyticity in the integrand.

[4]In this paper the cutoff, Λ, is the scale at which the contact operators of the effective relativistic theory are UV completed. The non-relativistic potentials derived from this theory are expansions in $\boldsymbol{q}^2/M^2$, where M is typically the mass of the scattering particle. For distances shorter than M^{-1}, higher order potential terms in $\boldsymbol{q}^2/M^2$ are significant when solving the Schrödinger equation. These terms are likely pertinent to resolving the behavior of singular potentials near the origin [215]. Ref. [216] takes a complementary, bottom-

In this manuscript we focus on the case where only one operator $\mathcal{O}^I$ is present so that we examine diagonal potentials $V_I \equiv V_{II}(\boldsymbol{r})$. While cross terms $V_{IJ\neq I}(\boldsymbol{r})$ may lead to interesting effects, they are necessarily accompanied by the diagonal potentials. Thus in the scope of fifth force searches it is sufficient to focus on diagonal potentials. Table 4.1 presents classification of spin structures arising in the potentials studied in this manuscript.

The non-relativistic formalism above takes only t-channel diagrams into account and also implies that sources are distinguishable. For certain applications, u-channel diagrams can also be relevant see e.g. Ref. [215] for a discussion in the context of self-interacting dark matter.

4.3.2 Spin Dependence and Spin Averaging

Both the amplitude for nucleon scattering, $i\mathcal{M}$, and the associated long range potential, $V(r)$, are matrices in spin-space. For instance, the N_1 current connects an incoming nucleon spinor to an outgoing nucleon spinor. The potential is a tensor product of spin matrices acting on N_1 and N_2. Each component gives the potential for a probe particle of a specified spin scattering off of a source of specified spin. The spin-dependent interactions are encoded in linear combinations of Pauli matrices $\boldsymbol{\sigma}_{1,2}$ acting on N_1 and N_2, respectively. The spin-independent pieces are proportional to the 2×2 identities $\mathbb{1}_1 \otimes \mathbb{1}_2$. The spin structures appearing in the potentials are always tensor products. In this manuscript, we omit

up approach and addresses singular potentials through a renormalization procedure based on physical observables and assuming only the leading $\boldsymbol{q}^2/M^2$ term.

the explicit $\otimes$ symbol. The relevant spin structures and their simplified notation are

$$\mathbb{1}_1 \otimes \mathbb{1}_2 \equiv \mathbb{1}_1 \mathbb{1}_2 \,, \quad \sigma_1^i \otimes \sigma_2^i \equiv \boldsymbol{\sigma}_1 \cdot \boldsymbol{\sigma}_2 \,, \quad \sigma_1^i \, \nabla^i \otimes \sigma_2^j \, \nabla^j \equiv (\boldsymbol{\sigma}_1 \cdot \boldsymbol{\nabla})(\boldsymbol{\sigma}_2 \cdot \boldsymbol{\nabla}) \equiv \not{\nabla}_1 \not{\nabla}_2 \quad (4.5)$$

where the $1, 2$ indices correspond to the N_1 and N_2 currents.

For unpolarized sources, one averages over the appropriate initial (or final) state spins in the potential. Observe that this is equivalent to summing together amplitudes with different initial states. This averaging does not change the spin-independent contributions, but causes the spin-dependent contributions to vanish. The scalar and vector potentials are unaffected by polarization average, while the pseudo-scalar and axial potentials vanish at all orders. For the tensor potential a spin-independent contribution remains at next to leading order in the non-relativistic expansion. Spin averaging is denoted by $\langle \sigma_2 \rangle$ in Table 4.1.

4.3.3 Orientation Averaging for Spin-Dependent Potentials

Spin-dependent potentials may be sensitive to scattering orientation. Consider scattering of a probe particle moving along a fixed axis towards the target. One may obtain the potential for isotropic scattering—for example, in a gas—by appropriate averaging over the polar angle. This is the *orientation-averaged limit*.

Let $\hat{\boldsymbol{r}} = \boldsymbol{r}/|\boldsymbol{r}|$ be the orientation of source N_1 with respect to source N_2. Certain spin-dependent potentials are proportional to $(\boldsymbol{\sigma}_1 \cdot \boldsymbol{\nabla})\,(\boldsymbol{\sigma}_2 \cdot \boldsymbol{\nabla})$. Averaging over this orientation yields

$$\langle V(\boldsymbol{r}) \rangle_{\hat{\boldsymbol{r}}} \propto \langle (\boldsymbol{\sigma}_1 \cdot \boldsymbol{\nabla})\,(\boldsymbol{\sigma}_2 \cdot \boldsymbol{\nabla})\; f(r) \rangle_{\hat{\boldsymbol{r}}} = \frac{1}{3}\,(\boldsymbol{\sigma}_1 \cdot \boldsymbol{\sigma}_2)\,\nabla^2 f(r) \;. \quad (4.6)$$

This particular relation is phenomenologically significant. In the Coulomb case, coming from the exchange of a single massless mediator particle, the radial dependence of the potential

is $f(r) \propto 1/r$. Because this is the Green's function of the three-dimensional Laplacian,

$$\langle V(\boldsymbol{r})\rangle_{\hat{\boldsymbol{r}}} \propto \nabla^2 f(r) = -4\pi\delta(\boldsymbol{r}) \ . \tag{4.7}$$

This is simply Gauss' law. This means that when a single, massless mediator is exchanged, the spin structure in (4.6) produces only a contact interaction and no finite-range contribution. Similarly, in case of a Yukawa interaction $f(r) \propto e^{-mr}/r$, $\nabla^2 f(r) = m^2 f(r) - 4\pi\delta(\boldsymbol{r})$ gives a finite range interaction suppressed by $O((mr)^2)$ with respect to the naive dimensional expectation of $1/r^3$. The suppression of finite-range interactions in the orientation-averaged limit are important for experimental prospects. We discuss this in Section 4.4.

Orientation averaging is denoted by $\langle\hat{r}\rangle$ in Table 4.1. The columns marked Yukawa have radial dependence characteristic of single particle exchange, whereas the columns marked exotic are general and may be generated by the models presented in this manuscript.

4.3.4 Higher-Order Terms

We remark on the contribution of higher-order Feynman diagrams:

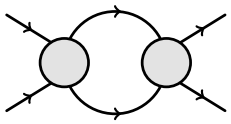

$$+\cdots \quad \propto \int \frac{d^4k}{(2\pi)^4} \langle N_{1,\text{out}}| \mathcal{O}_N^I \Delta_N O_N^I |N_{1,\text{in}}\rangle \, \Sigma_{\text{DS}} \langle N_{2,\text{out}}| \mathcal{O}_N^J \Delta_N O_N^J |N_{2,\text{in}}\rangle \ , \tag{4.8}$$

where Δ_N is the nucleon propagator. The size of such loop diagrams is suppressed compared to tree-level diagrams within the effective theory's regime of validity. A good estimate of the magnitude of these diagrams in the non-relativistic limit is obtained by taking $\Delta_N \sim -\mathbb{1}/m_N$. However, it is possible that the tree-level diagram may be suppressed by its spin-dependence while the loop diagram gives a spin-independent component. In this case, it

		$V_{S/V}$ $[\mathbb{1}/\gamma^\mu]$	V_P $[i\gamma^5]$		V_A $[\gamma^\mu\gamma^5]$		V_T $[\sigma_{\mu\nu}]$	
		Any	Exotic	Yukawa	Exotic	Yukawa	Exotic	Yukawa
no avg.	$\mathbb{1}_1\mathbb{1}_2$	✓					$m_N^{-2}r^{-2}$	$m^4m_N^{-2}r^2$
	$\not{\mathbb{V}}_1\not{\mathbb{V}}_2$		✓	✓	✓	✓	✓	✓
	$\boldsymbol{\sigma_1}\cdot\boldsymbol{\sigma_2}$				✓	✓	✓	m^2r^2
$\langle\hat{r}\rangle$	$\mathbb{1}_1\mathbb{1}_2$	✓					$m_N^{-2}r^{-2}$	$m^4m_N^{-2}r^2$
	$\boldsymbol{\sigma_1}\cdot\boldsymbol{\sigma_2}$		✓	$m^2r^2, \delta(r)$	✓	✓, $\delta(r)$	✓	m^2r^2
$\langle\hat{\sigma}_2\rangle$	$\mathbb{1}_1\mathbb{1}_2$	✓					$m_N^{-2}r^{-2}$	$m^4m_N^{-2}r^2$
	$\boldsymbol{p}\times\boldsymbol{\sigma_1}$						$m_N^{-2}r^{-1}$	$m^2m_N^{-2}r$
$\langle\hat{r}\rangle, \langle\hat{\sigma}_2\rangle$	$\mathbb{1}_1\mathbb{1}_2$	✓					$m_N^{-2}r^{-2}$	$m^4m_N^{-2}r^2$
	$\boldsymbol{p}\times\boldsymbol{\sigma_1}$							

Table 4.1: Spin structures, (4.5), generated by S, V, T, P, A nucleon operators in the cases of no averaging, the orientation-averaged limit, averaging over N_2 spins, and both the orientation-averaged limit and averaging over N_2 spin. Check marks indicate that the spin structure is generated. Other factors indicate extra suppression depending on the mediator mass, m, and the nucleon mass, m_N. Yukawa forces indicate a potential with radial dependence $f(r) \sim e^{-mr}/r$. Exotic forces indicate a radial dependence that is not Yukawa-like.

is possible that the loop-level contribution produces the most experimentally viable signal. See Section 4.4 for more details.

We explicitly illustrate the calculation of a higher order contribution with the case of a pseudoscalar, $\mathcal{L} = iy\phi\bar{N}\gamma_5 N$. The tree-level exchange of ϕ generates a spin-dependent Yukawa-type force, as indicated in Tab. 4.1. At one-loop order, a box diagram made of ϕ and N propagators exists. The diagram corresponds to substituting the blobs by tree-level exchange of ϕ in (4.8).[5] The vertices in the amplitude of (4.8) are $\mathcal{O}_N^{I,J} = -y\gamma_5$. In our approximation, we reduce the nucleon propagators Δ_N to $-\mathbb{1}/m_N$ in this amplitude. The two γ_5 simplify, giving $\mathcal{O}^I\Delta_N\mathcal{O}^I \approx -\mathbb{1}/m_N$. One then notices that such contracted diagram

[5] A cross-diagram also exists.

is equivalent to the exchange of a bubble of scalars induced by an effective operator

$$\frac{y^2}{2m_N}\phi^2\bar{N}N\,. \tag{4.9}$$

Such bubble loop diagram is much simpler to calculate than the original box, and has been evaluated in *e.g.* Ref. [46]. The effective vertex (4.9) gives the spin-independent potential

$$V(r) = -\frac{y^4}{64\pi^3 m_N^2 r^3}\,. \tag{4.10}$$

It turns out this result matches exactly the result obtained by evaluation of the full box diagram made in [52]. Note however that in general our approximation should give the correct behaviour of the potential but not necessarily reproduce the exact coefficient.

4.4 On Experimental Complementarity

Our effective theory study of the potentials in Section 4.3 and the corresponding classification of their properties in Table 4.1 are useful to evaluate experimental prospects. They can be used to sharpen a search strategy and delineate the theoretical motivations of a search. Whenever an experiment has potential sensitivity to a given type of potential, it is natural to ask whether another effect necessarily exists which may overwhelm the proposed search: either because an experimental bound is already set or because it provides a more promising search direction. In this section, we discuss some examples of experimental complementarity and point out the consequences for existing and future searches.

Two types of searches for fifth forces are neutron spin rotation and nuclear magnetic resonance experiments. Neutron spin rotation experiments pass a polarized neutron beam between metal plates that contain unpolarized spins. Spin–velocity potentials cause

the polarized neutron spins to precess about the direction of their three-momentum as they pass through the plates. The observation of this precession would be evidence for new physics that generates a spin–velocity potential. Nuclear magnetic resonance (NMR) experiments can probe new spin-dependent forces through the effective anomalous J-coupling of deuterated molecular hydrogen (HD). A gas of HD is in a disordered phase because collisions result in random reorientations of nuclei. The relative orientations between nuclei must be averaged for a fixed separation. This presents a way to search for orientation-averaged potentials. We present quantitative details of the experimental reach of NMR experiments in Section 4.5.1.

A simple example of this experimental complementarity is as follows. The vector–axial Yukawa cross-potential V_{VA} features a spin-velocity term that can be probed by neutron spin rotation experiments [51]. However, any effective theory that yields a V_{VA} potential must simultaneously furnish a vector–vector Yukawa potential V_V. This V_V potential is spin-independent and easier to probe experimentally. As a matter of fact, it is highly constrained. In the scope of the search for the dark sector, focusing on V_V is clearly more efficient than V_{VA} so that the search for V_{VA} is therefore not well-motivated. [6]

We see that the complementarity between spin-dependent and spin-independent searches is an important experimental consideration. To further illustrate this, consider the tree-level exchange of a single pseudoscalar versus the loop-level box diagram coming from the exchange of two pseudoscalars; see Sec. 4.3.4. The former term is spin-dependent while the loop contribution is spin-independent. It is natural to ask which of these contributions

[6]Note that if a new V_V potential were actually discovered, the cross term V_{VA} would then become an efficient way to search for a spin-dependent coupling of the newly discovered particle.

is a more effective channel to search for the new pseudoscalar particle. A search for the spin-dependent pseudoscalar potential has been done in [5] using NMR data. The experiment is in a disordered phase so that the potentials are calculated in the orientation-averaged limit. This means that the dominant contribution to the tree-level potential vanishes, and the main term is proportional to $e^{-mr}m^2/(m_N^2 r) \ll e^{-mr}/(m_N^2 r^3)$. On the other hand, the loop-level contribution force is proportional to $1/(m_N^2 r^3)$ at short distance, as shown in (4.10). The bound on this one-loop, spin-independent component can be readily obtained from [46]. It turns out that, except in a region of a few orders of magnitude around $m \sim 10$ keV where the NMR search is optimal, the bounds from the *spin-independent* component are the dominant ones. There is therefore complementarity between spin-dependent and spin-independent searches, and the spin-independent search turns out to be quite competitive in this example. See [217] for another example of this complementarity.

Another key aspect of experimental complementarity is the role of exotic versus Yukawa forces and the corresponding interplay with orientation and spin averages. To discuss orientation averaging, consider again the example of a pseudoscalar discussed above. The Yukawa-like spin-dependent force is suppressed because of Gauss' law. In particular, the force is suppressed by a $\mathcal{O}\left(m^2 r^2\right)$ factor such that the search sensitivity vanishes in the $m \to 0$ limit, while the spin-independent component does not. In contrast, an exotic force is—by definition—not subject to cancellations related to Gauss' law, and is therefore not suppressed in the same way. This affects the size of the spin-dependent force relative to higher-order spin-independent counterparts. Moreover, in contrast to scenarios with Yukawa-like forces, one typically expects that the higher-loop contributions to exotic

forces are subdominant and poorly constrained. From this, one concludes that exotic forces motivate experiments with disordered phases—such as NMR-based searches [5].

The case of a single polarized source is also interesting. Table 4.1 shows that the tensor potential features a mixed velocity–spin structure, $\boldsymbol{p} \times \boldsymbol{\sigma}_1$, in this limit. The complementarity of Yukawa versus exotic forces is again relevant in this case. For a Yukawa-type force, the velocity-dependent structure is $\mathcal{O}(m^2)$ and thus vanishes in the $m \to 0$ limit. This is not the case for an exotic force. One concludes that exotic forces motivate searches for velocity–spin dependent forces. These can be done in experiments with a polarized source—such as a neutron beam—at finite velocity. We expand on the theoretical ultraviolet completion of the tensor operator in Appendix G.

In summary, the possible existence of exotic spin-dependent forces motivates experiments with (i) disordered phases and (ii) polarized sources at finite velocity. Another general lesson is that the properties of Yukawa-like forces are rather non-generic and so they should not be used as the only benchmark for spin-dependent fifth force experiments. The following sections present well-motivated alternatives that can serve as benchmark models for the exotic potentials.

4.5 Spin-Dependent Quantum Forces

Our first example of an exotic force is when $\mathcal{O}_{\rm DS}$ in (4.1) is a bilinear of dark particles, each with mass m. The potential is generated by the exchange of *two* virtual particles [218]. In the scenario where the dark particles are dark matter, then the bilinear interaction with nucleons may be motivated from a $\mathbb{Z}_2$ symmetry that explains the particle's

stability. [7]

We extend the spin-independent study in Ref. [53] to the case of spin-dependent nucleon operators. We write the combined $\mathcal{O}_N\mathcal{O}_{\rm DS}$ operators in (4.1) as effective contact operators. Because $\mathcal{O}_{\rm DS}$ is a dark particle bilinear, it is possible to have dark particles of any spin. Here we consider spin-0, $\frac{1}{2}$, and 1. These operators are non-renormalizable so that the effective theory is valid above distance scales of

$$r \sim \max\left(\frac{1}{4\pi\Lambda}\,,\,\frac{1}{4\pi\Lambda_{\rm QCD}}\right)\,, \tag{4.11}$$

where Λ is the scale at which the contact operator description breaks down. This is defined by the underlying physics that generate the $\mathcal{O}_{\rm N}\mathcal{O}_{\rm DS}$ operators. We consider the operators:

$$\begin{aligned}
&\mathcal{O}_a^0 = \frac{1}{\Lambda^2}\bar{N}\gamma^\mu\gamma^5 N i\phi^*\overleftrightarrow{\partial_\mu}\phi && \mathcal{O}_a^{\frac{1}{2}} = \frac{1}{\Lambda^2}\bar{N}i\gamma^5 N\bar{\chi}i\gamma^5\chi && \mathcal{O}_a^1 = \frac{1}{\Lambda^3}\bar{N}i\gamma^5 N|X_{\mu\nu}|^2\\
&\mathcal{O}_b^0 = \frac{1}{\Lambda}\bar{N}i\gamma^5 N|\phi|^2 && \mathcal{O}_b^{\frac{1}{2}} = \frac{1}{\Lambda^2}\bar{N}i\gamma^5 N\bar{\chi}\chi && \mathcal{O}_b^1 = \frac{1}{\Lambda^3}\bar{N}i\gamma^5 N X_{\mu\nu}\widetilde{X}^{\mu\nu}\\
&\mathcal{O}_c^0 = \frac{1}{\Lambda^3}\bar{N}i\gamma^5 N|\partial_\mu\phi|^2 && \mathcal{O}_c^{\frac{1}{2}} = \frac{1}{\Lambda^2}\bar{N}\gamma^\mu\gamma^5 N\bar{\chi}\gamma_\mu\gamma^5\chi\\
&\mathcal{O}_d^0 = \frac{1}{\Lambda^3}\bar{N}\sigma^{\mu\nu}N(\partial_\mu\phi)(\partial_\nu\phi^*) && \mathcal{O}_d^{\frac{1}{2}} = \frac{1}{\Lambda^2}\bar{N}\gamma^\mu\gamma^5 N\bar{\chi}\gamma_\mu\chi\\
& && \mathcal{O}_e^{\frac{1}{2}} = \frac{1}{\Lambda^2}\bar{N}\sigma^{\mu\nu}N\bar{\chi}\sigma_{\mu\nu}\chi
\end{aligned}\,. \tag{4.12}$$

We write the dark particle as ϕ for scalars, χ for fermions, and X^μ for vectors. We use $\overleftrightarrow{\partial_\mu} \equiv \overrightarrow{\partial_\mu} - \overleftarrow{\partial_\mu}$. We assume that only one of these operators is active. That is, we do not consider any cases that mix vertices from different operators in a single Feynman diagram.

The potentials depend on modified Bessel functions of the second kind and on a

[7] The search for long-range potentials induced by the loop-level exchange of pairs of dark particles is then a search for virtual dark matter. In contrast to searches for on-shell dark matter in direct detection experiments, this is independent of the dark matter phase space distribution in the local galaxy.

Meijer G-function; we denote these by:

$$K_i \equiv K_i(2mr) \qquad\qquad G \equiv G^{2,0}_{2,4}\left(m^2 r^2 \middle| \begin{matrix} \frac{1}{2}, \frac{3}{2} \\ 0, 0, \frac{1}{2}, \frac{1}{2} \end{matrix} \right) . \tag{4.13}$$

We also introduce a discrete variable for whether or not the dark particle is self-conjugate:

$$\eta = \begin{cases} 0 & \text{if self-conjugate} \\ 1 & \text{otherwise} \end{cases} . \tag{4.14}$$

For these loop-induced potentials, the amplitude has a branch cut—appearing via a logarithm. The Fourier transform integral (4.4) is performed by analytical continuation into the complex $|\boldsymbol{q}|$ plane, reducing the integral over the real line to one on the discontinuity across the branch cut. Details are provided in Appendix I.

The operators produce the following potentials:

$$V_a^0 = -\eta\frac{m^2(\boldsymbol{\sigma_1}\cdot\boldsymbol{\sigma_2})}{8\pi^3\Lambda^4}\left(\frac{K_2}{r^3}\right) - \eta\frac{(\boldsymbol{\sigma_1}\cdot\boldsymbol{\nabla})(\boldsymbol{\sigma_2}\cdot\boldsymbol{\nabla})}{96\pi^3\Lambda^4}\left(\frac{-2mrK_1+4+m^2\pi^2r^2G}{r^3}\right) \tag{4.15}$$

$$V_b^0 = 2^\eta\frac{m(\boldsymbol{\sigma_1}\cdot\boldsymbol{\nabla})(\boldsymbol{\sigma_2}\cdot\boldsymbol{\nabla})}{128\pi^3\Lambda^2m_N^2}\left(\frac{K_1}{r^2}\right) \tag{4.16}$$

$$V_c^0 = 2^\eta\frac{m^2(\boldsymbol{\sigma_1}\cdot\boldsymbol{\nabla})(\boldsymbol{\sigma_2}\cdot\boldsymbol{\nabla})}{128\pi^3\Lambda^6m_N^2}\left(\frac{(15mr+m^3r^3)K_1+(30+6m^2r^2)K_2}{r^5}\right) \tag{4.17}$$

$$V_d^0 = \eta\frac{\left[(\boldsymbol{\sigma_1}\cdot\boldsymbol{\nabla})(\boldsymbol{\sigma_2}\cdot\boldsymbol{\nabla})-(\boldsymbol{\sigma_1}\cdot\boldsymbol{\sigma_2})\nabla^2\right]}{32\pi^3\Lambda^6}\left(\frac{m^2K_2}{r^3}\right) \tag{4.18}$$

$$V_a^{\frac{1}{2}} = 2^\eta\frac{(\boldsymbol{\sigma_1}\cdot\boldsymbol{\nabla})(\boldsymbol{\sigma_2}\cdot\boldsymbol{\nabla})}{32\pi^3m_N^2\Lambda^4}\left(\frac{3m^2K_2-2m^3rK_1}{r^3}\right) \tag{4.19}$$

$$V_b^{\frac{1}{2}} = 2^\eta\frac{(\boldsymbol{\sigma_1}\cdot\boldsymbol{\nabla})(\boldsymbol{\sigma_2}\cdot\boldsymbol{\nabla})}{32\pi^3m_N^2\Lambda^4}\left(\frac{3m^2K_2}{r^3}\right) \tag{4.20}$$

$$V_c^{\frac{1}{2}} = -2^\eta\frac{m^2(\boldsymbol{\sigma_1}\cdot\boldsymbol{\sigma_2})}{4\pi^3\Lambda^4}\left(\frac{K_2}{r^3}\right) + 2^\eta\frac{(\boldsymbol{\sigma_1}\cdot\boldsymbol{\nabla})(\boldsymbol{\sigma_2}\cdot\boldsymbol{\nabla})}{96\pi^3\Lambda^4}\left(\frac{\pi^2m^2r^2G+4mrK_1+4}{r^3}\right) \tag{4.21}$$

$$V_d^{\frac{1}{2}} = -\eta\frac{m^2(\boldsymbol{\sigma_1}\cdot\boldsymbol{\sigma_2})}{2\pi^3\Lambda^4}\left(\frac{mrK_1+K_2}{r^3}\right) + \eta\frac{(\boldsymbol{\sigma_1}\cdot\boldsymbol{\nabla})(\boldsymbol{\sigma_2}\cdot\boldsymbol{\nabla})}{48\pi^3\Lambda^4}\left(\frac{\pi^2m^2r^2G+4mrK_1+4}{r^3}\right) \tag{4.22}$$

$$V_e^{\frac{1}{2}} = -\eta\frac{m^2(\boldsymbol{\sigma_1}\cdot\boldsymbol{\sigma_2})}{\pi^3\Lambda^4}\left(\frac{K_2}{r^3}\right) - \eta\frac{\left[(\boldsymbol{\sigma_1}\cdot\boldsymbol{\nabla})(\boldsymbol{\sigma_2}\cdot\boldsymbol{\nabla})-(\boldsymbol{\sigma_1}\cdot\boldsymbol{\sigma_2})\nabla^2\right]}{12\pi^3\Lambda^4}\left(\frac{\pi^2m^2r^2G+4mrK_1+4}{r^3}\right) \tag{4.23}$$

$$V_a^1 = 2^\eta\frac{(\boldsymbol{\sigma_1}\cdot\boldsymbol{\nabla})(\boldsymbol{\sigma_2}\cdot\boldsymbol{\nabla})}{8\pi^3m_N^2\Lambda^6}\left[\left(\frac{30m^3}{r^4}+\frac{3m^5}{r^2}\right)K_1+\left(\frac{60m^2}{r^5}+\frac{12m^4}{r^3}\right)K_2\right] \tag{4.24}$$

$$V_b^1 = 2^\eta\frac{(\boldsymbol{\sigma_1}\cdot\boldsymbol{\nabla})(\boldsymbol{\sigma_2}\cdot\boldsymbol{\nabla})}{8\pi^3m_N^2\Lambda^6}\left(\frac{30m^3}{r^4}K_3+\frac{12m^4}{r^3}K_2\right)\ . \tag{4.25}$$

4.5.1 Orientation-Averaged Limit

We perform the orientation-averaging limit of Section 4.3.3 on the potentials of the previous section. We present these in the $r \ll m^{-1}$ limit. Note that by doing so, the mass dependence drops out. These take the limiting forms:

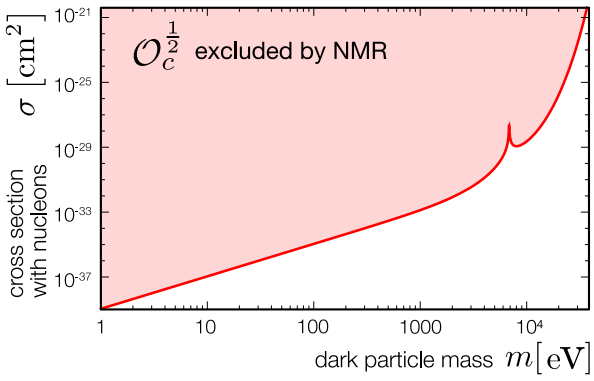

Figure 4.2: Bounds on $\mathcal{O}_c^{\frac{1}{2}}$ from NMR [5] on the direct detection plane. Note that this search is sensitive to much lighter masses than direct detection experiments, e.g. [6]. The cross section is for tree-level $2 \to 2$ scattering of dark matter off xenon. The bound vanishes in a narrow region around $m \approx 6850$ eV because orientation averaging causes $V_c^{\frac{1}{2}}$ to vanish at approximately $2mr \approx 5.2$.

$$
\begin{aligned}
V_a^0 &= -\eta \frac{\boldsymbol{\sigma_1}\cdot\boldsymbol{\sigma_2}}{24\pi^3\Lambda^4}\frac{1}{r^5} & V_a^{\frac{1}{2}} &= 2^\eta \frac{\boldsymbol{\sigma_1}\cdot\boldsymbol{\sigma_2}}{16\pi^3 m_N^2\Lambda^4}\frac{5}{r^7} & V_a^1 &= 2^\eta \frac{\boldsymbol{\sigma_1}\cdot\boldsymbol{\sigma_2}}{2\pi^3 m_N^2\Lambda^6}\frac{105}{r^9} \\
V_b^0 &= 2^\eta \frac{\boldsymbol{\sigma_1}\cdot\boldsymbol{\sigma_2}}{128\pi^3 m_N^2\Lambda^2}\frac{1}{r^5} & V_b^{\frac{1}{2}} &= 2^\eta \frac{\boldsymbol{\sigma_1}\cdot\boldsymbol{\sigma_2}}{16\pi^3 m_N^2\Lambda^4}\frac{5}{r^7} & V_b^1 &= 2^\eta \frac{\boldsymbol{\sigma_1}\cdot\boldsymbol{\sigma_2}}{2\pi^3 m_N^2\Lambda^6}\frac{105}{r^9} \\
V_c^0 &= 2^\eta \frac{\boldsymbol{\sigma_1}\cdot\boldsymbol{\sigma_2}}{64\pi^3 m_N^2\Lambda^6}\frac{105}{r^9} & V_c^{\frac{1}{2}} &= -2^\eta \frac{\boldsymbol{\sigma_1}\cdot\boldsymbol{\sigma_2}}{12\pi^3\Lambda^4}\frac{1}{r^5} & & \\
V_d^0 &= -\eta \frac{\boldsymbol{\sigma_1}\cdot\boldsymbol{\sigma_2}}{24\pi^3\Lambda^6}\frac{5}{r^7} & V_d^{\frac{1}{2}} &= -\eta \frac{\boldsymbol{\sigma_1}\cdot\boldsymbol{\sigma_2}}{6\pi^3\Lambda^4}\frac{1}{r^5} & & \\
& & V_e^{\frac{1}{2}} &= \eta \frac{\boldsymbol{\sigma_1}\cdot\boldsymbol{\sigma_2}}{6\pi^3\Lambda^4}\frac{1}{r^5} & &
\end{aligned}
\tag{4.26}
$$

Bounds on Dark Matter from NMR

The orientation-averaged form of the potential appears when forces are present in a disordered phase of matter. This is the case for NMR experiments in a gas phase. NMR data can be used to place bounds on the effective anomalous J-coupling of deuterated molecular hydrogen HD; Ref. [5] found that ΔJ_3 must be less than 9.8×10^{-16} eV. This, in

turn, bounds the strength of a possible spin-dependent potential between these nuclei. The proton-deuteron distance is of order $\langle r \rangle = 0.00038\,\mathrm{eV}^{-1}$. The relative orientations between nuclei are averaged because of random reorientation of HD molecules due to collisions.

If one of the dark particles ϕ, χ or X^μ is identified as the dark matter, the contact interactions (4.13) induce dark matter–nucleus scattering. This scattering process is probed by dark matter direct detection experiments. The sensitivity of such searches typically drops below $m \sim 1\,\mathrm{GeV}$. In contrast, NMR experiments probe dark particles that are much lighter than this scale—illustrating the complementarity between dark matter scattering and quantum force searches.

As a specific example, we provide bounds on Dirac dark matter interacting with xenon through the $\mathcal{O}_c^{\frac{1}{2}}$ axial-vector interaction. This is the standard benchmark case for spin-dependent direct detection. The bound is plotted in Fig. 4.2.

4.5.2 Spin-dependent Potentials with One Unpolarized Source

In the case in which one source is unpolarized, one must average over source's initial state spins. The corresponding nucleon bilinear vanishes for pseudoscalar ($Ni\gamma_5 N$) and axial vector ($\bar{N}\gamma_\mu\gamma_5 N$) interactions. This leaves only the operators with spin-0 or spin-1/2 dark particles interacting with the nucleon dipole. The resulting potentials include a term that is spin independent term and a term that is both spin and velocity dependent. We define the velocity, $\boldsymbol{v}$ as the average of the probe nucleon's incoming and outgoing momenta divided by the nucleon mass.

The general long-range potentials are:

$$V_d^0 = \eta \frac{2m_N \mathbb{1}_2 (\boldsymbol{v} \times \boldsymbol{\sigma_1}) \cdot \boldsymbol{\nabla} + \mathbb{1}_1 \mathbb{1}_2 \nabla^2}{128\pi^3 m_N^2 \Lambda^6} \nabla^2 \left(\frac{m^2 K_2}{r^3} \right) \tag{4.27}$$

$$V_e^{\frac{1}{2}} = \eta \frac{2m_N \mathbb{1}_2 (\boldsymbol{v} \times \boldsymbol{\sigma_1}) \cdot \boldsymbol{\nabla} + \mathbb{1}_1 \mathbb{1}_2 \nabla^2}{4\pi^3 m_N^2 \Lambda^4} m^2 \left(\frac{2mrK_1 + K_2}{r^3} \right) . \tag{4.28}$$

At distances much smaller than the dark particle's Compton wavelength, m^{-1}, these reduce to:

$$V_d^0(r \ll m^{-1}) = \eta \frac{5}{64\pi^3 m_N^2 \Lambda^6} \left(\frac{42 \mathbb{1}_1 \mathbb{1}_2}{r^9} + 2m_N \mathbb{1}_2 (\boldsymbol{v} \times \boldsymbol{\sigma_1}) \cdot \boldsymbol{\nabla} \frac{1}{r^7} \right) \tag{4.29}$$

$$V_e^{\frac{1}{2}}(r \ll m^{-1}) = \eta \frac{1}{8\pi^3 m_N^2 \Lambda^4} \left(\frac{20 \mathbb{1}_1 \mathbb{1}_2}{r^7} + 2m_N \mathbb{1}_2 (\boldsymbol{v} \times \boldsymbol{\sigma_1}) \cdot \boldsymbol{\nabla} \frac{1}{r^5} \right) . \tag{4.30}$$

4.6 Spin-Dependent Warped/Conformal Forces

Weakly coupled new physics in four dimensions produce potentials that carry negative integer powers of r. This section presents a departure from this behavior by examining effects from a five dimensional curved space and from a four-dimensional conformal sector.

4.6.1 Warped Dark Sector Scenario

The Standard Model may live on a four-dimensional brane lying at the boundary of a truncated five-dimensional AdS space with curvature k; see e.g. [28, 29, 155]. We refer to this brane as the UV brane. In this model, the effect of 5D gravity is mild as it is localized away from the UV brane. 5D gravity only induces a small $\mathcal{O}(k^{-2}r^{-3})$ correction to Newton potential. Such deviation is mildly constrained experimentally: torsion pendulum experiments put a lower bound $k \gtrsim 10^4$ TeV, which constitutes the leading constraint for

curvature in this model [46]. On the other hand, the AdS curvature k may be as high as the 4D Planck mass while staying consistent with the validity of the 5D effective theory.

Beyond this minimal braneworld model, matter fields can in principle propagate in the bulk of the extra dimension. These fields tend to be hidden from the UV brane as a result of the localization in the fifth dimension induced by the curvature. This framework therefore naturally gives rise to a dark sector [27] and is sketched in Fig. 4.3. As a concrete realization, consider the simplest case of a bulk scalar field, Φ that couples linearly to nucleons. The 5D matter action is

$$S_5 \supset \int_{\text{bulk}} d^5X \sqrt{|g|} \left(\frac{1}{2} \partial_M \Phi \partial^M \Phi - \frac{m_\Phi^2}{2} \Phi^2 \right) + \int_{\text{brane}} d^4X \sqrt{|\gamma|} \left(\mathcal{L}_{\text{SM}} + \frac{\lambda}{\sqrt{k}} \mathcal{O}_{\text{N}} \Phi - \frac{m_{\text{UV}}}{2} \Phi^2 \right) , \tag{4.31}$$

where $\gamma_{\mu\nu}$ is the induced metric on the brane, $\mathcal{O}_N$ is a nucleon bilinear, and λ is a dimensionless effective coupling which can be taken to be of order one. Using conformal coordinates and a $(+,-,-,-,-)$ signature, the AdS metric reads

$$ds^2 = g_{MN} X^M X^N = \frac{1}{(kz)^2} \left(\eta_{\mu\nu} dx^\mu dx^\nu - dz^2 \right) , \tag{4.32}$$

and the brane is localized at $z_0 = k^{-1}$.[8] We focus on the case of a brane-localized mass term satisfying the condition $m_{\text{UV}} = \sqrt{4k^2 + m_\Phi^2} - 2k$. This is consistent with the BPS brane condition from supergravity, and can be also motivated using holography, see [29] and references therein.

We consider couplings of the bulk scalar to the scalar ($\mathcal{O}_S$) and pseudoscalar ($\mathcal{O}_P$) nucleon operators in (4.2). The former generates a spin-independent force which we include

[8] Another common convention in the literature is to use the curvature radius of AdS, $R \equiv k^{-1}$.

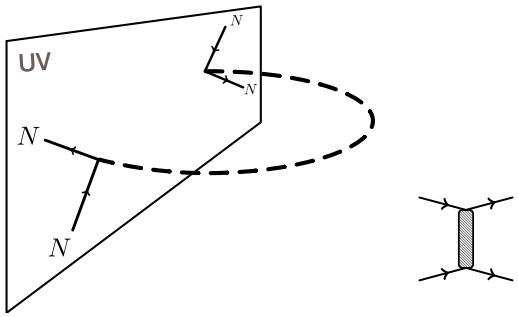

Figure 4.3: Diagram in 5D anti-de Sitter space giving rise to the conformal force.

as a useful benchmark. The axial coupling $\frac{1}{\Lambda}\bar{N}\gamma_5\gamma_\mu N\partial_\mu\Phi$ generates the same tree-level potential as the pseudoscalar. This can be seen directly at the level of the Lagrangian by integrating by part the interaction and using the nucleon equation of motion. [9]

4.6.2 Potential

The brane-to-brane Feynman propagator for Φ in mixed position/momentum space [219, 220] reads

$$\langle\Phi(p^\mu,z_0)\Phi(-p^\mu,z_0)\rangle \equiv \Delta_p(z_0,z_0) = \frac{i}{p}\frac{H^{(1)}_\alpha(p/k)}{H^{(1)}_{\alpha-1}(p/k)} \quad p=\sqrt{\eta_{\mu\nu}p^\mu p^\nu} \quad \alpha=\sqrt{4+\frac{m_\Phi^2}{k^2}}\,, \tag{4.33}$$

where $H^{(1)}$ is the Hankel function of the first kind. Regularity of the solution to the 5D equation of motion is imposed to obtain this propagator. For invariant four-momenta much

[9] The theories differ at higher order in their interactions. At loop level, for example, the spin-independent potential from a scalar with a derivative coupling to an axial vector current can be distinguished from a pseudoscalar [52].

less than the curvature, $p \ll k$, this gives

$$\Delta_p(z_0, z_0) \approx i \left[\frac{p^2}{2k(\alpha - 1)} - 2k \, \frac{\Gamma(1-\alpha)}{\Gamma(\alpha)} \left(-\frac{p}{2k} \right)^{2\alpha} \right]^{-1} . \tag{4.34}$$

For $\alpha > 1$, this propagator is dominated by the analytic term $\propto 1/p^2$. An observer on the UV brane thus mostly see a 4D massless field, similarly to the gravity case discussed above. For $\alpha < 1$, on the other hand, the propagator (4.34) is dominated by the non-analytic term with $p^{2\alpha}$ scaling.

One may qualitatively understand this behavior by imagining the presence of an IR brane at some distance $z_1 > z_0$ that creates a discrete spectrum of Kaluza–Klein modes. The parameter α controls the localization of these modes. For $\alpha > 1$ and any boundary condition on the IR brane, an ultralight mode localized on the UV brane exists. This corresponds to the 4D pole in $\Delta_p(z_0, z_0)$. For $\alpha < 1$, the light mode is instead localized towards the IR brane and an observer on the UV brane is primarily sensitive to the Kaluza–Klein excitations that are collectively encoded in the non-analytic $p^{2\alpha}$ term.

For the case $\alpha < 1$, the bulk scalar Φ generates an exotic long-range force between the nucleons on the UV brane. This force has *non-integer* dependence on the nucleon separation. The scalar and pseudo-scalar nucleon operators in (4.2) generate the following potentials:

$$V_S(r) = \frac{-\lambda^2}{2\pi^{\frac{3}{2}}} \frac{\Gamma(\frac{3}{2} - \alpha)}{\Gamma(1-\alpha)} \frac{1}{r(kr)^{2-2\alpha}} \tag{4.35}$$

$$V_P(r) = \frac{\lambda^2}{2\pi^{\frac{3}{2}}} \frac{\Gamma(\frac{3}{2} - \alpha)}{\Gamma(1-\alpha)} \frac{(\boldsymbol{\sigma_1} \cdot \boldsymbol{\nabla})(\boldsymbol{\sigma_2} \cdot \boldsymbol{\nabla})}{4m_N^2} \left(\frac{1}{r(kr)^{2-2\alpha}} \right) . \tag{4.36}$$

In the orientation-averaged limit, the pseudo-scalar potential becomes:

$$V_P(r) = \frac{2\lambda^2}{3\pi^{\frac{3}{2}}} \frac{(1-\alpha)\Gamma(\frac{5}{2} - \alpha)}{\Gamma(1-\alpha)} \frac{(\boldsymbol{\sigma_1} \cdot \boldsymbol{\sigma_2})}{4m_N^2} \frac{1}{r^3(kr)^{2-2\alpha}} . \tag{4.37}$$

4.6.3 A Conformal Model

The AdS/CFT correspondence relates the warped dark sector model to a purely four-dimensional conformal dark sector. For an exotic potential with $\alpha < 1$, the simplest realization of the duality is

$$\mathcal{L} = \mathcal{L}_{\rm SM} + \mathcal{L}_{\rm CFT} + \frac{1}{M^{\Delta_{\rm SM}+\Delta_{\rm CFT}-4}}\mathcal{O}_{\rm N}\mathcal{O}_{\rm CFT}\,. \tag{4.38}$$

The Lagrangian $\mathcal{L}_{\rm CFT}$ encodes the dynamics of the conformal field theory. The operator $\mathcal{O}_{\rm CFT}$ contains fields from the conformal sector. $\Delta_{\rm SM} = 3$ is the scaling dimension of the scalar or pseudo-scalar nucleon operators. We further define $\Delta \equiv \Delta_{\rm CFT}$, the dimension of the $\mathcal{O}_{\rm CFT}$ operator.

The symmetries of the CFT fully dictates the theory's behavior. In position space, conformal symmetry constrains the two-point correlation function to be

$$\langle \mathcal{O}_{\rm CFT}(0)\, \mathcal{O}_{\rm CFT}(x)\rangle = \frac{c}{4\pi^2(-|x|)^{2\Delta}}\ , \tag{4.39}$$

where c is an undetermined real number. In momentum space this is

$$\langle \mathcal{O}_{\rm CFT}(-p)\, \mathcal{O}_{\rm CFT}(p)\rangle = c\frac{i\,\Gamma(2-\Delta)}{4\,\Gamma(\Delta)}\left(\frac{-p^2}{4}\right)^{\Delta-2}\ . \tag{4.40}$$

By construction, nucleons source this correlation function and thus experience a force due to the conformal dynamics.

By comparing (4.40) to the non-analytical part of the brane-to-brane propagator in (4.34), one identifies $\Delta = 2-\alpha$. In the language of AdS/CFT, this is the "Δ_- branch" of the correspondence, in which the boundary of the bulk field is identified with the classical value of $\mathcal{O}_{\rm CFT}$ itself. This version of the duality is valid only for $0 < \alpha < 1$, i.e. $1 < \Delta < 2$.

In contrast, the Δ_+ branch identifies $\Delta = 2 + \alpha$ and is valid for any α. The Δ_- branch model is sufficient in the context of our study.

Taking the non-relativistic limit of the conformal two-point functions and transforming back to position space yields the *conformal* spin-dependent potentials analogous to (4.35–4.36):

$$V_S(r) = \frac{c}{4\pi^{3/2}} \frac{\Gamma(\Delta - 1/2)}{\Gamma(\Delta)} \frac{1}{r(Mr)^{2\Delta-2}} \tag{4.41}$$

$$V_P(r) = -\frac{c}{4\pi^{3/2}} \frac{\Gamma(\Delta - 1/2)}{\Gamma(\Delta)} \frac{(\boldsymbol{\sigma_1} \cdot \boldsymbol{\nabla})(\boldsymbol{\sigma_2} \cdot \boldsymbol{\nabla})}{4m_N^2} \left(\frac{1}{r(Mr)^{2\Delta-2}} \right) . \tag{4.42}$$

Both the warped and conformal models continuously interpolates between $1/r$ and $1/r^3$ as a function of a continuous parameter: either the bulk mass of the scalar field living AdS space, or—equivalently—the conformal dimension of the correlation function of conformal dynamics exchanged between nucleons.

4.7 Spin-Dependent Emergent Forces

A new force may emerge from a change in a theory's degrees of freedom at low energies. This may happen, for example, as a consequence of a phase transition. This scenario departs from Yukawa-like behavior and is thus exotic. Also, there is a priori no principle enforcing exact continuity of the potential between the short- and long-distance regimes, hence the potential might feature a smooth kink in the transition regime. We discuss this scenario from the perspective of a confining non-Abelian gauge theory and present a more explicit realization from a five-dimensional holographic setup.

4.7.1 Emergent Force from a Confining Dark Sector

Suppose a dark sector contains a non-Abelian gauge field with coupling g and field strength $X_{\mu\nu}$. This sector can couple to visible matter through gauge-invariant higher-dimensional operators of the form (4.1):

$$\mathcal{L} \supset \frac{c}{M^3}\mathcal{O}_{\rm N} X_{\mu\nu}X^{\mu\nu} + \cdots \ . \tag{4.43}$$

In the regime where the dark sector gauge theory is weakly coupled, it induces a quantum force (see Section 4.5), whose exact form is given by (4.25). Dimensional analysis requires the potential to scale as

$$V(r)_{\rm gauge} \sim \frac{c^2\, g^4}{M^6 r^7} \ . \tag{4.44}$$

When the gauge theory is asymptotically free, there is an infrared scale, $\mu \ll M$, at which the theory becomes strongly-interacting and confines. In this scenario, the theory may develop a mass gap analogous to QCD. Below the confinement scale, physics is described by an effective theory of composite states. Composite states with same quantum numbers as Tr $X_{\mu\nu}X^{\mu\nu}$ may arise as scalar glueball fields:

$$\mathcal{L}_{\rm conf} \supset \frac{c_\varphi \mu^3}{M^3}\mathcal{O}_{\rm SM}\,\varphi + \dots \ , \tag{4.45}$$

where φ is a CP-even scalar denoting the glueball excitation in the confined theory. See Refs. [221, 222] for earlier work on dark sectors described by glueball-like excitations. The c_φ coefficient arises from strong dynamics and is evaluated by dimensional analysis at strong coupling.

In the confined phase, $r \gg \mu^{-1}$, the potential is Yukawa-like,

$$V_{\rm conf}(r) \sim \frac{c_\varphi^2}{r}\frac{\mu^6}{M^6} \, . \tag{4.46}$$

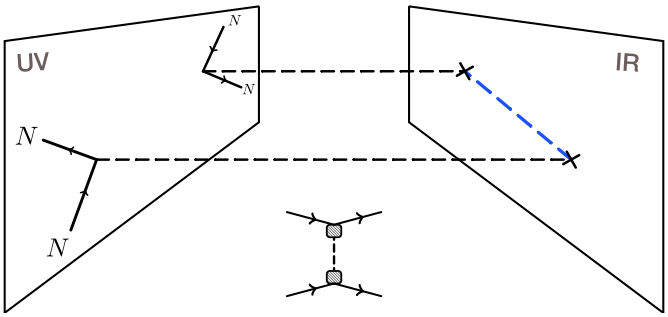

Figure 4.4: Diagram in 5D anti-de Sitter space giving rise to the emergent force. Blue line shows the propagator of the IR brane localized field. Crosses indicate mass mixing.

The potentials (4.44) and (4.46) appear to match at the level of dimensional analysis: the transition occurs at $r \sim 1/\mu$, where it turns out that $V_{\rm conf}(\mu^{-1}) \sim V_{\rm gauge}(\mu^{-1})$. However, the $c^2 g^4$ and c_φ^2 couplings are in principle different. The coupling g is perturbative at energies well above the confinement scale μ. In contrast, c_φ may typically be $\mathcal{O}(4\pi)$, hence it is possible that c_φ^2 be substantially larger than $c^2 g^4$. This implies that the spatial potential could undergo some enhancement when r enters the confined region at $r \sim 1/\mu$.

4.7.2 Holographic Emergent Force

This emergent force scenario can be realized more precisely in a five-dimensional model, as suggested by the AdS/CFT corresponddence. We sketch this in Fig. 4.4.

Consider the limit where the dark sector is a strongly-coupled gauge theory with large 't Hooft coupling and a large number of colors. The deconfined picture is similar to the picture described in Section 4.6.3. The key difference is that, at four-momentum of order of the confinement scale, an observer on the UV brane should see the appearance of a mass gap. The AdS/CFT correspondence relates confinement to presence of an IR brane

located at $z_1 = 1/\mu > z_0$. This IR brane encodes the spontaneous breaking of conformal symmetry in the infrared. States localized on the IR brane are identified with states that emerge below the confinement scale.

For example, a UV observer probing the bulk at low four-momentum observes a standard 4D theory. As four-momentum is increased beyond μ, the effect of the IR brane vanishes from the correlation functions because the bulk propagators are exponentially suppressed when probing the IR region $z > 1/p$ [110]. Hence for $p \gg \mu$, the IR region of the bulk becomes opaque to observers on the UV brane. In that limit, the observer sees only an infinite AdS bulk, as described in the conformal/warped force scenario of Section 4.6.3.

This mechanism can realize many versions of an emergent force. For simplicity, we focus on an extension of the model in Section 4.6.3. Assume a warped 5D AdS space with curvature k. The Standard Model is localized on the UV brane at $z_0 = 1/k$ and interacts with a bulk scalar field Φ. We introduce an IR brane at $z_1 = 1/\mu$. There may be a IR-localized mass term. This term is left as a free parameter and does not crucially affect the results. Let us assume the existence an IR-localized operator that interacts linearly with Φ:

$$S = S_5 + \int_{\text{IR brane}} d^4X \sqrt{|\gamma|} \left(\mathcal{L}_{\text{IR}} + \mathcal{O}_{\text{IR}} \Phi - \frac{m_{\text{IR}}^2}{2} \Phi^2 \right) , \tag{4.47}$$

where S_5 is the 5D action in (4.31).

The bulk Feynman propagator is readily expressed in terms of Bessel functions of the first and second kinds,

$$\Delta_p(z, z') = i \frac{\pi (kz)^2 (kz')^2}{2k} \quad \frac{\left[\widetilde{Y}_\alpha^{\text{UV}} J_\alpha (pz_<) - \widetilde{J}_\alpha^{\text{UV}} Y_\alpha (pz_<) \right] \left[\widetilde{Y}_\alpha^{\text{IR}} J_\alpha (pz_>) - \widetilde{J}_\alpha^{\text{IR}} Y_\alpha (pz_>) \right]}{\widetilde{J}_\alpha^{\text{UV}} \widetilde{Y}_\alpha^{\text{IR}} - \widetilde{Y}_\alpha^{\text{UV}} \widetilde{J}_\alpha^{\text{IR}}} , \tag{4.48}$$

where we define the extra-dimensional positions $z_< \equiv \min(z, z,')$, $z_> \equiv \max(z, z,')$, and the boundary functions

$$\widetilde{J}_\alpha^{\rm UV} \equiv \frac{p}{k}\, J_{\alpha-1}\left(\frac{p}{k}\right) \qquad\qquad \widetilde{J}_\alpha^{\rm IR} \equiv \frac{p}{\mu}\, J_{\alpha-1}\left(\frac{p}{\mu}\right) + b_{\rm IR}\, J_\alpha\left(\frac{p}{\mu}\right), \tag{4.49}$$

and similarly for the $\widetilde{Y}_\alpha$ functions.

We assume that a 4D field φ is present on the IR brane and mixes with Φ such that

$$\mathcal{O}_{\rm IR} = \omega\varphi\Phi\,. \tag{4.50}$$

with brane mass mixing parameter

$$\omega \equiv c_\varphi \frac{\mu^2}{\sqrt{k}}\,. \tag{4.51}$$

The magnitude of ω is set by dimensional analysis, such that $c_\varphi \sim \mathcal{O}(1)$. Since this is a bilinear interaction, the presence of the IR brane field φ can be rigorously included in the bulk propagator using the five-dimensional version of dressing, *i.e.* a geometric series representation of the brane–bulk mass mixing. The UV-to-UV brane propagator dressed by IR brane insertions is

$$\Delta_p^{\rm dr}(z_0, z_0) = \Delta_p(z_0, z_0) - \left[\Delta_p(z_0, z_1)\right]^2 \frac{i\,\omega^2}{p^2 - m_\varphi^2}\,. \tag{4.52}$$

We have introduced the φ mass as

$$m_\varphi^2 = m_{\varphi,0}^2 - i\,\omega^2 \Delta(m_{\varphi,0}; z_1, z_1)\,, \tag{4.53}$$

where $m_{\varphi,0}^2$ is a bare mass term and the $\Delta(p; z_1, z_1)$ term encodes the contribution to the mass from Kaluza–Klein modes. From dimensional analysis, both terms have a typical magnitude $\mathcal{O}(\mu^2)$. The first term of (4.52) corresponds to the undressed propagator. The

second term encodes the effect of the IR brane and generates the emergent force in the infrared.

4.7.3 Potential

The spatial potential follows from the dressed propagator, (4.52). However, the Fourier transform of this expression is only analytically tractable in the high- and low-energy limits. Let us consider the limits with space-like four-momentum $p = i|\mathbf{q}| \equiv iq$, as needed for the t-channel diagram that generates the potential. For $q \gg \mu$,

$$\Delta_p(z_0, z_0) \approx -i \frac{\Gamma(\alpha)}{\Gamma(1-\alpha)} \frac{2k}{q^2} \left(\frac{q}{2k}\right)^{2-2\alpha} \tag{4.54}$$

$$\Delta_p(z_0, z_1) \approx -i \frac{\sqrt{2\pi}}{\Gamma(1-\alpha)} \frac{2k}{q^{3/2}\sqrt{\mu}} \left(\frac{q}{2k}\right)^{1-\alpha} e^{-q/\mu} \tag{4.55}$$

$$\Delta_p(z_1, z_1) \approx -i \frac{k}{q\mu} \tanh(q/\mu)\,. \tag{4.56}$$

In the $q \ll \mu$ limit,

$$\Delta_p(z_0, z_0) \approx -i \frac{2\alpha + b_{\rm IR}}{2\alpha\, b_{\rm IR}} \frac{k}{\mu^2} \left(\frac{\mu}{k}\right)^{2-2\alpha} \tag{4.57}$$

$$\Delta_p(z_0, z_1) \approx -i \frac{k}{b_{\rm IR}\, \mu^2} \left(\frac{\mu}{k}\right)^{1-\alpha} \tag{4.58}$$

$$\Delta_p(z_1, z_1) \approx -i \frac{k}{b_{\rm IR}\, \mu^2}\,. \tag{4.59}$$

The behavior of the potential can be understood from these limits. In the $q \ll \mu$ limit, all Δ's are constant and only the IR-brane scalar remains in the spectrum. The dressed propagator takes the form of a 4D massive propagator, thereby generating a standard 4D Yukawa force. Equivalently, this is the behavior of the 4D effective theory whose Kaluza–Klein modes are integrated out. In the $q \gg \mu$ limit, the $\Delta(p; z_0, z_1)$ propagators are exponentially suppressed. Only the $\Delta(p; z_0, z_0)$ term remains, reproducing the conformal

scenario with *no* IR brane described in Section 4.6.3. In the 4D CFT interpretation, this is because the composite states have typical size $1/\mu$ and are not seen by probes with virtuality much higher than μ.

For the scalar nucleon operators, $\mathcal{O}^S$, the potential is:

$$V_S(r) \approx \begin{cases} -\dfrac{c_\varphi^2 \lambda^2}{b_{\rm IR}^2} \left(\dfrac{\mu}{k}\right)^{2-2\alpha} \dfrac{e^{-m_\varphi r}}{4\pi r} & \text{if} \quad r \gg 1/\mu \\ -\dfrac{\lambda^2}{2\pi^{3/2}} \dfrac{\Gamma(3/2-\alpha)}{\Gamma(1-\alpha)} \dfrac{1}{r} \dfrac{1}{(kr)^{2-2\alpha}} & \text{if} \quad r \ll 1/\mu \end{cases} \tag{4.60}$$

Analogously, for the pseudoscalar nucleon operators, $\mathcal{O}^P$, the potential is:

$$V_P(\boldsymbol{r}) \approx \begin{cases} \dfrac{c_\varphi^2 \lambda^2}{b_{\rm IR}^2} \left(\dfrac{\mu}{k}\right)^{2-2\alpha} \dfrac{(\boldsymbol{\sigma_1} \cdot \boldsymbol{\nabla})(\boldsymbol{\sigma_2} \cdot \boldsymbol{\nabla})}{4m_N^2} \dfrac{e^{-m_\varphi r}}{4\pi r} & \text{if} \quad r \gg 1/\mu \\ \dfrac{\lambda^2}{2\pi^{3/2}} \dfrac{\Gamma(3/2-\alpha)}{\Gamma(1-\alpha)} \dfrac{(\boldsymbol{\sigma_1} \cdot \boldsymbol{\nabla})(\boldsymbol{\sigma_2} \cdot \boldsymbol{\nabla})}{4m_N^2} \dfrac{1}{r} \dfrac{1}{(kr)^{2-2\alpha}} & \text{if} \quad r \ll 1/\mu \end{cases} . \tag{4.61}$$

Just like the case of an emergent force from a confining non-Abelian sector in Section 4.7.1, there is again an approximate continuity between the long and short distance regimes. This can be seen in the spatial potentials (4.60–4.61), and also at the level in the propagator itself by comparing the undressed and emergent parts of (4.52) at momentum of order μ.

Despite this approximate continuity, there may be a smooth kink around $r \sim 1/\mu$ if the emergent force is enhanced. This can happen for sufficiently large ω. In our simple scalar model this requires some tuning to keep m_φ small. The emergent force can also be enhanced if φ has some multiplicity, n_φ, in which case the emergent component of the force is increased by n_φ. Note however that n_φ cannot be arbitrarily increased because the local strong coupling scale decreases as $n_\varphi^{-1/2}$.

Finally, it is instructive to estimate how the emergent force vanishes at short

distances. In the $q \gg \mu$ regime, the emergent contribution is

$$\Delta_p^{\rm dr}(z_0, z_0) \supset \frac{k\mu^3}{q^5} \left(\frac{q}{k}\right)^{2-2\alpha} e^{-2q/\mu}\,, \tag{4.62}$$

where we have dropped all the $\mathcal{O}(1)$ factors for clarity. This approximation is valid for momenta larger than μ. We thus take $q > \widetilde{\mu}$ where $\widetilde{\mu}$ is an IR cutoff that may be taken to be around $\mathcal{O}(\text{few}) \times \mu$. The Fourier transform integrates over a momentum range $q \in [\widetilde{\mu}, \infty]$. Expanding in small $r\widetilde{\mu}$ shows that the emergent component of the potential behaves as

$$V(r)|_{r \ll 1/\mu} \sim c_\varphi^2 \lambda^2 e^{-2\widetilde{\mu}/\mu} \frac{\mu^4 r^2}{k} \left(\frac{\widetilde{\mu}}{k}\right)^{1-2\alpha} + \cdots\,. \tag{4.63}$$

This limit explicitly shows how the emergent force vanishes at short distance. This is only a crude approximation as the overall magnitude strongly depends on $\widetilde{\mu}$. An exact, numerical calculation of the holographic emergent force is beyond the scope of the present study.

4.8 Discussion

Hidden (dark) sectors with new particles may generate long-range forces between visible sector matter. This manuscript examines exotic long-range forces that differ from the Yukawa-like forces generated from single-particle exchange. We present three classes of exotic forces.

Quantum forces come from the loop-level exchange of pairs of dark sector particles. They are described by an effective theory and may themselves be the dark matter. We present the spin-dependent potentials including the spin- and orientation-averaged limits. As an example, we show the constraints on a light dark sector imposed from NMR bounds on the anomalous J-coupling of deuterium.

Conformal forces arise when visible particles couple to a dark sector with conformal symmetry. Such forces are also generated in the case of a "warped dark sector," which by the AdS/CFT correspondence is a five-dimensional realization of the conformal dark sector. These forces have non-integer behavior in r.

Emergent forces are induced by effective degrees of freedom arising in the infrared. We presented a qualitative picture in a 4D strongly-interacting dark sector, and a quantitative result from a specific realization of this scenario in a slice of AdS_5. In the AdS model, the emergent force comes from an IR brane-localized degree of freedom that becomes invisible to the UV-localized nucleons at short distances.

As an aside we classify the behavior of spin-dependent and spin-independent forces, for Yukawa and exotic cases, and for the ordinary, spin-averaged, and orientation-averaged cases. Such an analysis is required to form a coherent vision of existing and upcoming experimental prospects. We point out that in the orientation-averaged limit, the Yukawa forces are suppressed as a result of Gauss' law. A similar effect also occurs for the tensor force upon spin-averaging. This behavior is not true for exotic forces. Yukawa forces are thus non-generic compared to exotic forces.

It follows that experiments that use disordered phases of matter are particularly appropriate for searching for exotic spin-dependent forces. NMR-based experiments are one such type of setup. We find that searches for spin/velocity-dependent forces are especially sensitive to exotic tensor potentials.

Chapter 5

The Neutrino Casimir Force

5.1 Chapter Abstract

In the low energy effective theory of the weak interaction, a macroscopic force arises when pairs of neutrinos are exchanged. We calculate the neutrino Casimir force between plates, allowing for two different mass eigenstates within the loop. We also provide the general potential between point sources. We discuss the possibility of distinguishing whether neutrinos are Majorana or Dirac fermions using these quantum forces.

5.2 Introduction

For completeness, we study the general point-point neutrino-induced quantum force in Sec. 5.3. The evaluation uses the standard momentum-space formalism. We then introduce a mixed position-momentum space formalism and present the plate-plate and plate-point calculations in 5.4. We discuss the results in Sec. 5.5.

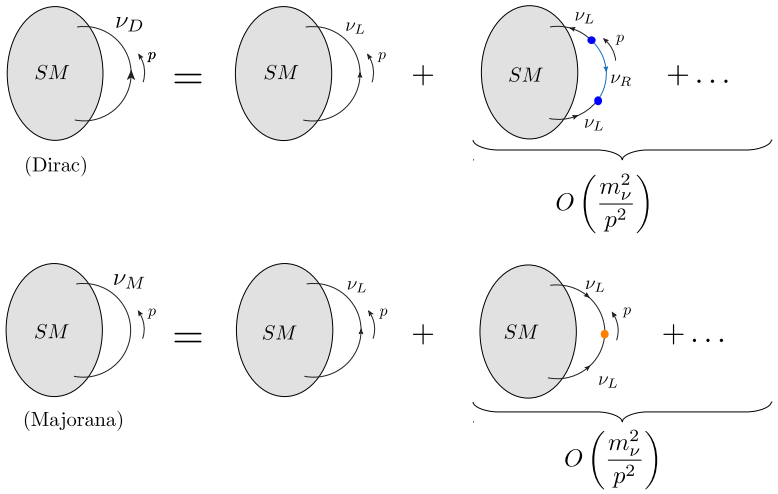

Figure 5.1: The Majorana-Dirac confusion theorem. The blob represents an arbitrary SM amplitude from which we single out an internal neutrino propagator. Dirac mass insertions (top) and Majorana mass insertions (bottom) become negligible for $p \gg m_\nu$ such that amplitudes become equivalent in this limit.

5.3 Potential Between Point Sources

We use the 4-component fermion formalism in our loop calculations. At energies below the electroweak scale, the Lagrangian describing neutrino mass eigenstates interacting with SM fermions is given by

$$\mathcal{L}_D = i\bar{\nu}_D^i \gamma^\mu \partial_\mu \nu_D^i - m_i \bar{\nu}_D^i \nu_D^i - \frac{G_F}{2\sqrt{2}} \left[\bar{\nu}_D^j \gamma^\mu \left(1-\gamma_5\right) \nu_D^i\right] \left[\bar{\psi}\gamma_\mu \left(g_{ij}^V - g_{ij}^A \gamma_5\right) \psi\right] \tag{5.1}$$

for Dirac neutrinos and

$$\mathcal{L}_M = \frac{i}{2}\bar{\nu}_M^i \gamma^\mu \partial_\mu \nu_M^i - \frac{m_i}{2} \bar{\nu}_M^i \nu_M^i + \frac{G_F}{2\sqrt{2}} \left[\bar{\nu}_M^j \gamma^\mu \gamma_5 \nu_M^i\right] \left[\bar{\psi}\gamma_\mu \left(g_{ij}^V - g_{ij}^A \gamma_5\right) \psi\right] \tag{5.2}$$

for Majorana neutrinos. The link to the 2-component fermion notation is given in App. K. The g_{ij}^V and g_{ij}^A coupling matrices depend on the SM field and on the neutrino generation. They are given in App. K for completeness.

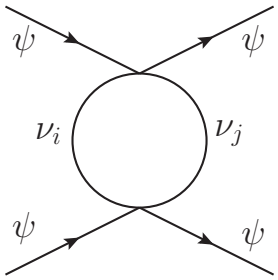

Figure 5.2: Quantum forces can be induced from the exchange of two neutrinos. The two virtual neutrinos can in principle have different masses $m_i \neq m_j$.

In this section, we present the force between two nonrelativistic fermions ψ arising from the exchange of two neutrinos, ν_i and ν_j. Similar results have already been presented in the literature, see for instance [7,68]. Here we present the most complete result including the spin-dependent part of the potential.

The calculation starts from the scattering amplitude in 4-momentum space. This formalism has been used in the literature (see *e.g.* [1, 52] for details), so we only present results here. See App. L for additional details.

We introduce a discrete variable to distinguish between the Majorana and Dirac cases:

$$\eta = \begin{cases} 0 & \text{if Majorana} \\ \\ 1 & \text{if Dirac} \end{cases} . \tag{5.3}$$

The full potential can be written using discontinuities (noted $\mathrm{D}\,[f]$) across branch cuts of a basis of f_{mn} functions

$$f_{mn} \equiv \int_0^1 dx x^m (1-x)^n \ln\left(\frac{x m_j^2 + (1-x) m_i^2 - x(1-x)\lambda^2}{\Lambda^2}\right), \tag{5.4}$$

which come from evaluating the loop integral. In this basis, the full potential is given by

$$V(\boldsymbol{r}) = \sum_{ij} V_{ij}(\boldsymbol{r}) = -iG_F^2 \sum_{ij} \frac{\left(\delta_0^\mu \mathbb{1}_1 g_{ij}^V \delta_0^\nu \mathbb{1}_2 g_{ji}^V + \delta_c^\mu \sigma_1^c g_{ij}^A \delta_d^\nu \sigma_2^d g_{ji}^A\right)}{(4\pi)^2} \int_{m_i+m_j}^{\infty} \frac{\lambda d\lambda}{(2\pi)^2} \times \tag{5.5}$$

$$\left(-g_{\mu\nu}\left(m_j^2 \mathrm{D}[f_{10}] + (1-\eta) m_i m_j \mathrm{D}[f_{00}] + m_i^2 \mathrm{D}[f_{01}] - 2\lambda^2 \mathrm{D}[f_{11}]\right) + 2\mathrm{D}[f_{11}] \delta_\mu^a \delta_\nu^b \nabla_a \nabla_b\right) \frac{e^{-\lambda r}}{r}$$

where $\boldsymbol{\sigma}_A$ denotes the Pauli matrices acting on the spinors of source fermion A. Latin indices, such as $a, b, ...$, are summed over $1, 2, 3$. We refer to the V_{ij} as partial potentials. Summing over all combinations of neutrinos from the 3 generations yields the full quantum potential from neutrinos.

We can perform the integral exactly for the diagonal terms ($m_i = m_j \equiv m$). These partial potentials take on the form

$$V_{ii}(\boldsymbol{r}) = G_F^2 \frac{\left(\delta_0^\mu \mathbb{1}_1 \left(g_{ii}^V\right)^2 \delta_0^\nu \mathbb{1}_2 + \delta_c^\mu \sigma_1^c \left(g_{ii}^A\right)^2 \delta_d^\nu \sigma_2^d\right)}{64\pi^4} \times \tag{5.6}$$

$$\left(g_{\mu\nu}\left(\eta \frac{4m^3 \pi K_3(2mr)}{r^2} + (1-\eta)\frac{8m^2\pi K_2(2mr)}{r^3}\right) + \delta_\mu^a \delta_\nu^b \nabla_a \nabla_b \frac{m\pi}{3r^2}\left(4K_1(2mr) + m\pi^2 r G(m^2 r^2)\right)\right)$$

where we have introduced the Meijer G-function

$$G(m^2 r^2) \equiv G_{2,4}^{2,0}\left(m^2 r^2 \middle| \begin{matrix} \frac{1}{2}, \frac{3}{2} \\ 0, 0, \frac{1}{2}, \frac{1}{2} \end{matrix}\right). \tag{5.7}$$

The spin-independent piece of (5.6) is given by

$$V_{ii}(r) = G_F^2 \frac{\left(g_{ii}^V\right)^2}{16\pi^3}\left(\eta \frac{m^3 K_3(2mr)}{r^2} + (1-\eta)\frac{2m^2 K_2(2mr)}{r^3}\right), \tag{5.8}$$

which corresponds to a repulsive force and is consistent with the literature (*e.g.* [7,68]). At short distances $mr \ll 1$, Dirac and Majorana predictions converge to

$$V_{ii}(r) = G_F^2 \frac{\left(g_{ii}^V\right)^2}{16\pi^3 r^5}, \tag{5.9}$$

as expected from the confusion theorem.

5.4 The Neutrino Casimir Force

Here we consider the quantum force between extended sources. Focusing on nonrelativistic, unpolarized sources formed by the SM fermions, we have $\bar{\psi}\gamma_\mu\gamma_5\psi \approx 0$, $\bar{\psi}\gamma_\mu\psi \approx \delta_{\mu 0}\psi^\dagger\psi = \delta_{\mu 0}\, n(\boldsymbol{x})$ were $n(\boldsymbol{x})$ is the number density operator. We denote by $J(\boldsymbol{x})$ the density expectation value in the presence of matter, $J(\boldsymbol{x}) = \langle\Omega|n(\boldsymbol{x})|\Omega\rangle$. We can write effective neutrino Lagrangians in the presence of such nonrelativistic static matter,

$$\mathcal{L}_D = i\bar{\nu}_D^i\gamma^\mu\partial_\mu\nu_D^i - m_i\bar{\nu}_D^i\nu_D^i - \frac{G_F}{2\sqrt{2}}\left[\bar{\nu}_D^j\gamma^0\left(1-\gamma_5\right)\nu_D^i\right] g_{ij}^V\, J \tag{5.10}$$

$$\mathcal{L}_M = \frac{i}{2}\bar{\nu}_M^i\gamma^\mu\partial_\mu\nu_M^i - \frac{m_i}{2}\bar{\nu}_M^i\nu_M^i + \frac{G_F}{2\sqrt{2}}\left[\bar{\nu}_M^j\gamma^0\gamma_5\nu_M^i\right] g_{ij}^V\, J\,. \tag{5.11}$$

We assume the matter density is compound of two pieces with density J_1, J_2, separated by a distance L. The full matter density is $J = J_1 + J_2$. The potential between these two sources can be obtained by varying the quantum vacuum energy of the system with respect to L.

In case of strong coupling to sources, the neutrino would acquire an effective mass inside the sources, which tends to repel the propagators. This strong coupling regime reproduces precisely the familiar Casimir force with Dirichlet boundary conditions on the sources [223]. Calculations of forces in the strong coupling limit can be found in [224]. Instead, in case of weak coupling to sources, which is the one relevant here, the potential is given by the leading term of the one-loop functional determinant. The force in this weakly coupled regime amounts to a "Casimir-Polder" force between extended objects. See App. M and Ref. [223] for details. For simplicity, and because the weak and strong regime of the force between extended objects have a unified description, we refer to the force in the weakly coupled regime as "Casimir force".

We find the potential induced by the neutrinos between extended sources J_1 and J_2 to be

$$V(L) = i\frac{G_F^2}{2^\eta\, 4}\int d^3\boldsymbol{x}\int d^4x'\sum_{ij}\mathrm{tr}\left[J_1(\boldsymbol{x})\Delta_i(x,x')\,\Gamma\, g_{ij}^V J_2(\boldsymbol{x}')\Delta_j(x',x)\,\Gamma\, g_{ji}^V\right] + \mathcal{O}\left(G_F^3\right) \tag{5.12}$$

where $\Gamma = \gamma_0(\eta - \gamma_5)$ encodes the Lorentz structure of the neutrino vertex. Here $\Delta(x,x')$ is the Feynman propagator of 4-component fermions. The trace is in spinor space. Notice that one of the integrals is in 3d space while the other is in spacetime. This reflects the fact that the quantum force is intrinsically relativistic.

In the limit of pointlike sources

$$J_1(\boldsymbol{x}) = \delta(\boldsymbol{x}) \qquad\qquad J_2(\boldsymbol{x}) = \delta(\boldsymbol{x} - \boldsymbol{L}), \tag{5.13}$$

(5.12) reproduces (L.9) and thus the point-point potential obtained in Sec. 5.3.

5.4.1 Potential Between Plates

We consider the sources are infinite plates with separation L. The plates are taken to have number densities n_1 and n_2 and are orthogonal to the z direction,

$$J_1(\boldsymbol{x}) = n_1\Theta(z<0) \qquad\qquad J_2(\boldsymbol{x}) = n_2\Theta(z>L) \tag{5.14}$$

The two transverse spatial coordinates are denoted by $x_\parallel$, hence $x_\mu = (t,\boldsymbol{x}) = (t, x_\parallel, z)$. It is also useful to introduce the (2+1) Lorentz indexes $\alpha = 0,1,2$ defining $x_\alpha = (t, x_\parallel)$.

A naive method to obtain the plate-plate potential would be to directly integrate the general point-point result (5.5). This is however rather challenging in the case of different masses. We show here a simpler path to the general result.

Since the sources are Lorentz-invariant along $x_\parallel$, we introduce Fourier transforms along these coordinates and time. This introduces the 3-momentum conjugate of the x_α coordinates. In this mixed position-momentum space, the fermion propagators are found to be

$$\Delta(k_\alpha, z-z') = \int \frac{dk_z}{2\pi} e^{ik_z(z-z')} \Delta(k_\mu) = \left(\not{k} + \omega_i \gamma^3 \mathrm{Sign}[z-z'] + m\right) \frac{e^{i\omega_i |z-z'|}}{2\omega_i} \tag{5.15}$$

with

$$\not{k} = \gamma^\alpha k_\alpha \,, \qquad \omega_i \equiv \sqrt{k^2 - m_i^2 + i\varepsilon} \,, \qquad k^2 = k_\alpha k^\alpha \,. \tag{5.16}$$

Introducing the mixed space propagator in Eq. (5.12) gives

$$\begin{aligned} V(L) = i\frac{G_F^2}{2^\eta\, 4} \int d^3\boldsymbol{x} \int d^4x' \int \frac{d^3k}{(2\pi)^3} \int \frac{d^3k'}{(2\pi)^3} e^{i(k-k')_\alpha (x-x')^\alpha} \\ \sum_{ij} \mathrm{tr}\left[J_1(z) \Delta_i(k_\alpha, z-z') \,\Gamma\, g_{ij}^V J_2(z') \Delta_j(k'_\alpha, z'-z) \,\Gamma\, g_{ji}^V\right] \end{aligned} \tag{5.17}$$

A momentum redefinition makes appear the loop integral, the external momentum q_α and the overall Fourier transform in q_α,

$$\begin{aligned} V(L) = i\frac{G_F^2}{2^\eta\, 4} \int d^3\boldsymbol{x} \int d^4x' \int \frac{d^3q}{(2\pi)^3} e^{iq_\alpha (x-x')^\alpha} \int \frac{d^3k}{(2\pi)^3} \\ \sum_{ij} \mathrm{tr}\left[J_1(z) \Delta_i(k_\alpha, z-z') \,\Gamma\, g_{ij}^V J_2(z') \Delta_j(k_\alpha + q_\alpha, z'-z) \,\Gamma\, g_{ji}^V\right] \end{aligned} \tag{5.18}$$

In the case of planar geometry considered here, it turns out that the external 3-momentum is set to zero because of

$$\int d^3x e^{iq_\alpha (x-x')^\alpha} = (2\pi)^3 \delta^{(3)}\left(q_\alpha\right) \,. \tag{5.19}$$

The fact that $q_0 = 0$ is a mere consequence of the nonrelativistic limit. The fact that $q_\parallel = 0$ is specific of the planar geometry and indicates that the force is dominated by fluctuations

with infinite transverse wavelengths. The remaining transverse integral is factored as a surface $\int d^2x_{\parallel} = S$, and the potential is given by

$$V(L) = i\frac{G_F^2}{2^\eta 4} S \int dz dz' \int \frac{d^3k}{(2\pi)^3} \sum_{ij} \mathrm{tr}\left[J_1(z)\Delta_i(k_\alpha, z-z')\,\Gamma\, g_{ij}^V J_2(z')\Delta_j(k_\alpha, z'-z)\,\Gamma\, g_{ji}^V\right] \tag{5.20}$$

Performing both remaining position integrals and evaluating the trace, we have

$$V(L) = -i\frac{S n_1 n_2 G_F^2}{4} \sum_{ij} g_{ij}^V g_{ji}^V \int \frac{d^3k}{(2\pi)^3} \left(\frac{2k_0^2 - k^2 - \omega_i\omega_j - (1-\eta)m_i m_j}{\omega_i\omega_j(\omega_i+\omega_j)^2}\right) e^{i(\omega_i+\omega_j)L}. \tag{5.21}$$

The only remaining integral is the loop integral. We Wick rotate the momentum integral from $2+1$ Lorentzian to 3-dimensional Euclidian space,

$$V(L) = \frac{-S n_1 n_2 G_F^2}{4} \sum_{ij} g_{ij}^V g_{ji}^V \int \frac{d^3k_E}{(2\pi)^3} \left(\frac{2k_{E0}^2 - k_E^2 - \omega_{Ei}\omega_{Ej} + (1-\eta)m_i m_j}{\omega_{Ei}\omega_{Ej}(\omega_{Ei}+\omega_{Ej})^2}\right) e^{-(\omega_{Ei}+\omega_{Ej})L}. \tag{5.22}$$

where we has defined $\omega_{Ei} = \sqrt{k_E^2 + m_i^2}$. We go to spherical coordinates and perform the angular integrals. For the remaining radial integral we introduce a dimensionless variable

$$u = |k_E| L\,, \qquad \rho_i = \sqrt{u^2 + m_i^2 L^2}\,. \tag{5.23}$$

The potential between plates is found to be

$$V(L) = \frac{S n_1 n_2 G_F^2}{8\pi^2 L} \sum_{ij} g_{ij}^V g_{ji}^V \int_0^\infty du u^2 \left(\frac{\frac{1}{3}u^2 + \rho_i\rho_j - (1-\eta)m_i m_j L^2}{\rho_i\rho_j(\rho_i+\rho_j)^2}\right) e^{-(\rho_i+\rho_j)}. \tag{5.24}$$

The rest of the integral cannot be performed analytically in general. Notice the loop integral is finite by construction because the two sources have finite separation. In this calculation there is no need for any loop integral regularization, expressions are finite at every step.

The pressure between the plates is given by

$$P(L) = \frac{-1}{S}\frac{\partial}{\partial L}V = \frac{n_1 n_2 G_F^2}{8\pi^2 L}\sum_{ij} g_{ij}^V g_{ji}^V \int_0^\infty du u^2 \left(\frac{\frac{1}{3}u^2 + \rho_i\rho_j - (1-\eta)m_i m_j L^2}{\rho_i\rho_j(\rho_i+\rho_j)}\right) e^{-(\rho_i+\rho_j)}. \tag{5.25}$$

The neutrino Casimir pressure is thus repulsive.

Finally, at short distance *i.e.* in the limit of $m_i, m_j \ll 1/L$, the integrals can be done exactly,

$$V(L) = \frac{S n_1 n_2 G_F^2}{48\pi^2 L}\sum_{ij} g_{ij}^V g_{ji}^V \qquad P(L) = \frac{n_1 n_2 G_F^2}{48\pi^2 L^2}\sum_{ij} g_{ij}^V g_{ji}^V. \tag{5.26}$$

In this regime the Majorana and Dirac predictions have become equal, as expected from the confusion theorem.

5.4.2 Potential Between a Plate and a Point Source

To obtain the plate-point potential, we consider sources of the form

$$J_1(\boldsymbol{x}) = n_1\Theta(z > L) \qquad J_2(\boldsymbol{x}) = \delta(\boldsymbol{x}) \tag{5.27}$$

with (5.18) and (5.19). Performing the remaining position integrals and evaluating the trace, we have

$$V(L) = \frac{-n_1 G_F^2}{4}\sum_{ij} g_{ij}^V g_{ji}^V \int \frac{d^3k}{(2\pi)^3}\left(\frac{2k_0^2 - k^2 - \omega_i\omega_j - (1-\eta)m_i m_j}{\omega_i\omega_j(\omega_i+\omega_j)}\right) e^{i(\omega_i+\omega_j)L}. \tag{5.28}$$

We follow the steps of the plate-plate calculation—Wick rotating, performing the angular integral, and using the definitions (5.23). We obtain

$$V(L) = \frac{n_1 G_F^2}{8\pi^2 L^2} \sum_{ij} g_{ij}^V g_{ji}^V \int_0^\infty du u^2 \left(\frac{\frac{1}{3}u^2 + \rho_i\rho_j - (1-\eta)m_i m_j L^2}{\rho_i\rho_j(\rho_i+\rho_j)} \right) e^{-(\rho_i+\rho_j)}. \quad (5.29)$$

At short distances, $m_i, m_j \ll 1/L$ for all (i,j), the integral can be done exactly, yielding

$$V(L) = \frac{n_1 G_F^2}{48\pi^2 L^2} \sum_{ij} g_{ij}^V g_{ji}^V. \quad (5.30)$$

We again find that any trace of the mass generation mechanism has vanished from the short-distance result.

5.5 Discussion

The neutrino Casimir force has not previously been determined in the literature, to the best of our knowledge. In this section, we elucidate its properties.

The expressions for the neutrino Casimir force (5.24), (5.29) contain only one numerical integral, just as for the point-point result (5.5). This property generalizes to plates with an arbitrary number of layers, which is easily obtainable in our formalism. In our calculation, we take into account loops with two different mass eigenstates, that we denote below as $m_> = \max(m_i, m_j), m_< = \min(m_i, m_j)$.

The Dirac and Majorana partial potentials V_{ij} converge to each other in the limit of short distance, $L \ll 1/m_>$. The convergence holds for all configurations of sources considered and is shown for the case of equal masses ($m_i = m_j$) in Fig. 5.3. This is the fingerprint of the confusion theorem—only the ν_L neutrino contributes to the pressure and thus any trace of the mass generation mechanism vanishes (see Fig. 5.1). The plate-plate, plate-point, and point-point potentials scale as $1/L$, $1/L^2$, and $1/L^5$ in this limit respectively

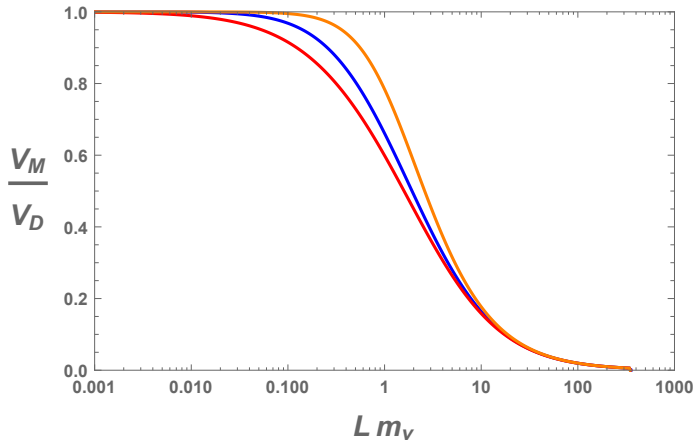

Figure 5.3: Ratios of the Dirac and Majorana potentials for point-point (orange), plate-point (blue), and plate-plate (red) configurations. Results are shown for equal masses ($m_i = m_j$). Majorana potentials are always weaker than Dirac potentials, consistent with prior results (*e.g.* [7]).

(see (5.26) and (5.30)).

For distances $L \gtrsim 1/m_>$, the partial potentials are exponentially suppressed for all configurations. We find that for $L \gtrsim 1/m_<$, the Dirac and Majorana partial potentials have distinct L-dependencies with $1 - V_M/V_D \sim \mathcal{O}(1)$. The latter effect occurs when the partial potential is already exponential suppressed, since $1/m_< \geq 1/m_>$. Hence we find that the contributions from the cross-term partial potentials ($m_i \neq m_j$) are not helpful in making a Dirac/Majorana distinction.

We find the current sensitivity to neutrino forces remains very low. For plates at a separation of $L \sim 1/m$ where $1 - V_M/V_D \sim \mathcal{O}(1)$, we use data from a recent Casimir force experiment[1] [225] to determine that 20 orders of magnitude still remain between current experimental limits and the quantum neutrino force.

Ref. [73] recently claimed that bounds from muonium spectroscopy place experi-

[1]This result is recast in [46] to bound the relevant quantum force.

mental limits just two orders of magnitude shy of being able to detect quantum forces from neutrinos. In their analysis, a non-relativistic formalism was used and it was assumed that the form of the potential (5.8) and electronic wavefunctions are valid down to $r \sim 1/m_Z$. It remains for this bound to be checked in a relativistic formalism. Unfortunately, even if the bounds in [73] hold, the confusion theorem renders a Dirac/Majorana distinction nearly impossible by this probe, as $1 - V_M/V_D \sim \mathcal{O}\left(10^{-11}\right)$ for $r_{\text{Bohr}} \sim L \ll 1/m$.

Chapter 6

Conclusions

Specific conclusions were presented at the end of each chapter. In this section, we offer a brief summary and focus on the broader themes and ideas present in this work.

6.1 On EFT in AdS

In chapter 2, we investigated how quantum dynamics affects the propagation of a scalar field in Lorentzian AdS_{d+1}. Among other results, we found that loop-level dressings by a self-energy with a bubble topology induce an exponential damping of the propagator in the $pz \gg 1$ region. This damping behaviour occurs even if a single point is in the conformally flat region, *i.e.* $pz_< \ll 1$, $pz_> \gg 1$, which includes the boundary-to-bulk propagator with $pz \gg 1$ as a particular case. This regime has no flat-space equivalent—the $pz \ll 1$ region vanishes if one Weyl-transforms to flat space. Renormalizable interactions may not give rise to an exponential damping, but operators of sufficiently high dimension—as present in an EFT—will induce it. In the EFT paradigm, the EFT breaks down when

higher dimensional operators give contributions to the self-energy of the same order. In AdS this occurs at sufficiently large pz, *i.e.* in the IR region of the Poincaré patch. Working in the EFT paradigm, we find that the exponential damping censors the region of EFT breakdown.

In a nutshell, opacity tells us that 2-point correlators are exponentially suppressed when one of the endpoints satisfies $pz \gtrsim 1$. Does this property apply to higher point correlators as well? If so, the IR region of AdS can be said to be *emergent* at low energies. This is what was investigated in chapter 3. It was found that in the regime in which opacity suppresses propagation to the IR brane, the spectrum of KK modes merge to form a continuum. In this continuum regime, cascade decays are suppressed and the IR is effectively emergent.

Now consider the "slice of AdS", in which the bulk of AdS is truncated by UV and IR branes at small and large z, respectively. Opacity tells us that 2-point correlators are exponentially suppressed when one of the endpoints satisfies $pz \gtrsim 1$, which implies the existence of a scale $\widetilde{\Lambda}$ above which propagation to the IR brane is exponentially suppressed. For timelike bulk propagators with momenta above this scale ($p > \widetilde{\Lambda}$), the IR brane is effectively absent. This scale separates the Kaluza–Klein and continuum regimes of the bulk propagator, as the IR brane is emergent for the propagator. Does this property apply to higher point correlators as well?

Naïvely, cascade decays could allow correlators with energy beyond $\widetilde{\Lambda}$ to be sensitive to the IR brane because the momentum is split between many offspring states. Therefore we studied cascade decays to better understand the notion of IR brane emergence in

chapter 3. We focused on a scalar with a bulk cubic interaction and investigate the squared matrix element integrated over final states that are the main ingredients of observable event rates. In the continuum regime, there exists a recursion relation between cascades of different branching depth, which we use to estimate the rate for arbitrarily deep cascade.

The cascade decay calculation provides a picture of soft bombs in the continuum regime of AdS. We find that the shape of the cascade events tend to be soft and spherical in the 4D Minkowski slices. This is because the branchings tend to be near-threshold with momentum evenly split between the offspring, which matches previous results for the CFT dual. Along the fifth dimension, the decays tend to occur near the region $z \sim 1/p$ where p is the parent four-momentum. Therefore the soft bomb diagram grows in the Minkowski direction and slowly progresses towards the IR. Once the typical momentum of the offspring reaches $\widetilde{\Lambda}$, the soft bomb enters the KK regime.

While there is no diagrammatic change between the KK and continuum regimes, the crucial change occurs in the behaviour of the propagators. In the KK regime, the narrow width approximation applies, such that amplitudes giving the soft bomb rate can effectively be cut. In the continuum regime the propagators do not have poles and the event cannot be cut before reaching the KK regime. The phase space factor associated with each of the final states accumulate and the soft bomb rate in the continuum regime acquires an exponential suppression. It follows that the continuum regime can be described by a high-energy effective theory with no IR brane. In other words, the operators on the IR brane effectively emerge at the energy scale $E \sim \widetilde{\Lambda}$, *i.e.* schematically $E[J]\big|_{p \gg \widetilde{\Lambda}} \approx E[J]_{\text{no IR brane}}$ in terms of generating functionals of correlators. We expect that the same conclusions

qualitatively apply to asymptotically AdS backgrounds with a metric deformation in the IR region, such as soft-wall models.

These features can lead to new possibilities for physics beyond the Standard Model, as already pointed out in [27]. In particular holographic dark sector scenarios may have bulk fields that mediate interactions between a UV-brane localized Standard Model and IR brane dark states that are emergent. This implies that a light dark particle can be invisible at high energy experiments. For instance, bounds from stellar cooling or missing energy searches may be alleviated if the dark particles are light enough. The many phenomenological consequences of an emergent dark sector require further studies.

6.2 On Exotic Forces from a Dark Sector

Hidden (dark) sectors with new particles may generate long-range forces between visible sector matter. Chapter 4 of this manuscript examines exotic long-range forces that differ from the Yukawa-like forces generated from single-particle exchange. We present three classes of exotic forces.

Quantum forces come from the loop-level exchange of pairs of dark sector particles. They are described by an effective theory and may themselves be the dark matter. We present the spin-dependent potentials including the spin- and orientation-averaged limits. As an example, we show the constraints on a light dark sector imposed from NMR bounds on the anomalous J-coupling of deuterium.

Conformal forces arise when visible particles couple to a dark sector with conformal symmetry. Such forces are also generated in the case of a "warped dark sector," which by

the AdS/CFT correspondence is a five-dimensional realization of the conformal dark sector. These forces have a non-integer power dependence on r.

Emergent forces are induced by effective degrees of freedom arising in the infrared. We presented a qualitative picture in a 4D strongly-interacting dark sector, and a quantitative result from a specific realization of this scenario in a slice of AdS_5. In the AdS model, the emergent force comes from an IR brane-localized degree of freedom that becomes invisible to the UV-localized nucleons at short distances.

As an aside, we classify the behavior of spin-dependent and spin-independent forces, for Yukawa and exotic cases, and for the ordinary, spin-averaged, and orientation-averaged cases. Such an analysis is required to form a coherent vision of existing and upcoming experimental prospects. We point out that in the orientation-averaged limit, the Yukawa forces are suppressed as a result of Gauss' law. A similar effect also occurs for the tensor force upon spin-averaging. This behavior is not true for exotic forces. Yukawa forces are thus non-generic compared to exotic forces.

It follows that experiments that use disordered phases of matter are particularly appropriate for searching for exotic spin-dependent forces. NMR-based experiments are one such type of setup. We find that searches for spin/velocity-dependent forces are especially sensitive to exotic tensor potentials.

6.3 On the Neutrino Casimir Force

The neutrino Casimir force has not previously been determined in the literature, to the best of our knowledge. Can this force be used to make a Dirac/Majorana distinction

as to the origin of the Neutrino mass?

In chapter 5, we determine the plate-plate and plate-point potentials and find that the current sensitivity to neutrino forces remains very low. We use data from a recent Casimir force experiment[1] [225] to determine that 20 orders of magnitude still remain between current experimental limits and the quantum neutrino force.

We thus conclude that there are still many orders of magnitude in sensitivity needed to make a Dirac/Majorana distinction with quantum neutrino forces. Perhaps in the distant future, the neutrino Casimir force can be used to confirm the Dirac/Majorana origin of the neutrino mass.

[1]This result is recast in [46] to bound the relevant quantum force.

Bibliography

[1] A. Costantino, S. Fichet, and P. Tanedo, *Exotic Spin-Dependent Forces from a Hidden Sector*, arXiv:1910.02972. .

[2] A. Costantino and S. Fichet, *The Neutrino Casimir Force*, *JHEP* **09** (2020) 122, [arXiv:2003.11032].

[3] A. Costantino, S. Fichet, and P. Tanedo, *Effective Field Theory in AdS: Continuum Regime, Soft Bombs, and IR Emergence*, arXiv:2002.12335.

[4] A. Costantino and S. Fichet, *Opacity from Loops in AdS*, arXiv:2011.06603.

[5] M. P. Ledbetter, M. Romalis, and D. F. Jackson-Kimball, *Constraints on short-range spin-dependent interactions from scalar spin-spin coupling in deuterated molecular hydrogen*, *Phys. Rev. Lett.* **110** (2013), no. 4 040402, [arXiv:1203.6894].

[6] **XENON** Collaboration, E. Aprile et al., *Constraining the spin-dependent WIMP-nucleon cross sections with XENON1T*, *Phys. Rev. Lett.* **122** (2019), no. 14 141301, [arXiv:1902.03234].

[7] J. A. Grifols, E. Masso, and R. Toldra, *Majorana neutrinos and long range forces*, *Phys. Lett.* **B389** (1996) 563–565, [hep-ph/9606377].

[8] J. Callan, Curtis G. and F. Wilczek, *INFRARED BEHAVIOR AT NEGATIVE CURVATURE*, *Nucl. Phys. B* **340** (1990) 366–386.

[9] D. McAvity and H. Osborn, *Conformal field theories near a boundary in general dimensions*, *Nucl. Phys. B* **455** (1995) 522–576, [cond-mat/9505127].

[10] S. Giombi and H. Khanchandani, *CFT in AdS and boundary RG flows*, arXiv:2007.04955.

[11] J. M. Maldacena, *The Large N Limit of Superconformal Field Theories and Supergravity*, *Int. J. Theor. Phys.* **38** (1999) 1113–1133, [hep-th/9711200]. [Adv. Theor. Math. Phys.2,231(1998)].

[12] S. S. Gubser, I. R. Klebanov, and A. M. Polyakov, *Gauge theory correlators from noncritical string theory*, *Phys. Lett.* **B428** (1998) 105–114, [hep-th/9802109].

[13] E. Witten, *Anti-de Sitter space and holography*, *Adv. Theor. Math. Phys.* **2** (1998) 253–291, [hep-th/9802150].

[14] D. Z. Freedman, S. D. Mathur, A. Matusis, and L. Rastelli, *Comments on 4 point functions in the CFT / AdS correspondence*, *Phys. Lett. B* **452** (1999) 61–68, [hep-th/9808006].

[15] H. Liu and A. A. Tseytlin, *On four point functions in the CFT / AdS correspondence*, *Phys. Rev. D* **59** (1999) 086002, [hep-th/9807097].

[16] D. Z. Freedman, S. D. Mathur, A. Matusis, and L. Rastelli, *Correlation functions in the CFT(d) / AdS(d+1) correspondence*, *Nucl. Phys. B* **546** (1999) 96–118, [hep-th/9804058].

[17] E. D'Hoker, D. Z. Freedman, and L. Rastelli, *AdS / CFT four point functions: How to succeed at z integrals without really trying*, *Nucl. Phys. B* **562** (1999) 395–411, [hep-th/9905049].

[18] E. D'Hoker, D. Z. Freedman, S. D. Mathur, A. Matusis, and L. Rastelli, *Graviton exchange and complete four point functions in the AdS / CFT correspondence*, *Nucl. Phys. B* **562** (1999) 353–394, [hep-th/9903196].

[19] O. Aharony, S. S. Gubser, J. M. Maldacena, H. Ooguri, and Y. Oz, *Large N field theories, string theory and gravity*, *Phys. Rept.* **323** (2000) 183–386, [hep-th/9905111].

[20] A. Zaffaroni, *Introduction to the AdS-CFT correspondence*, *Class. Quant. Grav.* **17** (2000) 3571–3597.

[21] H. Nastase, *Introduction to AdS-CFT*, arXiv:0712.0689.

[22] J. Kaplan, "Lectures on AdS/CFT from the Bottom Up." https://sites.krieger.jhu.edu/jared-kaplan/files/2016/05/AdSCFTCourseNotesCurrentPublic.pdf.

[23] L. Randall and R. Sundrum, *A Large mass hierarchy from a small extra dimension*, *Phys. Rev. Lett.* **83** (1999) 3370–3373, [hep-ph/9905221].

[24] B. von Harling and K. L. McDonald, *Secluded Dark Matter Coupled to a Hidden CFT*, *JHEP* **08** (2012) 048, [arXiv:1203.6646].

[25] K. L. McDonald and D. E. Morrissey, *Low-Energy Signals from Kinetic Mixing with a Warped Abelian Hidden Sector*, *JHEP* **02** (2011) 087, [arXiv:1010.5999].

[26] K. L. McDonald and D. E. Morrissey, *Low-Energy Probes of a Warped Extra Dimension*, *JHEP* **05** (2010) 056, [arXiv:1002.3361].

[27] P. Brax, S. Fichet, and P. Tanedo, *The Warped Dark Sector*, arXiv:1906.02199.

[28] L. Randall and R. Sundrum, *An Alternative to compactification*, *Phys. Rev. Lett.* **83** (1999) 4690–4693, [hep-th/9906064].

[29] P. Brax and C. van de Bruck, *Cosmology and brane worlds: A Review*, *Class. Quant. Grav.* **20** (2003) R201–R232, [hep-th/0303095].

[30] E. Witten, *Why Does Quantum Field Theory In Curved Spacetime Make Sense? And What Happens To The Algebra of Observables In The Thermodynamic Limit?*, arXiv:2112.11614.

[31] D. M. Hofman and J. Maldacena, *Conformal collider physics: Energy and charge correlations*, *JHEP* **05** (2008) 012, [arXiv:0803.1467].

[32] P. M. Chesler, K. Jensen, and A. Karch, *Jets in strongly-coupled N = 4 super Yang-Mills theory*, *Phys. Rev.* **D79** (2009) 025021, [arXiv:0804.3110].

[33] Y. Hatta, E. Iancu, and A. H. Mueller, *Deep inelastic scattering off a N=4 SYM plasma at strong coupling*, *JHEP* **01** (2008) 063, [arXiv:0710.5297].

[34] Y. Hatta, E. Iancu, and A. H. Mueller, *Jet evolution in the N=4 SYM plasma at strong coupling*, *JHEP* **05** (2008) 037, [arXiv:0803.2481].

[35] Y. Hatta and T. Matsuo, *Thermal hadron spectrum in e+e- annihilation from gauge/string duality*, *Phys. Rev. Lett.* **102** (2009) 062001, [arXiv:0807.0098].

[36] Y. Hatta and T. Matsuo, *Jet fragmentation and gauge/string duality*, *Phys. Lett.* **B670** (2008) 150–153, [arXiv:0804.4733].

[37] S. Knapen, S. Pagan Griso, M. Papucci, and D. J. Robinson, *Triggering Soft Bombs at the LHC*, *JHEP* **08** (2017) 076, [arXiv:1612.00850].

[38] C. Cesarotti and J. Thaler, *A Robust Measure of Event Isotropy at Colliders*, *JHEP* **08** (2020) 084, [arXiv:2004.06125].

[39] K. F. Di Petrillo, J. N. Farr, C. Guo, T. R. Holmes, J. Nelson, and K. Pachal, *Optimizing Trigger-Level Track Reconstruction for Sensitivity to Exotic Signatures*, arXiv:2211.05720.

[40] C. Csaki, M. Reece, and J. Terning, *The AdS/QCD Correspondence: Still Undelivered*, *JHEP* **05** (2009) 067, [arXiv:0811.3001].

[41] K. L. McDonald, *Sommerfeld Enhancement from Multiple Mediators*, *JHEP* **07** (2012) 145, [arXiv:1203.6341].

[42] A. Katz, M. Reece, and A. Sajjad, *Continuum-mediated dark matter–baryon scattering*, *Phys. Dark Univ.* **12** (2016) 24–36, [arXiv:1509.03628].

[43] M. J. Strassler, *Why Unparticle Models with Mass Gaps are Examples of Hidden Valleys*, arXiv:0801.0629.

[44] E. G. Adelberger, B. R. Heckel, and A. E. Nelson, *Tests of the gravitational inverse square law*, *Ann. Rev. Nucl. Part. Sci.* **53** (2003) 77–121, [hep-ph/0307284].

[45] E. J. Salumbides, W. Ubachs, and V. I. Korobov, *Bounds on fifth forces at the sub-Angstrom length scale*, *J. Molec. Spectrosc.* **300** (2014) 65, [arXiv:1308.1711].

[46] P. Brax, S. Fichet, and G. Pignol, *Bounding Quantum Dark Forces*, *Phys. Rev.* **D97** (2018), no. 11 115034, [arXiv:1710.00850].

[47] J. E. Moody and F. Wilczek, *New Macroscopic Forces?*, *Phys. Rev.* **D30** (1984) 130.

[48] B. A. Dobrescu and I. Mocioiu, *Spin-dependent macroscopic forces from new particle exchange*, *JHEP* **11** (2006) 005, [hep-ph/0605342].

[49] P. Fadeev, Y. V. Stadnik, F. Ficek, M. G. Kozlov, V. V. Flambaum, and D. Budker, *Revisiting spin-dependent forces mediated by new bosons: Potentials in the coordinate-space representation for macroscopic- and atomic-scale experiments*, *Phys. Rev.* **A99** (2019), no. 2 022113, [arXiv:1810.10364].

[50] F. M. Piegsa and G. Pignol, *Limits on the Axial Coupling Constant of New Light Bosons*, *Phys. Rev. Lett.* **108** (2012) 181801, [arXiv:1205.0340].

[51] H. Yan and W. M. Snow, *A New Limit on Possible Long-Range Parity-odd Interactions of the Neutron from Neutron Spin Rotation in Liquid ^4He*, *Phys. Rev. Lett.* **110** (2013), no. 8 082003, [arXiv:1211.6523].

[52] F. Ferrer and J. A. Grifols, *Long range forces from pseudoscalar exchange*, *Phys. Rev.* **D58** (1998) 096006, [hep-ph/9805477].

[53] S. Fichet, *Quantum Forces from Dark Matter and Where to Find Them*, *Phys. Rev. Lett.* **120** (2018), no. 13 131801, [arXiv:1705.10331].

[54] **Super-Kamiokande** Collaboration, Y. Fukuda et al., *Evidence for oscillation of atmospheric neutrinos*, *Phys. Rev. Lett.* **81** (1998) 1562–1567, [hep-ex/9807003].

[55] **SNO** Collaboration, Q. R. Ahmad et al., *Direct evidence for neutrino flavor transformation from neutral current interactions in the Sudbury Neutrino Observatory*, *Phys. Rev. Lett.* **89** (2002) 011301, [nucl-ex/0204008].

[56] **KamLAND** Collaboration, T. Araki et al., *Measurement of neutrino oscillation with KamLAND: Evidence of spectral distortion*, *Phys. Rev. Lett.* **94** (2005) 081801, [hep-ex/0406035].

[57] **K2K** Collaboration, M. H. Ahn et al., *Measurement of Neutrino Oscillation by the K2K Experiment*, *Phys. Rev.* **D74** (2006) 072003, [hep-ex/0606032].

[58] B. Kayser, *Majorana neutrinos and their electromagnetic properties*, *Phys. Rev. D* **26** (Oct, 1982) 1662–1670.

[59] K. M. Case, *Reformulation of the majorana theory of the neutrino*, *Phys. Rev.* **107** (Jul, 1957) 307–316.

[60] K. N. Abazajian and J. Heeck, *Observing Dirac neutrinos in the cosmic microwave background*, *Phys. Rev.* **D100** (2019) 075027, [arXiv:1908.03286].

[61] **KATRIN** Collaboration, M. Aker et al., *An improved upper limit on the neutrino mass from a direct kinematic method by KATRIN*, *Phys. Rev. Lett.* **123** (2019), no. 22 221802, [arXiv:1909.06048].

[62] **GERDA** Collaboration, M. Agostini et al., *Improved Limit on Neutrinoless Double-β Decay of ^{76}Ge from GERDA Phase II*, *Phys. Rev. Lett.* **120** (2018), no. 13 132503, [arXiv:1803.11100].

[63] **CUORE** Collaboration, D. Q. Adams et al., *Improved Limit on Neutrinoless Double-Beta Decay in ^{130}Te with CUORE*, arXiv:1912.10966.

[64] **KamLAND-Zen** Collaboration, A. Gando et al., *Search for Majorana Neutrinos near the Inverted Mass Hierarchy Region with KamLAND-Zen*, *Phys. Rev. Lett.* **117** (2016), no. 8 082503, [arXiv:1605.02889]. [Addendum: Phys. Rev. Lett.117,no.10,109903(2016)].

[65] J. Bernabeu, A. D. Rujula, and C. Jarlskog, *Neutrinoless double electron capture as a tool to measure the electron neutrino mass*, *Nuclear Physics B* **223** (1983), no. 1 15 – 28.

[66] S. Eliseev, C. Roux, K. Blaum, M. Block, C. Droese, F. Herfurth, H.-J. Kluge, M. I. Krivoruchenko, Y. N. Novikov, E. Minaya Ramirez, L. Schweikhard, V. M. Shabaev, F. Šimkovic, I. I. Tupitsyn, K. Zuber, and N. A. Zubova, *Resonant enhancement of neutrinoless double-electron capture in* ^{152}Gd, *Phys. Rev. Lett.* **106** (Feb, 2011) 052504.

[67] J. Bernabeu and A. Segarra, *Stimulated transitions in resonant atom Majorana mixing*, *JHEP* **02** (2018) 017, [arXiv:1706.08328].

[68] A. Segarra and J. Bernabeu, *Absolute neutrino mass and the Dirac/Majorana distinction from the weak interaction of aggregate matter*, arXiv:2001.05900.

[69] G. Feinberg and J. Sucher, *Long-range forces from neutrino-pair exchange*, *Phys. Rev.* **166** (Feb, 1968) 1638–1644.

[70] G. Feinberg, J. Sucher, and C.-K. Au, *The dispersion theory of dispersion forces*, *Physics Reports* **180** (1989), no. 2 83 – 157.

[71] S. D. H. Hsu and P. Sikivie, *Long range forces from two neutrino exchange revisited*, *Phys. Rev.* **D49** (1994) 4951–4953, [hep-ph/9211301].

[72] Q. Le Thien and D. E. Krause, *Spin-Independent Two-Neutrino Exchange Potential with Mixing and CP-Violation*, *Phys. Rev.* **D99** (2019), no. 11 116006, [arXiv:1901.05345].

[73] Y. V. Stadnik, *Probing Long-Range Neutrino-Mediated Forces with Atomic and Nuclear Spectroscopy*, *Phys. Rev. Lett.* **120** (2018), no. 22 223202, [arXiv:1711.03700].

[74] M. Ghosh, Y. Grossman, and W. Tangarife, *Probing the two-neutrino exchange force using atomic parity violation*, arXiv:1912.09444.

[75] B. V. Deriagin, *Analysis of friction and adhesion, IV. The theory of the adhesion of small particles* , *Kolloid Z.* **69** (1934) 155.

[76] I. Heemskerk, J. Penedones, J. Polchinski, and J. Sully, *Holography from Conformal Field Theory*, *JHEP* **10** (2009) 079, [arXiv:0907.0151].

[77] J. Penedones, *Writing CFT correlation functions as AdS scattering amplitudes*, *JHEP* **03** (2011) 025, [arXiv:1011.1485].

[78] L. Cornalba, M. S. Costa, and J. Penedones, *Eikonal approximation in AdS/CFT: Resumming the gravitational loop expansion*, *JHEP* **09** (2007) 037, [arXiv:0707.0120].

[79] A. Fitzpatrick and J. Kaplan, *Analyticity and the Holographic S-Matrix*, *JHEP* **10** (2012) 127, [arXiv:1111.6972].

[80] L. F. Alday and A. Bissi, *Loop Corrections to Supergravity on $AdS_5 \times S^5$*, *Phys. Rev. Lett.* **119** (2017), no. 17 171601, [arXiv:1706.02388].

[81] L. F. Alday and S. Caron-Huot, *Gravitational S-matrix from CFT dispersion relations*, *JHEP* **12** (2018) 017, [arXiv:1711.02031].

[82] L. F. Alday, A. Bissi, and E. Perlmutter, *Genus-One String Amplitudes from Conformal Field Theory*, *JHEP* **06** (2019) 010, [arXiv:1809.10670].

[83] L. F. Alday, *On Genus-one String Amplitudes on $AdS_5 \times S^5$*, arXiv:1812.11783.

[84] D. Meltzer, *Higher Spin ANEC and the Space of CFTs*, *JHEP* **07** (2019) 001, [arXiv:1811.01913].

[85] D. Ponomarev, E. Sezgin, and E. Skvortsov, *On one loop corrections in higher spin gravity*, *JHEP* **11** (2019) 138, [arXiv:1904.01042].

[86] M. Shyani, *Lorentzian inversion and anomalous dimensions in Mellin space*, arXiv:1908.00015.

[87] L. F. Alday and E. Perlmutter, *Growing Extra Dimensions in AdS/CFT*, *JHEP* **08** (2019) 084, [arXiv:1906.01477].

[88] L. F. Alday and X. Zhou, *Simplicity of AdS Supergravity at One Loop*, arXiv:1912.02663.

[89] D. Meltzer, *AdS/CFT Unitarity at Higher Loops: High-Energy String Scattering*, *JHEP* **05** (2020) 133, [arXiv:1912.05580].

[90] F. Aprile, J. Drummond, P. Heslop, and H. Paul, *Quantum Gravity from Conformal Field Theory*, *JHEP* **01** (2018) 035, [arXiv:1706.02822].

[91] F. Aprile, J. Drummond, P. Heslop, and H. Paul, *Unmixing Supergravity*, *JHEP* **02** (2018) 133, [arXiv:1706.08456].

[92] F. Aprile, J. Drummond, P. Heslop, and H. Paul, *Loop corrections for Kaluza-Klein AdS amplitudes*, *JHEP* **05** (2018) 056, [arXiv:1711.03903].

[93] S. Giombi, C. Sleight, and M. Taronna, *Spinning AdS Loop Diagrams: Two Point Functions*, *JHEP* **06** (2018) 030, [arXiv:1708.08404].

[94] C. Cardona, *Mellin-(Schwinger) representation of One-loop Witten diagrams in AdS*, arXiv:1708.06339.

[95] O. Aharony, L. F. Alday, A. Bissi, and E. Perlmutter, *Loops in AdS from Conformal Field Theory*, *JHEP* **07** (2017) 036, [arXiv:1612.03891].

[96] E. Y. Yuan, *Loops in the Bulk*, arXiv:1710.01361.

[97] E. Y. Yuan, *Simplicity in AdS Perturbative Dynamics*, arXiv:1801.07283.

[98] I. Bertan, I. Sachs, and E. D. Skvortsov, *Quantum ϕ^4 Theory in AdS_4 and its CFT Dual*, *JHEP* **02** (2019) 099, [arXiv:1810.00907].

[99] I. Bertan and I. Sachs, *Loops in Anti–de Sitter Space*, *Phys. Rev. Lett.* **121** (2018), no. 10 101601, [arXiv:1804.01880].

[100] J. Liu, E. Perlmutter, V. Rosenhaus, and D. Simmons-Duffin, *d-dimensional SYK, AdS Loops, and $6j$ Symbols*, *JHEP* **03** (2019) 052, [arXiv:1808.00612].

[101] D. Carmi, L. Di Pietro, and S. Komatsu, *A Study of Quantum Field Theories in AdS at Finite Coupling*, *JHEP* **01** (2019) 200, [arXiv:1810.04185].

[102] F. Aprile, J. Drummond, P. Heslop, and H. Paul, *Double-trace spectrum of $N = 4$ supersymmetric Yang-Mills theory at strong coupling*, *Phys. Rev. D* **98** (2018), no. 12 126008, [arXiv:1802.06889].

[103] K. Ghosh, *Polyakov-Mellin Bootstrap for AdS loops*, *JHEP* **02** (2020) 006, [arXiv:1811.00504].

[104] D. Mazac and M. F. Paulos, *The analytic functional bootstrap. Part II. Natural bases for the crossing equation*, *JHEP* **02** (2019) 163, [arXiv:1811.10646].

[105] M. Beccaria and A. A. Tseytlin, *On boundary correlators in Liouville theory on AdS_2*, *JHEP* **07** (2019) 008, [arXiv:1904.12753].

[106] S. M. Chester, *Genus-2 holographic correlator on $AdS_5 \times S^5$ from localization*, *JHEP* **04** (2020) 193, [arXiv:1908.05247].

[107] M. Beccaria, H. Jiang, and A. A. Tseytlin, *Supersymmetric Liouville theory in AdS_2 and AdS/CFT*, *JHEP* **11** (2019) 051, [arXiv:1909.10255].

[108] D. Carmi, *Loops in AdS: From the Spectral Representation to Position Space*, arXiv:1910.14340.

[109] F. Aprile, J. Drummond, P. Heslop, and H. Paul, *One-loop amplitudes in $AdS_5\times S^5$ supergravity from $\mathcal{N}=4$ SYM at strong coupling*, *JHEP* **03** (2020) 190, [arXiv:1912.01047].

[110] S. Fichet, *Opacity and effective field theory in anti–de Sitter backgrounds*, *Phys. Rev.* **D100** (2019), no. 9 095002, [arXiv:1905.05779].

[111] J. Drummond and H. Paul, *One-loop string corrections to AdS amplitudes from CFT*, arXiv:1912.07632.

[112] S. Albayrak, C. Chowdhury, and S. Kharel, *An étude of momentum space scalar amplitudes in AdS*, arXiv:2001.06777.

[113] S. Albayrak and S. Kharel, *On spinning loop amplitudes in Anti-de Sitter space*, arXiv:2006.12540.

[114] D. Meltzer and A. Sivaramakrishnan, *CFT Unitarity and the AdS Cutkosky Rules*, arXiv:2008.11730.

[115] S. Raju, *BCFW for Witten Diagrams*, *Phys. Rev. Lett.* **106** (2011) 091601, [arXiv:1011.0780].

[116] S. Raju, *Four Point Functions of the Stress Tensor and Conserved Currents in AdS_4/CFT_3*, *Phys. Rev. D* **85** (2012) 126008, [arXiv:1201.6452].

[117] S. Raju, *New Recursion Relations and a Flat Space Limit for AdS/CFT Correlators*, *Phys. Rev. D* **85** (2012) 126009, [arXiv:1201.6449].

[118] S. Raju, *Recursion Relations for AdS/CFT Correlators*, *Phys. Rev. D* **83** (2011) 126002, [arXiv:1102.4724].

[119] A. Bzowski, P. McFadden, and K. Skenderis, *Implications of conformal invariance in momentum space*, *JHEP* **03** (2014) 111, [arXiv:1304.7760].

[120] A. Bzowski, P. McFadden, and K. Skenderis, *Scalar 3-point functions in CFT: renormalisation, beta functions and anomalies*, *JHEP* **03** (2016) 066, [arXiv:1510.08442].

[121] A. Bzowski, P. McFadden, and K. Skenderis, *Renormalised CFT 3-point functions of scalars, currents and stress tensors*, *JHEP* **11** (2018) 159, [arXiv:1805.12100].

[122] A. Bzowski, P. McFadden, and K. Skenderis, *Evaluation of conformal integrals*, *JHEP* **02** (2016) 068, [arXiv:1511.02357].

[123] H. Isono, T. Noumi, and T. Takeuchi, *Momentum space conformal three-point functions of conserved currents and a general spinning operator*, *JHEP* **05** (2019) 057, [arXiv:1903.01110].

[124] H. Isono, T. Noumi, and G. Shiu, *Momentum space approach to crossing symmetric CFT correlators*, *JHEP* **07** (2018) 136, [arXiv:1805.11107].

[125] H. Isono, T. Noumi, and G. Shiu, *Momentum space approach to crossing symmetric CFT correlators. Part II. General spacetime dimension*, *JHEP* **10** (2019) 183, [arXiv:1908.04572].

[126] C. Corianò and M. M. Maglio, *Exact Correlators from Conformal Ward Identities in Momentum Space and the Perturbative TJJ Vertex*, *Nucl. Phys. B* **938** (2019) 440–522, [arXiv:1802.07675].

[127] C. Corianò, M. M. Maglio, A. Tatullo, and D. Theofilopoulos, *Exact Correlators from Conformal Ward Identities in Momentum Space and Perturbative Realizations*, *PoS* **CORFU2018** (2019) 072, [arXiv:1904.13174].

[128] C. Corianò and M. M. Maglio, *On Some Hypergeometric Solutions of the Conformal Ward Identities of Scalar 4-point Functions in Momentum Space*, *JHEP* **09** (2019) 107, [arXiv:1903.05047].

[129] M. Gillioz, *Momentum-space conformal blocks on the light cone*, *JHEP* **10** (2018) 125, [arXiv:1807.07003].

[130] C. Coriano, L. Delle Rose, E. Mottola, and M. Serino, *Solving the Conformal Constraints for Scalar Operators in Momentum Space and the Evaluation of Feynman's Master Integrals*, *JHEP* **07** (2013) 011, [arXiv:1304.6944].

[131] A. Bzowski, P. McFadden, and K. Skenderis, *Conformal n-point functions in momentum space*, *Phys. Rev. Lett.* **124** (2020), no. 13 131602, [arXiv:1910.10162].

[132] M. Gillioz, *Conformal 3-point functions and the Lorentzian OPE in momentum space*, arXiv:1909.00878.

[133] J. A. Farrow, A. E. Lipstein, and P. McFadden, *Double copy structure of CFT correlators*, *JHEP* **02** (2019) 130, [arXiv:1812.11129].

[134] B. Nagaraj and D. Ponomarev, *Spinor-helicity formalism for massless fields in AdS_4. Part II. Potentials*, *JHEP* **06** (2020) 068, [arXiv:1912.07494].

[135] S. Albayrak and S. Kharel, *Towards the higher point holographic momentum space amplitudes*, *JHEP* **02** (2019) 040, [arXiv:1810.12459].

[136] S. Albayrak and S. Kharel, *Towards the higher point holographic momentum space amplitudes. Part II. Gravitons*, *JHEP* **12** (2019) 135, [arXiv:1908.01835].

[137] S. Albayrak, C. Chowdhury, and S. Kharel, *New relation for Witten diagrams*, *JHEP* **10** (2019) 274, [arXiv:1904.10043].

[138] J. M. Maldacena, *Non-Gaussian features of primordial fluctuations in single field inflationary models*, *JHEP* **05** (2003) 013, [astro-ph/0210603].

[139] J. M. Maldacena and G. L. Pimentel, *On graviton non-Gaussianities during inflation*, *JHEP* **09** (2011) 045, [arXiv:1104.2846].

[140] I. Mata, S. Raju, and S. Trivedi, *CMB from CFT*, *JHEP* **07** (2013) 015, [arXiv:1211.5482].

[141] N. Kundu, A. Shukla, and S. P. Trivedi, *Constraints from Conformal Symmetry on the Three Point Scalar Correlator in Inflation*, *JHEP* **04** (2015) 061, [arXiv:1410.2606].

[142] A. Ghosh, N. Kundu, S. Raju, and S. P. Trivedi, *Conformal Invariance and the Four Point Scalar Correlator in Slow-Roll Inflation*, *JHEP* **07** (2014) 011, [arXiv:1401.1426].

[143] N. Arkani-Hamed and J. Maldacena, *Cosmological Collider Physics*, arXiv:1503.08043.

[144] N. Kundu, A. Shukla, and S. P. Trivedi, *Ward Identities for Scale and Special Conformal Transformations in Inflation*, *JHEP* **01** (2016) 046, [arXiv:1507.06017].

[145] C. Sleight, *A Mellin Space Approach to Cosmological Correlators*, *JHEP* **01** (2020) 090, [arXiv:1906.12302].

[146] C. Sleight and M. Taronna, *Bootstrapping Inflationary Correlators in Mellin Space*, *JHEP* **02** (2020) 098, [arXiv:1907.01143].

[147] C. Sleight and M. Taronna, *From AdS to dS Exchanges: Spectral Representation, Mellin Amplitudes and Crossing*, arXiv:2007.09993.

[148] N. Arkani-Hamed, P. Benincasa, and A. Postnikov, *Cosmological Polytopes and the Wavefunction of the Universe*, arXiv:1709.02813.

[149] N. Arkani-Hamed and P. Benincasa, *On the Emergence of Lorentz Invariance and Unitarity from the Scattering Facet of Cosmological Polytopes*, arXiv:1811.01125.

[150] P. Benincasa, *From the flat-space S-matrix to the Wavefunction of the Universe*, arXiv:1811.02515.

[151] P. Benincasa, *Cosmological Polytopes and the Wavefuncton of the Universe for Light States*, arXiv:1909.02517.

[152] N. Arkani-Hamed, D. Baumann, H. Lee, and G. L. Pimentel, *The Cosmological Bootstrap: Inflationary Correlators from Symmetries and Singularities*, *JHEP* **04** (2020) 105, [arXiv:1811.00024].

[153] D. Baumann, C. Duaso Pueyo, A. Joyce, H. Lee, and G. L. Pimentel, *The Cosmological Bootstrap: Weight-Shifting Operators and Scalar Seeds*, arXiv:1910.14051.

[154] D. Baumann, C. Duaso Pueyo, A. Joyce, H. Lee, and G. L. Pimentel, *The Cosmological Bootstrap: Spinning Correlators from Symmetries and Factorization*, arXiv:2005.04234.

[155] N. Arkani-Hamed, M. Porrati, and L. Randall, *Holography and phenomenology*, *JHEP* **08** (2001) 017, [hep-th/0012148].

[156] V. Balasubramanian, S. B. Giddings, and A. E. Lawrence, *What do CFTs tell us about Anti-de Sitter space-times?*, *JHEP* **03** (1999) 001, [hep-th/9902052].

[157] S. B. Giddings, *The Boundary S matrix and the AdS to CFT dictionary*, *Phys. Rev. Lett.* **83** (1999) 2707–2710, [hep-th/9903048].

[158] D. Meltzer, E. Perlmutter, and A. Sivaramakrishnan, *Unitarity Methods in AdS/CFT*, *JHEP* **03** (2020) 061, [arXiv:1912.09521].

[159] S. Caron-Huot, *Analyticity in Spin in Conformal Theories*, *JHEP* **09** (2017) 078, [arXiv:1703.00278].

[160] D. W. Dusedau and D. Z. Freedman, *Lehmann Spectral Representation for Anti-de Sitter Quantum Field Theory*, *Phys. Rev. D* **33** (1986) 389.

[161] C. J. Burges, D. Z. Freedman, S. Davis, and G. Gibbons, *Supersymmetry in Anti-de Sitter Space*, *Annals Phys.* **167** (1986) 285.

[162] S. Fichet, *Braneworld effective field theories — holography, consistency and conformal effects*, *JHEP* **04** (2020) 016, [arXiv:1912.12316].

[163] T. Leonhardt, R. Manvelyan, and W. Ruhl, *The Group approach to AdS space propagators*, *Nucl. Phys. B* **667** (2003) 413–434, [hep-th/0305235].

[164] "*NIST Digital Library of Mathematical Functions*." http://dlmf.nist.gov/, Release 1.0.28 of 2020-09-15. F. W. J. Olver, A. B. Olde Daalhuis, D. W. Lozier, B. I. Schneider, R. F. Boisvert, C. W. Clark, B. R. Miller, B. V. Saunders, H. S. Cohl, and M. A. McClain, eds.

[165] R. Zwicky, *A brief Introduction to Dispersion Relations and Analyticity*, in *Quantum Field Theory at the Limits: from Strong Fields to Heavy Quarks*, pp. 93–120, 2017. arXiv:1610.06090.

[166] M. E. Peskin and D. V. Schroeder, *An introduction to quantum field theory*. Westview, Boulder, CO, 1995.

[167] N. Birrell and P. Davies, *Quantum Fields in Curved Space*. Cambridge Monographs on Mathematical Physics. Cambridge University Press, 1984.

[168] M. F. Paulos, *Towards Feynman rules for Mellin amplitudes*, *JHEP* **10** (2011) 074, [arXiv:1107.1504].

[169] G. Mack, *D-dimensional Conformal Field Theories with anomalous dimensions as Dual Resonance Models*, *Bulg. J. Phys.* **36** (2009) 214–226, [arXiv:0909.1024].

[170] S. Kharel and G. Siopsis, *Tree-level Correlators of scalar and vector fields in AdS/CFT*, *JHEP* **11** (2013) 159, [arXiv:1308.2515].

[171] A. Fitzpatrick and J. Kaplan, *Unitarity and the Holographic S-Matrix*, *JHEP* **10** (2012) 032, [arXiv:1112.4845].

[172] M. S. Costa, V. Gonçalves, and J. Penedones, *Spinning AdS Propagators*, *JHEP* **09** (2014) 064, [arXiv:1404.5625].

[173] M. F. Paulos, J. Penedones, J. Toledo, B. C. van Rees, and P. Vieira, *The S-matrix bootstrap. Part I: QFT in AdS*, *JHEP* **11** (2017) 133, [arXiv:1607.06109].

[174] C. B. Jepsen and S. Parikh, *Recursion Relations in p-adic Mellin Space*, *J. Phys. A* **52** (2019), no. 28 285401, [arXiv:1812.09801].

[175] C. B. Jepsen and S. Parikh, *p-adic Mellin Amplitudes*, *JHEP* **04** (2019) 101, [arXiv:1808.08333].

[176] S. S. Gubser, C. Jepsen, and B. Trundy, *Spin in p-adic AdS/CFT*, *J. Phys. A* **52** (2019), no. 14 144004, [arXiv:1811.02538].

[177] E. Hijano, P. Kraus, E. Perlmutter, and R. Snively, *Witten Diagrams Revisited: The AdS Geometry of Conformal Blocks*, *JHEP* **01** (2016) 146, [arXiv:1508.00501].

[178] S. Parikh, *Holographic dual of the five-point conformal block*, *JHEP* **05** (2019) 051, [arXiv:1901.01267].

[179] C. B. Jepsen and S. Parikh, *Propagator identities, holographic conformal blocks, and higher-point AdS diagrams*, *JHEP* **10** (2019) 268, [arXiv:1906.08405].

[180] J. Penedones, J. A. Silva, and A. Zhiboedov, *Nonperturbative Mellin Amplitudes: Existence, Properties, Applications*, *JHEP* **08** (2020) 031, [arXiv:1912.11100].

[181] D. Ponomarev, *From bulk loops to boundary large-N expansion*, *JHEP* **01** (2020) 154, [arXiv:1908.03974].

[182] S. Caron-Huot and A.-K. Trinh, *All tree-level correlators in $AdS_5 \times S_5$ supergravity: hidden ten-dimensional conformal symmetry*, *JHEP* **01** (2019) 196, [arXiv:1809.09173].

[183] A. Fitzpatrick, J. Kaplan, J. Penedones, S. Raju, and B. C. van Rees, *A Natural Language for AdS/CFT Correlators*, *JHEP* **11** (2011) 095, [arXiv:1107.1499].

[184] S. Fichet, B. Jain, E. Ponton, M. Quiros, and R. Rosenfeld, "Private Communication."

[185] W. R. Inc., "Mathematica, Version 12.1." https://www.wolfram.com/mathematica.

[186] W. D. Goldberger and I. Z. Rothstein, *High-energy field theory in truncated AdS backgrounds*, *Phys. Rev. Lett.* **89** (2002) 131601, [hep-th/0204160].

[187] W. D. Goldberger and I. Z. Rothstein, *Effective field theory and unification in AdS backgrounds*, *Phys. Rev.* **D68** (2003) 125011, [hep-th/0208060].

[188] E. Ponton, *TASI 2011: Four Lectures on TeV Scale Extra Dimensions*, in *Theoretical Advanced Study Institute in Elementary Particle Physics: The Dark Secrets of the Terascale*, pp. 283–374, 2013. arXiv:1207.3827.

[189] Z. Chacko, M. A. Luty, and E. Ponton, *Massive higher dimensional gauge fields as messengers of supersymmetry breaking*, *JHEP* **07** (2000) 036, [hep-ph/9909248].

[190] K. Agashe, H. Davoudiasl, G. Perez, and A. Soni, *Warped Gravitons at the LHC and Beyond*, *Phys. Rev.* **D76** (2007) 036006, [hep-ph/0701186].

[191] A. Karch, E. Katz, D. T. Son, and M. A. Stephanov, *Linear confinement and AdS/QCD*, *Phys. Rev.* **D74** (2006) 015005, [hep-ph/0602229].

[192] U. Gursoy and E. Kiritsis, *Exploring improved holographic theories for QCD: Part I*, *JHEP* **02** (2008) 032, [arXiv:0707.1324].

[193] U. Gursoy, E. Kiritsis, and F. Nitti, *Exploring improved holographic theories for QCD: Part II*, *JHEP* **02** (2008) 019, [arXiv:0707.1349].

[194] S. S. Gubser and A. Nellore, *Mimicking the QCD equation of state with a dual black hole*, *Phys. Rev. D* **78** (2008) 086007, [arXiv:0804.0434].

[195] A. Falkowski and M. Perez-Victoria, *Electroweak Breaking on a Soft Wall*, *JHEP* **12** (2008) 107, [arXiv:0806.1737].

[196] B. Batell and T. Gherghetta, *Dynamical Soft-Wall AdS/QCD*, *Phys. Rev.* **D78** (2008) 026002, [arXiv:0801.4383].

[197] B. Batell, T. Gherghetta, and D. Sword, *The Soft-Wall Standard Model*, *Phys. Rev.* **D78** (2008) 116011, [arXiv:0808.3977].

[198] J. A. Cabrer, G. von Gersdorff, and M. Quiros, *Soft-Wall Stabilization*, *New J. Phys.* **12** (2010) 075012, [arXiv:0907.5361].

[199] G. von Gersdorff, *From Soft Walls to Infrared Branes*, *Phys. Rev.* **D82** (2010) 086010, [arXiv:1005.5134].

[200] J. A. Cabrer, G. von Gersdorff, and M. Quiros, *Suppressing Electroweak Precision Observables in 5D Warped Models*, *JHEP* **05** (2011) 083, [arXiv:1103.1388].

[201] D. Z. Freedman, S. S. Gubser, K. Pilch, and N. P. Warner, *Renormalization group flows from holography supersymmetry and a c theorem*, *Adv. Theor. Math. Phys.* **3** (1999) 363–417, [hep-th/9904017].

[202] E. Dudas and G. von Gersdorff, *Universal contributions to scalar masses from five dimensional supergravity*, *JHEP* **10** (2012) 100, [arXiv:1207.0815].

[203] E. E. Boos, Y. A. Kubyshin, M. N. Smolyakov, and I. P. Volobuev, *Effective Lagrangians for physical degrees of freedom in the Randall-Sundrum model*, *Class. Quant. Grav.* **19** (2002) 4591–4606, [hep-th/0202009].

[204] K. Hinterbichler, *Theoretical Aspects of Massive Gravity*, *Rev. Mod. Phys.* **84** (2012) 671–710, [arXiv:1105.3735].

[205] J. Polchinski and M. J. Strassler, *Deep inelastic scattering and gauge / string duality*, *JHEP* **05** (2003) 012, [hep-th/0209211].

[206] P. Breitenlöhner and D. Z. Freedman, *Stability in Gauged Extended Supergravity*, *Annals Phys.* **144** (1982) 249.

[207] P. Breitenlohner and D. Z. Freedman, *Positive Energy in anti-De Sitter Backgrounds and Gauged Extended Supergravity*, *Phys. Lett.* **115B** (1982) 197–201.

[208] A. Manohar and H. Georgi, *Chiral Quarks and the Nonrelativistic Quark Model*, *Nucl. Phys.* **B234** (1984) 189–212.

[209] H. Georgi and L. Randall, *Flavor Conserving CP Violation in Invisible Axion Models*, *Nucl. Phys.* **B276** (1986) 241–252.

[210] H. Georgi, *Generalized Dimensional Analysis*, *Phys. Lett.* **B298** (1993) 187–189, [hep-ph/9207278].

[211] G. Panico and A. Wulzer, *The Composite Nambu-Goldstone Higgs*, *Lect. Notes Phys.* **913** (2016) pp.1–316, [arXiv:1506.01961].

[212] **Particle Data Group** Collaboration, M. t. Tanabashi, *Review of particle physics*, *Phys. Rev. D* **98** (Aug, 2018) 030001.

[213] P. Creminelli, A. Nicolis, and R. Rattazzi, *Holography and the electroweak phase transition*, *JHEP* **03** (2002) 051, [hep-th/0107141].

[214] E. Witten, *Baryons in the 1/n Expansion*, *Nucl. Phys.* **B160** (1979) 57–115.

[215] F. Kahlhoefer, K. Schmidt-Hoberg, and S. Wild, *Dark Matter Self-Interactions from a General Spin-0 Mediator*, *JCAP* **1708** (2017), no. 08 003, [arXiv:1704.02149].

[216] B. Bellazzini, M. Cliche, and P. Tanedo, *Effective theory of self-interacting dark matter*, *Phys. Rev.* **D88** (2013), no. 8 083506, [arXiv:1307.1129].

[217] S. Aldaihan, D. E. Krause, J. C. Long, and W. M. Snow, *Calculations of the dominant long-range, spin-independent contributions to the interaction energy between two nonrelativistic Dirac fermions from double-boson exchange of spin-0 and spin-1 bosons with spin-dependent couplings*, *Phys. Rev.* **D95** (2017), no. 9 096005, [arXiv:1611.01580].

[218] G. Feinberg and J. Sucher, *Long-Range Forces from Neutrino-Pair Exchange*, *Phys. Rev.* **166** (1968) 1638–1644.

[219] M. Puchwein and Z. Kunszt, *Radiative corrections with 5-D mixed position / momentum space propagators*, *Annals Phys.* **311** (2004) 288–313, [hep-th/0309069].

[220] M. Carena, A. Delgado, E. Ponton, T. M. P. Tait, and C. E. M. Wagner, *Precision electroweak data and unification of couplings in warped extra dimensions*, *Phys. Rev.* **D68** (2003) 035010, [hep-ph/0305188].

[221] K. K. Boddy, J. L. Feng, M. Kaplinghat, Y. Shadmi, and T. M. P. Tait, *Strongly Interacting Dark Matter: Self-Interactions and keV Lines*, *Phys. Rev.* **D90** (2014), no. 9 095016, [arXiv:1408.6532].

[222] K. K. Boddy, J. L. Feng, M. Kaplinghat, and T. M. P. Tait, *Self-Interacting Dark Matter from a Non-Abelian Hidden Sector*, *Phys. Rev.* **D89** (2014), no. 11 115017, [arXiv:1402.3629].

[223] P. Brax and S. Fichet, *Quantum Chameleons*, *Phys. Rev.* **D99** (2019), no. 10 104049, [arXiv:1809.10166].

[224] K. Milton, *The Casimir Effect: Physical Manifestations of Zero-point Energy*. EBL-Schweitzer. World Scientific, 2001.

[225] Y. J. Chen, W. K. Tham, D. E. Krause, D. Lopez, E. Fischbach, and R. S. Decca, *Stronger Limits on Hypothetical Yukawa Interactions in the 30?8000 nm Range*, *Phys. Rev. Lett.* **116** (2016), no. 22 221102, [arXiv:1410.7267].

[226] D. Karateev, P. Kravchuk, and D. Simmons-Duffin, *Harmonic Analysis and Mean Field Theory*, *JHEP* **10** (2019) 217, [arXiv:1809.05111].

[227] B. Holdom, *Searching for ϵ Charges and a New U(1)*, *Phys. Lett.* **B178** (1986) 65–70.

[228] B. Holdom, *Two U(1)'s and Epsilon Charge Shifts*, *Phys. Lett.* **166B** (1986) 196–198.

[229] S. Fichet, *Shining Light on Polarizable Dark Particles*, *JHEP* **04** (2017) 088, [arXiv:1609.01762].

[230] G. Feinberg, J. Sucher, and C. K. Au, *The Dispersion Theory of Dispersion Forces*, *Phys. Rept.* **180** (1989) 83.

Appendix A

Dressed Equation of Motion

In this appendix we derive the equation of motion in the presence of a generic self-energy using the path integral formalism. The approach amounts to requiring invariance of a given path integral quantity under an infinitesimal change in the field variable. This method was used in [166] in the free case.

We first derive the homogeneous equation of motion. Start from the partition function of the interacting theory

$$Z = \int \mathcal{D}\Phi\mathcal{D}\varphi e^{iS[\Phi,\varphi]}\,, \quad S[\Phi,\varphi] = \int d^{d+1}X\sqrt{|\gamma|}\left(\mathcal{L}_0[\Phi] + \mathcal{L}[\varphi] + \lambda\Phi\mathcal{O}(\varphi)\right)\,. \tag{A.1}$$

In the fundamental action, $\mathcal{L}_0[\Phi]$ is the free Lagrangian for Φ, given by

$$\mathcal{L}_0[\Phi] = -\frac{1}{2}\Phi(X)\mathcal{D}\Phi(X)\,. \tag{A.2}$$

$\mathcal{L}[\varphi]$ encodes the properties of other fields φ and does not need to be specified. The (generally composite) operator $\mathcal{O}$ is here assumed to depend on the φ fields only. A very similar calculation can be done if Φ has self-interactions. We recall the definition of the expectation

value of an operator A dictated by the partition function,

$$\langle A\rangle(X) = Z^{-1}\int \mathcal{D}\Phi\mathcal{D}\varphi\, A(X)\, e^{i\int d^{d+1}X'\, S[\Phi,\varphi]}\,. \tag{A.3}$$

Starting from Z, we perform an infinitesimal change of variable of the field $\Phi(X) \equiv \widetilde{\Phi}(X) + \epsilon(X)$. The path integral measure remains unchanged, $\mathcal{D}\Phi = \mathcal{D}\widetilde{\Phi}$. Expanding the exponential at first order in ϵ gives

$$\begin{aligned} Z &= \int \mathcal{D}\Phi\mathcal{D}\varphi e^{i\int d^{d+1}X'\sqrt{|\gamma|}(\mathcal{L}_0[\Phi]+\mathcal{L}[\varphi]+\lambda\Phi\mathcal{O})}\left(1 + i\int d^{d+1}X\epsilon(X)\sqrt{|\gamma|}\,[-\mathcal{D}\Phi(X)+\lambda\mathcal{O}(X)]\right) \\ &= Z + i\int d^{d+1}X\sqrt{|\gamma|}\epsilon(X)\int \mathcal{D}\Phi\mathcal{D}\varphi e^{i\int d^{d+1}X'\sqrt{|\gamma|}(\mathcal{L}_0[\Phi]+\mathcal{L}[\varphi]+\lambda\Phi\mathcal{O})}\,[-\mathcal{D}\Phi(X)+\lambda\mathcal{O}(X)]\,. \end{aligned} \tag{A.4}$$

The second term in the last line must vanish for any $\epsilon(X)$, implying the quantum equation of motion

$$\int \mathcal{D}\Phi\mathcal{D}\varphi e^{iS[\Phi,\varphi]}\,[\mathcal{D}\Phi(X) - \lambda\mathcal{O}(X)] = 0\,. \tag{A.5}$$

Using the definition of the expectation value from Eq. (A.3) and introducing the notation $\langle\Phi\rangle = \Phi_{\rm cl}$, $\langle\mathcal{O}\rangle = \mathcal{O}_{\rm cl}$ we have

$$\mathcal{D}\Phi_{\rm cl}(X) - \lambda\mathcal{O}_{\rm cl}(X) = 0\,. \tag{A.6}$$

The second term involves the expectation value of the composite operator $\mathcal{O}$

$$\mathcal{O}_{\rm cl}(X) = Z^{-1}\int \mathcal{D}\Phi\mathcal{D}\varphi\,\mathcal{O}(X)\, e^{i\int d^{d+1}X\sqrt{|\gamma|}(\mathcal{L}_0[\Phi]+\mathcal{L}[\varphi]+\lambda\Phi\mathcal{O})}\,. \tag{A.7}$$

We now seek to express $\mathcal{O}_{\rm cl}$ as a quantity involving $\Phi_{\rm cl}$. We can notice the Φ field acts as a source for $\mathcal{O}$. It is convenient to introduce a generating functional of the $\mathcal{O}$ correlators $E[\Phi_{\rm cl}]$ such that

$$E[\Phi_{\rm cl}] = i\log Z[\Phi_{\rm cl}]\,, \quad Z[\Phi_{\rm cl}] = \int \mathcal{D}\varphi e^{i\int d^{d+1}X\sqrt{|\gamma|}(\mathcal{L}_0[\Phi]+\mathcal{L}[\varphi]+\lambda\Phi_{\rm cl}\mathcal{O})} \tag{A.8}$$

From $E[\Phi_{\rm cl}]$ we have the standard identities

$$\frac{\delta E[\Phi_{\rm cl}]}{\delta\Phi_{\rm cl}(X)} = -\lambda\sqrt{|\gamma|}\mathcal{O}_{\rm cl}(X)\,. \tag{A.9}$$

$$\frac{\delta^2 E}{\delta\Phi_{\rm cl}(X)\delta\Phi_{\rm cl}(X')} = -i\lambda^2\sqrt{|\gamma|}_X\sqrt{|\gamma|}_{X'}\langle\mathcal{O}(X)\mathcal{O}(X')\rangle_{\rm conn} \tag{A.10}$$

where we display the connected correlator of $\mathcal{O}$. The self-energy $i\Pi$ is defined such as it absorbs the metric factors and the $(i\lambda)^2$ vertices, giving

$$\frac{\delta^2 E}{\delta\Phi_{\rm cl}(X)\delta\Phi_{\rm cl}(X')} = -\Pi(X,X')\,. \tag{A.11}$$

Finally we also have

$$-\lambda\sqrt{|\gamma|}\Phi_{\rm cl}(X) = \frac{\delta E[\Phi_{\rm cl}]}{\delta\mathcal{O}_{\rm cl}(X)}\,. \tag{A.12}$$

Given these identities, we can rewrite $-\lambda\sqrt{|\gamma|}\mathcal{O}_{\rm cl}(X)$ as follows. Using the chain rule for functional derivatives in Eq. (A.9) we get

$$-\lambda\sqrt{|\gamma|}\mathcal{O}_{\rm cl}(X) = \int d^{d+1}X'\frac{\delta\mathcal{O}_{\rm cl}(X')}{\delta\Phi(X)}\frac{\delta E[\Phi]}{\delta\mathcal{O}_{\rm cl}(X')} = \int d^{d+1}X'\frac{\delta\mathcal{O}_{\rm cl}(X')}{\delta\Phi(X)}\left(-\lambda\sqrt{|\gamma|_{X'}}\right)\Phi_{\rm cl}(X')\,. \tag{A.13}$$

Then using again Eq. (A.9) notice that

$$-\lambda\sqrt{|\gamma|_{X'}}\frac{\delta\mathcal{O}_{\rm cl}(X')}{\delta\Phi(X)} = \frac{\delta^2 E[\Phi]}{\delta\Phi(X)\delta\Phi(X')} = -\Pi(X,X')\,. \tag{A.14}$$

Therefore we have shown that

$$\lambda\sqrt{|\gamma|}\mathcal{O}_{\rm cl}(X) = \int d^{d+1}X'\Pi(X,X')\Phi_{\rm cl}(X'). \tag{A.15}$$

Hence the dressed equation of motion takes the form

$$\mathcal{D}\Phi_{\rm cl}(X) - \frac{1}{\sqrt{|\gamma|}}\Pi * \Phi_{\rm cl}(X) = 0\,. \tag{A.16}$$

In order to compute the dressed equation of motion for the Feynman propagator, one proceeds similarly with an extra insertion of Φ in the path integral such that the starting quantity considered amounts to $Z\Phi_{\rm cl}(X)$. An infinitesimal shift of the field variable gives

$$
\begin{aligned}
&Z\Phi_{\rm cl}(X) = \qquad\qquad (A.17)\\
&\int \mathcal{D}\Phi\mathcal{D}\varphi e^{iS}\left(\Phi(X)+\int d^{d+1}X'\epsilon(X')\left(i\sqrt{|\gamma|}\left[-\mathcal{D}\Phi(X')+\lambda\mathcal{O}\right]\Phi(X)+\delta^{(d+1)}(X-X')\right)\right)\\
&= Z\Phi_{\rm cl}(X)+\\
&\int d^{d+1}X'\epsilon(X')\int \mathcal{D}\Phi\mathcal{D}\varphi e^{iS}\left(i\sqrt{|\gamma|}\left[-\mathcal{D}\Phi(X')+\lambda\mathcal{O}\right]\Phi(X)+\delta^{(d+1)}(X-X')\right).
\end{aligned}
$$

The second term must vanish for any $\epsilon(X)$, hence we have

$$\int \mathcal{D}\Phi\mathcal{D}\varphi e^{iS}\left(i\sqrt{|\gamma|}\left[-\mathcal{D}\Phi(X')+\lambda\mathcal{O}\right]\Phi(X)+\delta^{(d+1)}(X-X')\right)=0. \qquad (A.18)$$

In terms of expectation values, we find that the previous statement is equivalent to

$$\sqrt{|\gamma|}_X\mathcal{D}_X\langle\Phi(X)\Phi(X')\rangle-\lambda\sqrt{|\gamma|}_X\langle\Phi(X)\mathcal{O}(X')\rangle_{\rm conn}=-i\delta^{(d+1)}(X-X'). \qquad (A.19)$$

Using similar manipulations as above [1] we find

$$\lambda\sqrt{|\gamma|}_X\langle\Phi(X)\mathcal{O}(X')\rangle=i\lambda^2\sqrt{|\gamma|}_X\sqrt{|\gamma|}_{X'}\langle\mathcal{O}(X)\mathcal{O}(\widetilde{X})\rangle_{\rm conn}*G(\widetilde{X},X')=\Pi*G(X,X'). \qquad (A.20)$$

The dressed equation of motion is thus

$$\sqrt{|\gamma|}\mathcal{D}_XG(X,X')-\Pi*G(X,X')=-i\delta^{(d+1)}(X-X'), \qquad (A.21)$$

which completes the proof of Eq. (2.9).

[1] One can for instance introduce a generating functional with sources for Φ and $\mathcal{O}$ which are set to zero at the end of the calculation.

Appendix B

Proof of Conformal Completeness Relation

We prove Eq. (2.24) in two steps. In App. B.1, we show that the integral vanishes for $z \neq z'$. In App. B.2, we integrate Eq. (2.24) over z' to determine the normalization of the delta function.

B.1 $z \neq z'$

Here we evaluate

$$\int_{-i\infty}^{i\infty} d\alpha \Omega_p(\alpha) = \int_{i\infty}^{i\infty} d\alpha \frac{i\alpha \sin(\pi\alpha)}{\pi^2} (k^2 z z')^{d/2} K_\alpha(\sqrt{-p^2} z) K_\alpha(\sqrt{-p^2} z') \tag{B.1}$$

for $z > z'$. This choice is unimportant—it simply controls how we close the contour for some of the terms. We use the series representation of the Bessel functions, Eq. (2.72). Four

terms emerge. These reduce to two terms under a $\alpha \to -\alpha$ relabeling. We are left with

$$\int_{-i\infty}^{i\infty} d\alpha \Omega_p(\alpha) = \tag{B.2}$$
$$(k^2 z z')^{d/2} \int_{i\infty}^{i\infty} d\alpha \frac{i\alpha}{2\sin(\pi\alpha)} \sum_{m,n=0} \frac{1}{m!n!} \left(\frac{\sqrt{-p^2}z'}{2}\right)^{2n} \left(\frac{\sqrt{-p^2}z}{2}\right)^{2m} \times$$
$$\left[\frac{1}{\Gamma(n-\alpha+1)} \left(\frac{\sqrt{-p^2}z'}{2}\right)^{-\alpha}\right] \left[\frac{1}{\Gamma(m-\alpha+1)} \left(\frac{\sqrt{-p^2}z}{2}\right)^{-\alpha} - \frac{1}{\Gamma(m+\alpha+1)} \left(\frac{\sqrt{-p^2}z}{2}\right)^{\alpha}\right].$$

We promote the line integral to a contour and close this contour in a large half-circle towards the negative reals. We then apply the residue theorem and sum over the poles of the $1/\sin(\pi\alpha)$ function. A sequence of poles are cancelled by the roots of $1/\Gamma(m+\alpha+1)$ in the second term. The remaining terms (labeled by T_1 and T_2) are

$$T_1 = (k^2 z z')^{d/2} \times \tag{B.3}$$
$$\sum_{m,n=0} \sum_{l=1}^{\infty} \frac{il(-1)^l}{m!n!} \left(\frac{\sqrt{-p^2}z'}{2}\right)^{2n+l} \left(\frac{\sqrt{-p^2}z}{2}\right)^{2m+l} \frac{1}{\Gamma(n+l+1)\Gamma(m+l+1)}$$

$$T_2 = -(k^2 z z')^{d/2} \times \tag{B.4}$$
$$\sum_{m=1,n=0} \sum_{l=1}^{m} \frac{il(-1)^l}{m!n!} \left(\frac{\sqrt{-p^2}z'}{2}\right)^{2n} \left(\frac{\sqrt{-p^2}z}{2}\right)^{2m} \frac{1}{\Gamma(n+l+1)\Gamma(m-l+1)} \left(\frac{z'}{z}\right)^{l}.$$

We introduce $c \equiv m + l$ in T_1 and convert the sums over m, l into sums over c, l. Upon a relabeling, this gives $T_1 = -T_2$ and thus

$$\int_{-i\infty}^{i\infty} d\alpha \, \Omega_p(\alpha) = 0 \tag{B.5}$$

for $z \neq z'$.

B.2 Normalization

To obtain the normalization and thus prove Eq. (2.24), we evaluate

$$\int_0^\infty dz' \int_{-i\infty}^{i\infty} d\alpha \Omega_p(\alpha) = \tag{B.6}$$
$$\int_0^\infty dz' \int_{-i\infty}^{i\infty} d\alpha \frac{i\alpha \sin(\pi\alpha)}{\pi^2} (k^2 z z')^{d/2} K_\alpha(\sqrt{-p^2} z) K_\alpha(\sqrt{-p^2} z') \,.$$

We directly perform the integral over z' and use the series representation Eq. (2.72) to expand the remaining Bessel function. We then let $\alpha \to -\alpha$ to reduce the two terms to one. We are left with

$$\int_0^\infty dz' \int_{-i\infty}^{i\infty} d\alpha \Omega_p(\alpha) = \frac{i}{2\pi\sqrt{-p^2}} \left(\frac{2zk^2}{\sqrt{-p^2}}\right)^{d/2} \sum_{m=0} \frac{1}{m!} \left(\frac{\sqrt{-p^2} z}{2}\right)^{2m} \times \tag{B.7}$$
$$\int_{-i\infty}^{i\infty} d\alpha \left[\frac{\alpha}{\Gamma(m-\alpha+1)} \left(\frac{\sqrt{-p^2} z}{2}\right)^{-\alpha}\right] \Gamma\left(\frac{1}{4}(d-2\alpha+2)\right) \Gamma\left(\frac{1}{4}(d+2\alpha+2)\right) \,.$$

We promote the line integral to a contour and close to the negative reals. A straightforward application of the residue theorem yields

$$\int_0^\infty dz' \int_{-i\infty}^{i\infty} d\alpha \Omega_p(\alpha) = \tag{B.8}$$
$$\frac{(kz)^{d+1}}{k} \sum_{m,n=0} \frac{(-1)^n}{m!n!} \left[\frac{(2n+\frac{d}{2}+1)\Gamma\left(n+\frac{d}{2}+1\right)}{\Gamma(m+(2n+\frac{d}{2}+1)+1)} \left(\frac{\sqrt{-p^2} z}{2}\right)^{2n+2m}\right] .$$

By introducing $c \equiv m+n$ and reorganizing the sums, we obtain

$$\int_0^\infty dz' \int_{-i\infty}^{i\infty} d\alpha \Omega_p(\alpha) = \tag{B.9}$$
$$\frac{(kz)^{d+1}}{k} \sum_{c=0}^{\infty} \left(\frac{\sqrt{-p^2} z}{2}\right)^{2c} \sum_{n=0}^{c} \frac{(-1)^n (2n+\frac{d}{2}+1)}{(c-n)!n!} \frac{\Gamma\left(n+\frac{d}{2}+1\right)}{\Gamma(c+(n+\frac{d}{2}+1)+1)} \,.$$

We directly perform the sum over n with

$$\sum_{n=0}^{c} \frac{(-1)^n}{(c-n)!n!} \frac{\Gamma\left(n+1+\frac{d}{2}\right)(2n+\frac{d}{2}+1)}{\Gamma(c+(n+\frac{d}{2}+1)+1)} = \delta_{c0} \,, \tag{B.10}$$

which we obtained through the use of Mathematica [185]. This gives

$$\int_0^\infty dz' \int_{-i\infty}^{i\infty} d\alpha \Omega_p(\alpha) = \frac{(kz)^{d+1}}{k} \,,$$

which completes the proof of Eq. (2.24).

Appendix C

Elements of AdS/CFT in Momentum Space

In this Appendix we give elements of CFT in d-dimensional Minkowski space and introduce the AdS bulk-to-boundary propagator. All these notions are consistently translated into Lorentzian momentum space. We recall the chosen metric has mostly-minus signature $(+,-,\ldots,-)$. The Fourier transform convention is

$$\mathcal{O}(x) = \int \frac{d^d p}{(2\pi)^d} \mathcal{O}(p) e^{-ip\cdot x} \,. \tag{C.1}$$

C.1 Bulk Mass and Conformal Dimensions

The relation between a scalar bulk field in AdS with bulk mass $m_\Phi^2 = \left(\alpha^2 - \frac{d^2}{4}\right) k^2$ and a scalar primary operator with scaling dimension Δ from the dual CFT is given by (see

e.g. [13])

$$\alpha^2 = \frac{M^2}{k^2} + \frac{d^2}{4} \equiv \left(\Delta - \frac{d}{2}\right)^2 . \tag{C.2}$$

The relation implies $\Delta = \frac{d}{2} \pm \alpha$. In general we have $\alpha \in \mathbb{R}$. As done in Sec. 2.3, we restrict to $\alpha \in \mathbb{R}_+$ without loss of generality, and define

$$\Delta_\pm = \frac{d}{2} \pm \alpha \,. \tag{C.3}$$

Unitarity requires $\Delta \geq d/2 - 1$. Hence for $\alpha > 1$ only the dual CFT operator with Δ_+ exists. For $0 < \alpha < 1$, both Δ_- and Δ_+ branches of the correspondence exist. [1]

C.2 CFT Correlators

We are interested in scalar primary operators noted $\mathcal{O}_i$. These representations of the conformal group are labelled by the scaling dimension Δ_i.

2-point In position space a 2-point correlator is constrained by conformal invariance to the form

$$\langle \mathcal{O}_i(x_1)\mathcal{O}_i(x_2)\rangle = \frac{1}{(-x_{12}^2)^{\Delta_i}} \,, \tag{C.4}$$

up to an overall coefficient.

We introduce the reduced correlator

$$\langle \mathcal{O}(p_1)\mathcal{O}(p_2)\rangle = (2\pi)^d \delta^{(d)}(p_1 + p_2) \langle\!\langle \mathcal{O}(p_1)\mathcal{O}(p_2)\rangle\!\rangle \,. \tag{C.5}$$

[1] Notice α is analytically continued to the complex plane in the spectral conformal representation, see Sec. 2.3.2. Also, when studying the Euclidian principal series representation, the conformal dimension is usually defined as $\Delta = \frac{d}{2} + i\nu$, $\nu \in \mathbb{R}$. Here we rather use $\alpha \equiv i\nu$, which is typically used in other momentum space works such as [114].

We get $\langle \mathcal{O}(x_1)\mathcal{O}(x_2)\rangle = \int \frac{d^dp}{(2\pi)^d} \langle\!\langle \mathcal{O}(p)\mathcal{O}(-p)e^{-ip\cdot x_{12}}\rangle\!\rangle$ and obtain

$$\langle\!\langle \mathcal{O}(p)\mathcal{O}(-p)\rangle\!\rangle = -i\frac{\pi^{d/2}\Gamma(d/2-\Delta)}{\Gamma(\Delta)}\left(\frac{4}{-p^2}\right)^{d/2-\Delta} \tag{C.6}$$

Notice that for $d=4$ and $\Delta = d/2-1 = 1$, one recovers the usual 4d relation

$$\frac{-1}{4\pi^2x^2} = \int \frac{d^4p}{(2\pi)^4}\frac{i}{p^2}e^{-ip\cdot x}\,. \tag{C.7}$$

Using $\Delta = d/2+\alpha$, the correlator reads

$$\langle\!\langle \mathcal{O}_i(p)\mathcal{O}_i(-p)\rangle\!\rangle = -i\frac{\pi^{d/2}\Gamma(-\alpha)}{\Gamma(\alpha+d/2)}\left(\frac{-p^2}{4}\right)^{\alpha}\,. \tag{C.8}$$

3-point 3-point correlators of the CFT are constrained by conformal invariance to the form

$$\langle \mathcal{O}_1(x_1)\mathcal{O}_2(x_2)\mathcal{O}_3(x_3)\rangle = \frac{1}{\sqrt{-x_{12}^2}^{\Delta_1+\Delta_2-\Delta_3}\sqrt{-x_{23}^2}^{\Delta_2+\Delta_3-\Delta_1}\sqrt{-x_{13}^2}^{\Delta_1+\Delta_3-\Delta_2}}\,. \tag{C.9}$$

Using $\Delta_i = d/2+\alpha_i$, we have

$$\langle \mathcal{O}_1(x_1)\mathcal{O}_2(x_2)\mathcal{O}_3(x_3)\rangle = \frac{1}{\sqrt{-x_{12}^2}^{\alpha_1+\alpha_2-\alpha_3+d/2}\sqrt{-x_{23}^2}^{\alpha_2+\alpha_3-\alpha_1+d/2}\sqrt{-x_{13}^2}^{\alpha_1+\alpha_3-\alpha_2+d/2}}\,. \tag{C.10}$$

In momentum space one introduces the reduced correlator

$$\langle \mathcal{O}(p_1)\mathcal{O}_1(p_2)\mathcal{O}_2(p_3)\rangle = (2\pi)^d\delta^{(d)}(p_1+p_2+p_3)\langle\!\langle \mathcal{O}(p_1)\mathcal{O}_1(p_2)\mathcal{O}_2(p_3)\rangle\!\rangle\,. \tag{C.11}$$

By direct calculation using *e.g.* Schwinger parametrization (see [119]), one obtains

$$i\langle\!\langle \mathcal{O}_1(p_1)\mathcal{O}_2(p_2)\mathcal{O}_3(p_3)\rangle\!\rangle = \tag{C.12}$$
$$\frac{\pi^d 2^{4-\alpha_1-\alpha_2-\alpha_3}}{\Gamma(\frac{\alpha_1+\alpha_2+\alpha_3+d/2}{2})\Gamma(\frac{\alpha_1+\alpha_2-\alpha_3+d/2}{2})\Gamma(\frac{\alpha_1-\alpha_2+\alpha_3+d/2}{2})\Gamma(\frac{-\alpha_1+\alpha_2+\alpha_3+d/2}{2})}\times$$
$$\left(-p_1^2\right)^{\alpha_1/2}\left(-p_2^2\right)^{\alpha_2/2}\left(-p_3^2\right)^{\alpha_3/2}\int_0^\infty dz z^{d/2-1}K_{\alpha_1}\left(\sqrt{-p_1^2}z\right)K_{\alpha_2}\left(\sqrt{-p_2^2}z\right)K_{\alpha_3}\left(\sqrt{-p_3^2}z\right).$$

C.3 Shadow Transform

In conformal field theory a scalar operator $\mathcal{O}$ is accompanied by a "shadow" operator $\widetilde{\mathcal{O}}$ with dimension

$$\widetilde{\Delta} = d - \Delta \,. \tag{C.13}$$

Equivalently, if $\Delta = d/2+\alpha$, then $\widetilde{\Delta} = d/2-\alpha$. $\mathcal{O}$ and $\widetilde{\mathcal{O}}$ have a natural conformal-invariant pairing $\int d^d x \mathcal{O}(x)\widetilde{\mathcal{O}}(x)$. Such operation can connect the legs of different CFT correlators to build loop diagrams, see Sec. C.4.

In a given n-point correlator, an operator $\mathcal{O}_i$ is shadow-transformed into $\widetilde{\mathcal{O}}_i$ by convoluting the correlator with the corresponding shadow 2-pt function $\langle\widetilde{\mathcal{O}}_i(x)\widetilde{\mathcal{O}}_i(x')\rangle$ [226]. Here we give the transformation for a 3-pt correlator. The shadow transform of the position space 3-pt correlator [158, 226] in Minkowski metric is given by

$$i\int d^d x_3' \langle\widetilde{\mathcal{O}}_3(x_3)\widetilde{\mathcal{O}}_3(x_3')\rangle\langle\mathcal{O}_1(x_1)\mathcal{O}_2(x_2)\mathcal{O}_3(x_3')\rangle = S_{\Delta_3}^{\Delta_1,\Delta_2}\langle\mathcal{O}_1(x_1)\mathcal{O}_2(x_2)\widetilde{\mathcal{O}}_3(x_3)\rangle \tag{C.14}$$

with the coefficient

$$S_{\Delta_3}^{\Delta_1,\Delta_2} = \frac{\pi^{d/2}\Gamma(\alpha_3)}{\Gamma(d/2-\alpha_3)}\frac{\Gamma(\frac{\alpha_3+\alpha_1-\alpha_2+d/2}{2})\Gamma(\frac{\alpha_3-\alpha_1+\alpha_2+d/2}{2})}{\Gamma(\frac{-\alpha_3+\alpha_1-\alpha_2+d/2}{2})\Gamma(\frac{-\alpha_3-\alpha_1+\alpha_2+d/2}{2})}\,. \tag{C.15}$$

We introduce the Fourier transform of the operators as in Eq. (C.1). The shadow transform in momentum space becomes a product

$$\begin{aligned} &i\int d^d x_3' \langle\widetilde{\mathcal{O}}_3(x_3)\widetilde{\mathcal{O}}_3(x_3')\rangle\langle\mathcal{O}_1(x_1)\mathcal{O}_2(x_2)\mathcal{O}_3(x_3')\rangle \\ &= i\int\frac{d^d p_1}{(2\pi)^d}\int\frac{d^d p_2}{(2\pi)^d}\int\frac{d^d p_3}{(2\pi)^d}e^{i(p_1.x_1+p_2.x_2+p_3.x_3)}\langle\!\langle\widetilde{\mathcal{O}}_3(p_3)\widetilde{\mathcal{O}}_3(-p_3)\rangle\!\rangle\langle\!\langle\mathcal{O}_1(p_1)\mathcal{O}_2(p_2)\mathcal{O}_3(p_3)\rangle\!\rangle \\ &= S_{\Delta_3}^{\Delta_1,\Delta_2}\int\frac{d^d p_1}{(2\pi)^d}\int\frac{d^d p_2}{(2\pi)^d}\int\frac{d^d p_3}{(2\pi)^d}e^{i(p_1.x_1+p_2.x_2+p_3.x_3)}\langle\!\langle\mathcal{O}_1(p_1)\mathcal{O}_2(p_2)\widetilde{\mathcal{O}}_3(p_3)\rangle\!\rangle. \end{aligned} \tag{C.16}$$

The relation in momentum space can be read from the two last lines.

Using the explicit expression for the 2-point shadow correlator (given by Eq. (C.8) with $\alpha \to -\alpha_3$) the shadow transform in momentum space becomes simply

$$\langle\!\langle \mathcal{O}_1(p_1)\mathcal{O}_2(p_2)\widetilde{\mathcal{O}}_3(p_3)\rangle\!\rangle = \frac{1}{S^{\Delta_1,\Delta_2}_{\Delta_3}} \frac{\pi^{d/2}\Gamma(\alpha_3)}{\Gamma(d/2-\alpha_3)} \left(\frac{-p_3^2}{4}\right)^{-\alpha_3} \langle\!\langle \mathcal{O}_1(p_1)\mathcal{O}_2(p_2)\mathcal{O}_3(p_3)\rangle\!\rangle \quad \text{(C.17)}$$
$$= \frac{\Gamma(\frac{-\alpha_3+\alpha_1-\alpha_2+d/2}{2})\Gamma(\frac{-\alpha_3-\alpha_1+\alpha_2+d/2}{2})}{\Gamma(\frac{\alpha_3+\alpha_1-\alpha_2+d/2}{2})\Gamma(\frac{\alpha_3-\alpha_1+\alpha_2+d/2}{2})} \left(\frac{-p_3^2}{4}\right)^{-\alpha_3} \langle\!\langle \mathcal{O}_1(p_1)\mathcal{O}_2(p_2)\mathcal{O}_3(p_3)\rangle\!\rangle .$$

We can use this identity Eq. (C.17) on the explicit representation of the momentum-space 3-pt correlator Eq. (C.12). When doing so, one explicitly sees that the shadow transform Eq. (C.17) precisely amounts to flip the sign of α_3 in Eq. (C.12).

C.4 CFT Bubble

In the calculation of the dressed AdS propagator in the conformal spectral representation, a CFT bubble diagram appears. It is made of two 3-pt correlators whose legs are connected via pairing between $\mathcal{O}_i$ and $\widetilde{\mathcal{O}}_i$, or equivalently the legs are connected by 2-pt shadow correlators, see Sec. C.3.

The CFT bubble evaluation is well known [158,226]. Translating to our conventions we have [2]

$$\int d^dx_1 d^dx_2 \langle \mathcal{O}_a(x)\mathcal{O}_1(x_1)\mathcal{O}_2(x_2)\rangle\langle \widetilde{\mathcal{O}}_1(x_1)\widetilde{\mathcal{O}}_2(x_2)\widetilde{\mathcal{O}}_b(x')\rangle \quad \text{(C.18)}$$
$$= \mathcal{B}_{\mathcal{O}}\delta_{ab}2\pi \left(\delta^{(d)}(x-x')\delta(\alpha-\alpha') - i\left(\frac{\Gamma(\alpha+d/2)\Gamma(d/2-\alpha)}{\pi^d\Gamma(\alpha)\Gamma(-\alpha)}\right)^{1/2} \frac{\delta(\alpha+\alpha')}{(-(x-x')^2)^{\alpha+d/2}}\right)$$
$$= \mathcal{B}_{\mathcal{O}}\delta_{ab}2\pi \left(\delta^{(d)}(x-x')\delta(\alpha-\alpha') + s.t.\right)$$

[2] One uses $\delta(x_E) = i\delta(x)$, $\delta(\nu) = \delta(-i\alpha)$. The latter will be integrated along the imaginary line, such that the argument of the Dirac delta is real. However one can check that one can equivalently use $\delta(-i\alpha) = i\delta(\alpha)$, that we use throughout.

where the second term in the parenthesis corresponds to the shadow transform of the first one—the $-i$ results from Minkowski metric. Below we denote this second term by *s.t.* The bubble coefficient is given by

$$\mathcal{B}_{\mathcal{O}} = \frac{2\pi^{3d/2}}{\Gamma(d/2)} \frac{\Gamma(\alpha)\Gamma(-\alpha)}{\Gamma(\alpha + d/2)\Gamma(d/2 - \alpha)} \,. \tag{C.19}$$

Introducing the Fourier tranform of the operators, one obtains the CFT bubble in momentum space (involving the reduced correlators). It is given by

$$\int \frac{d^d q}{(2\pi)^d} \langle\!\langle \mathcal{O}_a(p)\mathcal{O}_1(q)\mathcal{O}_2(-p-q)\rangle\!\rangle \langle\!\langle \widetilde{\mathcal{O}_1}(-q)\widetilde{\mathcal{O}}_2(p+q)\widetilde{\mathcal{O}}_b(-p)\rangle\!\rangle = 2\pi \mathcal{B}_{\mathcal{O}} \delta_{ab} \delta(\alpha - \alpha') + s.t. \tag{C.20}$$

On the left-hand side we recognize the integration over the internal d-momentum running inside the loop.

C.5 Boundary-to-Bulk Propagators

Here we come back to AdS. We introduce the boundary-to-bulk propagator $\mathcal{K}(z, x, x')$, a Green function for sources placed on the AdS boundary (see *e.g.* [13, 201]). From the bulk-to-bulk AdS propagator $G^{(0)}(X, X')$, $\mathcal{K}(z, x, x')$ can be obtained by sending *e.g.* z' to the AdS boundary, while including an appropriate scaling factor in z' such that the obtained object is non zero and finite for $z \neq 0$. Boundary-to-bulk propagators are closely related to the dual CFT operators and can be directly labelled with the corresponding scaling dimension Δ.

The boundary-to-bulk propagator associated with a CFT operator with dimension

Δ_+ (Δ_-) is defined as

$$\mathcal{K}_{\Delta_\pm}(x,x',z) = \frac{\Gamma(\Delta_\mp)}{\pi^{d/2}\Gamma(\Delta_\mp - \frac{d}{2})}\left(\frac{z}{z^2-(x-x')^2}\right)^{\Delta_\mp} \tag{C.21}$$

where $\Delta_- = d - \Delta_+$, according to definitions in Eq. (C.3)). [3]

Introducing the Fourier transform, we define the boundary-to-bulk propagator in position-momentum space as $\mathcal{K}_{\Delta_+}(p,z) = k^{d/2}\int d^dx\, \mathcal{K}_{\Delta_+}(x,x',z)e^{ip.(x-x')}$. [4] The result is

$$\mathcal{K}_{\Delta_\pm}(p,z) = i(kz)^{d/2}\frac{2}{\Gamma(\Delta_\mp - d/2)}\left(\frac{\sqrt{-p^2}}{2}\right)^{\Delta_\mp - d/2} K_{d/2-\Delta_\mp}(\sqrt{-p^2}z)\,. \tag{C.22}$$

We see that the Bessel K function appears. We also see that multiplying $\mathcal{K}_{\Delta_+}(p,z)$ and $\mathcal{K}_{\Delta_-}(p,z)$ cancels out the overall factor of p, giving the dimensionless quantity

$$\mathcal{K}_{\Delta_+}(p,z)\mathcal{K}_{\Delta_-}(p,z') = 4\frac{\alpha\sin(\pi\alpha)}{\pi}(k^2zz')^{d/2}K_\alpha(\sqrt{-p^2}z)K_\alpha(\sqrt{-p^2}z')\,. \tag{C.23}$$

This product reproduces precisely the form of the conformal spectral function $\Omega_\alpha(p;z,z')$ (see Eq. (2.23)) such that

$$\Omega_\alpha(p,z,z') = \frac{i}{4\pi}\mathcal{K}_{\Delta_-}(p,z)\mathcal{K}_{\Delta_+}(p,z')\,. \tag{C.24}$$

Such feature is expected—it amounts to introduce the "split" representation [163] in position-momentum space. Since in position space the split representation would involve a convolution on the AdS boundary, in position-momentum space the split representation involves a simple product.

For our calculation of the dressed AdS propagator, the well-known correspondence between $\mathcal{K}$ and CFT 2-pt correlator is not needed. On the other hand, bulk cubic interactions will involve the convolution of three different boundary-to-bulk propagagors. We

[3] These propagators satisfy $\mathcal{K}_{\Delta_\pm}(z\to 0) = iz^{\Delta_\pm}\delta^{(d)}(x)$. A bulk field $\phi(z,x)$ sourced by a boundary field (*i.e.* "boundary data") $\phi_0(x)$ satisfies $\phi(z,x) = -iz^{-\Delta_\pm}\int d^dy\mathcal{K}_{\Delta_+}(z,x-y)\phi_0(y)\,.$

[4] Defined that way, $\mathcal{K}_{\Delta_+}$ and $\mathcal{K}_{\Delta_-}$ have opposite mass dimensions, $[\mathcal{K}_{\Delta_-}] = -[\mathcal{K}_{\Delta_+}] = \alpha$.

introduce the notation $\mathcal{K}_{\Delta_\pm}(p,z) = \mathcal{K}^\pm_\alpha(p,z)$. For the product of three generic $\mathcal{K}^-$, using Eq. (C.12) we find

$$\begin{aligned}\int \frac{du}{(ku)^{d+1}} &\mathcal{K}^-_{\alpha_1}(p_1;u)\mathcal{K}^-_{\alpha_2}(p_2;u)\mathcal{K}^-_{\alpha_3}(p_3;u) \\ &= -i\frac{2^{3-\alpha_1-\alpha_2-\alpha_3}}{\Gamma(\alpha_1)\Gamma(\alpha_2)\Gamma(\alpha_3)}(-p_1^2)^{\alpha_1/2}(-p_2^2)^{\alpha_2/2}(-p_3^2)^{\alpha_3/2} \\ &\qquad \times \int du\,(ku)^{d/2-1} K_{\alpha_1}\left(\sqrt{-p_1^2}u\right) K_{\alpha_2}\left(\sqrt{-p_2^2}u\right) K_{\alpha_3}\left(\sqrt{-p_3^2}u\right) \\ &= c_{\alpha_1,\alpha_2,\alpha_3} k^{d/2-1} \langle\!\langle \mathcal{O}_1(p_1)\mathcal{O}_2(p_2)\mathcal{O}_3(p_3)\rangle\!\rangle \ .\end{aligned} \tag{C.25}$$

with the dimensionless coefficient

$$c_{\alpha_1,\alpha_2,\alpha_3} = \frac{\Gamma(\frac{\alpha_1+\alpha_2+\alpha_3+d/2}{2})\Gamma(\frac{\alpha_1-\alpha_2+\alpha_3+d/2}{2})\Gamma(\frac{\alpha_1+\alpha_2-\alpha_3+d/2}{2})\Gamma(\frac{-\alpha_1+\alpha_2+\alpha_3+d/2}{2})}{2\pi^d\,\Gamma(\alpha_1)\Gamma(\alpha_2)\Gamma(\alpha_3)} \tag{C.26}$$

Eq. (C.25) relates a 3-pt bulk diagram (first line) to a 3-pt CFT correlator (last line), explicitly showing AdS/CFT at work.

Convolutions involving $\mathcal{K}^+$ propagators are obtained from Eq. (C.25) by a shadow transform. As seen in Sec. C.3, this amounts to flipping the signs of the corresponding α_i in the $c(\alpha_1,\alpha_2,\alpha_3)$ coefficient. We have for instance

$$\int \frac{du}{(ku)^{d+1}} \mathcal{K}^-_{\alpha_1}(p_1;u)\mathcal{K}^-_{\alpha_2}(p_2;u)\mathcal{K}^+_{\alpha_3}(p_3;u) = c(\alpha_1,\alpha_2,-\alpha_3)k^{d/2-1}\langle\!\langle \mathcal{O}_1(p_1)\mathcal{O}_2(p_2)\widetilde{\mathcal{O}}_3(p_3)\rangle\!\rangle \ . \tag{C.27}$$

Appendix D

Momentum Spectral Integrals at Large pz

We first review aspects of the spectral integral $\int_0^A dm\Omega_m(z,z')$. We are interested in the $Az \gg 1$, $Az' \gg 1$ limit at fixed α, hence for our purposes the α-dependence is negligible and we can set $\alpha = 1/2$. The spectral integral is then proportional to

$$\int_0^A dm \sin(mz)\sin(mz') = \frac{1}{2}\frac{\sin(A(z-z'))}{z-z'} - \frac{1}{2}\frac{\sin(A(z+z'))}{z+z'}\,. \tag{D.1}$$

If we let $A \to \infty$ at fixed z, z', using the definition of the sinc function as a nascent Dirac delta, the first term of Eq. (D.1) becomes proportional to a Dirac delta and the second vanishes—proving Eq. (2.30). We recall this is understood in the distribution sense. The second term oscillates infinitely rapidly for any z, z' such that under a z integral, for any appropriate test function the second term averages to zero under the integral. This happens similarly for the first term of Eq. (D.1) except for $A(z-z') \ll 1$, which asymptotically gives rise to the Dirac delta.

Instead of letting $A \to \infty$ in Eq. (D.1), we can introduce $\bar{z} = \frac{z+z'}{2}$, $z - z' = \bar{z}\epsilon$, and let $\bar{z} \to \infty$ at fixed A and ϵ. This gives the same result as the $A \to \infty$ limit since

$$\frac{\sin(A(z-z'))}{z-z'} = \frac{\sin(A\bar{z}\epsilon)}{\bar{z}\epsilon} = \frac{A}{\bar{z}}\frac{\sin(A\bar{z}\epsilon)}{A\epsilon} \xrightarrow[\bar{z}\to\infty]{} \frac{\pi A}{\bar{z}}\delta(A\epsilon) = \pi\delta(z-z')\,. \tag{D.2}$$

Again, this limit is understood in the distribution sense. For our purposes, taking the limit of large $\bar{z}$ at fixed interval $[0, A]$ is more convenient.

Consider then the spectral integral

$$\int_0^A dm \sin(mz)\sin(mz')F(m,A) \tag{D.3}$$

where the $F(m, A)$ function is smooth in m and is independent of z, z'. Taking the large $\bar{z}$ limit at A fixed, for large enough $\bar{z}$ we have $\partial_m\left(\sin(mz)\sin(mz')\right) \gg \partial_m F(m, A)$ everywhere on the interval and we can approximate the rapidly oscillating function by its average over $[0, A]$,

$$\int_0^A dm \sin(mz)\sin(mz')F(m,A) \approx \left(\frac{1}{2}\frac{\sin(A(z-z'))}{A(z-z')} - \frac{1}{2}\frac{\sin(A(z+z'))}{A(z+z')}\right)\int_0^A dmF(m,A) \tag{D.4}$$

Taking the large $\bar{z}$ limit as above gives asymptotically

$$\left(\frac{1}{2}\frac{\sin(A(z-z'))}{A(z-z')}\right)\int_0^A dmF(m,A) \xrightarrow[\bar{z}\to\infty]{} \frac{\pi}{2A}\delta(z-z')\int_0^A dmF(m,A) \tag{D.5}$$

in the distribution sense.

We can apply the preliminary results above to evaluate the double spectral integral of Eq. (2.108)

$$\int_0^{A_1} dm_1 \int_0^{A_2} dm_2 \Omega_{m_1}(z,z')\Omega_{m_2}(z,z')F(m_1,m_2,A_i) \tag{D.6}$$

where $A_1 = p$, $A_2 = p - m_1$ in the large pz limit. We keep p finite and take the limit of large $\bar{z}$. Taking $\alpha = 1/2$, the integral is proportional to

$$\int_0^{A_1} dm_1 \int_0^{A_2} dm_2 \sin(m_1 z) \sin(m_1 z') \sin(m_2 z) \sin(m_2 z') F(m_1, m_2, A_i) \tag{D.7}$$

F is assumed to be smooth in m_1 and m_2 such that the limit for rapidly oscillating function introduced above applies. We first approximate the m_2 integral, giving

$$\int_0^{A_1} dm_1 \sin m_1 z \sin m_1 z' \left(\frac{1}{2} \frac{\sin(A_2(z-z'))}{A_2(z-z')} - \frac{1}{2} \frac{\sin(A_2(z+z'))}{A_2(z+z')} \right) \int_0^{A_2} dm_2 F(m_1, m_2, A_i) \,. \tag{D.8}$$

Then we use that $\frac{1}{A_2} \int_0^{A_2} dm_2 F(m_1, m_2, A_i)$ is smooth in m_1 with respect to the whole oscillating function such that the latter can be averaged and extracted from the m_1 integral. Combining the sines we have

$$\begin{aligned} &= \frac{1}{4A_1} \int_0^{A_1} dm_1 \left(\cos(m_1(z-z')) - \cos(m_1(z+z')) \right) \left(\frac{\sin(A_2(z-z'))}{z-z'} - \frac{\sin(A_2(z+z'))}{z+z'} \right) \\ &\qquad \times \int_0^{A_1} dm_1 \int_0^{A_2} dm_2 \frac{1}{A_2} F(m_1, m_2, A_i) \end{aligned} \tag{D.9}$$

The first line contains the average of the oscillating function in m_1. The integrals of the four terms give

$$\frac{1}{A_1} \int_0^{A_1} dm_1 \cos(m_1(z-z')) \frac{\sin(A_2(z-z'))}{z-z'} = \frac{1}{2(z-z')} \sin p(z-z') \tag{D.10}$$

$$\frac{1}{A_1} \int_0^{A_1} dm_1 \cos(m_1(z-z')) \frac{\sin(A_2(z+z'))}{z+z'} = \frac{1}{2pzz'} \sin pz \sin pz' \tag{D.11}$$

$$\frac{1}{A_1} \int_0^{A_1} dm_1 \cos(m_1(z+z')) \frac{\sin(A_2(z-z'))}{z-z'} = \frac{1}{2pzz'} \sin pz \sin pz' \tag{D.12}$$

$$\frac{1}{A_1} \int_0^{A_1} dm_1 \cos(m_1(z+z')) \frac{\sin(A_2(z+z'))}{z+z'} = \frac{1}{2(z+z')} \sin p(z+z') \tag{D.13}$$

In the large $\bar{z}$ limit the first term Eq .(D.10) dominates, the other become negligible. Again, this term gives rise a nascent Dirac delta in the large $\bar{z}$ limit,

$$\frac{1}{2(z-z')}\sin p(z-z') = \frac{1}{2\bar{z}\epsilon}\sin p\bar{z}\epsilon = \frac{p}{2\bar{z}}\frac{\sin p\bar{z}\epsilon}{p\epsilon} \xrightarrow[\bar{z}\to\infty]{} \frac{p}{\bar{z}}\frac{\pi}{2}\delta(p\epsilon) = \frac{\pi}{2}\delta(z-z')\,, \quad \text{(D.14)}$$

understood in the distribution sense.

We have thus obtained that the double spectral integral Eq. (D.7) tends to

$$\frac{\pi}{8}\delta(z-z')\int_0^p dm_1 \int_0^{p-m_1} dm_2 \frac{1}{A_2} F(m_1, m_2, A_i) \quad \text{(D.15)}$$

at large $\bar{z}$. This delta function, as mentioned throughout this section, is best thought of as being under an integral. When interested in the value of ImΠ itself, this delta may naively seem like a divergence. One should remember that this is a nascent delta and is hence replaced as $z - z'$ becomes arbitrarily small.

In our bubble calculation, $F(m_1, m_2) = \Xi(d, p, m_1, m_2)$. Even though the remaining double integral may be difficult, we see that all the dependence in z is factored out. Hence the scaling in p is obtained by simple dimensional analysis, giving p^{d-3}. Putting together all the factors leads to the asymptotic scaling given in Eq. (2.122).

Appendix E

Kinematic Approximation: Numerical Checks

Fig. E.1 shows examples of $\mathrm{Im}\Pi(z, z')$ in the kinematic approximation introduced in Sec. 2.6.3. We can see that a side effect of the kinematic approximation is to somewhat smoothen the oscillations. It also renders $\mathrm{Im}\Pi$ positive for any $z \neq z'$. These details have a mild impact on the subsequent results. Upon performing the z integrals, the results match with $O(10)\%$ accuracy.

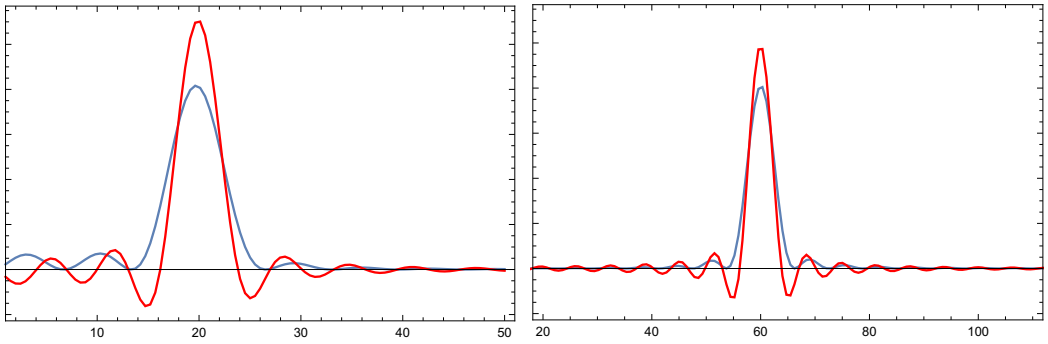

Figure E.1: The exact (red) and approximate (blue) profiles of $(zz')^{\frac{d-1}{2}}\mathrm{Im}\Pi(z,z')$ as a function of pz, taking $pz'=20$ (left) and $pz'=60$ (right), and taking $d=4$.

Appendix F

Bubble Diagrams

In these calculations, we consider bubbles formed of $\lambda\Phi\Phi_1\Phi_2$ and $\xi\Phi\partial_M\Phi_1\partial^M\Phi_2$ vertices, hence the fields and propagators are not treated as identical. We use standard manipulations (Feynman parameterization, dimensional regularization) to evaluate the loop. We define $\Delta = -x(1-x)p^2 + xm_1^2 + (1-x)m_2^2$.

When taking the imaginary part of Π, we use the kinematic approximation of Sec. 2.6.3 to obtain

$$\mathrm{Im}\int_{x_-}^{x_+} \log\Delta = -\pi \tag{F.1}$$

$$\mathrm{Im}\int_{x_-}^{x_+} x\log\Delta = \mathrm{Im}\int_{x_-}^{x_+} (1-x)\log\Delta = -\frac{\pi}{2} \tag{F.2}$$

$$\mathrm{Im}\int_{x_-}^{x_+} x(1-x)\log\Delta = -\frac{\pi}{6} \tag{F.3}$$

$$\mathrm{Im}\int_{x_-}^{x_+} x^2(1-x)\log\Delta = \mathrm{Im}\int_{x_-}^{x_+} x(1-x)^2\log\Delta = -\frac{\pi}{12} \tag{F.4}$$

$$\mathrm{Im}\int_{x_-}^{x_+} x^2(1-x)^2\log\Delta = -\frac{\pi}{30}\,. \tag{F.5}$$

F.1 $\Phi^3 - \Phi^3$

The amplitude of the bubble induced by two $\lambda\Phi\Phi_1\Phi_2$ vertices is

$$i\Pi_{\lambda\lambda}(z_1,z_2) = \lambda^2 \frac{1}{k^4 z_1 z_2} \int dq_1 dq_2 q_1 q_2 \int \frac{d^4q}{(2\pi)^4} \frac{J_{\alpha_1}(q_1 z_1) J_{\alpha_1}(q_1 z_2) J_{\alpha_2}(q_2 z_1) J_{\alpha_2}(q_2 z_2)}{(q^2 - q_1^2)((q+p)^2 - q_2^2)} \,. \tag{F.6}$$

We introduce a Feynman parameter x and use dimensional regularization to evaluate the loop. We have

$$i\Pi_{\lambda\lambda}(z_1,z_2) = \tag{F.7}$$
$$\lambda^2 \frac{1}{k^4 z_1 z_2} \int dq_1 dq_2 q_1 q_2 \int_0^1 dx \frac{-i}{16\pi^2} \log\left(\frac{\Delta}{\Lambda^2}\right) J_{\alpha_1}(q_1 z_1) J_{\alpha_1}(q_1 z_2) J_{\alpha_2}(q_2 z_1) J_{\alpha_2}(q_2 z_2) + \ldots$$

Λ is the regularization scale and the ellipses represent the divergent part of the loop diagram. Both the divergence and the Λ-dependence vanish upon taking the imaginary part of Π. Taking the imaginary part gives Eq. (2.150).

F.2 $\Phi^3 - \Phi(\partial\Phi)^2$

The amplitude of the bubble induced by one $\lambda\Phi\Phi_1\Phi_2$ and one $\xi\Phi\partial_M\Phi_1\partial^M\Phi_2$ vertex is given by

$$i\Pi_{\lambda\zeta}(z_1,z_2) = \tag{F.8}$$
$$-\lambda\zeta \frac{(kz_2)^2}{k^4 z_1 z_2} \int dq_1 dq_2 q_1 q_2 \int \frac{d^4q}{(2\pi)^4} \left(q.(p+q) - \partial_{z_2}^{(1)}\partial_{z_2}^{(2)}\right) \frac{J_{\alpha_1}(q_1 z_1) J_{\alpha_1}(q_1 z_2) J_{\alpha_2}(q_2 z_1) J_{\alpha_2}(q_2 z_2)}{(q^2 - q_1^2)((q+p)^2 - q_2^2)}$$

plus its $(1 \leftrightarrow 2)$ counterpart. The $\partial_z^{(i)}$ derivative acts only on the $G_{q_i}(z_1,z_2)$ propagator, *i.e.* only on the $J_{\alpha_i}(q_i z)$ Bessel function in the above expression and subsequent ones. We introduce a Feynman parameter x and perform the loop integral via dimensional regularization.

We obtain

$$i\Pi_{\lambda\zeta}(z_1,z_2) = -\lambda\zeta\frac{z_2^2}{k^2 z_1 z_2}\int dq_1 dq_2 q_1 q_2 \int_0^1 dx \tag{F.9}$$
$$\frac{-i}{16\pi^2}\log\left(\frac{\Delta}{\Lambda^2}\right)\left(2\Delta - x(1-x)p^2 - \partial_{z_2}^{(1)}\partial_{z_2}^{(2)}\right) J_{\alpha_1}(q_1 z_1) J_{\alpha_1}(q_1 z_2) J_{\alpha_2}(q_2 z_1) J_{\alpha_2}(q_2 z_2) + \ldots$$

Λ is the regularization scale and the ellipses represent the divergent part of the loop diagram. Both vanish upon taking the imaginary part of Π. Taking the imaginary part and including the $(1 \leftrightarrow 2)$ contribution gives Eq. (2.154).

F.3 $\Phi(\partial\Phi)^2 - \Phi(\partial\Phi)^2$

The amplitude of the bubble induced by two $\xi\Phi\partial_M\Phi_1\partial^M\Phi_2$ vertices is

$$i\Pi_{\zeta\zeta}(z_1,z_2) = \zeta^2\frac{(kz_1)^2(kz_2)^2}{k^4 z_1 z_2}\int dq_1 dq_2 q_1 q_2 \int \frac{d^4q}{(2\pi)^4} \tag{F.10}$$
$$\left(q.(p+q) - \partial_{z_1}^{(1)}\partial_{z_1}^{(2)}\right)\left(q.(p+q) - \partial_{z_2}^{(1)}\partial_{z_2}^{(2)}\right)\frac{J_{\alpha_1}(q_1 z_1) J_{\alpha_1}(q_1 z_2) J_{\alpha_2}(q_2 z_1) J_{\alpha_2}(q_2 z_2)}{(q^2 - q_1^2)((q+p)^2 - q_2^2)}\,.$$

We introduce a Feynman parameter x and perform the loop integral via dimensional regularization to obtain

$$i\Pi_{\zeta\zeta}(z_1,z_2) = \zeta^2\frac{z_1^2 z_2^2}{z_1 z_2}\int dq_1 dq_2 q_1 q_2 \int_0^1 dx \frac{-i}{16\pi^2}\log\left(\frac{\Delta}{\Lambda^2}\right) \tag{F.11}$$
$$\left(3\Delta^2 + \left(\frac{1}{2} - 6x(1-x)\right)p^2\Delta + x^2(1-x)^2 p^4\right.$$
$$\left. - (2\Delta - x(1-x)p^2)\left(\partial_{z_1}^{(1)}\partial_{z_1}^{(2)} + \partial_{z_2}^{(1)}\partial_{z_2}^{(2)}\right) + \partial_{z_1}^{(1)}\partial_{z_1}^{(2)}\partial_{z_2}^{(1)}\partial_{z_2}^{(2)}\right)$$
$$J_{\alpha_1}(q_1 z_1) J_{\alpha_1}(q_1 z_2) J_{\alpha_2}(q_2 z_1) J_{\alpha_2}(q_2 z_2) + \ldots$$

Λ is the regularization scale and the ellipses represent the divergent part of the loop diagram. Evaluating the x integrals and taking the imaginary part of Π gives

$$\begin{aligned}\mathrm{Im}\Pi_{\zeta\zeta}(z_1,z_2) = \zeta^2 \frac{z_1^2 z_2^2}{z_1 z_2}\frac{1}{16\pi}\int dq_1 dq_2 q_1 q_2 \\ \left(q_1^4+q_2^4+q_1^2q_2^2-\frac{3}{4}p^2(q_1^2+q_2^2)+\frac{p^4}{4}\right. \\ \left.-\left(q_1^2+q_2^2-\frac{p^2}{2}\right)\left(\partial_{z_1}^{(1)}\partial_{z_1}^{(2)}+\partial_{z_2}^{(1)}\partial_{z_2}^{(2)}\right)+\partial_{z_1}^{(1)}\partial_{z_1}^{(2)}\partial_{z_2}^{(1)}\partial_{z_2}^{(2)}\right) \\ J_{\alpha_1}(q_1z_1)J_{\alpha_1}(q_1z_2)J_{\alpha_2}(q_2z_1)J_{\alpha_2}(q_2z_2)\,.\end{aligned} \tag{F.12}$$

F.4 Scalar-Graviton Bubble

The amplitude induced by the scalar component of the graviton multiplet is

$$\begin{aligned}i\Pi^{\phi}(z_1,z_2) = \frac{-1}{3\,M_*^3}\left(\frac{m_\Phi^2}{2(kz_1)^2}-\frac{3}{2}\partial_{z_1}\partial_{z_1}^{G_\Phi}\right)\left(\frac{m_\Phi^2}{2(kz_2)^2}-\frac{3}{2}\partial_{z_2}\partial_{z_2}^{G_\Phi}\right) \\ \frac{1}{(kz_1)(kz_2)}\int\frac{dq^4}{(2\pi)^4}G_\alpha^\Phi(q_1,z_1,z_2)G^\phi(q_2,z_2,z_1)\,.\end{aligned} \tag{F.13}$$

The $\partial_z^{G_\Phi}$ derivatives act only on the internal Φ propagator (henceforth the term contained in square brackets). Introducing the propagators in their momentum spectral representations, we have

$$\begin{aligned}i\Pi^{\phi}(z_1,z_2) = \frac{1}{3\,M_*^3}\left(\frac{m_\Phi^2}{2(kz_1)^2}-\frac{3}{2}\partial_{z_1}\partial_{z_1}^{G_\Phi}\right)\left(\frac{m_\Phi^2}{2(kz_2)^2}-\frac{3}{2}\partial_{z_2}\partial_{z_2}^{G_\Phi}\right) \\ \frac{1}{z_1z_2}\int dq_1dq_2q_1q_2\int\frac{dq^4}{(2\pi)^4}\frac{\left[z_1^2z_2^2J_\alpha(q_1z_1)J_\alpha(q_1z_2)\right]J_0(q_2z_1)J_0(q_2z_2)}{(q^2-q_1^2)((q+p)^2-q_2^2)}\,.\end{aligned} \tag{F.14}$$

We introduce a Feynman parameter and perform the loop integral to obtain

$$\begin{aligned}i\Pi^{\phi}(z_1,z_2) = \frac{-i}{48\pi^2\,M_*^3}\left(\frac{m_\Phi^2}{2(kz_1)^2}-\frac{3}{2}\partial_{z_1}\partial_{z_1}^{G_\Phi}\right)\left(\frac{m_\Phi^2}{2(kz_2)^2}-\frac{3}{2}\partial_{z_2}\partial_{z_2}^{G_\Phi}\right) \\ \frac{1}{z_1z_2}\int dq_1dq_2q_1q_2\int_0^1 dx\log\left(\frac{\Delta}{\Lambda^2}\right)\left[z_1^2z_2^2J_\alpha(q_1z_1)J_\alpha(q_1z_2)\right]J_0(q_2z_1)J_0(q_2z_2)\,.\end{aligned} \tag{F.15}$$

Taking the imaginary part gives Eq. (2.185).

Appendix G

The Dipole Potential

The four operators $\mathcal{O}_N^{\mathrm{S,P,A,V}}$ can couple to a dark mediator with renormalizable couplings. In contrast, the tensor operator $\mathcal{O}_N^{\mathrm{T}}$ can only couple to other fields through a higher-dimensional operator. This is a consequence of its two Lorentz indexes. Since $\sigma_{\mu\nu}$ is antisymmetric, the only operator available is a field strength tensor $X_{\mu\nu}$ which couples to the tensor operator as

$$\frac{m_N}{\Lambda^2}\bar{N}\sigma_{\mu\nu}NX^{\mu\nu} \qquad\qquad \frac{m_N}{\Lambda^2}\bar{N}\sigma_{\mu\nu}N\widetilde{X}^{\mu\nu}\,. \tag{G.1}$$

It is natural to assume that $X_{\mu\nu}$ is the field strength of a hidden gauge group. The operators in (G.1) then describe *dark* magnetic and electric dipole moments. We assume the gauge group is Abelian and denote it $U(1)_X$. We refer to the gauge boson as the dark photon.

The Standard Model particles themselves may have hidden charge. This possibility is highly constrained due to the chiral structure of the Standard Model: either new chiral fermions must be carefully introduced to cancel anomalies, or Wess–Zumino terms are generated in the low-energy theory. A less constrained possibility is that all Standard

Model fields are singlets under $U(1)_X$. In that case, the dark photon may have a kinetic mixing with the visible photon [227, 228]. This mixing is typically loop induced so that the dark photon has a small coupling to visible electric currents.

Even without kinetic mixing, visible sector fields can interact with the dark photon through multipole operators. Complex and Dirac fields can have dipoles, and self-conjugate fields can have dark polarizability. [1] In particular, nucleons (or quarks), have dark dipole operators like those in (G.1). Two ways to generate a dark polarization are: (i) The polarization may be induced by loops of heavy particles coupled to the Standard Model. (ii) The polarization could be a consequence of the compositeness of Standard Model particles if the underlying constituents are charged under $U(1)_X$. In the latter case, the dipole moment is a low-energy manifestation of the internal structure of the Standard Model particle. This is analogous to the electromagnetic moments of hadrons. In this "dark dipole scenario," some amount of photon–dark photon kinetic mixing should also be present, at least as a result of loops contributing to $F^{\mu\nu} - X^{\mu\nu}$ mixing. However, this loop-induced mixing via Standard Model fields can be expected to be small.

If the hidden gauge boson is sufficiently light, the nucleon dipole operator induces a spin-dependent force of tensor-type:

$$V_{\rm T}(\boldsymbol{r}) = \frac{-4m_N^2[(\boldsymbol{\sigma_1}\cdot\boldsymbol{\sigma_2})\nabla^2 - (\boldsymbol{\sigma_1}\cdot\boldsymbol{\nabla})(\boldsymbol{\sigma_2}\cdot\boldsymbol{\nabla})]}{\Lambda^4}\left(\frac{e^{-mr}}{4\pi r}\right) \ . \tag{G.2}$$

Upon spin averaging $\boldsymbol{\sigma_2}$, the dominant piece is

$$V_{\rm T}(\boldsymbol{r}) = \frac{\{\mathbb{1}_2[(\boldsymbol{p_1}+\boldsymbol{p_1'})\times\boldsymbol{\sigma_1}]\cdot\boldsymbol{\nabla} + \mathbb{1}_1\mathbb{1}_2\nabla^2\}}{\Lambda^4}\nabla^2\left(\frac{e^{-mr}}{4\pi r}\right) \ . \tag{G.3}$$

[1] See *e.g.* [229] for more details on polarizability operators in the context of a dark sector.

If, instead, the dark photon is heavy, then (G.1) generates the $\bar{N}\sigma_{\mu\nu}N\mathcal{O}_{\rm DS}^{\mu\nu}$ tensor interaction. This operator induces a quantum force, presented in the analysis of Section 4.5. We leave further study of this "dipole portal" scenario for future work.

Appendix H

Fourier Transforms and Effective Theory

While the technique to derive a non-relativistic potential from a field theory amplitude is not new (see e.g. [230]), some aspects related to the effective theory framework are usually left implicit and deserve clarification. [1]

The integral in the Fourier transform (4.4) spans three-momenta up to infinity. However, whenever working within a low-energy effective theory, momenta higher than the effective theory cutoff Λ should not be used in a calculation because it probes physics beyond the validity of the theory. For finite, low-energy predictions—like the potentials studied here—the details of the momentum truncation are ultraviolet details that should have negligible impact.

However, this leads to an apparent paradox. Amplitudes arising in the effective

[1] This appendix is based on discussions between S. F., G. von Gersdorff, and E. Ponton.

theory can grow with energy with a polynomial form such that the integrand in (4.4) takes typically the form $e^{iqr}q^n \ln q^2$, with $n > 0$, $q \equiv |\mathbf{q}|$, $r \equiv |\mathbf{r}|$. An integral up to infinity diverges and requires an ultraviolet cutoff. One may impose the cutoff by introducing a step function $\Theta(|\mathbf{q}| < \Lambda)$ in the integrand. In the presence of this factor the integral produces oscillating Λ-dependent terms such as $\Lambda^n \sin(\Lambda r)$ in addition to Λ-independent terms from the low-energy region of the Fourier integral. These Λ terms are unsuppressed and do not vanish in the $\Lambda \to \infty$ limit.

The same paradox occurs if one attempts an analytic continuation to transform the integral along the real line as an integral over the branch cut of the amplitude, as described in Appendix I and used in Section 4.5. In that case, the integral along the branch cut provides the universal long-distance contribution, while the integral over the large arcs of radius Λ needed to close the contour gives rise to the Λ-dependent oscillating terms described above.

These Λ-dependent contributions originate from the fact that a hard cutoff factor $\Theta(|\mathbf{q}| < \Lambda)$ introduces a non-analyticity at $|\mathbf{q}| = \Lambda$ because it is not continuous across this boundary. The Λ-dependent contributions are thus artifacts of the truncation of momentum space. The solution to the paradox is then clear: A smooth cutoff should be used in order to avoid the spurious Λ-dependent contributions.

Such smooth cutoff is conveniently implemented by convolving the step function with a smooth distribution, π. For example:

$$\Theta(|\mathbf{q}| < \Lambda) \to \int d\xi\, \Theta(|\mathbf{q}| < \Lambda + \xi)\pi(\xi) \qquad \pi(\xi) = \frac{1}{\sqrt{2\pi}\sigma} e^{-\xi^2/(2\sigma^2)}\,, \tag{H.1}$$

where $\sigma \ll \Lambda$ is the width of the smoothing function. The Fourier integral takes the form

$$\int \frac{d^3q}{(2\pi)^3} e^{i\boldsymbol{q}\cdot\boldsymbol{r}} \mathcal{M}_{IJ} \int d\xi\, \Theta(|\mathbf{q}| < \Lambda + \xi)\pi(\xi)\,. \tag{H.2}$$

The ξ integral is most conveniently performed after the Fourier transform. The Λ-dependent contribution to the potential is exponentially suppressed by a factor $e^{-r^2\sigma^2}$, thereby leaving the universal long-distance contribution as the main contribution to the potential.

Appendix I

Calculation of the Quantum Potentials

We present additional details for the calculation of the quantum potentials in Section 4.5.

I.1 Loop Calculation

The relevant one-loop amplitudes for the operators of Section 4.5 are:

$$i\mathcal{M}_a^0 = \frac{\eta}{\Lambda^4}(\bar{u}_{p_1'}\gamma^\mu\gamma^5 u_{p_1}\bar{u}_{p_2'}\gamma^\nu\gamma^5 u_{p_2})\int\frac{d^4k}{(2\pi)^4}\frac{2k_\mu+q_\mu}{k^2-m^2}\frac{2k_\nu+q_\nu}{(q+k)^2-m^2} \tag{I.1}$$

$$i\mathcal{M}_b^0 = \frac{2^{\eta-1}}{\Lambda^2}(\bar{u}_{p_1'}i\gamma^5 u_{p_1}\bar{u}_{p_2'}i\gamma^5 u_{p_2})\int\frac{d^4k}{(2\pi)^4}\frac{1}{k^2-m^2}\frac{1}{(q+k)^2-m^2} \tag{I.2}$$

$$i\mathcal{M}_c^0 = \frac{2^{\eta-1}}{\Lambda^6}(\bar{u}_{p_1'}i\gamma^5 u_{p_1}\bar{u}_{p_2'}i\gamma^5 u_{p_2})\int\frac{d^4k}{(2\pi)^4}\frac{k^2+k\cdot q}{k^2-m^2}\frac{k^2+k\cdot q}{(q+k)^2-m^2} \tag{I.3}$$

$$i\mathcal{M}_d^0 = \frac{\eta}{\Lambda^6}(\bar{u}_{p_1'}\sigma^{\mu\nu} u_{p_1}\bar{u}_{p_2'}\sigma^{\alpha\beta} u_{p_2})\int\frac{d^4k}{(2\pi)^4}\frac{k_\mu(k+q)_\nu}{k^2-m^2}\frac{k_\alpha(k+q)_\beta}{(q+k)^2-m^2} \tag{I.4}$$

$$i\mathcal{M}_a^{\frac{1}{2}} = \frac{-2^{\eta-1}}{\Lambda^4}(\bar{u}_{p_1'}i\gamma^5 u_{p_1}\bar{u}_{p_2'}i\gamma^5 u_{p_2})\int\frac{d^4k}{(2\pi)^4}\mathrm{Tr}\left[\frac{(\not{k}+m)i\gamma^5}{k^2-m^2}\frac{(\not{q}+\not{k}+m)i\gamma^5}{(q+k)^2-m^2}\right] \tag{I.5}$$

$$i\mathcal{M}_b^{\frac{1}{2}} = \frac{-2^{\eta-1}}{\Lambda^4}(\bar{u}_{p_1'}i\gamma^5 u_{p_1}\bar{u}_{p_2'}i\gamma^5 u_{p_2})\int\frac{d^4k}{(2\pi)^4}\mathrm{Tr}\left[\frac{(\not{k}+m)}{k^2-m^2}\frac{(\not{q}+\not{k}+m)}{(q+k)^2-m^2}\right] \tag{I.6}$$

$$i\mathcal{M}_c^{\frac{1}{2}} = \frac{-2^{\eta-1}}{\Lambda^4}(\bar{u}_{p_1'}\gamma^\mu\gamma^5 u_{p_1}\bar{u}_{p_2'}\gamma^\nu\gamma^5 u_{p_2})\int\frac{d^4k}{(2\pi)^4}\mathrm{Tr}\left[\frac{(\not{k}+m)\gamma_\mu\gamma^5}{k^2-m^2}\frac{(\not{q}+\not{k}+m)\gamma_\nu\gamma^5}{(q+k)^2-m^2}\right] \tag{I.7}$$

$$i\mathcal{M}_d^{\frac{1}{2}} = \frac{-\eta}{\Lambda^4}(\bar{u}_{p_1'}\gamma^\mu\gamma^5 u_{p_1}\bar{u}_{p_2'}\gamma^\nu\gamma^5 u_{p_2})\int\frac{d^4k}{(2\pi)^4}\mathrm{Tr}\left[\frac{(\not{k}+m)\gamma_\mu}{k^2-m^2}\frac{(\not{q}+\not{k}+m)\gamma_\nu}{(q+k)^2-m^2}\right] \tag{I.8}$$

$$i\mathcal{M}_e^{\frac{1}{2}} = \frac{-\eta}{\Lambda^4}(\bar{u}_{p_1'}\sigma^{\mu\nu} u_{p_1}\bar{u}_{p_2'}\sigma^{\alpha\beta} u_{p_2})\int\frac{d^4k}{(2\pi)^4}\mathrm{Tr}\left[\frac{(\not{k}+m)\sigma_{\mu\nu}}{k^2-m^2}\frac{(\not{q}+\not{k}+m)\sigma_{\alpha\beta}}{(q+k)^2-m^2}\right] \tag{I.9}$$

$$i\mathcal{M}_a^1 = \frac{2^{\eta+3}}{\Lambda^6}(\bar{u}_{p_1'}i\gamma^5 u_{p_1}\bar{u}_{p_2'}i\gamma^5 u_{p_2})\int\frac{d^4k}{(2\pi)^4}\frac{1}{k^2-m^2}\frac{2(k\cdot(k+q))^2+k^2(k+q)^2}{(q+k)^2-m^2} \tag{I.10}$$

$$i\mathcal{M}_b^1 = \frac{2^{\eta+4}}{\Lambda^6}(\bar{u}_{p_1'}i\gamma^5 u_{p_1}\bar{u}_{p_2'}i\gamma^5 u_{p_2})\int\frac{d^4k}{(2\pi)^4}\frac{1}{k^2-m^2}\frac{(k\cdot(k+q))^2-k^2(k+q)^2}{(q+k)^2-m^2}\ , \tag{I.11}$$

where $q = p_1 - p_1' = p_2' - p_2$. Unprimed momenta represent the initial states, and primed momenta represent the final states. We introduce Feynman parameters to simplify the

integral in the usual way. The resulting integrals are

$$\int \frac{d^4l}{(2\pi)^4}\frac{1}{(l^2-\Delta)^2} \longrightarrow \frac{-i}{(4\pi)^2}\ln\left(\frac{\Delta}{\Lambda^2}\right) \tag{I.12}$$

$$\int \frac{d^4l}{(2\pi)^4}\frac{l^2}{(l^2-\Delta)^2} \longrightarrow \frac{-2i\Delta}{(4\pi)^2}\ln\left(\frac{\Delta}{\Lambda^2}\right) \tag{I.13}$$

$$\int \frac{d^4l}{(2\pi)^4}\frac{(l^2)^2}{(l^2-\Delta)^2} \longrightarrow \frac{-3i\Delta^2}{(4\pi)^2}\ln\left(\frac{\Delta}{\Lambda^2}\right) \tag{I.14}$$

with $\Delta = m^2 - x(1-x)q^2$. The amplitudes can then be written in a basis of integrals over the Feynman parameters,

$$f_n = \int_0^1 dx(x(1-x))^n \ln\left(\frac{\Delta}{\Lambda^2}\right) \ . \tag{I.15}$$

$\ln(y)$ has a branch cut along the real axis for $y < 0$. The discontinuity in f_n due to this branch cut is given by

$$\mathrm{Disc}(f_n) = 2\pi i \int_{x_-}^{x_+} dx(x(1-x))^n \qquad\qquad x_\pm = \frac{1}{2} \pm \frac{1}{2q}\sqrt{q^2-4m^2} \ . \tag{I.16}$$

I.2 Amplitude to Spatial Potential

The spatial potential is a Fourier transform of the relativistic scattering amplitude $\mathcal{M}$,

$$V(\boldsymbol{r}) = \int \frac{d^3q}{(2\pi)^3}\frac{-\mathcal{M}(\boldsymbol{q})}{4m_N^2}e^{i\boldsymbol{q}\cdot\boldsymbol{r}} \qquad\qquad \mathcal{M}(\boldsymbol{q}) = \sum_A \mathcal{S}_A(\boldsymbol{q}) f_A(|\boldsymbol{q}|) \ . \tag{I.17}$$

Here A indexes possible tensor structures in spin space as carried by the factors $\mathcal{S}_A(\boldsymbol{q})$. Observe that $\mathcal{S}_A(\boldsymbol{q})$ may depend on $\boldsymbol{q}$ through $(\boldsymbol{q}\cdot\sigma_1)(\boldsymbol{q}\cdot\sigma_2)$. This is the only piece of the amplitude that may depend on $\boldsymbol{q}$ as a spatial vector rather than just its magnitude. Inside the Fourier transform, we may identify the transfer momentum with a gradient, $\boldsymbol{q} = -i\nabla$.

This gives an expression for the potential that is a Fourier transform of a function that only depends on the magnitude, $\rho = |\boldsymbol{q}|$:

$$V(\boldsymbol{r}) = \sum_A \frac{-i\mathcal{S}_A(-i\nabla)}{4m_N^2} \int_{-\infty}^{\infty} \frac{d\rho}{(2\pi)^2} \rho f_A(\rho) e^{i\rho r} \ , \tag{I.18}$$

where we have performed the angular integrals and have extended the radial integral to the entire real line. The remaining integral may be performed by analytic continuation into the complex plane, minding the branch cuts in the $f_A(\rho)$ functions along the imaginary ρ-axis starting at $\rho = 2im$. Deforming the integration contour then maps the integral to the discontinuity across this branch cut:

$$\int_{-\infty}^{\infty} \frac{d\rho}{(2\pi)^2} \rho f_A(\rho) \frac{e^{i\rho r}}{r} = \int_{2im+\varepsilon}^{i\infty+\varepsilon} \frac{d\rho}{(2\pi)^2} \rho f_A(\rho) \frac{e^{i\rho r}}{r} - \int_{2im-\varepsilon}^{i\infty-\varepsilon} \frac{d\rho}{(2\pi)^2} \rho f_A(\rho) \frac{e^{i\rho r}}{r} \ . \tag{I.19}$$

Changing integration variables then yields:

$$V(\boldsymbol{r}) = \sum_A \frac{i\mathcal{S}_A(-i\nabla)}{4m_N^2} \int_{2m}^{\infty} \frac{d\lambda}{(2\pi)^2} \lambda \, \mathrm{Disc}\left[f_A(\lambda)\right] \frac{e^{-\lambda r}}{r} \ . \tag{I.20}$$

To complete the remaining integral, we use

$$\int_{2m}^{\infty} d\lambda \sqrt{\lambda^2 - 4m^2} e^{-\lambda r} = \frac{2m}{r} K_1(2mr) \tag{I.21}$$

$$\int_{2m}^{\infty} d\lambda \lambda^2 \sqrt{\lambda^2 - 4m^2} e^{-\lambda r} = \frac{8m^3}{r} K_1(2mr) + \frac{12m^2}{r^2} K_2(2mr) \tag{I.22}$$

$$\int_{2m}^{\infty} d\lambda \lambda^4 \sqrt{\lambda^2 - 4m^2} e^{-\lambda r} = \frac{32m^4}{r^2} K_2(2mr) + \left(\frac{120m^3}{r^3} + \frac{32m^5}{r}\right) K_3(2mr) \tag{I.23}$$

$$\int_{2m}^{\infty} d\lambda \lambda^6 \sqrt{\lambda^2 - 4m^2} e^{-\lambda r} = 2m^8 \left[\frac{K_1(2mr)}{2mr} + \frac{9K_2(2mr)}{(2mr)^2} + \frac{45K_3(2mr)}{(2mr)^3} + \frac{105K_4(2mr)}{(2mr)^4}\right] \tag{I.24}$$

$$\int_{2m}^{\infty} \frac{d\lambda}{\lambda^2} \sqrt{\lambda^2 - 4m^2} e^{-\lambda r} = \frac{1}{4m^2 r^2} \left(4 + \pi m^3 r^3 + \pi^2 m^2 r^2 G(m^2 r^2)\right) \ . \tag{I.25}$$

$G(m^2r^2)$ is shorthand for one of the Meijer G–functions,

$$G(m^2r^2) \equiv G^{2,0}_{2,4}\left(m^2r^2 \middle| \begin{matrix} \frac{1}{2}, \frac{3}{2} \\ 0, 0, \frac{1}{2}, \frac{1}{2} \end{matrix} \right) \ . \tag{I.26}$$

The orientation-averaged form for the potentials is equivalent to the replacement

$$\partial_i \partial_j \longrightarrow \frac{1}{3}\delta_{ij}\nabla^2 \ . \tag{I.27}$$

Appendix J

Non-Relativistic Spinor Limits

For convenience, we present results of spinor contractions to leading order in the non-relativistic limit. Latin indices refer to spatial directions.

J.1 Both Sources Polarized

$$\bar{u}_{p_1'} u_{p_1} \bar{u}_{p_2'} u_{p_2} \approx 4m_N^2 \mathbb{1}_1 \mathbb{1}_2 \tag{J.1}$$

$$\bar{u}_{p_1'} \gamma^\mu u_{p_1} \bar{u}_{p_2'} \gamma^\nu u_{p_2} \approx 4m_N^2 \delta_0^\mu \delta_0^\nu \mathbb{1}_1 \mathbb{1}_2 \tag{J.2}$$

$$\bar{u}_{p_1'} \sigma^{\mu\nu} u_{p_1} \bar{u}_{p_2'} \sigma^{\rho\lambda} u_{p_2} \approx 4m_N^2 \varepsilon^{ijk} \varepsilon^{lmn} \delta_i^\mu \delta_j^\nu \delta_l^\rho \delta_m^\lambda \sigma_1^k \sigma_2^n \tag{J.3}$$

$$\bar{u}_{p_1'} \gamma^\mu \gamma^5 u_{p_1} \bar{u}_{p_2'} \gamma^\nu \gamma^5 u_{p_2} \approx 4m_N^2 \delta_i^\mu \delta_j^\nu \sigma_1^i \sigma_2^j \tag{J.4}$$

$$\bar{u}_{p_1'} i\gamma^5 u_{p_1} \bar{u}_{p_2'} i\gamma^5 u_{p_2} \approx q_j q_k \sigma_1^j \sigma_2^k \ . \tag{J.5}$$

J.2 One Source Polarized, Other Unpolarized

The above results change when one source of nucleons is unpolarized. Take $\boldsymbol{\sigma_2}$ to represent the spin of the unpolarized nucleon current. The long-range potential is the average of the initial spins. The spin-independent $\mathcal{O}^S$ and $\mathcal{O}^V$ bilinears remain unchanged. The axial and pseudo-scalar combinations vanish at all order:

$$\bar{u}_{p_1'}\gamma^\mu\gamma^5 u_{p_1}\bar{u}_{p_2'}\gamma^\nu\gamma^5 u_{p_2} = 0 \qquad\qquad \bar{u}_{p_1'}i\gamma^5 u_{p_1}\bar{u}_{p_2'}i\gamma^5 u_{p_2} = 0\ . \tag{J.6}$$

The tensor combination at leading order is

$$\bar{u}_{p_1'}\sigma^{\mu\nu}u_{p_1}\bar{u}_{p_2'}\sigma^{\rho\lambda}u_{p_2} \approx -iq_a\mathbb{1}_2[((\boldsymbol{p_1}+\boldsymbol{p_1'})\times\boldsymbol{\sigma_1})_i - iq_i\mathbb{1}_1](\delta_i^\mu\delta_0^\nu - \delta_i^\nu\delta_0^\mu)(\delta_a^\rho\delta_0^\lambda - \delta_a^\lambda\delta_0^\rho)\ . \tag{J.7}$$

Appendix K

Neutrino Lagrangians

Here we give more details on Lagrangians in the 2 and 4-component formalisms. The 2-component neutrino charged under $SU(2)_L$ is denoted ν_L, the singlet neutrino is denoted ν_R. The L and R labels only refer to the gauge charge. ν_L and ν_R are left-handed *i.e.* transform as the $(1/2, 0)$ representation of the Lorentz group.

The free Lagrangian for ν_L in case of Dirac and Majorana masses are given by

$$\mathcal{L}_{D,\text{kin}} = i\nu_L^{i\dagger}\bar{\sigma}^\mu\partial_\mu\nu_L^i + i\nu_R^{i\dagger}\bar{\sigma}^\mu\partial_\mu\nu_R^i - m_i\left(\nu_L^i\nu_R^i + \nu_L^{i\dagger}\nu_R^{i\dagger}\right) \tag{K.1}$$

$$\mathcal{L}_{M,\text{kin}} = i\nu_L^{i\dagger}\bar{\sigma}^\mu\partial_\mu\nu_L^i - \frac{m_i}{2}\left(\nu_L^i\nu_L^i + \nu_L^{i\dagger}\nu_L^{i\dagger}\right). \tag{K.2}$$

Integrating out the Z boson in the electroweak Lagrangian gives the effective interaction

$$\mathcal{L}_{\text{int}}^Z = \frac{4G_\text{F}}{\sqrt{2}}J_Z^\mu J_{Z\mu} \supset \frac{4G_\text{F}}{\sqrt{2}}(\nu_L^{i\dagger}\bar{\sigma}^\mu\nu_L^i)J_{\psi\mu} \tag{K.3}$$

where $J_{\psi\mu}$ is the weak neutral current for fields other than neutrinos. Integrating out the W bosons gives

$$\mathcal{L}_{\text{int}}^W = \frac{8G_\text{F}}{\sqrt{2}}J_W^{\mu-}J_{W\mu}^+ \supset \frac{4G_\text{F}}{\sqrt{2}}(e_L^\dagger\bar{\sigma}^\mu\nu_L^i)(\nu_L^{i\dagger}\bar{\sigma}^\mu e_L) = -\frac{4G_\text{F}}{\sqrt{2}}(\nu_L^{i\dagger}\bar{\sigma}^\mu\nu_L^i)(e_L^\dagger\bar{\sigma}^\mu e_L). \tag{K.4}$$

We used a Fierz rearrangement in the last step.

The ν_L field can be described as a 4-component Majorana fermion

$$\nu_M = \begin{pmatrix} \nu_L \\ \\ \nu_L^\dagger \end{pmatrix} \tag{K.5}$$

The ν_L, ν_R can be combined into a Dirac fermion

$$\nu_D = \begin{pmatrix} \nu_L \\ \\ \nu_R^\dagger \end{pmatrix} . \tag{K.6}$$

This provides the Dirac and Majorana fields used in our calculations. The neutrino bilinear in the various representations is expressed as

$$\nu_L^\dagger \bar{\sigma}^\mu \nu_L = -\frac{1}{2} \bar{\nu}_M \gamma^\mu \gamma_5 \nu_M = \bar{\nu}_D \gamma^\mu \frac{1-\gamma_5}{2} \nu_D \, . \tag{K.7}$$

Using this and the definitions (K.5), (K.6) in $\mathcal{L}_{D/M,\text{kin}} + \mathcal{L}_{\text{int}}$ gives the 4-component Lagrangians (5.1), (5.2).

In these 4-component Lagrangians, the relevant couplings to SM fermions in case of unpolarized matter are the vector ones. We find

$$g_{ij}^V = (1 - 4s_w^2)\delta_{ij} \qquad \text{if} \qquad \psi = p \tag{K.8}$$

$$g_{ij}^V = -\delta_{ij} \qquad \text{if} \qquad \psi = n \tag{K.9}$$

$$g_{ij}^V = 2U_{ie}U_{ej}^\dagger - (1 - 4s_w^2)\delta_{ij} \qquad \text{if} \qquad \psi = e. \tag{K.10}$$

Appendix L

Point-Point Neutrino Force Derivation

For this calculation, we follow the steps outlined in [1, 46]. The scattering amplitude corresponding to the loop diagram in Fig. 5.2 is given by

$$i\mathcal{M}_{ij} = -S^{\mu\nu} \int \frac{d^4k}{(2\pi)^4} \mathrm{Tr}\left[\left(\frac{(\not{k} + m_i)\gamma_\mu(\eta - \gamma_5)}{k^2 - m_i^2 + i\varepsilon} \right) \left(\frac{(\not{q} + \not{k} + m_j)\gamma_\nu(\eta - \gamma_5)}{(q+k)^2 - m_j^2 + i\varepsilon} \right) \right] \tag{L.1}$$

with

$$S^{\mu\nu} \equiv 2^{-2-\eta} G_F^2 \bar{u}_{p_1'} \gamma^\mu \left(g_{ij}^V - g_{ij}^A \gamma_5 \right) u_{p_1} \bar{u}_{p_2'} \gamma^\nu \left(g_{ji}^V - g_{ji}^A \gamma_5 \right) u_{p_2}. \tag{L.2}$$

When both point sources are nonrelativistic and polarized, the spin structure simplifies to

$$\bar{u}_{p_1'} \gamma^\mu u_{p_1} \approx 2m_\psi \delta_0^\mu \mathbb{1} \qquad \bar{u}_{p_1'} \gamma^\mu \gamma^5 u_{p_1} \approx 2m_\psi \delta_a^\mu \sigma^a \ . \tag{L.3}$$

We introduce Feynman parameters to simplify the loop integral. Upon dimensional

regularization, the resulting integrals are given by

$$\int \frac{d^4l}{(2\pi)^4}\frac{1}{(l^2-\Delta_{ij})^2} \longrightarrow \frac{-i}{(4\pi)^2}\ln\left(\frac{\Delta_{ij}}{\Lambda^2}\right) \tag{L.4}$$

$$\int \frac{d^4l}{(2\pi)^4}\frac{l^2}{(l^2-\Delta_{ij})^2} \longrightarrow \frac{-2i\Delta_{ij}}{(4\pi)^2}\ln\left(\frac{\Delta_{ij}}{\Lambda^2}\right) \tag{L.5}$$

with $\Delta_{ij} = xm_j^2 + (1-x)m_i^2 - x(1-x)q^2$. The remaining function can be decomposed into the basis of

$$f_{mn} \equiv \int_0^1 dx\, x^m(1-x)^n \ln\left(\frac{\Delta_{ij}}{\Lambda^2}\right) \ . \tag{L.6}$$

These functions have a branch cut when $\Delta_{ij} < 0$. The discontinuity across this branch cut is

$$\mathrm{D}[f_{mn}] = 2\pi i \int_{x_-}^{x_+} dx x^m(1-x)^n \tag{L.7}$$

for

$$x_\pm \equiv \frac{q^2 + \left(m_i^2 - m_j^2\right) \pm \sqrt{(q^2-(m_i-m_j)^2)\,(q^2-(m_i+m_j)^2)}}{2q^2}. \tag{L.8}$$

The amplitude is related to the spatial potential by

$$V_{ij}(\boldsymbol{r}) = \int \frac{d^3q}{(2\pi)^3}\frac{-\mathcal{M}_{ij}(\boldsymbol{q}, q_0 \approx 0)}{4m_\psi^2} e^{i\boldsymbol{q}\cdot\boldsymbol{r}}. \tag{L.9}$$

Inside the Fourier transform, we identify the transfer momentum with a gradient, $\boldsymbol{q} = -i\nabla$. This gives an expression for the potential that is a Fourier transform of a function that only depends on the magnitude $|\boldsymbol{q}|$ and the gradient. [1] The magnitude is analytically continued as $|\boldsymbol{q}| = i\lambda$, and after some manipulations we find

$$V_{ij}(\boldsymbol{r}) = \frac{1}{4m_\psi^2}\int_{m_i+m_j}^{\infty} \frac{d\lambda}{(2\pi)^2}\lambda\,\mathrm{D}\left[i\mathcal{M}_{ij}\left(\lambda, -i\boldsymbol{\nabla}, q_0 \approx 0\right)\right]\frac{e^{-\lambda r}}{r}\,. \tag{L.10}$$

Summing the partial potentials from three generations of neutrinos then yields (5.5).

[1] For more details, please see [1, 46].

Appendix M

Casimir Force from the Path Integral

We show how to derive the potential between generic extended sources, shown in (5.12). Start from an effective Lagrangian with a bilinear coupling between a Dirac fermion Ψ and a nonrelativistic density of matter J,

$$\mathcal{L} = i\bar{\Psi}\partial\!\!\!/\Psi - m\bar{\Psi}\Psi + \bar{\Psi}\Gamma\Psi J(\boldsymbol{x}) \tag{M.1}$$

where Γ can be any Lorentz structure.

We are interested in calculating the energy of a configuration involving two objects J_1, J_2 acting as sources, both described by the distribution $J = J_1 + J_2$. The relevant information is contained in the generating functional of connected correlators $W[J]$, given by

$$Z[J] = \int \mathcal{D}\bar{\Psi}\mathcal{D}\Psi e^{i\int d^4x \mathcal{L}[\Psi,J]} = e^{-iW[J]}\,. \tag{M.2}$$

When the source is static, $W[J] = E[J]T$ where $T = \int dt$ is the integral over time. $E[J]$

is the quantum vacuum energy. At one-loop level, the vacuum energy $E[J]$ is given by the functional determinant (see *e.g.* [166])

$$E[J] = i \ln \mathrm{Det}\left[i\not{\partial} - m + \Gamma J\right] \tag{M.3}$$

$$= i\left(\sum_{n=1}^{\infty} \frac{(-1)^{n+1}}{n}\left(\frac{\Gamma J}{i\not{\partial} - m}\right)^n + \mathrm{Tr}\ln\left[i\not{\partial} - m\right]\right), \tag{M.4}$$

where Det/Tr is the determinant/trace in the functional sense.

$E[J]$ contains infinities—the observable quantity is rather the variation $\partial_L E[J]$, which gives the Casimir force. In the limit where the ΓJ contribution can be treated perturbatively, the leading contribution to $\partial_L E[J]$ is from the $n = 2$ term,

$$\partial_L E[J] \supset i \int d^3\boldsymbol{x} \int d^4x' \,\mathrm{tr}\left[\Gamma \partial_L J(\boldsymbol{x}) \Delta(x - x') \Gamma J(\boldsymbol{x}') \Delta(x' - x)\right] \tag{M.5}$$

where tr is the trace on spinor indexes. The piece of potential associated to this term is found to be

$$V(L) = i \int d^3\boldsymbol{x} \int d^4x' \,\mathrm{tr}\left[\Gamma J_1(\boldsymbol{x}) \Delta(x - x') \Gamma J_2(\boldsymbol{x}') \Delta(x' - x)\right] . \tag{M.6}$$

Restoring the coupling constant yields (5.12) in the Dirac case.